

UC San Diego

UC San Diego Electronic Theses and Dissertations

Title

The use of Metal-Binding Pharmacophores as Druglike Small Molecule Metalloenzyme Inhibitors

Permalink

<https://escholarship.org/uc/item/0xx07972>

Author

Adamek, Rebecca

Publication Date

2020

Peer reviewed|Thesis/dissertation

UNIVERSITY OF CALIFORNIA SAN DIEGO

The use of Metal-Binding Pharmacophores as Druglike Small Molecule Metalloenzyme
Inhibitors

A dissertation submitted in partial satisfaction of the
requirements for the degree Doctor of Philosophy

in

Chemistry

by

Rebecca Noel Adamek

Committee in charge:

Professor Seth Cohen, Chair
Professor Carlo Ballatore
Professor Joshua Figueroa
Professor Thomas Hermann
Professor Jerry Yang

2020

Copyright

Rebecca Noel Adamek, 2020

All rights reserved.

The Dissertation of Rebecca Noel Adamek is approved, and it is acceptable in quality and form for publication on microfilm and electronically:

Chair

University of California San Diego

2020

DEDICATION

To my family and my friends, those I have now, and those that are yet to come. God must really love me to so richly bless my life with your presence. I could not have made it through this adventure without your unending love and support. Thank you all. I love you all, so, so much!!

And of course, I give my praise and thanks to Jesus Christ, the LORD, who is the rock of my salvation, and from whom all blessings flow. It is by the grace of God that I made it through this journey. Praise and glory be to the Lord God almighty! Amen!

TABLE OF CONTENTS

Signature Page	iii
Dedication	iv
Table of Contents	v
List of Abbreviations and Symbols	viii
List of Figures	xiv
List of Schemes	xvii
List of Tables	xix
Acknowledgements	xx
Vita	xxiii
Abstract of the Dissertation	xxv
Chapter 1: Introduction to Metalloenzymes and Medicinal Chemistry	1
1.1: The Science of Medicinal Chemistry	2
1.2: High Throughput Screening verses Fragment-Based Drug Discovery	5
1.3: Metalloenzymes and Metalloenzyme Inhibition	8
1.4: Metal-Binding Pharmacophores as Metalloenzyme Inhibitors	14
1.5: Improving the Druglikeness of the MBP library	17
1.6: Conclusions	18
1.7: Acknowledgements	18
1.8: References	19
Chapter 2: Isosteres of Hydroxypyridinethione as Druglike Pharmacophores for Metalloenzyme Inhibition	23
2.1: Introduction	24
2.2: Materials and Methods	29

2.3: Results and Discussion	32
2.4: Conclusions	42
2.5: Experimental	42
2.6: Acknowledgements	85
2.7: References	85
Chapter 3: Isosteres of Hydroxypyridinethione as Inhibitors of Human Insulin Degrading Enzyme	90
3.1: Introduction	91
3.2: Results and Discussion	97
3.3: Future Work	105
3.4: Conclusions	107
3.5: Experimental	108
3.6: Acknowledgements	136
3.7: References	136
Chapter 4: MBP Isosteres as Inhibitors of Metallo- β -Lactamase	140
4.1: Introduction	141
4.2: Hydroxyquinoline-Based Inhibitors of NDM-1.....	146
4.2.1: 7-Derivatized 8-hydroxyquinolines	149
4.2.2: 2-Derivatized 8-hydroxyquinolines	151
4.2.3: 5-Derivatized 8-hydroxyquinolines	154
4.2.4: Conclusions on 8-Hydroxyquinoline as a Scaffold for NDM-1 Inhibition.....	156
4.3: Hydroxypyridine Thione-Based Inhibitors of NDM-1	157
4.3.1: NDM-1 Assay Screening of 1,2-HOPTO Derivatives	161
4.3.2: Conclusions on 1,2-HOPTO Based NDM-1 Inhibitors	164

4.4: Conclusions	165
4.5: Experimental	166
4.6: Acknowledgements	189
4.7: References	190
Chapter 5: MBPs as Inhibitors of Human Arginase 1	193
5.1: Introduction to Arginase-1	194
5.2: Assay Protocol and Screening Results	199
5.3: MBP Inhibitor Development against Arg1	202
5.3.1: Catechol based inhibitors of Arg1	203
5.3.2: Oxazoline based inhibitors of Arg1	206
5.3.3: Hydroxamic acid based inhibitors of Arg1	210
5.3.4: Unnatural amino acid MBP inhibitors of Arg1	212
5.4: Conclusions	216
5.5: Experimental	217
5.6: Acknowledgements	249
5.7: References	250

LIST OF ABBREVIATIONS AND SYMBOLS

ABH	6-Aminohexaboronic acid
ADA	Adenosine deaminase
ADMET	Absorption, distribution, metabolism, excretion and toxicity
AD	Alzheimer's Disease
Arg1	Human Arginase 1
Arg2	Human Arginase 2
BBB	Blood brain barrier
Bn	Benzyl
BnBr	Benzyl bromide
br	Broad singlet
CCDC	Cambridge Crystallographic Data Center
d	Doublet
Da	Dalton
DCM	Dichloromethane; methylene chloride
dd	Doublet of doublets
DMF	Dimethyl formamide
DMSO	Dimethyl sulfoxide
dt	Doublet of triplets
DTT	Dithiothreitol
<i>E. coli</i>	Escherichia coli
EDC	1-Ethyl-3-(3-dimethylaminopropyl)carbodiimide
EDTA	Ethylenediaminetetraacetic acid

ESI	Electrospray ionization
Et	Ethyl group
EtOAc	Ethyl acetate
EtOH	Ethanol
FBDD	Fragment-based drug discovery
FBLD	Fragment-based lead discovery
FDA	American food and drug administration
g	Times gravity
h	Hours
HATU	1-[bis(dimethylamino)methylene]-1H-1,2,3-triazolo[4,5-b]pyridinium 3-oxid Hexafluorophosphate
HBA	Hydrogen bond acceptor
HBD	Hydrogen bond donor
HEPES	4-(2-hydroxyethyl)-1-piperazineethanesulfonic acid
HOBt	Hydroxybenzotriazole
HOPO	Hydroxypyridinone
HOPTO	Hydroxypyridinethione
hCAII	Human carbonic anhydrase
hGlo-1	Human glyoxalase 1
HIV	Human immunodeficiency virus
HOAc	Acetic acid
HPLC	High pressure liquid chromatography
HRMS	High-resolution mass spectrometry

HTS	High throughput screening
Hz	Hertz
IC ₅₀	50% inhibition concentration; inhibitory activity
IDE	Insulin degrading enzyme
IMI	Imipenem
IMP-1	Imipenemase-1
IPA	Isopropyl alcohol
J	Coupling constant
K_d	Dissociation constant
K_i	Inhibitory constant
kDa	Kilodalton
L	Liters
M	Molar
m	Multiplet
MBI	Metal binding isostere
MBL	Metallo- β -lactamase
MBP	Metal binding pharmacophore
mCPBA	<i>m</i> -Chloroperoxybenzoic acid
MCR-1	Mobilized colistin resistance-1
MDSC	Myeloid Derived Suppressor Cell
MeOH	Methanol
MHz	Megahertz
min	Minutes

mL	Milliliters
mM	Millimolar
MMP	Matrix metallopeptidase
MMP-3	Stromelysin-1; Matrix metallopeptidase-3
MMP-12	Matrix metallopeptidase 12
MMSF	U.C. San Diego Molecular Mass Spectrometry Facility
MOE	Molecular operating environment software
MS	Mass spectrometry
NDM-1	New Delhi metallo- β -lactamase-1
NEM	N-ethylmaleimide
nm	Nanometers
nM	Nanomolar
NME	New molecular entities
NMR	Nuclear magnetic resonance spectroscopy
NOHA	N-Omega-hydroxy-L-arginine
nor-NOHA	nor-N-Omega-hydroxy-L-arginine
OD600	Optical density at 600 nm
PAINS	Pan-assay interference compounds
PAN	Influenza A virus RNA-dependent RNA polymerase PA N-terminal endonuclease
PDB	Protein data bank
PK	Physiochemical properties
pK _a	Acid dissociation constant

pM	Picomolar
ppm	Parts per million
PSA	Polar surface area
q	Quartet
R&D	Research and development
RO5	Rule of Five
RT	Room temperature
s	Singlet
SAR	Structure activity relationships
sec	Seconds
T	Temperature
t	Triplet
T3P	Propanephosphonic acid anhydride
tBu	Tertbutyl group
TEA	Triethylamine
TFA	Trifluoroacetic acid
THF	Tetrahydrofuran
TLC	Thin layer chromatography
Tris	Tris(hydroxymethyl)aminomethane
VIM-2	Verona Integrase Metallo- β -Lactamase-2
$[(\text{Tp}^{\text{Ph,Me}})\text{Zn}]$	Zinc hydrotris(3,5-phenylmethylpyrazolyl)borate
δ	Chemical shift; ppm
Δ	Difference

ΔT_M	Change in melting temperature
$^{\circ}\text{C}$	Degree Celsius
μL	Microliters
μM	Micromolar

LIST OF FIGURES

- Figure 1.1.** The stereotypical drug discovery pipeline, illustrating the process of candidate lead development to eventual FDA approval. In this example, emphasis is placed on the lead optimization to drug candidate phase. Adapted from lecture notes by Dr. Thomas Hermann, as well as Scott et al.....4
- Figure 1.2.** Lead discovery comparison using a generic enzyme active site of HTS (*left*) versus FBDD (*right*). HTS begins with full-length compounds that have moderate activity, and attenuate leads to better fit the active site pockets. FBDD searches for fragment molecules that fit within active site pockets, and either grows or links fragments to improve active site.....7
- Figure 1.3.** Representative MBP fragments for metalloenzyme inhibition. Adapted from Jacobsen et al.....15
- Figure 1.4.** Diagram of the strengths of different molecular interactions in kcal/mol. The relative strength of metal coordination in MBPs is highlighted as a star. H-bonding strength can reach up to 40 kcal/mol in certain cases, but these are considered semi-covalent bonds; as such, this region of semi-covalent H-bond strength is represented as a dashed line.....17
- Figure 2.1.** a) The three HOPTO isomers, as well as a few examples of compounds containing HOPTO-like core scaffolds; b) The typical mode of HOPTO metal coordination is exemplified by the structures of Zn(1,2-HOPTO)₂ (CCDC: OXPZND) as well as c) [(Tp^{Ph,Me})Zn(1,2-HOPTO)] complex (CCDC: TADXUS).....25
- Figure 2.2.** a) Assembled library of 22 HOPTO isostere compounds; b) HOPTO isostere derivatives demonstrating the potential for additional functionalization.....27
- Figure 2.3.** Structures of metalloenzyme active sites used in this study. Metalloenzymes are shown as ribbons with coordinating residues shown in detail. Zn²⁺ is colored in orange spheres with Mn²⁺/Mg²⁺ in purple, and coordination bonds are displayed as yellow dashes; a) MMP-12 (2OXU); b) hCAII (1CA2); c) NDM-1 (3SPU); d) influenza endonuclease (5DES).....29
- Figure 2.4.** The [(Tp^{Ph,Me})Zn(MBI)] complexes of compounds **2.4**, **2.9**, and **2.14**.....37
- Figure 2.5.** Dose-response curve of compounds **2.4**, **2.5**, **2.6**, and **2.9** against NDM-1. This plot was fit using Graphpad Prism, using four-variable response parameters to determine IC₅₀ values.....82
- Figure 3.1.** The structure of IDE. a) The entirety of IDE, with the N-Domain in blue and green, and the C-Domain in yellow and red, with the connecting hinge in white; b) Close-up of the buried catalytic Zn²⁺ and metal coordinating residues within the IDE active site, with Zn²⁺ shown as an orange sphere, water as a red sphere, and coordination bonds as yellow dashes.....92
- Figure 3.2.** Demonstration of the paradoxical ability of IDE to bind and hydrolyze a broad range of substrates, as exemplified by Insulin (a), Glucagon (b), and amyloid-β (c). The full structure

of IDE bound to each substrate is shown on the top, with a close-up of the catalytic site below. For glucagon and amyloid- β , the apo-IDE was used so as to prevent substrate hydrolysis.....94

Figure 3.3. Structures and inhibition values of all reported IDE inhibitors. a) Cystine modifying IDE inhibitors. b) Metal-binding IDE inhibitors, with inset showing crystal structure of hydroxamate-based **3.2** coordinating to the active site Zn^{2+} . c) Exo-site binding IDE inhibitors, with inset showing crystal structure of **3.4** bound to the IDE exo-site, with insulin.....96

Figure 3.4. Model of **2.4** bound to the catalytic Zn^{2+} within the IDE active site. a) Superpose of **2.4** and **3.2**, which was used to create b) the center model of **2.4** bound to the Zn^{2+} in the IDE active site. c) A 2-D representation of the model, with Zn^{2+} in orange, coordination bonds as pink dashes, interactions as green arrows, and solvent exposed regions as blue spheres.....99

Figure 3.5. Prepared non-metal-binding IDE control compounds.....106

Figure 3.6. a) The HPLC trace of **5c** in 1:4 MeOH to water with no additives. The peak at 8.25 min correlates to the dimer, whereas the peak at 9.64 min is **5c**; b) The HPLC trace of **5c** in 1:4MeOH to water with 0.5 mM DTT. The presence of DTT reduces the dimer peak.....135

Figure 4.1. The mechanism of β -lactam inhibition of transpeptidase enzyme. The upper portion displays the normal action of transpeptidase cross-linking, whereas the bottom pathway displays the mechanism of covalent inhibition by a generic β -lactam. Adapted from Patrick.....142

Figure 4.2. a) Full structure of NDM-1 (PDB 3SPU). b) Close-up of the NDM-1 active site (PDB 3SPU). c) Demonstration of the broad-spectrum activity of NDM-1 showing the overlaid hydrolysis products of three different classes of β -lactam (PDB 4RL2, 4EYL, and 4EY2).....144

Figure 4.3. The proposed mechanism of β -lactam hydrolysis within the NDM-1 active site. Adapted from Yang et al.....145

Figure 4.4. A representative selection of previously reported NDM-1 inhibitors.....146

Figure 4.5. a) Percent inhibition of hit 8-hydroxyquinoline fragments against NDM-1 at 200 μ M. Quinoline scaffold numbering is shown on **4.1** in blue. b) Proposed model of **4.4** bound to the NDM-1 active site (3SPU).....147

Figure 4.6. Regions of interest for exploration of the 8-hydroxyquinoline scaffold.....149

Figure 4.7. Time-kill cell assay of **4.12a** against NDM-1 expressing *E. coli* grown for 24 hours, with the optical density displayed below each test tube.....154

Figure 4.8. a) Relative tryptophan fluorescence of **2.6** and **2.31** binding NDM-1, with L-captopril and EDTA as controls. **2.6** and **2.31** display binding as indicated by the decrease in relative tryptophan fluorescence intensity at 348 nm; b) Equilibrium dialysis of the Zn^{2+} content of NDM-1 (8 μ M) with **2.6** and **2.31** as inhibitors.....160

Figure 4.9. Effects of DMSO on NDM-1 fluorocillin green assay. a) Dose-response curves for 2.6 (red) and 2.30 (blue) with no additives in the assay buffer, resulting in enzyme activation at low concentrations of inhibitor; b) Dose-response curves for 2.6 (red) and 2.30 (blue) with 1% DMSO in the assay buffer, demonstrating correction of the previously observed.....	162
Figure 4.10. a) Graph of NDM-1 activity over time, measured in relative fluorescence units, at 100 pM enzyme, where the inclusion of DMSO increases the rate of enzyme activity. b) Graph of NDM-1 activity over time, measured in relative fluorescence units, at 50 pM enzyme, where the inclusion of DMSO no longer affects the rate of enzyme activity.....	163
Figure 5.1. Structure of human Arg1 (PDB 1HQG). a) Full structure of the Arg1 homotrimer; b) close up of the Arg1 active site; c) structure of the hydrolyzed substrate, L-ornithine and urea, bound to the Arg1 active site; d) mechanism of Arg1 mediated L-arginine hydrolysis. The transition state intermediate is boxed in red.....	195
Figure 5.2. a) Summary of noteworthy Arg1 inhibitors; b) Crystal structures of lead Arg1 inhibitors, with important hydrogen bonds shown as magenta dashes. <i>Left:</i> Structure of ABH bound to the active site (PDB 2AEB). <i>Right:</i> Structure of nor-NOHA bound to the active site (PDB: 1HQH).....	198
Figure 5.3. a) Mechanism of the Arg1 assay, where the thioarginine substrate is hydrolyzed by Arg1 to produce a free thiol that reacts with Ellman’s Reagent, generating the chromophore 5-mercapto-2-nitrobenzoic acid (shown in gold starburst), which is monitored at 412 nm; b) Results of screening the MBP library against Arg1 at 200 μ M.....	200
Figure 5.4. Structures and IC ₅₀ values of identified lead MBP scaffolds for Arg1 inhibition. A proposed model of the mode of binding is shown beneath each MBP. Models were prepared using the structure PDB 3K2V.....	201
Figure 5.5. General plan for inhibitor design against Arg1, using a generic example of a catechol-based compound on the left.....	202
Figure 5.6. Summary of catechol analogues and isosteres tested against Arg1.....	203
Figure 5.7. Summary of the various oxazoline analogues and isosteres tested against Arg1....	207
Figure 5.8. Summary of the various hydroxamic acid analogues and isosteres tested against Arg1.....	210
Figure 5.9. Summary of the various unnatural amino acid MBPs tested against Arg1.....	213

LIST OF SCHEMES

Scheme 2.1. General synthetic method to preparing 1,2-HOPTO based compounds 2.2 and 2.4 – 2.9 , using 2.4 as a general example.....	46
Scheme 2.2. Route to 2.10	51
Scheme 2.3. Route to 2.11	52
Scheme 2.4. Route to 2.14	55
Scheme 2.5. Route to 2.15	56
Scheme 2.6. Route to 2.16	57
Scheme 2.7. Route to 2.18	58
Scheme 2.8. Route to 2.19	60
Scheme 2.9. Route to 2.22	61
Scheme 2.10. Route to derivatives 2.23 – 2.26	63
Scheme 2.11. General route to derivatives 2.27 – 2.28	66
Scheme 2.12. General route to derivatives 2.29 – 2.32	68
Scheme 2.13. Route to derivatives 2.33 and 2.34	73
Scheme 2.14. Route to derivatives 2.35 and 2.36	78
Scheme 3.1. Synthesis of sulfonamide HOPTO derivatives.....	101
Scheme 4.1. Synthesis of 7-derivatized 8-hydroxyquinolines.....	150
Scheme 4.2. Synthesis of 2-derivatized 8-hydroxyquinolines.....	152
Scheme 4.3. Synthesis of 5-derivatized 8-hydroxyquinolines.....	155
Scheme 5.1. Synthetic methods for used preparing various catechol-based MBPs, where a) represents a general method of ester deprotection using 5.9b as a representative example, and b) and c) are specific examples.....	205
Scheme 5.2. General method for oxazoline synthesis by: a) cyclizing ethanolamine or aminopropanol with an aromatic nitrile (5.32b as a representative example), or b) by cyclizing amide-coupled ethanolamine (5.34b as a representative example).....	208

Scheme 5.3. General method for hydroxamic synthesis by: a) performing a nucleophilic addition-substitution using hydroxylamine hydrochloride (5.46 as a representative example), or b) by using acid chloride mediated nucleophilic attack (5.57 as a representative example).....211

Scheme 5.4. General method for unnatural amino acid MBP synthesis, using **5.64f** as a representative example.....214

LIST OF TABLES

Table 1.1. List of selected relevant guidelines for good druglikeness and the pharmacokinetic properties they govern.....	5
Table 1.2. List of FDA-approved metal-binding metalloenzyme inhibitors. Adapted and updated from Chen/Adamek et al.....	10
Table 1.3. List of FDA approved metal-binding metalloenzyme inhibitors, organized by MBP scaffold used for metal-chelation. On the right are shown representatives of the most common MBP scaffolds, with the MBP portion highlighted in red.....	13
Table 2.1. Summary of the properties used to assess the druglikeness of small molecules, as applied to both fully elaborated leads and fragments. The calculated PK values for each member of the HOPTO library is displayed below.....	36
Table 2.2. Percent inhibition at 200 μ M of the HOPTO isostere library against various metalloenzymes. Percent inhibition is colored as a heat map with compounds that have no activity in yellow, and gradually moves towards compounds displaying complete inhibition in red (see section 2.3 for assay details).....	38
Table 2.3. Crystal data and structure refinement for [(Tp ^{Ph,Me})Zn] model complexes.....	84
Table 3.1. K_i values of parent HOPTO compounds against the various tested IDE substrates. Compounds 3.6c and 3.7c are included as amide variants of the sulfonamide.....	102
Table 3.2. Inhibitory activity of thiophene sulfonamide derivatives against the IDE substrates.....	104
Table 4.1. Summary of IC ₅₀ values of 8-hydroxyquinoline derivatized at the 7-position.....	151
Table 4.2. Summary of IC ₅₀ values of 8-hydroxyquinoline derivatized at the 2-position.....	153
Table 4.3. Summary of IC ₅₀ values of 8-hydroxyquinoline derivatized at the 5-position.....	156
Table 4.4. IC ₅₀ values of 1,2-HOPTO based compounds tested against NDM-1.....	158
Table 4.5. Summary of HOPTO IC ₅₀ values under different assay conditions.....	164
Table 5.1. Results of screening the prepared catechol derivatives against Arg1.....	206
Table 5.2. Results of screening the prepared oxazoline derivatives against Arg1.....	209
Table 5.3. Results of screening the prepared hydroxamic acid derivatives against Arg1.....	212
Table 5.4. Results of screening the prepared unnatural amino acid MBPs against Arg1.....	215

ACKNOWLEDGEMENTS

I thank my amazing family for seeing me through this time. My Mama, my Papa, my Nathan, my Liam – I could not have undertaken this grand adventure without your love and support. I also want to thank my brothers for their favorite line of advice, “...*Do it!*” it has been very helpful. I thank the rest of my family, my grandparents, my aunts, my uncles, and all of my cousins for their endless love and encouragement as well.

To Seth, you were the reason I choose this wonderful lab group, thank you for helping me pursue Medicinal Chemistry under your tutelage. I could not have made through this journey without your mentorship and assistance. I also thank all of my Cohen lab members, both past and present for your friendship, guidance, and counsel over these past six years. A special shout out to Dr. Cy Credille, who mentored my early years and taught me how to do synthesis, hope you’re doing well! And to Sergio, you were the best late-night lab buddy!

To my dearest friends – I will always cherish our weekly Friday gatherings. See you soon; I’m winning the next round of Spicy Uno!

I want to thank Dr. Douglas Behenna, my Pfizer advisor, for being an endless fount of knowledge and sage advice, and for generously providing an un-ending supply of NMR tubes!

I want to thank our amazing janitor, Aaron Watkins, you helped keep our lab running, and you always had the best stories. Hope you’re enjoying retirement!

Thank you to my external collaborators, these projects would not have worked without you. Thank you to Caitlyn Suire and Dr. Malcolm Leissring at UC Irvine for their help and contributions with Insulin Degrading Enzyme. Thank you to my collaborators at UT Austin, Dr. Pei Thomas and Dr. Walter Fast, as well as Dr. Michael Crowder and Dr. Bonomo at Miami University, Ohio for their contributions towards the New Delhi Metallo- β -Lactamase-1 project.

Chapters 1, 4, and 5 are, in part, a reprint of materials published in the following paper: Targeting Metalloenzymes for Therapeutic Intervention, Chen, Y.A.;* Adamek, R.N.;* Dick, B.L.; Credille, C.V.; Morrison, C.N.; Cohen, S.M.; *Chem. Rev.* **2018**, *118*, ASAP article. DOI: 10.1021/ACS.CHEMREV.8B00201. The dissertation author was the primary researcher and the primary author for the reprinted data presented herein. The dissertation author thanks the remaining co-authors for their contributions. Reprinted with permission from Chemical Reviews. Copyright 2018 American Chemical Society.

*These authors contributed equally to this work

Chapter 2, in large part, is a reprint of materials published in the following paper: Isosteres of Hydroxypyridinethione as Druglike Pharmacophores for Metalloenzyme Inhibition, Adamek, R.N.; Credille, C.V.; Dick, B.L.; Cohen, S.M.; *J. Biol. Inorg. Chem.* **2018**, *23*, 1129-1138. DOI: 10.1007/S00775-018-1593-1. The dissertation author was the primary researcher and the primary author for the reprinted data presented herein. The dissertation author thanks the remaining co-authors for their contributions. Reprinted with permission from Journal of Biological Inorganic Chemistry. Copyright 2018 Springer Nature.

Chapter 3, in part, is currently being prepared for submission for publication of the material. Adamek, R.N.; Suire, C.; Leissring, M.; Cohen, S.M. The dissertation author was the primary researcher and the primary author for the reprinted data presented herein. The dissertation author thanks the remaining co-authors for their contributions

Chapter 5 is, in part, submitted for publication as the following manuscript: Identification of Adenosine Deaminase Inhibitors by Metal-binding Pharmacophore Screening, Adamek, R.N.;* Ludford, P.;* Duggan, S.M.; Tor, Y.; Cohen, S.M.; *ChemMedChem* **2020** (*in submission*). The dissertation author was the primary researcher and the primary author for the

reprinted data presented herein. The dissertation author thanks the remaining co-authors for their contributions.

*These authors contributed equally to this work

VITA

EDUCATION

- 2020 Doctor of Philosophy, Chemistry, University of California San Diego, La Jolla, California
- 2016 Master of Science, Chemistry, University of California San Diego, La Jolla, California
- 2014 Bachelor of Science, Chemistry, California State University Fullerton, Fullerton, California

PROFESSIONAL EXPERIENCE

- 2018 Industry Intern, Pfizer, La Jolla, California
- 2014 – 2020 Graduate Student Researcher, University of California San Diego, La Jolla, California
- 2014 – 2020 Teaching Assistant, University of California San Diego, La Jolla, California
- 2013 – 2014 Supplementary Instruction Leader, California State University Fullerton, Fullerton, California
- 2012 – 2014 Undergraduate Student Researcher, California State University Fullerton, Fullerton, California

PUBLICATIONS

1. **Rebecca N. Adamek**,* Paul Ludford,* Stephanie M. Duggan, Yitzhak Tor, Seth M. Cohen, Identification of Adenosine Deaminase Inhibitors by Metal-binding Pharmacophore Screening, *ChemMedChem* **2020** (*in submission*).
***These authors contributed equally to this work**
2. Cy V. Credille, Benjamin L. Dick, Ryjul W. Stokes, **Rebecca N. Adamek**, Nicholas Wu, Ian Wilson, and Seth M. Cohen, "Structure-Activity Relationships in Metal-Binding Pharmacophores for Influenza Endonuclease" *J. Med. Chem.* **2018**, *61*, 10206-10217.
DOI: 10.1021/ACS.JMEDCHEM.8B01363
2. Allie Y. Chen,* **Rebecca N. Adamek**,* Benjamin L. Dick, Cy V. Credille, Christine N. Morrison, and Seth M. Cohen, "Targeting Metalloenzymes for Therapeutic Intervention" *Chem. Rev.* **2018**, *118*, ASAP article.
DOI: 10.1021/ACS.CHEMREV.8B00201
***These authors contributed equally to this work**
3. **Rebecca N. Adamek**, Cy V. Credille, Benjamin L. Dick, and Seth M. Cohen, "Isosteres of Hydroxypyridinethione as Druglike Pharmacophores for Metalloenzyme Inhibition" *J.*

Biol. Inorg. Chem. **2018**, *23*, 1129-1138.
DOI: 10.1007/S00775-018-1593-1

- Anastasia A. Martinez, Bianca A. Espinosa, **Rebecca N. Adamek**, Brent A. Thomas, Jennifer Chau, Edwardo Gonzalez, Niroshika Keppetipola, Nicholas T. Salzameda, “Breathing new life into West Nile virus therapeutics; discovery and study of zafirlukast as an NS2B-NS3 protease inhibitor” *Eur. J. Med. Chem.* **2018**, *157*, 1202-1213.
DOI: 10.1016/j.ejmech.2018.08.077
- Rebecca N. Adamek**; Maniquis, R.V.; Khakoo, S.; Bridges, M.D.; Salzameda, N.T.; “A FRET-based Assay for the Discovery of West Nile Virus NS2B-NS3 Protease Inhibitors.” *Bioorg. and Med. Chem. Lett.*, **2013**, *23*, 4848-4850.

PATENTS

- U.S. Provisional Patent 62/680,396, Cohen, S.M.; Dick, B.L.; Chen, Y.A.; and **Adamek, R.N.**; “Metal Binding Isosteres as Pharmacophores for Inhibitor Development”, June 4, 2018

ABSTRACT OF THE DISSERTATION

The use of Metal-Binding Pharmacophores as Druglike Small Molecule Metalloenzyme
Inhibitors

by

Rebecca Noel Adamek

Doctor of Philosophy in Chemistry

University of California San Diego, 2020

Professor Seth M. Cohen, Chair

Metalloenzymes are enzymes that require one or more metal ion cofactors for catalytic activity. These enzymes have been estimated to represent up to one-third of the proteome, and are responsible for carrying out a broad range of functions relevant to life. Despite their ubiquity, the metalloenzyme family has been largely underrepresented in terms of drug discovery efforts, with only ~67 drugs having attained FDA approval for metalloenzyme inhibition. To develop new metalloenzyme inhibitors, the Cohen laboratory has developed a library of metal-

binding pharmacophores (MBPs) containing ~350 small molecules ideally suited for metalloenzyme inhibitor development. These compounds act by coordinating to the metal ion cofactor necessary for metalloenzyme activity, thereby blocking off the active site and preventing further enzymatic activity. By screening this MBP library against disease relevant metalloenzymes, it is possible to identify MBP scaffolds with both high affinity and specificity for target metalloenzymes. Then through a series of rational fragment growth and structural activity relationship studies, it is possible to elaborate these fragment MBPs into full-length inhibitors.

To further improve this library and facilitate the use of MBPs as metalloenzyme inhibitors, the work described in this thesis has sought to improve the druglikeness of MBP fragments. Chapter 2 deals with a case study of expanding the hydroxypyridinethione (HOPTO) MBP scaffold to by creating sublibrary of HOPTO isostere and analogue compounds designed to enhance the druglikeness of the HOPTO MBP. Chapter 3 then takes this expanded HOPTO sublibrary, and applies it towards drug discovery efforts against human Insulin Degrading Enzyme (IDE), a target relevant for both Type 2 diabetes and neurodegeneration. This work resulted in the discovery of a new, sulfonamide HOPTO inhibitor of IDE. In Chapter 4, this HOPTO sublibrary, as well as a set of derivatized 8-hydroxyquinoline compounds, were applied against New Delhi Metallo- β -lactamase-1 (NDM-1), a mononuclear Zn^{2+} metalloenzyme responsible for β -lactam antibiotic resistance. Finally, Chapter 5 deals with the use of MBPs to develop new inhibitors of human Arginase-1, a dinuclear Mn^{2+} metalloenzyme relevant to cancer immunotherapy. In this work, catechol, oxazoline, and hydroxamic acid scaffolds were all explored as MBP warheads against this target.

Chapter 1: Introduction to Metalloenzymes and Medicinal Chemistry

1.1 The Science of Medicinal Chemistry

The term science is derived from the Latin *scire*, meaning “knowledge of”,¹ whereas in Medicinal Chemistry, the word medicinal is sourced from the Latin word *medicina*, meaning “the healing art”,² and chemistry is a phonetic shortening of the Medieval term alchemy.³ In turn, alchemy is derived from the Arabic prefix *al-* meaning of, and the Egyptian word *khem*,⁴ the ancient name of the land of Egypt, meaning blackness, in reference to the fertile soil of the Nile. Therefore, the science of medicinal chemistry, in etymological terms, can informally be translated as “knowledge of healing black earth magic”.

Today, Medicinal Chemistry, is understood to be the practice of developing therapeutics for the treatment of various diseases, and is a field at the intersection of the practices of organic chemistry and pharmacy.⁵⁻⁶ The following section is by no means a comprehensive review of the art of medicinal chemistry, but a brief overview of the field, intended to guide the reader through the essential fundamentals. Most medicinal chemistry is focused on the development of small molecules (as opposed to biologics) that interact with a target enzyme relevant to disease, to elicit a beneficial effect.^{5, 7} As such, the majority of small molecule drugs operate by binding to a target enzyme, either at the active site or an allosteric site, to block the enzyme from further function, preventing enzymatic activity and thereby treating the disease of interest.⁵⁻⁶

It is useful to consider this inhibitor-binding event through the lens of thermodynamics and kinetics. When successful, the act of ligand binding is a spontaneous and therefore exothermic event, meaning that by Gibbs free energy, it is desirable for ΔG to be as low as possible. Breaking the analysis down according to $\Delta G = \Delta H - T\Delta S$ reveals that much of the ligand binding is governed by the enthalpic and entropic contributions. During the binding event, both ligand and protein must be first be desolvated of their respective water shells, and upon

subsequent ligand entry to the active site, interactions between the ligand and enzyme must occur to stabilize and form favorable interactions within the active site.⁸⁻⁹ The initial desolvation step is enthalpically disfavored yet entropically favored, as the release of water results in a loss of coordination. However, the second phase of forming protein-ligand interactions is enthalpically favored with a loss of entropy due the formation of favorable interactions.⁸⁻⁹ Successful drug discovery is usually based on a balance of these enthalpic and entropic components.

A generic pipeline of the drug discovery process is presented in Figure 1.1 below. Upon selection of a relevant enzymatic target, various small molecule libraries are screened for their ability to inhibit enzymatic activity, until a lead with good inhibitory activity, usually in the low micromolar range, is found. This inhibitory activity is often measured in IC_{50} values, the concentration of inhibitor required to reduce enzymatic activity by half in an in vitro enzymatic assay, so that lower IC_{50} values correlate with more potent inhibitors; many other types of affinity measures are also employed to evaluate binding strength, as detailed by Pennington et.al.¹⁰ This inhibitor screening is typically some form of bioaffinity measurement, ranging from any combination of colorimetric/fluorescent in vitro enzymatic assays to in vitro cellular assays.¹⁰ The lead is then elaborated or otherwise modified and the screening process is repeated, so that through a series of iterative modifications and screenings, the drug lead is modified until a low nanomolar, preferable picomolar, drug candidate is found.⁶ Upon selection of drug candidate, pre-clinical ADMET (absorption, distribution, metabolism, excretion, and toxicity) studies are carried out, and upon success, the drug candidate advances to human clinical trials.⁵⁻⁶ Should the drug candidate prove to be both non-toxic and efficacious in the three phases of clinical trials, it is passed on towards the FDA for final review and approval.⁶

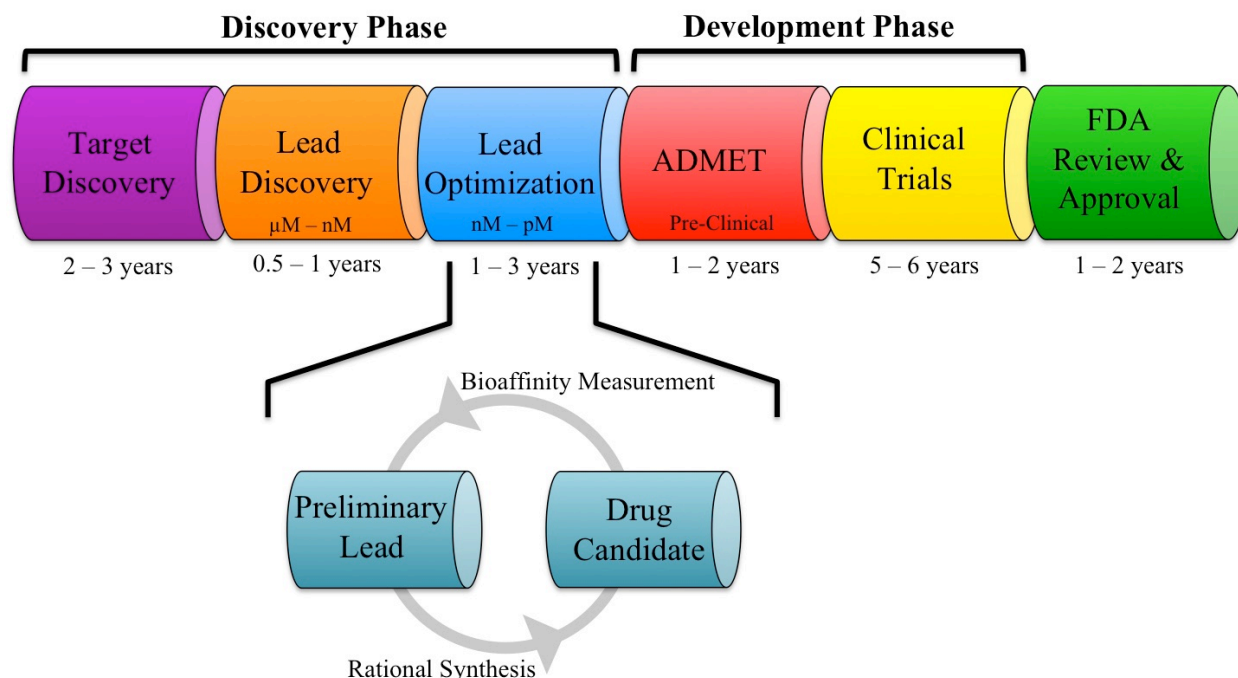


Figure 1.1. The stereotypical drug discovery pipeline, illustrating the process of candidate lead development to eventual FDA approval. In this example, emphasis is placed on the lead optimization to drug candidate phase. Adapted from lecture notes by Dr. Thomas Hermann,¹¹ as well as Scott et al.¹²

While high potency, target specificity, and lack of toxicity are obviously among the most desired traits in drug candidates, there are other chemical and physical properties that dictate the success and failure of lead compounds in clinical trials. These properties are often referred to as druglikeness, the qualitative assessment of how drug-like a compound is in comparison to other known drugs. Considering this is a rather circular definition, in an effort to more broadly define the constraints of druglike space, seminal work by Christopher Lipinski of Pfizer developed the Rule of Five (RO5) to describe the parameters for success in orally bioavailable drugs.¹³ These guidelines and their rationale are presented in the first four entries in Table 1.1 below. In large part, these rules can be summarized as ensuring drug molecules have the right balance of lipophilicity and aqueous solubility to achieve permeability across membranes. Compounds that break two or more of these rules usually fail as clinical candidates.¹³ Of course, being within

these parameters by no means guarantees the success of a drug, and there are always exceptions of drugs that break these rules that are extremely useful as clinical drugs; the RO5 is simply a highly useful set of guidelines. Over the following years, many other parameters have been added to the RO5 to predict good druglikeness,¹⁴⁻¹⁵ some of these are also included in Table 1.1.

Table 1.1. List of selected relevant guidelines for good druglikeness and the pharmacokinetic properties they govern.

Parameter	Rationale
MW \leq 500 g/mol	Compounds with too high MW have difficulty with intestinal and Blood Brain Barrier (BBB) permeation.
ClogP \leq 5	A measure of lipophilicity, defined as the ratio of octanol solubility verses water solubility. Compounds with high ClogP tend to be too soluble in lipids and have poor aqueous solubility.
Hydrogen Bond Acceptors (HBA) \leq 10	Too many HBA groups hinder membrane bilayer permeability.
Hydrogen Bond Donors (HBD) \leq 5	Too many HBD groups hinder membrane bilayer permeability.
Polar Surface Area (PSA) \leq 140 Å	High PSA tends to correlate with poor intestinal and BBB absorption.
Rotatable Bonds \leq 10	Too many rotatable bonds tend to correlate with poor intestinal permeability.

1.2 High Throughput Screening verses Fragment-Based Drug Discovery

Once a target enzyme has been selected, it is critical to decide what small molecules to screen against said target. This chemical library selection is no small undertaking, as the realm of chemical space is near infinite. It has been conservatively estimated that for all possible chemical combinations of C, N, O, and S, limited to \leq 30 atoms, there exists $\sim 10^{63}$ possible molecules; a number far exceeding the grains of sand on the Earth and stars in the universe.¹⁶⁻¹⁷ As it is near impossible by current human standards to develop and maintain a chemical library of this magnitude, chemical libraries are instead designed to be representative of the myriad possible chemical scaffolds. In this regard, the two mainstream approaches towards chemical

library development are High Throughput Screening (HTS) and Fragment-Based Drug Discovery (FBDD), which is interchangeably referred to as Fragment-Based Lead Discovery (FBLD).

Historically, drug discovery programs were predominately phenotypic screening based, with the focus on producing efficacious results, and often achieved success through fortunate serendipity, rather than identification of the actual drug target.^{13, 18} Around the 1970s, the paradigm began to shift towards rational drug development, with drug discovery programs choosing to start with established biological targets believed to be the root of disease, and search for inhibitors of these targets.¹³ This rational drug discovery approach, fueled by the advent of combinatorial synthetic methods lead to the development of HTS in the early 1990s as a method of lead generation.¹³ HTS libraries can contain up to the millions of full-length compounds, typically up to 500 g/mol, and usually follow the guidelines of the RO5. Leads discovered by HTS tend to have relatively strong binding affinities in the low micromolar to nanomolar regime, but also have a tendency to have more entropy driven attraction, with potency derived from strategically placed lipophilic bulk rather than polar interactions, as exemplified in Figure 1.2.¹² Upon identification of initial hit compounds, synthetic modifications are made to the core scaffold to improve both activity and selectivity through better interactions with the active site, until a lead drug candidate is developed.

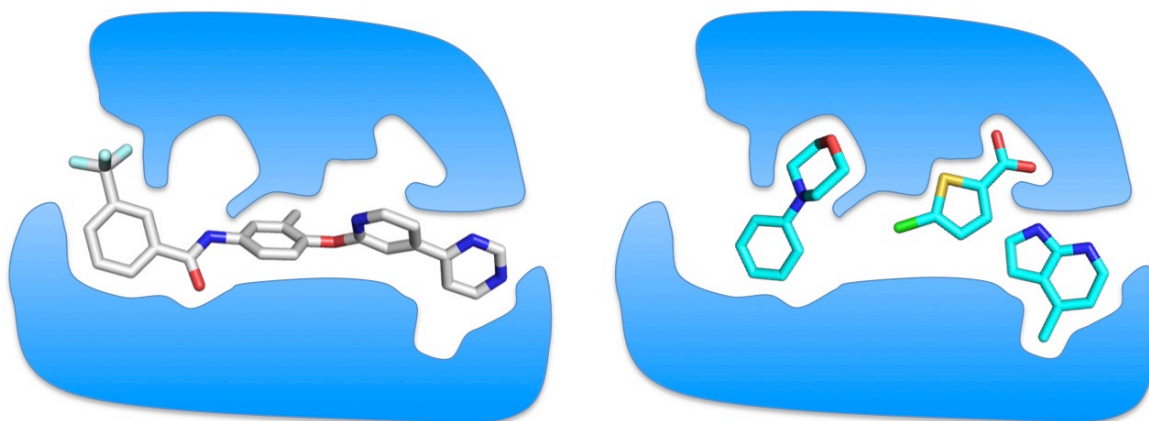


Figure 1.2. Lead discovery comparison using a generic enzyme active site of HTS (*left*) versus FBDD (*right*). HTS begins with full-length compounds that have moderate activity, and attenuate leads to better fit the active site pockets. FBDD searches for fragment molecules that fit within active site pockets, and either grows or links fragments to improve active site interactions. Adapted from Scott et al.¹²

In the hands of industry, HTS approaches have been fruitful in lead generation, but the HTS methodology remains plagued by concerns of high lipophilicity, poor thermodynamic solubility, and false positive leads.¹² As such, trends have shifted towards FBDD as an alternative method of hit generation. As the name implies, fragments are small molecules with $MW \leq 300$ g/mol, that, due to their small size, typically have much lower target affinity than HTS, in the millimolar range.¹⁹ However, these fragment interactions must be of high-quality in order to be detected, meaning that fragment based interactions tend to be more specific and enthalpically driven.¹² As such, FBDD has become increasingly popularized as a method of lead discovery, with vemurafenib (marketed as zelboraf) being the first FBDD derived therapeutic to ever attain FDA approval in 2011.²⁰⁻²¹ Upon identification of lead scaffolds, fragment hits are developed into full-length compounds via either fragment linking to join together active fragments, or fragment growth to elaborate the scaffold into available binding pockets (Figure 1.2).

1.3 Metalloenzymes and Metalloenzyme Inhibition

Metalloproteins are proteins that require one or more metal ions in order to function; it has been estimated that between 40 to 50% of all proteins can be categorized as metalloproteins.²²⁻²⁴ The metalloprotein family can be further subdivided into proteins that utilize the metal ion to maintain structural organization, those that require metal for electron transfer, and those that use the metal to carry out catalytic function.²⁵ This latter class is referred to as metalloenzymes, enzymes that require one or more metal-ion cofactors within the active site for catalytic activity.²⁵ Typically, metalloenzymes are easy to distinguish from other metalloproteins, as the catalytic metal typically has one or more ‘open’ coordination sites occupied by water, whereas in structural metalloproteins, the metal is fully coordinated by amino acid residues.²⁵ This open coordination site on the metal within metalloenzymes can then serve as a site for substrate binding or aid in transition state stabilization, facilitating the catalytic process. Often, the metal serves to act as a Lewis acid, and activates bound water by stabilizing the more nucleophilic hydroxide form to carry out subsequent catalysis.²⁵

Metalloenzymes are capable of, and responsible for, carrying out a broad range of functions, including oxidation and reduction, substrate ligation, substrate isomerization, functional group transfer, and substrate hydrolysis.²⁵ Correlating to this myriad functionality, metalloenzyme activity has been implicated in a broad range of disease states, including heart disease, cancer, diabetes, neurodegeneration, and pathogenic infections.²⁶ As such, directly targeting the metal-ion cofactor through the use of metal-binding pharmacophores (MBPs) presents an innovative method of metalloenzyme inhibition to treat these various disease states. Broadly speaking, metal-binding inhibitors are described as having an MBP domain that serves

to anchor the inhibitor to the active-site metal through one or more donor atoms, and a backbone portion that affords additional specificity through interactions with the remainder of the active site. MBP-based inhibitors serve the dual function of physically blocking substrate access to the active site, and deprive the metalloenzyme of its capacity for metal-mediated catalysis.

Despite the tantalizing prospects of metalloenzyme inhibition through metal-binding inhibitors, metalloenzymes have historically been vastly under-represented in the drug discovery space. As of December 31, 2019, there have only been ~67 FDA approved metal-binding metalloenzyme inhibitors (Table 1.2). This number is based off of initial studies by Liao²⁷ and Chen/Adamek et al.,²⁶ with updates to reflect the recent FDA approval of baloxavir marboxil²⁸ for the treatment of influenza, and the approval of bictegravir for HIV as a fixed component of the combination antiretroviral drug bictarvy.²⁹ Considering there are ~1,565 FDA approved small molecule drugs, metalloenzyme inhibitors then represent less than 5% of all FDA approved drugs, an underwhelming number, especially in consideration of the extreme prevalence of metalloenzymes within the proteome.

Table 1.2. List of FDA-approved metal-binding metalloenzyme inhibitors. Adapted and updated from Chen/Adamek et al.

Metalloenzyme Target	FDA-approved, metal-binding metalloenzyme inhibitors (~67 total)	Number of Inhibitors (%)
4-Hydroxyphenylpyruvate dioxygenase	nitisinone	1 (~1.5 %)
Angiotensin converting enzyme	benazepril, captopril, enalapril, fosinopril, lisinopril, moexipril, perindopril, quinapril, ramipril, trandolapril	10 (~15 %)
carbonic anhydrase	acetazolamide, bendroflumethiazide, benzthiazide, brinzolamide, chlorothiazide, cyclothiazide, diclofenamide, dorzolamide, ethoxzolamide, furosemide, hydrochlorothiazide, hydroflumethiazide, methazolamide, methyclothiazide, quinethazone, topiramate, trichlormethiazide, zonisamide	19 (~28 %)
cytochrome P4503A4	ritonavir	1 (~1.5 %)
histone deacetylase	belinostat, panobinostat, romidepsin, vorinostat	4 (~6 %)
HIV-1 integrase	bictegravir, ^a dolutegravir, elvitegravir, raltegravir	4 (~6 %)
Human alcohol dehydrogenase	fomepizole	1 (~1.5 %)
lanosterol 14 α -demethylase	albaconazole, bifonazole, butoconazole, clotrimazole, econazole, efinaconazole, fenticonazole, fluconazole, isavuconazole, isoconazole, itraconazole, ketoconazole, luliconazole, miconazole, omoconazole, oxiconazole, posaconazole, ravuconazole, sertaconazole, sulconazole, terconazole, tioconazole, voriconazole	23 (~34 %)
lipoxygenase	zileuton	1 (~1.5 %)
matrix metalloproteinase	periostat	1 (~1.5 %)
phosphodiesterase 4	crisaborole	1 (~1.5 %)
PA _N Endonuclease	baloxavir marboxil ^b	1 (~1.5 %)
tyrosinase	hydroquinone	1 (~1.5 %)

^abictegravir is currently only approved as a component of a fixed-dose combination antiretroviral therapy.

^bbaloxavir marboxil is the pro-drug form of the active species baloxavir

In part, this disparity between the small amount of metalloenzyme inhibitors, relative to the plethora of disease-related metalloenzyme targets, can be sourced to concerns that arose during the attempts of industry to develop MBP inhibitors of MMP for cancer therapeutics. While there was a wide breadth of chemical diversity present in the various inhibitors developed against the various MMP isoforms, they were all reliant on a single MBP warhead, the hydroxamic acid, to achieve metal coordination to the active site Zn^{2+} .³⁰ Unfortunately, these projects all suffered costly-late stage drug candidate failures, with only the repurposed antibiotic doxycycline achieving FDA approval, and even then only for niche use in periodontal disease.³¹ It was later ascertained that these failures derived not from the MBP, but from on-target effects, as the biological roles MMP were not fully validated, and the full repercussions of MMP inhibition were not understood.³²⁻³³ As this work represented the first concerted effort on the part of industry to develop MBP inhibitors, the hydroxamic acid evolved from these origins to become the first, and often only, MBP scaffold used in drug-discovery efforts.

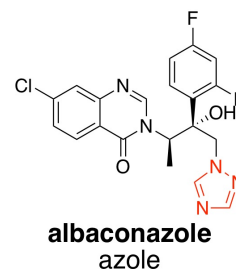
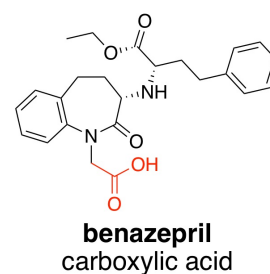
This disproportionate reliance on the hydroxamic acid MBP has in turn created a stigma against MBPs as a whole, that they lack specificity and exhibit broad, off-target toxic effects due to indiscriminate metalloenzyme inhibition.³⁴ To address this latter point, studies by Day and Chen have demonstrated that MBP containing molecules, when optimized for their respective drug targets, retain specificity for their designated target, even when challenged with excess levels of competing metalloenzyme sources.

The other primary factor as to why metalloenzymes have been under-represented as a drug target can be attributed to a lack of diversity in available MBP warheads. The vast majority of lead-discovery efforts against metalloenzymes have historically utilized an extremely small subset of MBPs, namely the carboxylic acid, hydroxamic acid, and thiol, which expectedly does

not cover a wide breadth of chemical space. Moving on from discovery efforts and examining only the ~67 FDA-approved metal-binding metalloenzymes, it becomes rapidly apparent that only a few privileged metal-binding scaffolds have attained approval. The carboxylic acid, sulfonamide, andazole MBPs comprising the bulk of approved metal-binding scaffolds at a total of 52 out of 67 compounds, or ~76%. Upon further analysis and comparison between Table 1.2 and Table 1.3, it is evident that these select scaffolds are geared towards only a few metalloenzymes, with carboxylic acids targeting angiotensin converting enzyme, sulfonamides towards carbonic anhydrase, and azoles, with the exception of fomepizole, inhibiting lanosterol 14 α -demethylase. This lack of diversity within metal-binding inhibitors, coupled with the small amount of metalloenzymes that are the validated targets of FDA-approved compounds, again serves to indicate the extent of how unexploited the metalloenzyme space is in regards to therapeutic potential.

Table 1.3. List of FDA approved metal-binding metalloenzyme inhibitors, organized by MBP scaffold used for metal-chelation. On the right are shown representatives of the most common MBP scaffolds, with the MBP portion highlighted in red.

MBP Scaffold	FDA-approved, metal-binding metalloenzyme inhibitors (~67 total)	Number of Inhibitors (%)
4-oxo-nicotinic acid	elvitegravir	1 (~1.5%)
boronic acid	crisaborole	1 (~1.5%)
carboxylic acid	benazepril, enalapril, fosinopril, lisinopril, moexipril, perindopril, quinapril, ramipril, trandolapril	9 (~13%)
hydroxamic acid	belinostat, panobinostat, vorinostat, zileuton ^a	4 (~6%)
hydroxypyridone (family)	bictegravir, dolutegravir, raltegravir, baloxavir marboxil	4 (~6%)
imidazole	bifonazole, butoconazole, clotrimazole, econazole, fenticonazole, isoconazole, ketoconazole, luliconazole, miconazole, omoconazole, oxiconazole, sertaconazole, sulconazole, tioconazole	14 (~21%)
polyphenol/polyketone	Periostat, hydroquinone, nitisinone	3 (~4%)
pyrazole	fomepizole	1 (~1.5%)
sulfonamide	acetazolamide, bendroflumethiazide, benzthiazide, brinzolamide, chlorothiazide, cyclothiazide, diclofenamide, dorzolamide, ethoxzolamide, furosemide, hydrochlorothiazide, furosemide, hydroflumethiazide, methazolamide, methyclothiazide, quinethazone, topiramate, trichlormethiazide, zonisamide	19 (~28%)
thiazole	ritonavir	1 (~1.5%)
thiol	captopril, romidepsin	2 (~3%)
triazole	albaconazole, efinaconazole, fluconazole, isavuconazole, itraconazole, posaconazole, ravuconazole, terconazole, voriconazole	9 (~13%)



^aWhile the MBP in zilueton is not a true hydroxamic acid, it is structurally similar enough to be considered to bind through the same coordination found in hydroxamic acids.

1.4 Metal-Binding Pharmacophores as Metalloenzyme Inhibitors

While the MBPs listed in Table 1.3 are known and useful warheads for metal-coordination, over-reliance on these scaffolds is imaginably insufficient to optimize metal coordination. Different metals have different charge states and different electronic configurations all dictated by their intrinsic atomic properties, and these properties result in different preferences for the coordination sphere of a metal-ion; and the metal-ions found in metalloenzymes are no different. Indeed, in addition to intrinsic ligand coordination preferences of the metal ion, the metal coordination sphere within metalloenzymes is further impacted by active site constraints of the enzyme itself.³⁵⁻³⁶ This concept was exemplified in work by Martin, demonstrating that when hydroxypyridinethione binds to the active site Zn^{2+} in carbonic anhydrase, the lipophilic wall of active site is capable forcing strong deviations from preferred ligand coordination modes.³⁶ Therefore, when designing MBP ligands for metalloenzyme inhibition, it is important to consider the properties of the both the metal and the enzyme itself. To address this shortcoming and design ligands better suited towards metalloenzyme inhibition, previous works by the Cohen lab have sought to extensively expand the breadth of MBP warheads, resulting in a library of ~350 MBP fragment molecules, with each member containing a unique MBP. A representative sample of this library is shown in Figure 1.3 below.

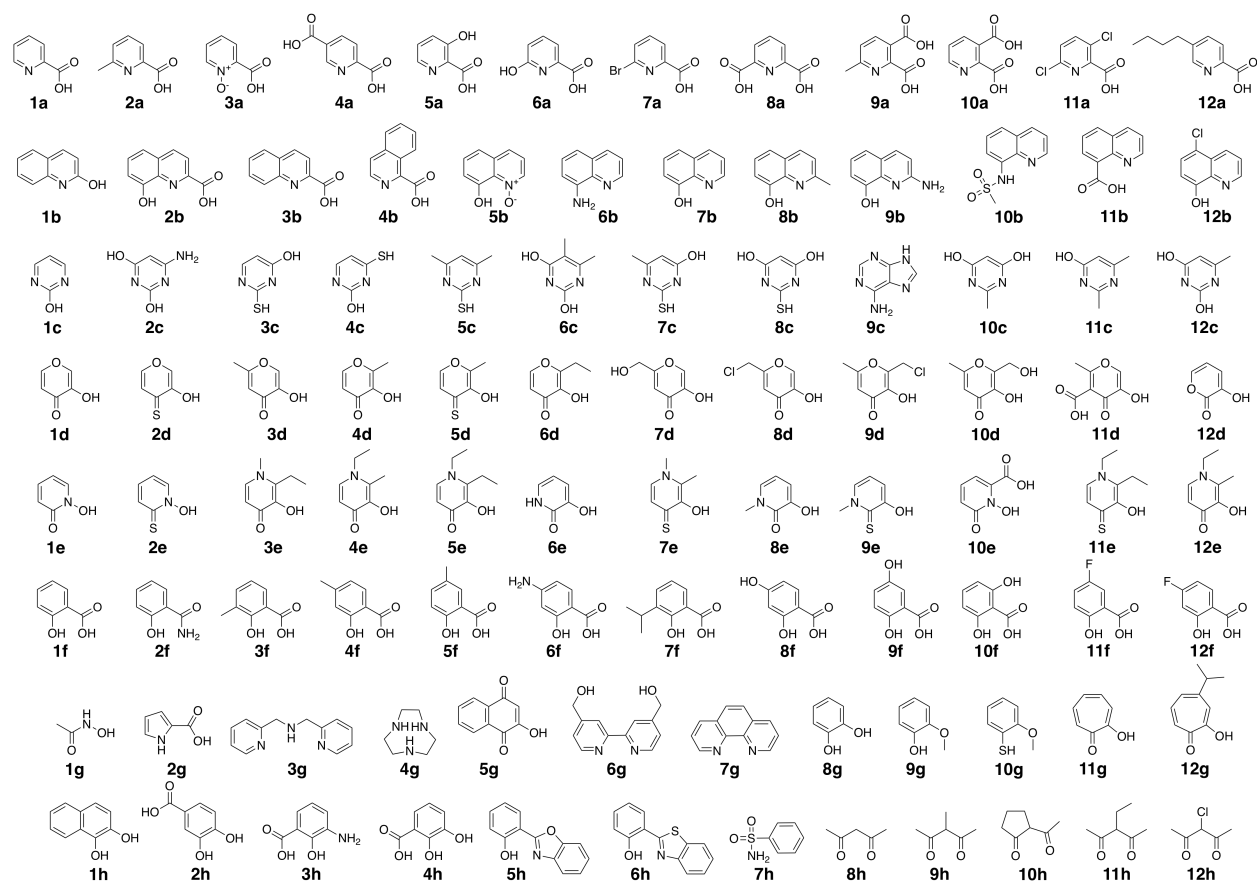


Figure 1.3. Representative MBP fragments for metalloenzyme inhibition. Adapted from Jacobsen et al.³⁷

This MBP library is ideally suited towards discovering novel metal-binding lead scaffolds for hit to lead drug development against metalloenzymes. The library was largely curated from the wealth of knowledge available in the inorganic field, and converted ligands previously utilized in siderophores or in metal catalysis, and adapted them as fragments for use in drug discovery. This inhibitor class acts by forming one or more coordination bonds with the active site metal, resulting in a strong, reversible, and non-covalent interaction. The ligands are predominantly comprised of aromatic rings to afford rigidity, and through one or more donor atoms, are able to act as Lewis bases and donate a lone pair of electrons to the metal, forming the strong coordinate bonds. These fragments are composed of a wide selection of different

donating groups, coupled with an assortment of heterocycles, so that when combined, there is an intrinsically large array of chemical diversity within the MBP library. This diversity in turn allows for tuning of the MBP ligand to fit the individual metalloenzyme active site, as the diversified donor atom set and carbon backbone respectively provide optimal interactions with the both metal and amino acid residues of the active site.

As coordinate bond formation is an enthalpy driven process, a large amount of binding affinity can be gained by optimizing these metal-centric interactions (Figure 1.4). Therefore, MBP fragment hits typically display affinities in the low micromolar regime, ranking them far more potent than the millimolar ranges typically seen in traditional FBDD hits, and roughly on par with the affinities seen in HTS hits. Considering MBP fragments are by definition, low molecular weight compounds, they naturally have much higher ligand efficiency; again evidencing the utility of MBPs as candidates for discovery efforts against metalloenzymes. Upon identification of a potent MBP scaffold for a given target metalloenzyme, the fragment is elaborated through a series of growth and merging strategies until a selective, full-length inhibitor is attained. This strategy has been used with great success by the Cohen lab, and has lead to a number of published MBP metalloenzyme inhibitors.^{26, 38-43}

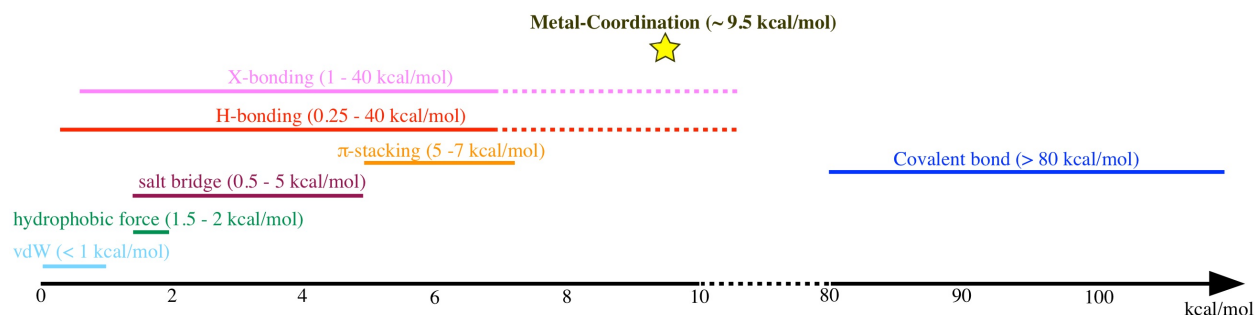


Figure 1.4. Diagram of the strengths of different molecular interactions in kcal/mol. The relative strength of metal coordination in MBPs is highlighted as a star. H-bonding strength can reach up to 40 kcal/mol in certain cases, but these are considered semi-covalent bonds; as such, this region of semi-covalent H-bond strength is represented as a dashed line.⁴⁴⁻⁴⁵ In consideration that halogen bonds have similar strengths to H-bonds, the upper regions of X-bond strength are also represented as a dashed line.⁴⁶⁻⁴⁷ Figure adapted from Zhou, P. et al.⁴⁷⁻⁴⁸

1.5 Improving the Druglikeness of the MBP library

To aid the incorporation of MBPs in future medicinal chemistry efforts, the work described in this thesis has sought to improve the druglikeness of MBP scaffolds. Within the medicinal chemistry community, there are known strategies to improve druglikeness, such as the incorporation of nitrogen heteroatoms, isosteric replacement, and incorporation of sp^3 hybridization, and the work of this thesis shows that these traditional medicinal chemistry methods are amenable to MBP scaffolds as well. Therefore, the goal of the thesis work described herein is to expand the utility of MBPs by improving the druglikeness of common MBP scaffolds, and employing these compounds as inhibitors of historically challenging and elusive metalloenzymes. As such, Chapter 2 will focus on a case study of improving the druglikeness of the HOPTO scaffold, and Chapters 3 and 4 will demonstrate the utility of these modifications in hit to lead development against IDE and NDM-1 respectively. Finally, Chapter 5 deals with a separate example of using similar strategies to expand the utility of catechol warhead to other MBPs against Arg1.

1.6 Conclusions

Metalloenzymes account for approximately 30% of the proteome, yet are vastly underrepresented as drug targets. Less than 5% of all FDA-approved drugs are metal-binding inhibitors of metalloenzymes, and of these approved compounds, three metalloenzymes are targeted by 52 of the 67 approved compounds. To facilitate the use of MBPs as metalloenzyme inhibitors, the work described in this thesis has sought to improve the druglikeness of MBP fragments. In a case study described in Chapter 2, a library of HOPTO compounds was prepared, and demonstrated to have a good range of pharmacokinetic properties, as well as selectivity between various metalloenzymes, despite all compounds bearing the same MBP. Therefore, this HOPTO library was employed against two different Zn^{2+} metalloenzymes, IDE and NDM-1, and used to develop new inhibitor classes against these target enzymes in Chapters 3 and 4 respectively. Finally Chapter 5 also demonstrates the benefits of improving the druglikeness of MBPs by using catechol as well as oxazoline and hydroxamic acid based inhibitors against Arg1.

1.7 Acknowledgements

Chapters 1 is, in part, a reprint of materials published in the following paper: Targeting Metalloenzymes for Therapeutic Intervention, Chen, Y.A.;* Adamek, R.N.;;* Dick, B.L.; Credille, C.V.; Morrison, C.N.; Cohen, S.M.; *Chem. Rev.* **2018**, *118*, ASAP article. DOI: 10.1021/ACS.CHEMREV.8B00201. The dissertation author was the primary researcher and the primary author for the reprinted data presented herein. Reprinted with permission from Chemical Reviews. Copyright 2018 American Chemical Society.

*These authors contributed equally to this work

1.8 References

1. Harper, D., Science. In *Online Etymology Dictionary*.
2. Harper, D., Medicine. In *Online Etymology Dictionary*.
3. Harper, D., Chemistry. In *Online Etymology Dictionary*.
4. Harper, D., Alchemy. In *Online Etymology Dictionary*.
5. Patrick, G. L., Drugs and Drug Targets: An Overview. In *An Introduction to Medicinal Chemistry, Fourth Edition*, Oxford University Press: 2009.
6. Silverman, R. B.; Holladay, M. W., Chapter 1: Introduction. In *The Organic Chemistry of Drug Design and Drug Action, Third Edition*, Elsevier Inc.: 2015.
7. Stevens, E., Chapter 1: The Modern Drug Discovery Process. In *Medicinal Chemistry, The Modern Drug Discovery Process*, Pearson Education, Inc: 2014.
8. Freire, E., Chapter 1: The Binding Thermodynamics of Drug Candidates. In *Thermodynamics and Kinetics of Drug Binding*, Wiley-VCH Verlag GmbH & Co. KGaA: 2015.
9. Keserü, G. M., Chapter 4: Thermodynamics-Guided Optimizations in Medicinal Chemistry. In *Thermodynamics and Kinetics of Drug Binding*, Wiley-VCH Verlag GmbH & Co. KGaA: 2015.
10. Pennington, L. D.; Aquila, B. M.; Choi, Y.; Valiulin, R. A.; Muegge, I., Positional Analogue Scanning: An Effective Strategy for Multiparameter Optimization in Drug Design. *J. Med. Chem.* **2020**.
11. Hermann, T. Lecture 3: Drug Discovery, Development & Approval http://tch.ucsd.edu/chem259/259_lecture_03_2012.pdf.
12. Scott, D. E.; Coyne, A. G.; Hudson, S. A.; Abell, C., Fragment-Based Approaches in Drug Discovery and Chemical Biology. *Biochemistry* **2012**, *51*, 4990-5003.
13. Lipinski, C. A.; Lombardo, F.; Dominy, B. W.; Feeney, P. J., Experimental and Computational Approaches to Estimate Solubility and Permeability in Drug Discovery and Development Settings. *Adv. Drug. Deliv. Rev.* **2001**, *46*, 3-26.
14. Clark, D. E.; Pickett, S. D., Computational Methods for the Prediction of 'Drug-Likeness'. *Drug Discov. Today* **2000**, *5*, 49-58.
15. Veber, D. F.; Johnson, S. R.; Cheng, H. Y.; Smith, B. R.; Ward, K. W.; Kopple, K. D., Molecular Properties that Influence the Oral Bioavailability of Drug Candidates. *J. Med. Chem.* **2002**, *45*, 2615-23.
16. Bohacek, R. S.; McMartin, C.; Guida, W. C., The Art and Practice of Structure-Based Drug Design: A Molecular Modeling Perspective. *Med. Res. Rev.* **1996**, *16*, 3-50.

17. Erlanson, D. A.; Fesik, S. W.; Hubbard, R. E.; Jahnke, W.; Jhoti, H., Twenty Years On: The Impact of Fragments on Drug Discovery. *Nat. Rev. Drug. Discov.* **2016**, *15*, 605-619.
18. Kubinyi, H., Strategies and Recent Technologies in Drug Discovery. *Pharmazie* **1995**, *50*, 647-62.
19. Kuntz, I. D.; Chen, K.; Sharp, K. A.; Kollman, P. A., The Maximal Affinity of Ligands. *Proc. Natl. Acad. Sci. U. S. A.* **1999**, *96*, 9997-10002.
20. Tsai, J.; Lee, J. T.; Wang, W.; Zhang, J.; Cho, H.; Mamo, S.; Bremer, R.; Gillette, S.; Kong, J.; Haass, N. K.; Sproesser, K.; Li, L.; Smalley, K. S.; Fong, D.; Zhu, Y. L.; Marimuthu, A.; Nguyen, H.; Lam, B.; Liu, J.; Cheung, I.; Rice, J.; Suzuki, Y.; Luu, C.; Settachatgul, C.; Shellooe, R.; Cantwell, J.; Kim, S. H.; Schlessinger, J.; Zhang, K. Y.; West, B. L.; Powell, B.; Habets, G.; Zhang, C.; Ibrahim, P. N.; Hirth, P.; Artis, D. R.; Herlyn, M.; Bollag, G., Discovery of a Selective Inhibitor of Oncogenic B-Raf Kinase with Potent Antimelanoma Activity. *Proc. Natl. Acad. Sci. U. S. A.* **2008**, *105*, 3041-6.
21. Staton, T. Roche Melanoma Drug Wins Early FDA Nod. <https://www.fiercepharma.com/pharma/roche-melanoma-drug-wins-early-fda-nod>.
22. Andreini, C.; Bertini, I.; Cavallaro, G.; Holliday, G. L.; Thornton, J. M., Metal Ions in Biological Catalysis: From Enzyme Databases to General Principles. *J. Biol. Inorg. Chem.* **2008**, *13*, 1205-18.
23. Solomon, E. I.; Sundaram, U. M.; Machonkin, T. E., Multicopper Oxidases and Oxygenases. *Chem. Rev.* **1996**, *96*, 2563-2606.
24. Waldron, K. J.; Rutherford, J. C.; Ford, D.; Robinson, N. J., Metalloproteins and Metal Sensing. *Nature* **2009**, *460*, 823-30.
25. Bertini, I.; Gray, H. B.; Stiefel, E. I.; Valentine, J. S., Metal-Dependent Lyase and Hydrolase Enzymes. (I) General Metabolism. In *Biological Inorganic Chemistry Structure and Reactivity*, University Science Books: 2007; pp 175-184.
26. Chen, A. Y.; Adamek, R. N.; Dick, B. L.; Credille, C. V.; Morrison, C. N.; Cohen, S. M., Targeting Metalloenzymes for Therapeutic Intervention. *Chem. Rev.* **2019**, *119*, 1323-1455.
27. Yang, Y.; Hu, X. Q.; Li, Q. S.; Zhang, X. X.; Ruan, B. F.; Xu, J.; Liao, C., Metalloprotein Inhibitors for the Treatment of Human Diseases. *Curr. Top. Med. Chem.* **2016**, *16*, 384-96.
28. Hunt, A., FDA Approves New Drug to Treat Influenza. FDA, Ed. 2018.
29. Gilead, U.S. Food and Drug Administration Approves Gilead's Biktarvy® (Bictegravir, Emtricitabine, Tenofovir Alafenamide) for Treatment of HIV-1 Infection. 2018.
30. Whittaker, M.; Floyd, C. D.; Brown, P.; Gearing, A. J., Design and Therapeutic Application of Matrix Metalloproteinase Inhibitors. *Chem. Rev.* **1999**, *99*, 2735-76.

31. Peterson, J. T., Matrix Metalloproteinase Inhibitor Development and the Remodeling of Drug Discovery. *Heart Fail. Rev.* **2004**, *9*, 63-79.
32. Murphy, G., Riding the Metalloproteinase Roller Coaster. *J. Biol. Chem.* **2017**, *292*, 7708-7718.
33. Vandenbroucke, R. E.; Libert, C., Is There New Nope for Therapeutic Matrix Metalloproteinase Inhibition? *Nat. Rev. Drug Discov.* **2014**, *13*, 904-27.
34. Baell, J.; Walters, M. A., Chemistry: Chemical Con Artists Foil Drug Discovery. *Nature* **2014**, *513*, 481-3.
35. Martin, D. P.; Hann, Z. S.; Cohen, S. M., Metalloprotein-Inhibitor Binding: Human Carbonic Anhydrase II as a Model for Probing Metal-Ligand Interactions in a Metalloprotein Active Site. *Inorg. Chem.* **2013**, *52*, 12207-15.
36. Martin, D. P.; Blachly, P. G.; McCammon, J. A.; Cohen, S. M., Exploring the Influence of the Protein Environment on Metal-Binding Pharmacophores. *J. Med. Chem.* **2014**, *57*, 7126-35.
37. Jacobsen, J. A.; Fullagar, J. L.; Miller, M. T.; Cohen, S. M., Identifying Chelators for Metalloprotein Inhibitors Using a Fragment-Based Approach. *J. Med. Chem.* **2011**, *54*, 591-602.
38. Perez, C.; Barkley-Levenson, A. M.; Dick, B. L.; Glatt, P. F.; Martinez, Y.; Siegel, D.; Momper, J. D.; Palmer, A. A.; Cohen, S. M., Metal-Binding Pharmacophore Library Yields the Discovery of a Glyoxalase 1 Inhibitor. *J. Med. Chem.* **2019**, *62* (3), 1609-1625.
39. Li, J.; Zhang, Y.; Da Silva Sil Dos Santos, B.; Wang, F.; Ma, Y.; Perez, C.; Yang, Y.; Peng, J.; Cohen, S. M.; Chou, T. F.; Hilton, S. T.; Deshaies, R. J., Epidithiodiketopiperazines Inhibit Protein Degradation by Targeting Proteasome Deubiquitinase Rpn11. *Cell. Chem. Biol.* **2018**, *25* (11), 1350-1358 e9.
40. Credille, C. V.; Dick, B. L.; Morrison, C. N.; Stokes, R. W.; Adamek, R. N.; Wu, N. C.; Wilson, I. A.; Cohen, S. M., Structure-Activity Relationships in Metal-Binding Pharmacophores for Influenza Endonuclease. *J. Med. Chem.* **2018**, *61* (22), 10206-10217.
41. Chen, A. Y.; Thomas, P. W.; Stewart, A. C.; Bergstrom, A.; Cheng, Z.; Miller, C.; Bethel, C. R.; Marshall, S. H.; Credille, C. V.; Riley, C. L.; Page, R. C.; Bonomo, R. A.; Crowder, M. W.; Tierney, D. L.; Fast, W.; Cohen, S. M., Dipicolinic Acid Derivatives as Inhibitors of New Delhi Metallo-beta-lactamase-1. *J. Med. Chem.* **2017**, *60* (17), 7267-7283.
42. Chen, A. Y.; Thomas, P. W.; Cheng, Z.; Xu, N. Y.; Tierney, D. L.; Crowder, M. W.; Fast, W.; Cohen, S. M., Investigation of Dipicolinic Acid Isosteres for the Inhibition of Metallo-beta-Lactamases. *ChemMedChem* **2019**, *14* (13), 1271-1282.
43. Adamek, R. N.; Credille, C. V.; Dick, B. L.; Cohen, S. M., Isosteres of hydroxypyridinethione as drug-like pharmacophores for metalloenzyme inhibition. *J. Biol. Inorg. Chem.* **2018**, *23* (7), 1129-1138.

44. Steiner, T., The Hydrogen Bond in the Solid State. *Angew. Chem. Int. Ed. Engl.* **2002**, *41*, 49-76.
45. Desiraju, G. R., Hydrogen Bridges in Crystal Engineering: Interactions without Borders. *Acc. Chem. Res.* **2002**, *35*, 565-73.
46. Metrangolo, P.; Neukirch, H.; Pilati, T.; Resnati, G., Halogen Bonding Based Recognition Processes: A World Parallel to Hydrogen Bonding. *Acc. Chem. Res.* **2005**, *38*, 386-95.
47. Zhou, P.; Lv, J.; Zou, J.; Tian, F.; Shang, Z., Halogen-Water-Hydrogen Bridges in Biomolecules. *J. Struct. Biol.* **2010**, *169*, 172-82.
48. Zhou, P.; Huang, J.; Tian, F., Specific Noncovalent Interactions at Protein-Ligand Interface: Implications for Rational Drug Design. *Curr. Med. Chem.* **2012**, *19*, 226-38.

Chapter 2: Isosteres of Hydroxypyridinethione as Druglike Pharmacophores for Metalloenzyme Inhibition

2.1 Introduction

Metalloenzymes constitute at least one-third of all enzymes, are involved in a broad range of in vivo functions, and represent a validated class of clinical targets.¹⁻³ Metalloenzymes have been linked to a number of human diseases including cancer and heart disease,⁴ and have been implicated as targets in both pathogenic bacterial⁵ and viral vectors.⁶ Small molecule therapeutics containing metal-binding pharmacophores (MBPs) designed to coordinate the active site metal ion offer an appealing approach in treating diseases linked to metalloenzymes.⁷

Hydroxypyridinethiones (HOPTOs) are natural products derived from the *Allium stipitatum* or drumstick onion plant,⁸ and are a chemical scaffold highly suited for metal binding. There are three isomeric HOPTO scaffolds, with each bearing a thione and hydroxyl donor atom metal coordination motif, as shown in Figure 2.1. These ligands are well established in the field of inorganic chemistry and are known to form stable, 5-member coordination rings with a variety of metal ions.⁹ This strong metal binding combined with the heterocyclic nature of the HOPTO scaffold imparts a high binding affinity for metalloenzymes, implying that HOPTOs can be a useful warhead for drug discovery campaigns against metalloenzymes.

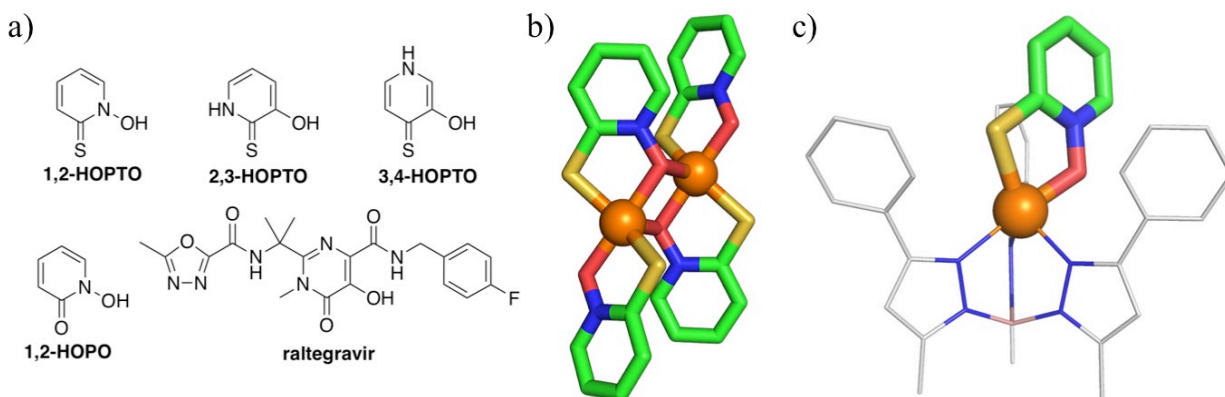


Figure 2.1. a) The three HOPTO isomers, as well as a few examples of compounds containing HOPTO-like core scaffolds; b) The typical mode of HOPTO metal coordination is exemplified by the structures of $\text{Zn}(1,2\text{-HOPTO})_2$ (CCDC: OXPZND) as well as c) $[(\text{Tp}^{\text{Ph,Me}})\text{Zn}(1,2\text{-HOPTO})]$ complex (CCDC: TADXUS). Structures are colored by atom type: boron = pink, carbon = green or gray, nitrogen = blue, oxygen = red, sulfur = gold, and zinc = orange (spheres).

However, despite their strong affinity for metal ions and metalloenzymes, the therapeutic potential of the HOPTO MBP has been underexploited. Only zinc pyrithione (a.k.a., 1,2-HOPTO = 1-hydroxypyridine-2(1*H*)-thione) (Figure 2.1) is widely used for its anti-microbial properties¹⁰ as the active ingredient of anti-dandruff shampoos¹¹ and in anti-fouling agents for paints.¹² There are no reports of FDA approved drugs containing the HOPTO scaffold for human internal use. This is in contrast to the analogous hydroxy-pyridinone (HOPO) MBP, which have been used in a plethora of applications, ranging from food additives to anti-cancer agents.¹³ In particular, HOPO and HOPO isosteres have been used as MBPs in metalloenzyme inhibitors, such as the FDA-approved HIV integrase inhibitors raltegravir¹⁴ (Figure 2.1), and dolutegravir,¹⁵ in addition to being utilized as a MBP warhead in innumerable metalloenzyme inhibitor campaigns. Considering that HOPTOs and HOPOs only differ by a thione versus ketone respectively, it is surprising that the HOPTO scaffold has not enjoyed the same therapeutic utility as the HOPO scaffold.

In large part, the lack of use of the HOPTO scaffold can be attributed to a broader general concern around metalloenzyme inhibitors, of which those containing thiols are viewed with particular reservation (despite the clinical success of compounds such as Captopril).¹⁶⁻¹⁸ Metalloenzyme inhibitors have suffered under the impression that if a molecule is able to bind metal, it will act indiscriminately and display broad off-target effects by inhibiting all available metalloenzymes.¹⁹ However, studies by Chen²⁰ and Day²¹ demonstrate otherwise, showing that metalloenzyme inhibitors are as selective in binding to their respective targets as other small molecule inhibitors, and are not titrated away by the presence of alternate, off-target metalloenzymes. Furthermore, metalloenzymes are the validated target of multiple drug discovery campaigns, with there being approximately 68 FDA-approved metal-binding metalloenzyme inhibitors,^{4, 22-23} clearly indicating that the presence of a MBP does not diminish the therapeutic potential of a molecule.

As for the thiol, there has been concern over potential toxicity issues. There have been reports of terminal thiol inhibitors such as L-744,832 against farnesyl transferase, which failed Phase I clinical trials due to off-target effects.²⁴⁻²⁵ However, it is critical to understand that the thione present in the HOPTO scaffold is not a thiol and therefore has a different physiochemical and PK profile. As the HOPTO thione predominately exists in the sp^2 hybridization with 53:1 thione to thiol,²⁶ it is not subjected to the same reactivity (and hence toxicity) associated with the thiol moiety. Furthermore, the bidentate metal-binding profile of HOPTOs grants potentially greater metalloenzyme specificity than the monodentate nature of a terminal thiol.

Outside of the stigma associated with MBPs, the only real drawback associated with the HOPTO scaffold has been a relatively poor logP, leading to limited aqueous solubility,²⁷ as well as a limited scope of meaningful structure activity relationship (SAR) studies on how

modifications to the MBP itself affect overall metal-binding and inhibitory activity. Thus, detailed herein is a summary of useful HOPTO isosteres and analogues designed with the purpose of improving PK and maintaining metal binding properties (Figure 2.2). We have prepared a 22 component HOPTO metal-binding isostere (MBI) library, demonstrating that it is possible to access a wealth of synthetic diversity with electronic and PK tunability while maintaining donor atoms critical for metal binding. In addition to this library, we have also prepared routes to derivatives of select members of this HOPTO library as a means of demonstrating their potential for fragment growth and merging strategies.

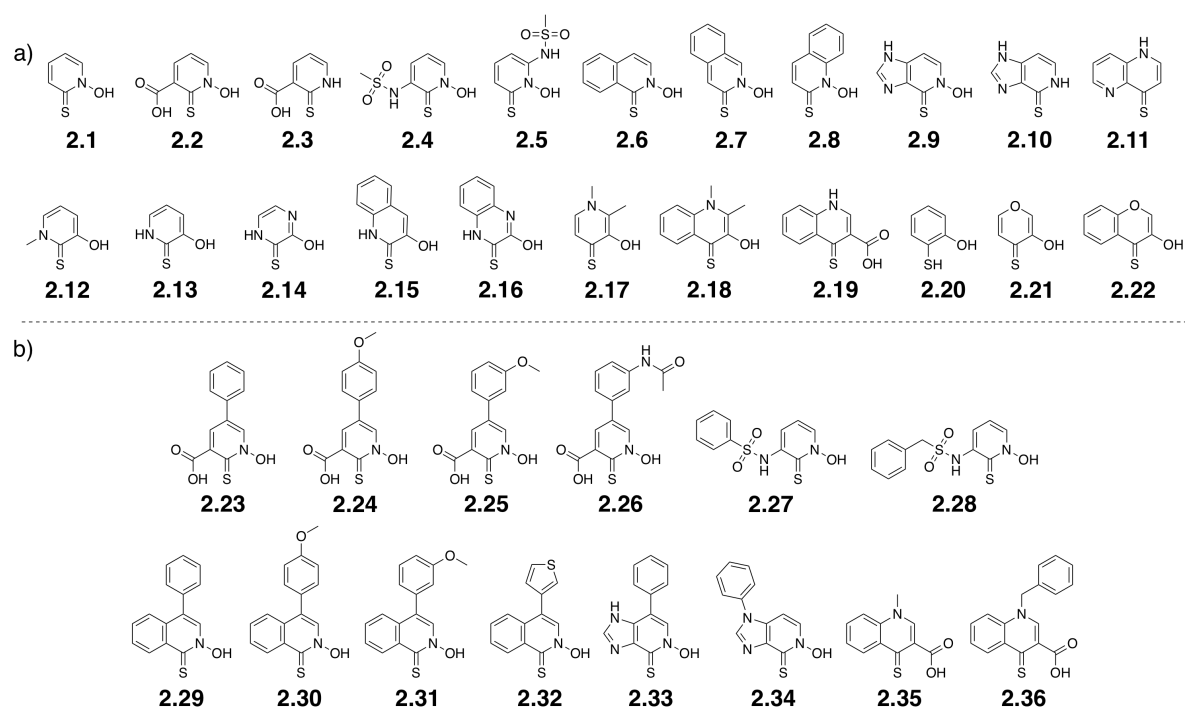


Figure 2.2. a) Assembled library of 22 HOPTO isostere compounds; b) HOPTO isostere derivatives demonstrating the potential for additional functionalization.

Finally, for the purpose of evaluating these novel HOPTO scaffolds as fragments useful to medicinal chemistry, human carbonic anhydrase II (hCAII), matrix metalloprotease-12 (MMP-12), New Delhi Metallo- β -lactamase-1 (NDM-1), and influenza endonuclease (PA_N) were

selected as metalloenzyme targets to test the validity and selectivity of the HOPTO library (Figure 2.3). hCAII and MMP-12 are both mononuclear Zn^{2+} -dependent human metalloenzymes, where hCAII regulates blood pH and the MMPs have long been established as cancer targets. NDM-1 is a dinuclear Zn^{2+} -dependent metalloenzyme that confers bacterial resistance to β -lactam antibiotics, and PA_N is a conserved dinuclear Mn^{2+} -dependent metalloenzyme vital for influenza virus replication. PA_N was included as the *O,S* donor is expected to be less suitable for the Mn^{2+} active site (based on hard-soft acid-base theory) when compared to the Zn^{2+} -dependent metalloenzymes studied here.²⁸⁻²⁹ HOPTOs **2.1** – **2.22** were screened against these four metalloenzymes at 200 μ M and demonstrate that taking a metal-centric approach and fine-tuning the SAR of just the core MBP generates different selectivity amongst these metalloenzymes even though the ligand donor set is maintained.

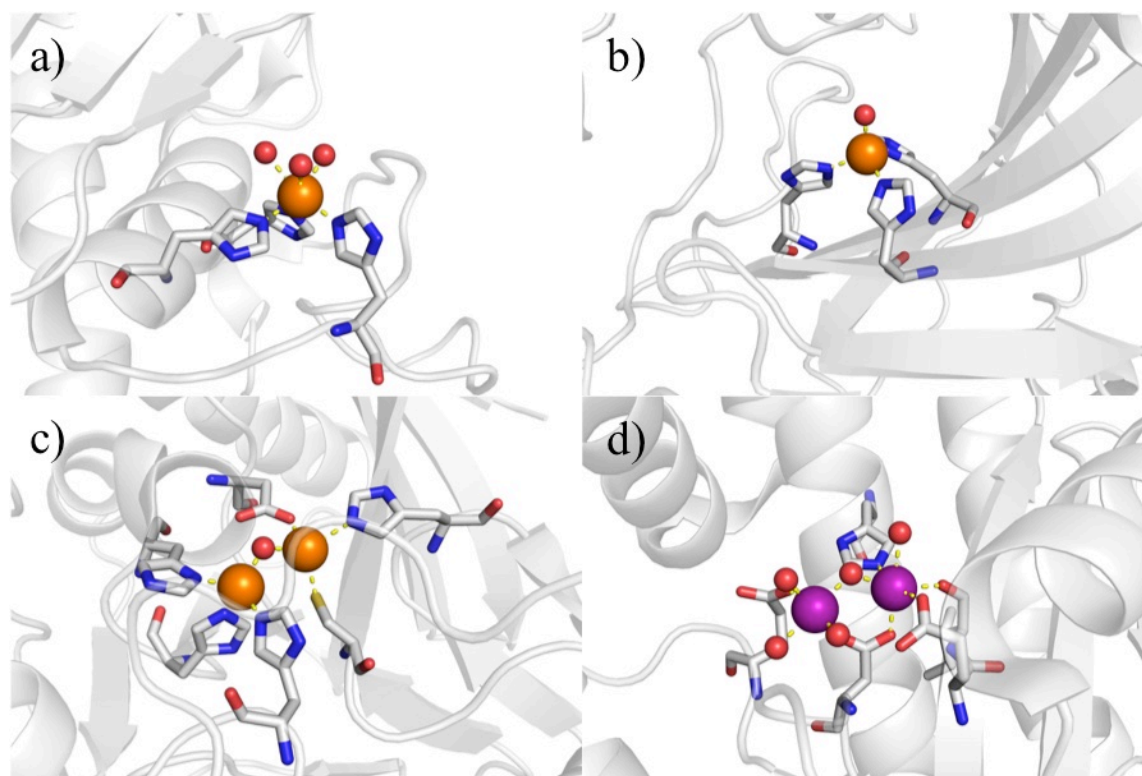


Figure 2.3. Structures of metalloenzyme active sites used in this study. Metalloenzymes are shown as ribbons with coordinating residues shown in detail. Zn^{2+} is colored in orange spheres with Mn^{2+}/Mg^{2+} in purple, and coordination bonds are displayed as yellow dashes; a) MMP-12 (2OXU); b) hCAII (1CA2); c) NDM-1 (3SPU); d) influenza endonuclease (5DES).

2.2 Materials and Methods

Materials

All reactants and reagents were purchased from either Sigma-Aldrich, Alfa-Aesar, or Combi-blocks and used with no additional purification. Synthetic protocols and details for **2.1** – **2.37** are reported in the Experimental Section 2.5. Absorbance assays were performed using a BioTek Synergy HT microplate reader. Fluorescence assays were performed using either a BioTek Synergy HT microplate reader or a BioTek Synergy H4 microplate reader. hCAII was prepared as previously reported,³⁰ MMP-12 was purchased from Enzo Life Sciences

(Farmingdale, NY, USA), NDM-1 was supplied as a gift from Dr. David Tierney (U. Miami, Ohio), and influenza endonuclease was expressed and purified as previously reported.³¹

Pharmacokinetic Properties

All calculated PK data was determined through ChemAxon. Experimental logP and logD_{7.4} for **2.1**, **2.4**, **2.9**, and **2.14** was determined using a Sirius T₃ instrument. Both pK_a and logP were performed in 0.15 M KCl with 0.5 M HCl and KOH. First the pK_a was experimentally determined through triplicate potentiometric titrations,³²⁻³³ Sample sizes contained approximately 0.70 mg of MBI for pK_a measurements. The experiments were titrated from pH 12.0 to 2.0, and standard deviations were determined from fitting the three replicate runs. As **2.1** had poor aqueous solubility, it was necessary to include HPLC grade MeOH in the sample analysis.

logP was experimentally determined through potentiometric titrations in the presence of differing ratios of octanol and water in triplicate runs.³²⁻³³ Sample sizes contained approximately 0.50 mg of MBI for logP measurements. Again the experiments were titrated from pH 12.0 to 2.0, and standard deviations were determined from fitting the three replicate runs. LogD_{7.4} was then calculated from the measured pK_a and logP values.

MMP-12 Assays

MMP-12 and OmniMMP fluorogenic substrate were purchased as an assay kit from Enzo Life Sciences, and the assay was performed in a Costar black 96-well plate. Each well contained a total volume of 100 μ L including buffer (50 mM HEPES, 10 mM CaCl₂, 0.05% Brij-35, pH 7.5), human recombinant MMP-12 (0.7 U per well, Enzo Life Sciences), inhibitor (200 μ M), and

fluorogenic OmniMMP substrate (4 μ M MCA-Pro-Leu-Gly-Leu-DPA-Ala-Arg-NH₂-AcOH, Enzo Life Sciences). The enzyme and inhibitor were initially incubated together for 15 min at 37 °C, after which the reaction was initiated by substrate addition. The change in fluorescence was monitored for 20 min with excitation at 320 nm and reading emission at 400 nm. The negative control wells contained no inhibitor and were arbitrarily set as 100% enzyme activity.

hCAII Assays

hCAII was prepared as previously reported,³⁰ and the assay was performed in a Costar clear 96-well plate. Each well contained a total volume of 100 μ L including buffer (50 mM HEPES, 100 mM NaSO₄, pH 8.0), hCAII (100 nM), inhibitor (200 μ M), and *p*-nitrophenyl acetate substrate (500 μ M). The enzyme and inhibitor were initially incubated together for 15 min at room temperature, after which the reaction was initiated by substrate addition. The change in absorbance was monitored for 20 min at 405 nm. The negative control wells contained no inhibitor and were arbitrarily set as 100% enzyme activity.

NDM-1 Assays

NDM-1 was supplied as a gift from David Tierney, and the Fluorocillin Green substrate was purchased from ThermoFisher. The assay was performed in a Costar black 96-well plate. Each well contained a total volume of 100 μ L including buffer (50 mM HEPES, 2 mM CHAPS, 5 μ M Zn-SO₄, pH 7.0), NDM-1 (100 pM), inhibitor (200 μ M), and fluorocillin green substrate (87 nM). The enzyme and inhibitor were initially incubated together for 20 min at room temperature, after which the reaction was initiated by substrate addition. The change in fluorescence was monitored for 20 min with excitation at 485 nm and reading emission at 528

nm. The negative control wells contained no inhibitor and were arbitrarily set as 100% enzyme activity. IC_{50} values were determined by incubating various concentrations of inhibitor with the enzyme using the aforementioned conditions, and dose response curves were generated, fitted, and analyzed using GraphPad Prism graphing software using four-variable response parameters.

PA_N Assays

PA_N was prepared as previously reported,³¹ and the fluorescent ssDNA-oligo substrate was purchased from Sigma-Aldrich. The assay was performed in a Costar black 96-well plate. Each well contained a total volume of 100 μ L including buffer (20 mM Tris, 150 mM NaCl, 2 mM MnCl₂, 2 mM MgCl₂, 10 mM β -mercaptoethanol, 0.2% Triton-X100, pH 8.0), PA_N (25 nM), inhibitor (200 μ M), and fluorescent ssDNA-oligo substrate (200 nM). A single-stranded, 17-mer DNA substrate labeled with a 5'-FAM fluorophore and a 3'-TAMRA quencher ([6-FAM]AATCGCAGGCAGCACTC[TAM]) was synthesized by Sigma-Aldrich and was used to measure PA_N cleavage. There was no pre-incubation period, and the reaction was initiated by substrate addition. The change in fluorescence was monitored for 45 min at 37 °C with excitation at 485 nm and reading emission at 528 nm. The negative control wells contained no inhibitor and were arbitrarily set as 100% enzyme activity.

2.3 Results and Discussion

Library Development

The HOPTO library was synthesized as detailed in the SI. Particular focus was placed on the inclusion of heteroatoms as a means of fine-tuning the HOPTO ring electronics, as seen in **2.14**, as well as the use of bicyclic systems to introduce more lipophilicity and directionality

(Figure 2.2). In particular, **2.6 – 2.8** can be considered as ‘naphthyl’ isosteres of 1,2-HOPTO and as a group are designed to evaluate the effect of moving the steric bulk of an additional phenyl ring around the 1,2-HOPTO core. Likewise, **2.15** and **2.16** are also bicyclic analogues of 2,3-HOPTO, and **2.18** presents the bicyclic version of 3,4-HOPTO. Compound **2.9** is a deazapurine analogue of 1,2-HOPTO that was designed to have improved water solubility; however, as **2.9** has a potential alternate metal binding site, **2.10** and **2.11** were prepared as probes of this secondary metal-binding functionality. Furthermore, as **2.2**, **2.4**, and **2.5** are also designed to contain a secondary metal-binding site, **2.3** was included as a control for this second metal-binding site. Finally **2.20** and **2.21** are included as analogues of the HOPTO scaffold itself with no heteroatom and an oxygen heteroatom, respectively.

Elaborated HOPTO Derivatives

Derivatives of select HOPTO isosteres were prepared as described in Section 2.5. Compounds **2.2**, **2.4**, **2.6**, **2.9**, and **2.19** were selected as representative scaffolds for derivatization as the fragment growth protocols applied to these molecules are easily extrapolated to other members of the HOPTO library. Derivatization focused on fragment growth methods commonly seen in fragment-based drug discovery (FBDD) strategies, with a particular emphasis was placed on techniques such as metal catalyzed cross couplings (**2.23 – 2.26**, **2.30 – 2.34**), sulfonamide couplings (**2.27 – 2.29**), as well as nucleophilic substitution (**2.35 – 2.37**). The ability to elaborate these HOPTO isosteres through such varied synthetic methodologies demonstrates that this library is more than just novel MBP fragments, but contains structures that readily have the capacity to be developed into lead molecules. Routes to

prepare such derivatives will facilitate future medicinal chemistry efforts based on these HOPTO scaffolds, as described in Chapters 3 and 4.

Pharmacokinetics

In terms of assessing the druglike potential of a molecule, Lipinski's Rule-of-Five has long been the standard guideline for determining oral bioavailability,³⁴ along with addendums by Veber³⁵ and Clark.³⁶ Briefly, some of the more pertinent values include ClogP as a measure of lipophilicity, ClogD a pH sensitive measure of lipophilicity that takes into account ionization states, ClogS accounts for aqueous solubility (note that ClogD and ClogS are typically reported at or near physiological pH 7.4), rotatable bonds affect molecular flexibility, and (topological) polar surface (PSA or TPSA) area impacts the potential for membrane permeability.³⁴⁻³⁶ As fragments typically have overall less molecular weight than fully elaborated lead molecules, it has been suggested that fragments require a more scaled-down approach than the Rule-of-Five, and that a "Rule-of-Three" is more amenable in assessing fragment-based leads for drug discovery.³⁷ A summary of the idealized values of these PK constraints for both fragments and elaborated leads is shown in Table 2.1, with a comparison of how they apply to each member of the HOPTO library. In particular, PSA, ClogP, ClogD, and ClogS were chosen as the primary criteria to evaluate the druglikeness of the HOPTO library as the other considerations of molecular weight, number of hydrogen bond donors and acceptors, and rotatable bonds are readily met.

Pharmacokinetic (PK) values were calculated using available software from ChemAxon, following the precedent by Lassalas et al.³⁸ Briefly, the PSA ranges from 55.56 to 110.11 Å², with ClogP ranging from -0.52 to 2.54, CLogD_{7.0} from -2.44 to 2.41, and ClogS_{7.0} from -3.72 to

0.03, so that there is a 3 – 5 log difference between the calculated log values (Table 2.1). It is worth noting that these calculated values are well within the acceptable parameters for the Rule-of-Three. Moreover, the fact that these compounds cover a 3 – 5 log range is highly encouraging from a drug discovery perspective, as this breadth of values is indicative of tunability in terms of PK properties, a necessary feature for drug development. In terms of the PSA, the library is well tolerated by the Rule-of-Five, but is technically slightly high by the Rule-of-Three for fragments. This polarity is a necessary feature for metal binding as Lewis bases are required to engage in meaningful interactions with metal cations. The higher PSA is not particularly concerning, as a general profile to avoid drug toxicity is a PSA greater than 75 \AA^2 coupled with a logP less than 3,³⁹ which are values well matched by the HOPTO MBIs.

In order to corroborate the calculated PK values with actual experimental data, the logP and logD_{7.4} were experimentally determined for **2.1**, **2.4**, **2.9**, and **2.14** as representative compounds. For **2.1** the logP = 0.51 ± 0.01 and logD_{7.4} = -1.86; for **2.4** the logP = 0.49 ± 0.02 and logD_{7.4} = -1.78; for **2.9** the logP = 0.37 ± 0.03 and logD_{7.4} = -2.00; and for **2.14** the logP = -1.02 ± 0.18 and logD_{7.4} = -1.15. The measured logD_{7.4} values are not identical to the predicted calculated values; however, this is not atypical as cyclic, acidic moieties have been previously reported to have similar discrepancies between computational and experimental logD values.³⁸ Furthermore, the experimentally determined logD_{7.4} for **2.1**, **2.4**, **2.9**, and **2.14** were much lower than the ClogD_{7.0}, indicating that these HOPTOs are likely to be more water soluble than predicted; a property that bodes well for the druglikeness of these HOPTO based compounds. In short, the HOPTO library is tolerated by the canonical Rule-of-Three used to evaluate fragments for lead development, which is an excellent indicator for the potential of the HOPTO scaffold as a lead in inhibitor development against metalloenzymes.

Table 2.1. Summary of the properties used to assess the druglikeness of small molecules, as applied to both fully elaborated leads and fragments. The calculated PK values for each member of the HOPTO library is displayed below.

Compound	PSA (Å ²)	ClogP	ClogD _{7.0}	ClogS _{7.0}	H-Bond Donors	H-Bond Acceptors	Rotatable Bonds
Rule-of-Five	≤140 Å ²	≤5	≤5	≤-4	≤5	≤10	≤5
Rule-of-Three	≤ 60 Å ²	≤3	≤3	≤-4	≤3	≤3	≤3
2.1	55.56	0.91	0.90	-1.33	1	2	0
2.2	92.86	0.42	-2.44	0.49	2	4	1
2.3	81.42	0.63	-2.20	0.00	2	3	1
2.4	110.11	-0.38	-0.70	-1.24	2	4	2
2.5	110.11	-0.52	-0.32	-1.80	2	4	2
2.6	55.56	2.26	2.21	-3.29	1	2	0
2.7	55.56	0.99	1.06	-3.26	1	2	0
2.8	55.56	1.94	2.12	-3.18	1	2	0
2.9	84.24	0.13	0.33	-1.84	2	3	0
2.10	72.80	0.34	0.38	-2.85	2	2	0
2.11	57.01	1.40	1.36	-2.30	1	2	0
2.12	55.56	1.29	0.88	-1.11	1	2	0
2.13	64.35	1.04	0.66	-1.92	2	2	0
2.14	76.71	1.20	0.31	-1.15	2	3	0
2.15	64.35	2.54	2.22	-3.72	2	2	0
2.16	76.71	2.48	0.45	-0.78	2	3	0
2.17	55.56	1.73	1.50	-0.75	1	2	0
2.18	55.56	2.42	2.63	-2.55	1	2	0
2.19	81.42	1.82	1.07	-3.01	2	3	1
2.20	59.03	1.85	0.86	-0.56	1	1	0
2.21	61.55	1.63	1.23	-1.33	1	2	0
2.22	61.55	2.40	2.31	-3.15	1	2	0

Model Complexes

Zinc hydrotris(3,5-phenylmethylpyrazolyl)borate [(Tp^{Ph,Me})Zn(MBI)] complexes were prepared of **2.4**, **2.9**, and **2.14**; these complexes were crystallized and their structure determined by single-crystal X-ray diffraction (Figure 2.4). These compounds were selected as representative models of the HOPTO library and all demonstrate that the typical HOPTO binding

motif (as exemplified by 1,2-HOPTO, Figure 2.1) is conserved even after significant electronic and structural changes have been introduced to the HOPTO ring. These complexes maintain the binding pose of equatorial thione and axial oxygen with no perturbations to the surrounding ligand environment of the TP complex. This HOPTO binding is consistent with the 1,2-HOPTO, 2,3-HOPTO, and 3,4-HOPTO previously reported.^{9, 40} The only discernable difference is that the ligands show different canted angles where the HOPTO ligand is tilted further forward or back compared to 1,2-HOPTO, but this effect could very well be artifacts of crystal packing. These $[(\text{Tp}^{\text{Ph,Me}})\text{Zn}(\text{MBI})]$ model complexes demonstrate that the HOPTO isosteres maintain the same metal binding mode as the parent HOPTO scaffolds, regardless of how the electronics and substituents are modified.

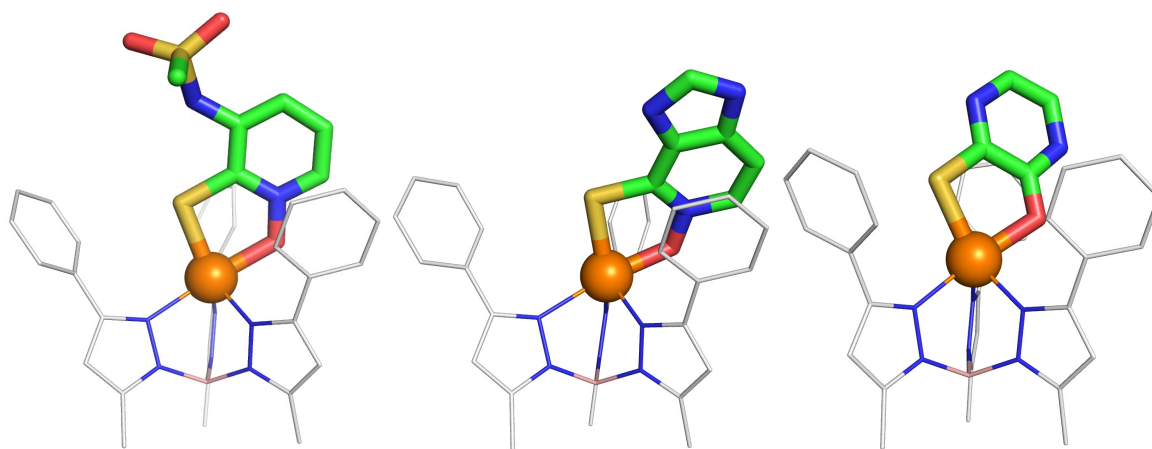


Figure 2.4. The $[(\text{Tp}^{\text{Ph,Me}})\text{Zn}(\text{MBI})]$ complexes of compounds **2.4**, **2.9**, and **2.14**.

Metalloenzyme Assays

The activity of each metalloenzyme was monitored via kinetic assays that measured either an increase in fluorescence or absorbance upon substrate hydrolysis (see section 2.3 for details). All compounds were incubated with each metalloenzyme at a fragment concentration of

200 μM , with the percent inhibition of each fragment displayed in Table 2.2. The results of these activity screens shows widely varying SAR preferences for each individual metalloenzyme, even though the same core ligand donor atoms are maintained across all of the MBIs.

Table 2.2. Percent inhibition at 200 μM of the HOPTO isostere library against various metalloenzymes. Percent inhibition is colored as a heat map with compounds that have no activity in yellow, and gradually moves towards compounds displaying complete inhibition in red (see section 2.3 for assay details).

Compound	MMP-12	hCAII	NDM-1	PA _N
2.1	11	13	69	43
2.2	40	0	77	70
2.3	34	0	0	10
2.4	99	3	100	73
2.5	94	10	96	93
2.6	98	88	100	33
2.7	13	41	5	98
2.8	23	29	8	44
2.9	28	9	93	42
2.10	56	5	0	16
2.11	96	9	100	30
2.12	53	4	40	40
2.13	40	10	83	40
2.14	42	0	12	41
2.15	44	23	54	24
2.16	50	24	41	3
2.17	94	11	98	0
2.18	44	0	38	37
2.19	53	2	63	32
2.20	14	22	19	0
2.21	66	19	93	100
2.22	35	47	79	90

Both MMP-12 and hCAII have similar active sites that rely on a tris(histidine) coordinated Zn²⁺ ion for catalytic activity, yet hCAII displays far fewer hits with only **2.6** having relevant inhibition against hCAII (.

Table 2.2), whereas **2.4**, **2.5**, **2.6**, **2.11**, and **2.17** all display 94% or better inhibition against MMP-12. A likely reason for the selectivity observed in hCAII, as previously detailed in work by Martin,⁴¹ is that the protein active site environment can impart a great deal of control on what ligands are able to effectively access the Zn²⁺ ion within the active site. The hCAII active site is fairly sterically and electrostatically constricted with both hydrophobic and hydrophilic regions, and therefore only allows a select number of ligands to bind efficiently. Conversely, the active site of MMP-12 is relatively more open and therefore allows more ligands to bind.

Additionally, it is interesting that **2.4** and **2.5** displayed strong inhibition against MMP-12 and not against hCAII. As terminal sulfonamide MBP warheads have been a privileged scaffold for hCAII inhibition,⁴² it is surprising that **2.4** and **2.5** show no activity against hCAII. This lack of activity can likely be attributed to the terminal -CH₃ sterically blocking the amide from engaging in metal-binding. As for MMP-12, it makes sense that **2.4** and **2.5** displayed some of the strongest inhibition against this metalloenzyme, as sulfonamide groups have long been successfully used as peptidomimetic linkers in designing MMP inhibitors.⁴³⁻⁴⁴ It is likely that the sulfonamide groups in **2.4** and **2.5** are fulfilling some similar role as a linking group instead of participating in metal-binding interactions against MMP-12.

While most reported metallo- β -lactamases (MBLs) all have similar active site coordination geometry, NDM-1 was selected as a representative MBL as it is the most prevalently occurring worldwide,⁴⁵ and is currently an important target due to its relevance in causing antibiotic resistance.⁴⁶ The NDM-1 active site is dinuclear Zn²⁺ with Zn₁ coordinated by a tris-His group in tetrahedral geometry, and Zn₂ coordinated by Cys, Asp, and His in a distorted tetrahedral geometry.⁴⁷ A catalytic water sits coordinated μ between the two Zn²⁺ ions, and is

used as the nucleophile to hydrolyze β -lactam bonds during NDM-1 activity.⁴⁷ During inhibition assays, as the Zn_2 site is relatively less tightly bound with a K_d value of 2 μM ,⁴⁸ excess Zn^{2+} was supplied at a concentration of 5 μM to ensure the Zn_2 site was fully occupied. In addition, the presence of excess metal in the assay buffer prevents metal stripping by the HOPTO ligands, which may be an issue at the relatively high concentrations of fragment utilized in these early screens. While it is possible to make the argument that including excess Zn^{2+} in the assay buffer would only result in titrating away the ligand due to formation of the $Zn(HOPTO)_2$ complex, this is not a concern as this homoleptic complex would still be able to dissociate and allow for ligand binding at the enzyme active site to occur. In turn, such event would indicate that the HOPTO ligand has a preference for the metal in the active site over the free metal in solution, again highlighting the selectivity dictated by active site environment argument.

From the inhibitor screen at 200 μM , **2.4**, **2.5**, **2.6**, **2.9**, **2.11**, **2.17**, and **2.21** all performed well against NDM-1, with greater than 90% inhibition. All of the compounds that may have additional donor atoms (**2.2**, **2.4**, **2.5**, and **2.9**) for binding both metal centers were among the most active NDM-1 inhibitors. It is possible that these compounds are binding both of the active site Zn^{2+} ions, thereby generating increased inhibitory activity. Without structural data, it is difficult to predict if both of the Zn^{2+} ions are coordinated by these HOPTO ligands, but it is reasonable to assume that these ligands are bound to one metal ion and likely bridging between the two Zn^{2+} ions.

Additionally, IC_{50} values for **2.4**, **2.5**, **2.6**, and **2.9** were found to be 35.2, 101, 40.3, and 42.8 μM respectively against NDM-1 (Figure 2.5), again highlighting the strong affinity and good activity of these ligands. It is encouraging that many members of the HOPTO library performed this well against NDM-1, even when challenged with excess Zn^{2+} , indicating that

these HOPTO fragments have great potential to be used in inhibitor discovery campaigns against MBLs such as NDM-1. In particular, **2.9** stands out as a lead fragment for further development as it was the most selective for NDM-1 over MMP-12 and hCAII.

PA_N was used as a compliment to NDM-1 as it is also a dinuclear metalloenzyme but relies on active site Mn²⁺ for catalysis, providing a control for a hard Lewis acid metal in comparison to the softer Zn²⁺. The PA_N active site consists of Mn₁ bound by Glu, Asp, and four waters in an octahedral geometry, and Mn₂ bound by His, Asp, Glu, two waters, and the carbonyl backbone of an Ile in a distorted octahedral geometry (Figure 2.3).⁴⁹ As the Mn₁ is relatively more labile, the influenza endonuclease assay also contained excess Mn²⁺ (and Mg²⁺), to be consistent with previous reports of PA_N activity assays and for similar reasons as described in the NDM-1 assay.³¹ However, the effect of excess Mn²⁺ metal ions on the overall inhibitory activity of metal binding inhibitors has been found to be insignificant so long as the total concentration of metal ions is above the *K_d* of the more labile metal binding site.⁵⁰ Overall **2.5**, **2.7**, **2.21**, and **2.22** had the best activity against endonuclease with greater than 90% inhibition. It is expected that fewer compounds emerged as hits against PA_N than NDM-1 due to hard-soft Lewis acid base theory. Furthermore, it is also interesting to note that the two naphthyl HOPTO isosteres, **2.6** and **2.7**, showed widely varying activity that was contrary to that observed with the other three metalloenzymes studied here.

Finally, it is worth noting that control compound **2.20** showed little to no activity against any of the metalloenzymes tested. As **2.20** still has the same *O,S* donor atoms and therefore the same binding motif, the lack of activity in **2.20** is indicative of the importance of the nitrogen heteroatom in the HOPTO MBP. As stated previously, the nitrogen heteroatom promotes the thione hybridization, so that the HOPTO ligand exists as a monoanionic species, thereby

facilitating metal binding under physiological conditions. In short, the HOPTO scaffold is well suited and useful pharmacophore for designing inhibitors against metalloenzymes.

2.4 Conclusions

The goal of this work was to enhance the druglikeness of the HOPTO MBP, and make it a more appealing scaffold for future medicinal chemistry efforts. This was accomplished through the incorporation of isosteres and N-heteroatom replacement to attain different scaffolds within the realm of the HOPTO MBP. As such, this library of HOPTO isosteres demonstrate that the HOPTO scaffold is electronically tunable, and can access a wide range of PK properties without sacrificing metal-binding capacity. Moreover, these HOPTO fragments display strong inhibition activity, and despite containing the same ligand donor atoms, they have remarkable selectivity between different metalloenzymes. These results once again highlight the validity of a metal-centric approach and demonstrate, even at the fragment level, small modifications to the SAR of the MBP can have drastic effects on metalloenzyme inhibition. In all, this work should help to expand the utility of metal binding inhibitor scaffolds such as HOPTOs and eventually lead to new avenues of therapeutics against metalloenzymes, as demonstrated in Chapters 3 and 4.

2.5 Experimental

Synthesis of HOPTO and HOPTO isosteres

Unless otherwise noted, all reagents and solvents were purchased from commercial suppliers and used with no additional purification. Microwave reactions were performed using a CEM Discover series S-class microwave reactor in pressure-sealed vessels. Silica gel column

chromatography was performed using a CombiFlash Rf⁺ Teledyne ISCO system, using hexane, ethyl acetate, CH₂Cl₂ or MeOH as eluents. Reverse phase separations utilized a C18-column on the same instrument with a 0.1% formic acid in water and MeOH as eluents. Separations were monitored via a Teledyne ISCO Rf⁺ PurIon ESI-MS detector with 1 Da resolution. ¹H NMR spectra were obtained using Varian 400 MHz spectrometers at the Department of Chemistry and Biochemistry at UC San Diego. ¹H NMR data is reported in parts per million relative to the residual non-deuterated solvent signals, and spin multiplicities are given as s (singlet), *br s* (broad singlet), d (doublet), dd (doublet of doublets), t (triplet), dt (doublet of triplets), q (quartet), and m (multiplet). When available, coupling constants (J) are reported in hertz (Hz). The purity of compounds **2.1** – **2.37** was determined to be at least 90% by ¹H NMR analysis. Standard resolution mass spectrometry was performed at either the UC San Diego Molecular Mass Spectrometry Facility or on the previously described Teledyne ISCO Rf⁺ PurIon ESI-MS detector. Compounds **2.1**, **2.3**, and **2.20** were purchased from commercial suppliers. Compound **2.2** was prepared by Dr. Cy Credille, whereas compound **2.11** was prepared by Dr. Yuyoung Ma. Compounds **2.12**, **2.13**, **2.17**, and **2.21** were prepared as previously reported.⁷

General Oxidation Protocol A: Oxidation with mCPBA. The starting material was dissolved in 10 mL of a 1:1 CH₂Cl₂/MeOH solution, and cooled to 0 °C. Three equiv of mCPBA was dissolved in an 10 mL of a 1:1 CH₂Cl₂/MeOH, and the mCPBA solution was added dropwise to the solution containing the starting material. The reaction mixture was placed under nitrogen atmosphere and was allowed to slowly warm to room temperature, after which the mixture was stirred for 24 h. The reaction mixture was concentrated under reduced pressure and the resulting residue was purified by column chromatography, using a gradient of 100% hexanes to 100% ethyl acetate, and then from 100% CH₂Cl₂ to 15% MeOH in CH₂Cl₂. The desired products elute

in 0-10% MeOH in CH₂Cl₂. Fractions containing the desired product were concentrated under reduced pressure to obtain the desired products.

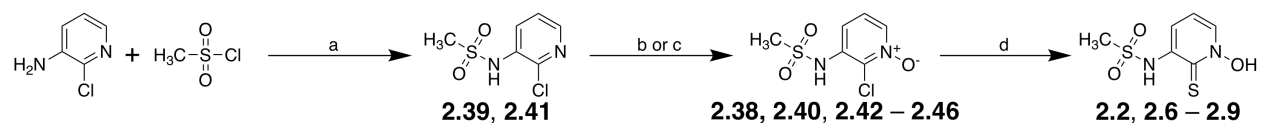
General Oxidation Protocol B: Oxidation with H₂O₂ and TFA. The starting material was dissolved in 60 mL TFA and add 20 mL of 30% H₂O₂, being careful to maintain a 3:1 ratio of TFA to H₂O₂. The reaction mixture was heated at 80 °C for 3 h, and then the reaction mixture was concentrated under reduced pressure. The resulting residue was purified by column chromatography, using a gradient of 100% CH₂Cl₂ to 20% MeOH in CH₂Cl₂. The desired products elute in 10-15 % MeOH in CH₂Cl₂. Fractions containing the desired product were concentrated under reduced pressure to obtain the desired products.

General Thionation Protocol: The starting material was dissolved in 5 mL DI water with a minimal amount of MeOH to dissolve as needed. Then 5 mL of saturated sodium hydrogen sulfide solution (excess) was added to the solution containing the starting material. The reaction mixture was allowed to react at 0-100 °C for 1-16 h. Then the reaction mixture was slowly quenched with 6 M HCl. After waiting approximately 5 min to allow the resultant H₂S gas to evolve and disperse, the resulting solids were collected via vacuum filtration and washed with a small amount of DI water. The crude solid was then purified by column chromatography, using a gradient of 100% hexanes to 100% ethyl acetate. When necessary, reverse phase chromatography was also used, using a gradient of 100% water to 100% MeOH. Fractions containing the desired product were concentrated under reduced pressure to obtain the desired products.

General Thionation Protocol B: The starting material and 3 equivalents of KI were dissolved in 5 mL DI water with a minimal amount of MeOH to dissolve as needed. Then 5 mL of saturated sodium hydrogen sulfide solution (excess) was added to the solution containing the starting material, and the reaction mixture was heated to reflux at 100 °C for 8 h. Then the reaction mixture was cooled to room temperature, and then submerged in an ice bath. Then the reaction mixture was slowly quenched with 6 M HCl. After waiting approximately 5 min to allow the resultant H₂S gas to evolve and disperse, the resulting solids were extracted into organic using 3×20 mL ethyl acetate. The organic layers were combined, washed with brine, and concentrated under reduced pressure. The resulting residue was purified by reverse phase column chromatography, using a gradient of 100% water to 100% MeOH. Fractions containing the desired product were concentrated under reduced pressure to obtain the desired products.

General Sulfonamide Coupling Protocol: Unless otherwise noted, the following sulfonamide coupling procedure was used. Using a 5 mL microwave vessel with stir bar, 2-chloropyridin-3-amine (0.200g, 1.56 mmol) was dissolved in 2 mL dry pyridine. Then sulfonyl chloride (2.33 mmol) was added and the reaction mixture was heated in the microwave reactor at 130°C for 3 min at power 300. After cooling to room temperature, the reaction mixture was poured into 12 mL ice water, and extracted using 3×10 mL CH₂Cl₂. The combined organic layers were washed with 15 mL 1 M HCl and dried over magnesium sulfate. The solids were filtered off and discarded, and the filtrate was concentrated under reduced pressure. The resulting crude oil was then purified by column chromatography, using a gradient of 100% hexanes to 100% ethyl acetate. The desired products elute in 30-70% ethyl acetate in hexanes. Fractions containing the desired product were concentrated under reduced pressure to obtain the desired products.

General cross-coupling procedure: Unless otherwise noted, the following sulfonamide coupling procedure was used. The starting material, 0.1 equiv of S-Phos, and 1.1 equiv of the appropriate boronic acid were dissolved in 2 mL 1,4-dioxane. Then 3 equiv of tribasic potassium phosphate was dissolved in 0.5 mL water, and the aqueous was added to the solution containing the starting material. The reaction mixture was degassed under vacuum for 10 min, after which 0.07 mol percent PdCl₂(dppf) was added. The reaction mixture was heated at 100 °C for 1 h and was then hot filtered over a thin layer of celite and rinsed with a 1:1 solution of CH₂Cl₂ and MeOH. The filtrate was concentrated under reduced pressure and the resulting residue was purified by column chromatography, using a gradient of 100% hexanes to 100% ethyl acetate. Fractions containing the desired product were concentrated under reduced pressure to obtain the desired products.



Scheme 2.1. General synthetic method to preparing 1,2-HOPTO based compounds **2.2** and **2.4 – 2.9**, using **2.4** as a general example. Reagents and conditions: (a) 2-chloropyridin-3-amine, methyl sulfonyl chloride, pyridine, microwave irradiation, 130 °C, 15 min, 42 – 62%; (b) mCPBA, 1:1 CH₂Cl₂ to MeOH, 25 °C, 24 h, 21 – 44%; (c) TFA, H₂O₂, 45 °C, 60 h, 42%; (d) NaSH, KI, H₂O, 25 – 80 °C, 27 – 82%.

2-Bromo-3-carboxypyridine-1-oxide (2.38): 2-Bromonicotinic acid (1.0 g, 4.95 mmol) was dissolved in 25 mL TFA and stirred. Hydrogen peroxide solution (37%, 10.11 mL, 99 mmol) was added and the mixture was heated to 45 °C for 60 h. The solvent was then removed under vacuum and the residue was co-evaporated with methanol several times to remove residual TFA.

The resultant solids were taken up in methanol, sonicated briefly, and isolated by filtration to yield crude **2.38** (0.45 g, 2.10 mmol, 42%) as a reddish-brown solid which was taken forward with no further purification. $^1\text{H NMR}$ (400 MHz, $\text{DMSO-}d_6$) δ : 8.54 (dd, $J = 6.4, 1.5$ Hz, 1H), 7.54 (dd, $J = 7.8, 1.5$ Hz, 1H), 7.50 – 7.45 (m, 1H); ESI-MS(-): m/z 218.24 $[\text{M} - \text{H}]^-$.

1-Hydroxy-2-thioxo-1,2-dihydropyridine-3-carboxylic acid (2.2): 2.38 (0.30 g, 1.38 mmol) was taken up in a 1:1 mixture of water and saturated NaSH solution (20 mL total volume) and was stirred at room temperature for 2 h. The solution was then carefully acidified with 4 M HCl, and the resultant H_2S gas was allowed to effervesce with stirring in a fume hood. After 30 minutes of stirring, the cloudy mixture was extracted three times with 30 mL portions of ethyl acetate. The combined organic fractions were dried and concentrated, and the residue purified by silica chromatography eluting in 5% methanol in CH_2Cl_2 to afford **2.2** (0.92 g, 0.55 mmol, 40%) as a yellow solid. $^1\text{H NMR}$ (400 MHz, $\text{DMSO-}d_6$) δ : 8.69 (dd, $J = 6.6, 1.2$ Hz, 1H), 8.12 (d, $J = 7.5$ Hz, 1H), 7.04 (d, $J = 6.6$ Hz, 1H); ESI-MS(+): m/z 170.38 $[\text{M} - \text{H}]^-$.

N-(2-chloropyridin-3-yl)methanesulfonamide (2.39): Using the following modified version of the general sulfonamide cross-coupling procedure, 2-chloropyridin-3-amine (0.50 g, 3.89 mmol) was dissolved in 2 mL dry pyridine with methanesulfonyl chloride (0.45 mL, 5.83 mmol) in the microwave reactor at 130 °C for 6 min to obtain **2.39** (0.34 g, 1.64 mmol, 42%) as a yellow oil. $^1\text{HNMR}$ (400 MHz, $\text{DMSO-}d_6$) δ : 9.74 (*br s*, 1H), 8.26 (d, $J = 6.0$ Hz, 1H), 7.87 (d, $J = 8.0$ Hz, 1H), 7.46 – 7.43 (m, 1H), 3.11 (s, 3H); ESI-MS(+): m/z 207 $[\text{M} + \text{H}]^+$.

2-Chloro-3-(methylsulfonamido)pyridine 1-oxide (2.40): Following general oxidation protocol A, **2.39** (0.34 g, 1.64 mmol) and mCPBA (0.85 g, 4.92 mmol) were dissolved in 10 mL chloroform and allowed to react at 0-25 °C for 24 h to obtain **2.40** (0.13 g, 0.59 mmol, 34%) as a slightly impure tan solid. ¹HNMR (400 MHz, DMSO-*d*₆) δ: 9.96 (s, 1H), (dd, *J*₁ = 6.4 Hz, *J*₂ = 1.2 Hz, 1H), 7.44-7.36 (m, 2H), 3.15 (s, 3H); ESI-MS(+): *m/z* 223 [M + H]⁺.

N-(1-hydroxy-2-thioxo-1,2-dihydropyridin-3-yl)methanesulfonamide (2.4): Using the following modified general thionation protocol B, from **2.40** (0.10 g, 0.45 mmol) with KI (0.075 g, 0.45 mmol), **2.4** (0.085 g, 0.38 mmol, 86%) was obtained as a very pale yellow crystalline solid. ¹HNMR (400 MHz, DMSO-*d*₆) δ: 8.93 (*br s*, 1H), 8.22 (dd, *J*₁ = 6.8 Hz, *J*₂ = 1.2 Hz, 1H), 7.51 (dd, *J*₁ = 7.6 Hz, *J*₂ = 1.2 Hz, 1H), 6.90 (t, *J* = 6.8 Hz, 1H), 3.17 (s, 3H); ESI-MS(-): *m/z* 219.14 [M - H]⁻.

N-(6-bromopyridin-2-yl)methanesulfonamide (2.41): Following the general sulfonamide cross-coupling procedure, 6-bromopyridin-2-amine (0.50 g, 2.89 mmol) was dissolved in 2 mL dry pyridine with methanesulfonyl chloride (0.45 mL, 5.78 mmol) in the microwave reactor at 130 °C for 6 min to obtain **2.41** (0.49 g, 2.89 mmol, 68%) as a yellow oil that solidified upon standing. ¹HNMR (400 MHz, DMSO-*d*₆) δ: 10.91 (*br s*, 1H), 7.66 (t, *J* = 7.6 Hz, 1H), 7.27 (d, *J* = 7.6 Hz, 1H), 6.97 (d, *J* = 8.0 Hz, 1H), 3.29 (s, 3H); ESI-MS(+): *m/z* 251 [M + H]⁺.

2-bromo-6-(methylsulfonamido)pyridine 1-oxide (2.42): Following general oxidation protocol A, from **2.41** (0.49 g, 1.99 mmol) in 15 mL of 1:1 CH₂Cl₂ and MeOH with mCPBA (1.96 g, 7.97 mmol) at 40 °C for 72 h, **2.42** (0.15 g, 0.54 mmol, 27%) was obtained as a white

solid. $^1\text{HNMR}$ (400 MHz, Acetone- d_6) δ : 7.98 (d, $J = 7.2$ Hz, 1H), 7.67 (d, $J = 8.8$ Hz, 1H), 7.56 (t, $J = 7.6$ Hz, 1H), 2.06 (s, 3H); ESI-MS(+): m/z 267 $[\text{M} + \text{H}]^+$.

N-(1-hydroxy-6-thioxo-1,6-dihydropyridin-2-yl)methanesulfonamide (2.5): Following general thionation protocol B, from **2.42** (0.07 g, 0.26 mmol) with KI (0.13 g, 0.79 mmol), **2.5** (0.016 g, 0.07 mmol, 27%) was obtained as an off-white waxy solid. $^1\text{HNMR}$ (400 MHz, Acetone- d_6) δ : 7.45 (t, $J = 8.4$ Hz, 1H), 7.32 (dd, $J_1 = 8.4$ Hz, $J_2 = 1.2$ Hz, 1H), 7.10 (dd, $J_1 = 8.0$ Hz, $J_2 = 1.2$ Hz, 1H), 3.38 (s, 3H); ESI-MS(+): m/z 223 $[\text{M} + \text{H}]^+$.

1-Chloroisoquinoline 2-oxide (2.43): Following general oxidation protocol B, from 1-chloroisoquinoline (0.85 g, 0.67 mmol), **2.43** (0.20 g, 1.09 mmol, 21%) was obtained. $^1\text{HNMR}$ (400 MHz, DMSO- d_6) δ : 8.36 (d, $J = 7.2$ Hz, 1H), 8.03 (d, $J = 8.0$ Hz, 2H), 7.96 (d, $J = 7.2$ Hz, 1H), 7.80 (t, $J = 8.0$ Hz, 1H), 7.70 (t, $J = 7.2$ Hz, 1H); ESI-MS(+): m/z 180.32 $[\text{M} + \text{H}]^+$, 202.11 $[\text{M} + \text{Na}]^+$.

2-Hydroxyisoquinoline-1(2H)-thione (2.6): Following general thionation protocol A, from **2.43** (0.15 g, 0.84 mmol) at 0 °C for 2 h, **2.6** (0.10 g, 0.58 mmol, 69%) was obtained as a light yellow solid. $^1\text{HNMR}$ (400 MHz, DMSO- d_6) δ : 12.09 (*br s*, 1H), 8.71 (d, $J = 8.4$ Hz, 1H), 8.21 (d, $J = 7.2$ Hz, 1H), 7.88 (d, $J = 8.0$ Hz, 1H), 7.79 (t, $J = 8.0$ Hz, 1H), 7.69 (t, $J = 7.2$ Hz, 1H), 7.30 (d, $J = 7.6$ Hz, 1H); ESI-MS(+): m/z 178.26 $[\text{M} + \text{H}]^+$.

3-Chloroisoquinoline 2-oxide (2.44): Following general oxidation protocol B, from 3-chloroisoquinoline (1.00 g, 0.67 mmol), **2.44** (0.36 g, 1.99 mmol, 33%) was obtained. $^1\text{HNMR}$

(400 MHz, DMSO- d_6) δ : 9.22 (s, 1H), 8.42 (s, 1H), 7.90-7.89 (m, 2H), 7.66-7.64 (m, 2H); ESI-MS(+): m/z 180.23 [M + H]⁺.

2-Hydroxyisoquinoline-3(2H)-thione (2.7): Following general thionation protocol B, from **2.44** (0.300 g, 1.67 mmol) with KI (0.83 g, 5.01 mmol) at 100 °C for 16 h, followed by additional purification by reverse chromatography and crystallization from CH₂Cl₂ and hexanes, **2.7** (0.011 g, 0.06 mmol, 4%) was obtained as a light tan solid. ¹HNMR (400 MHz, DMSO- d_6) δ : 9.28 (*br s*, 1H), 8.06 (d, J = 6.4 Hz, 1H), 7.93 (d, J = 7.6 Hz, 2H), 7.74 (t, J = 7.6 Hz, 1H), 7.66 – 7.53 (m, 2H); ESI-MS(+): m/z 177.25 [M]⁺.

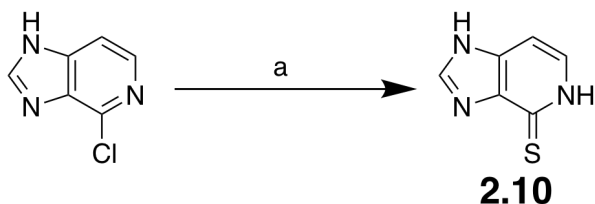
2-Chloroquinoline 1-oxide (2.45): Following general oxidation protocol B, from 2-chloroquinoline (1.0 g, 6.11 mmol), **2.45** (0.27 g, 1.50 mmol, 25%) was obtained. ¹HNMR (400 MHz, DMSO- d_6) δ : 8.32 (d, J = 8.8 Hz, 1H), 8.12 (d, J = 8.0 Hz, 1H), 7.95 (d, J = 8.8 Hz, 1H), 7.87 (t, J = 8.8 Hz, 1H), 7.81-7.74 (m, 2H); ESI-MS(+): m/z 180.25 [M + H]⁺.

1-Hydroxyquinoline-2(1H)-thione (2.8): Following general thionation protocol A, from **2.45** (0.27 g, 1.50 mmol) at 60 °C for 1.75 h, **2.8** (0.15 g, 0.83 mmol, 55%) was obtained as a light yellow solid. ¹HNMR (400 MHz, DMSO- d_6) δ : 12.14 (*br s*, 1H), 7.92-7.90 (m, 2H), 7.84-7.76 (m, 2H), 7.52-7.45 (m, 2H); ESI-MS(+): m/z 177 [M + H]⁺.

4-Chloro-1H-imidazo[4,5-c]pyridine 5-oxide (2.46): Following general oxidation protocol A, from 4-chloro-1H-imidazo[4,5-c]pyridine (0.50 g, 3.26 mmol), at 40 °C for 14 h, **2.46** (0.24 g,

1.42 mmol, 44%) was obtained as a white solid. $^1\text{H NMR}$ (400 MHz, $\text{DMSO-}d_6$) δ : 7.88 (s, 1H), 7.62-7.60 (m, 1H), 7.50-7.46 (m, 1H); ESI-MS(+): m/z 170.43 $[\text{M}+\text{H}]^+$.

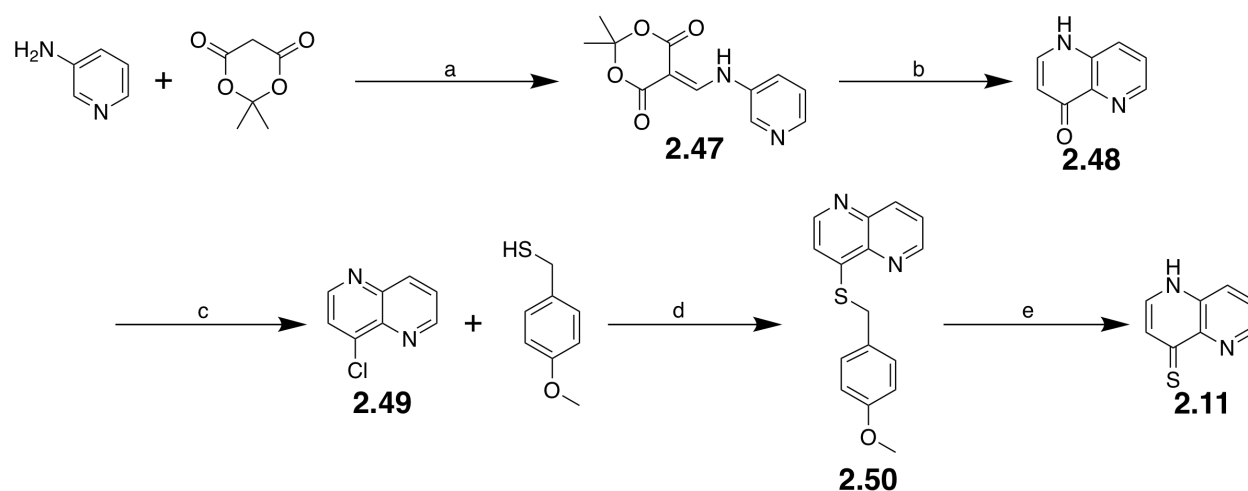
5-Hydroxy-1,5-dihydro-4H-imidazo[4,5-c]pyridine-4-thione (2.9): Following the general thionation protocol A, from **2.46** (0.24 g, 1.42 mmol) at room temperature for 2 h and purification by reverse phase chromatography running gradient from 100% water to 100% MeOH, **2.9** (0.13 g, 0.80 mmol, 57%) was obtained as a pale yellow solid. $^1\text{H NMR}$ (400 MHz, $\text{DMSO-}d_6$) δ : 8.31 (s, 1H), 8.10 (d, $J = 7.2$ Hz, 1H), 7.12 (d, $J = 7.2$ Hz, 1H); ESI-MS(-): m/z 166.30 $[\text{M}-\text{H}]^-$.



Scheme 2.2. Route to **2.10**. Reagents and conditions: (a) 4-chloro-1H-imidazo[4,5-c]pyridine, NaSH, 1:1 H_2O to MeOH, 60 $^\circ\text{C}$, 2.5 h, 33%.

1,5-Dihydro-4H-imidazo[4,5-c]pyridine-4-thione (2.10): Following a modified version of general thionation protocol A, 4-chloro-1H-imidazo[4,5-c]pyridine (0.24 g, 1.56 mmol) was suspended in 10 mL of a 1:1 solution of DI water and MeOH, and sonicated to dissolve. Then 5 mL of saturated sodium hydrogen sulfide solution was added to the solution containing the starting material. The reaction mixture was placed under nitrogen atmosphere and heated at 60 $^\circ\text{C}$ for 2.5 h. Then the reaction mixture was slowly quenched with 6 M HCl. After waiting approximately 5 min to allow the resultant H_2S gas to evolve and disperse, the solution was adjusted to pH 8 using NaOH. The reaction mixture was concentrated under reduced pressure.

The resulting crude solid was taken up in 50 mL of a 1:1 solution of CH₂Cl₂ and MeOH to preclude the salts, which were filtered off and discarded. The filtrate was concentrated under reduced pressure and the resulting residue was purified by reverse phase chromatography, using a gradient of 100% water to 100% MeOH. The desired product eluted in 20% MeOH in water. Fractions containing the desired product were concentrated under reduced pressure to obtain **2.10** (0.078 g, 0.52 mmol, 33%) as a white powdery solid. ¹HNMR (400 MHz, DMSO-*d*₆) δ: 8.47 (s, 1H), 7.48 (t, *J* = 6.0 Hz, 1H), 7.10 (d, *J* = 6.8 Hz, 1H); ESI-MS(+): *m/z* 152 [M + H]⁺.



Scheme 2.3. Route to **2.11**. Reagents and conditions: (a) pyridine-3-amine, methyl sulfonyl chloride, 2,2-dimethyl-1,3-dioxane-4,6-dione, triethyl orthoformate, 105 °C, 2 h, theoretical yield; (b) Dowtherm[®]A, 250 °C, 2.5 h, 75%; (c) POCl₃, toluene, 110 °C, 2 h, 41%; (d) (4-methoxyphenyl)methanethiol, NaH, DMF, 25 °C, 2 h, 69%; (e) *m*-cresol, TFA, 100 °C, 16 h, 94%.

2,2-Dimethyl-5-((pyridin-3-ylamino)methylene)-1,3-dioxane-4,6-dione (2.47): A mixture of pyridine-3-amine (1.88 g, 20 mmol) and 2,2-dimethyl-1,3-dioxane-4,6-dione (3.46 g, 24 mmol) was pre-heated to 90 °C, at which point triethyl orthoformate (20.0 mL, 120 mmol) was added. The reaction mixture was then heated at 105 °C for 2 h. The reaction was allowed to cool to room temperature, and the resulting solid was collected via vacuum filtration to obtain **2.47** (5.30

g, 21.36 mmol, excess yield) as a red solid, which was immediately used without any further purification. ¹HNMR (400 MHz, CDCl₃) δ: 11.25 (d, *J* = 12.0 Hz, 1H), 8.65 (s, 1H), 8.60 (s, 1H), 8.54 (d, *J* = 4.0, 1H), 7.61 (dd, *J*₁ = 8.0 Hz, *J*₂ = 4.0 Hz, 1H), 7.41 (dd, *J*₁ = 8.0 Hz, *J*₂ = 4.0 Hz, 1H), 1.77 (s, 6H); ESI-MS(+): *m/z* 248.90 [M + H]⁺, 270.82 [M + Na]⁺.

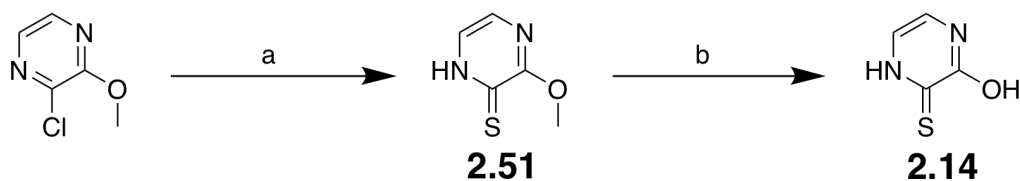
1,5-Naphthyridin-4(1H)-one (2.48): A solution of **2.47** (2.60 g, 2.4 mmol) in Dowtherm[®] A (150 mL) was placed in a pre-heated bath at 250 °C and stirred for 2.5 h. Then the reaction mixture was allowed to cool to room temperature to obtain **2.48** (1.14 g, 10.50 mmol, 75%) as a dark solid that was used in the next step without any further purification. ¹HNMR (400 MHz, (CD₃OD) δ: 9.07 (d, *J* = 4.0 Hz, 1H), 8.72 (d, *J* = 8.0 Hz, 1H), 8.61 (d, *J* = 8.0 Hz, 1H), 8.22 (dd, *J*₁ = 12.0 Hz, *J*₂ = 8.0 Hz, 1H), 7.07 (d, *J* = 8.0 Hz, 1H); ESI-MS(+): *m/z* 147.29 [M + H]⁺.

4-Chloro-1,5-naphthyridine (2.49): To a mixture of **2.48** (0.80 g, 5.57 mmol) in 20 mL toluene, POCl₃ (1.02 mL, 11.0 mmol) was added, and the reaction mixture was heated to reflux for 2 h. The reaction mixture was allowed to cool to room temperature, at which point a white precipitate formed. The white precipitate was collected via vacuum filtration to obtain **2.49** (0.365 g, 2.22 mmol, 41%) without any additional purification. ¹HNMR (400 MHz, CDCl₃) δ: 8.92 (d, *J* = 8.0, 1H), 8.69 (d, *J* = 4.0, 1H), 8.26 (d, *J* = 8.0, 1H), 7.60 (d, *J* = 4.0, 1H), 7.57 (dd, *J*₁ = 8.0, *J*₂ = 4.0, 1H); ESI-MS(+): *m/z* 165.28 [M + H]⁺.

4-((4-Methoxybenzyl)thio)-1,5-naphthyridine (2.50): To a solution of **2.49** (0.90 g, 5.50 mmol) and (4-methoxyphenyl)methanethiol (1.14 mL, 8.20 mmol) in 10 mL DMF at room temperature, NaH (0.40 g, 16.5 mmol) was added, and the reaction was allowed to stir at room

temperature for 2 h. Then the reaction was acidified with 1 M HCl to pH 7, diluted with water, and extracted into ethyl acetate. The combined organic layers were dried over Na₂SO₄, filtered, and concentrated under reduced pressure. The resulting crude was taken up in ethyl acetate, and filtered to remove solids. The filtrate was then purified by column chromatography, running gradient from 100% hexanes to 100% ethyl acetate to obtain **2.50** (1.07 g, 3.79 mmol, 69%) as a white solid. ¹HNMR (400 MHz, CDCl₃) δ: 8.91 (d, *J* = 4.0 Hz, 1H), 8.69 (d, *J* = 4.0 Hz, 1H), 8.33 (d, *J* = 8.0 Hz, 1H), 7.64 (dd, *J*₁ = 8.0 Hz, *J*₂ = 4.0 Hz, 1H), 7.40 (d, *J* = 8.0 Hz, 2H), 7.35 (d, *J* = 4.0 Hz, 1H), 6.87 (d, *J* = 8.0 Hz, 2H), 4.24 (s, 2H), 3.77 (s, 3H); ESI-MS(+): *m/z* 283.05 [M + H]⁺.

1,5-Naphthyridine-4(1*H*)-thione (2.11): To a solution of **2.50** (0.70 g, 2.48 mmol) in 20 mL TFA, *m*-cresol (1.3 mL, 12.41 mmol) was added, and the reaction mixture was heated to reflux for 16 h. Then the reaction was allowed to cool to room temperature, and was concentrated under reduced pressure. The crude was taken up in ethyl acetate, and neutralized with saturated sodium bicarbonate solution so that an orange-red precipitate formed. The resulting precipitate was collected via vacuum filtration and washed with acetone and DI water to obtain **2.11** (0.38 g, 2.33 mmol, 94%). ¹HNMR (400 MHz, DMSO-*d*₆) δ: 8.67 (d, *J* = 4.0 Hz, 1H), 8.03 (d, *J* = 8.0 Hz, 1H), 7.96 (d, *J* = 4.0 Hz, 1H), 7.46 (dd, *J*₁ = 8.0 Hz, *J*₂ = 4.0 Hz, 1H), 7.41 (d, *J* = 8.0 Hz, 1H); ESI-MS(+): *m/z* 163.23 [M + H]⁺.

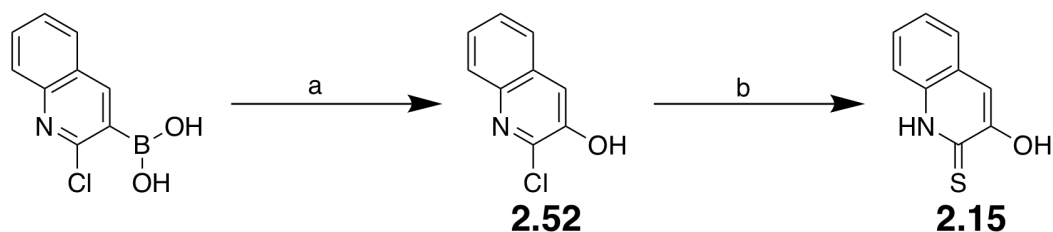


Scheme 2.4. Route to **2.14**. Reagents and conditions: (a) NaSH, KI, H₂O, 100 °C, 16 h, 52%; (b) HBr, acetic acid, MeOH, 100 °C, 16 h, 45%.

3-Methoxypyrazine-2(1H)-thione (2.51): Following a modified version of general thionation protocol B, 2-chloro-3-methoxypyrazine (1.00 g, 6.92 mmol) and KI (3.45 g, 20.8 mmol) were dissolved in 5 mL of a 1:1 solution of MeOH and water. Then 5 mL of saturated sodium hydrosulfide solution was dropwise to the solution containing the starting material. The reaction mixture was heated to reflux at 100 °C for 14 h. Then the reaction mixture was allowed to cool to room temperature and was placed in an ice bath. Then the reaction mixture was slowly quenched with 6 M HCl. After waiting approximately 5 min to allow the resultant H₂S gas to evolve and disperse, the resulting yellow precipitate was collected via vacuum filtration, washing with a small amount of DI water. The crude solid was further purified by column chromatography, using a gradient of 100% hexanes to 100% ethyl acetate. The desired product eluted over 50% ethyl acetate in hexanes to 100% ethyl acetate. Fractions containing the desired product were concentrated under reduced pressure to obtain **2.51** (0.51 g, 6.92 mmol, 52%) as a bright yellow solid. ¹HNMR (400 MHz, DMSO-*d*₆) δ: 7.35 (d, *J* = 3.6 Hz, 1H), 7.25 (d, *J* = 4.0 Hz, 1H), 3.84 (s, 3H); ESI-MS(+): *m/z* 143.11 [M+H]⁺.

3-Hydroxypyrazine-2(1H)-thione (2.14): To a solution of **2.51** (0.45 g, 3.17 mmol) in glacial acetic acid (5.0 mL, 87 mmol) with approximately 15 mL of MeOH, HBr (0.57 mL, 5.06 mmol) was added. The reaction mixture was placed under a nitrogen atmosphere and heated to reflux at 100°C for 16 h. Then the reaction mixture was allowed to cool to room temperature and was

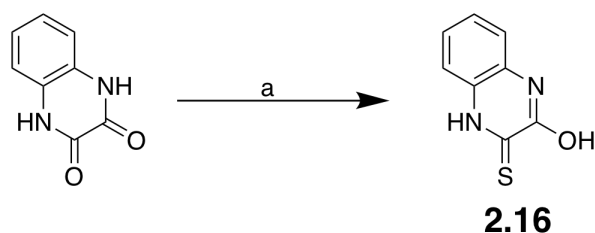
concentrated under reduced pressure. The resulting residue was purified by reverse phase column chromatography, using a gradient of 100% water to 100% MeOH. The desired product eluted in 100% water. Fractions containing the desired product were concentrated under reduced pressure to obtain **2.14** (0.18 g, 1.43 mmol, 45%) as a bright yellow solid. $^1\text{H NMR}$ (400 MHz, $\text{DMSO-}d_6$) δ : 11.49 (*br s*, 1H), 6.76 (d, $J = 5.2$ Hz, 1H), 6.44 (d, $J = 5.2$ Hz, 1H); ESI-MS(+): m/z 129.11 $[\text{M}+\text{H}]^+$, 151.00 $[\text{M}+\text{Na}]^+$.



Scheme 2.5. Route to **2.15**. Reagents and conditions: (a) H_2O_2 , NH_4Cl , ethanol, H_2O , 25 °C, 16 h, 74%; (b) NaSH , KI , H_2O , 100 °C, 14 h, 30%.

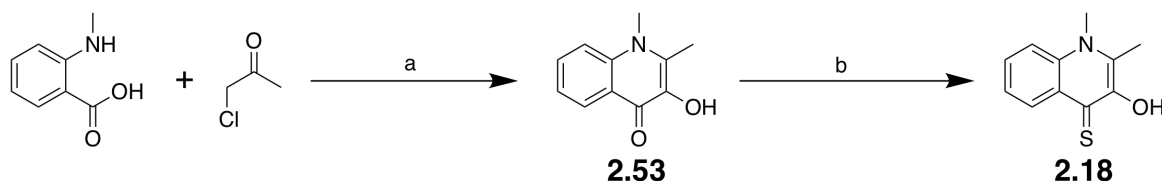
2-Chloroquinolin-3-ol (2.52): (2-chloroquinolin-3-yl)boronic acid (0.828 g, 3.99 mmol) was dissolved in 6 mL ethanol. Ammonium chloride (0.400 g, 7.39 mmol) was separately dissolved in 6 mL of DI water, and the aqueous solution was added dropwise to the solution to the starting material. Then 50% H_2O_2 (2.1 mL, 33.5 mmol) was added dropwise to the solution containing the starting material. The reaction was allowed to stir at room temperature for 16 h, after which a white precipitate formed. The resulting white precipitate was collected via vacuum filtration and rinsed with a small amount of cold 1:1 EtOH/water to obtain **2.52** (0.53 g, 2.93 mmol, 74%) as a white solid. $^1\text{H NMR}$ (400 MHz, $(\text{CD}_3)_2\text{SO}$): 11.09 (*br s*, 1H), 7.83 (t, $J = 8.0$ Hz, 2H), 7.66 (s, 1H), 7.57-7.50 (m, 4H); ESI-MS(+): m/z 180.20 $[\text{M}+\text{H}]^+$.

3-Hydroxyquinoline-2(1H)-thione (2.15): Following a modified version of thionation protocol B, **2.52** (0.40 g, 2.23 mmol) and KI (1.11 g, 6.68 mmol) were dissolved in 5 mL of a 1:1 solution of MeOH and water. Then 5 mL of saturated sodium hydrosulfide solution (excess) was added dropwise to the reaction mixture. The reaction mixture was heated to reflux at 100 °C for 16 h. Then the reaction mixture was allowed to cool to room temperature and was placed in an ice bath. Then the reaction mixture was slowly quenched with 6 M HCl. After waiting approximately 5 min to allow the resultant H₂S gas to evolve and disperse, the resulting yellow precipitate was collected via vacuum filtration and rinsed with a small amount of DI water. The resulting crude was purified by column chromatography, using a gradient of 100% hexanes to 100% ethyl acetate. The desired product eluted impure in 28% ethyl acetate in hexanes. Fractions containing the desired product were concentrated under reduced pressure and further purified by reverse phase chromatography, using a gradient of 100% water to 100% MeOH. The desired product eluted in 60% MeOH in water. Fractions containing the desired product were concentrated under reduced pressure to obtain **2.15** (0.12 g, 0.66 mmol, 30%) as a light yellow solid. ¹HNMR (400 MHz, DMSO-*d*₆) δ: 8.59 (*br s*, 1H), 7.71 (dd, *J*₁ = 8.0 Hz, *J*₂ = 2.0 Hz, 1H), 7.63 (dd, *J*₁ = 8.4 Hz, *J*₂ = 2.4 Hz, 1H), 7.49-7.43 (m, 2 H), 7.34 (t, *J* = 8.0, 1H); ESI-MS(-): *m/z* 176.32 [M-H].



Scheme 2.6. Route to **2.16**. Reagents and conditions: (a) P₄S₁₀, pyridine, H₂O, 120 °C, 5 h, 10%.

3-Thioxo-3,4-dihydroquinoxalin-2(1H)-one (2.16): To a suspension of 1,4-dihydroquinoxaline-2,3-dione (0.50 g, 3.08 mmol) partially dissolved in 10 mL pyridine, approximately 5 drops DI water was added, followed by phosphorous pentasulfide (1.03 g, 4.63 mmol). The reaction mixture was heated to reflux at 120 °C for 5 h. The reaction mixture was allowed to cool to room temperature, and was concentrated under reduced pressure to remove volatiles. The resulting crude oil was taken up in 50 mL DI water and heated at 100 °C for 2 h. The reaction mixture was then cooled to room temperature, and submerged in an ice bath. The solution was and basified using 30% ammonium hydroxide solution. The resulting solids were filtered off and discarded. The filtrate was acidified using acetic acid and the resulting dark yellow precipitate was collected via vacuum filtration. The crude solid was purified by reverse phase chromatography, using a gradient of 100% water to 100% MeOH. The desired product eluted in 20% MeOH in water. Fractions containing the desired product were concentrated under reduced pressure to obtain **2.17** (0.05 g, 0.03 mmol, 10%) as a bright yellow solid. ¹HNMR (400 MHz, DMSO-*d*₆) δ: 12.11 (*br s*, 1H), 7.36 (*d*, *J* = 8.0 Hz, 1H), 7.21-7.14 (*m*, 3H); ESI-MS(+): *m/z* 179.20 [M+H]⁺, 201.06 [M+Na]⁺.



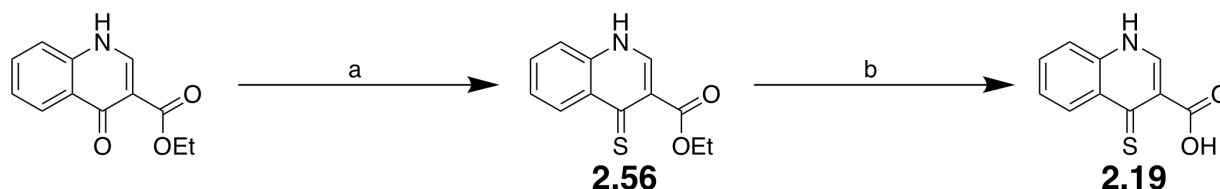
Scheme 2.7. Route to **2.18**. Reagents and conditions: (a) 2-(methylamino)benzoic acid, chloroacetone, DIPEA, microwave irradiation, NMP, 200 °C, 45 min, 16%; (b) Lawesson's reagent, HMPA, 100 °C, 3 h, 46%.

3-Hydroxy-1,2-dimethylquinolin-4(1H)-one (2.53): To a solution of 2-(methylamino)benzoic acid (0.50 g, 3.31 mmol) in 3 mL NMP, chloroacetone (0.27 mL, 3.31 mmol) and DIPEA (0.69

mL, 3.97 mmol) were sequentially added. The reaction mixture was heated at 200°C for 45 min in the microwave reactor. The reaction mixture was allowed to cool to room temperature and was neutralized by pouring into 20 mL DI water. The solution was then concentrated under reduced pressure to remove volatiles. The resulting residual oil was purified by column chromatography, using a gradient of 100% hexanes to 100% CH₂Cl₂, and then to 15% MeOH in CH₂Cl₂. The desired product eluted impure in 6% MeOH in CH₂Cl₂. Fractions containing the desired product were concentrated under reduced pressure to obtain the product as an impure oily tan solid. The product was recrystallized from 1:3 CH₂Cl₂/IPA and the resulting solid was collected via vacuum filtration. The solid was rinsed with a small amount of cold IPA to obtain **2.53** (0.10 g, 0.53 mmol, 16%) as a fluffy, off-white solid. ¹HNMR (400 MHz, DMSO-*d*₆) δ : 8.21 (d, *J* = 8.0 Hz, 1H), 7.76 (d, *J* = 8.8 Hz, 1H), 7.64 (t, *J* = 7.2 Hz, 1H), 7.30 (t, *J* = 7.6 Hz, 1H), 3.78 (s, 3H), 2.51 (s, 3H); ESI-MS(+): *m/z* 190.40 [M+H]⁺.

3-Hydroxy-1,2-dimethylquinoline-4(1*H*)-thione (2.18): Using a sealed vessel, to a partially dissolved solution of **2.53** (0.08 g, 0.423 mmol) in 5 mL HMPA, Lawesson's reagent (0.10 g, 0.25 mmol) was added. The reaction mixture was heated at 100°C for 3 h, after which the reaction mixture was allowed to cool to room temperature. The reaction was then and neutralized with 30 mL of 1 M HCl and the product was extracted using 3×20 mL ethyl acetate. The combined organic layers were washed with brine and dried over magnesium sulfate. Then the organic was concentrated under reduced pressure and resulting residue was purified by column chromatography, using gradient of 100% hexanes to 100% CH₂Cl₂ to 10% MeOH in CH₂Cl₂. The desired product eluted in 20% CH₂Cl₂ in hexanes. Fractions containing the desired product were and concentrated under reduced pressure to obtain **2.18** (0.040 g, 0.20

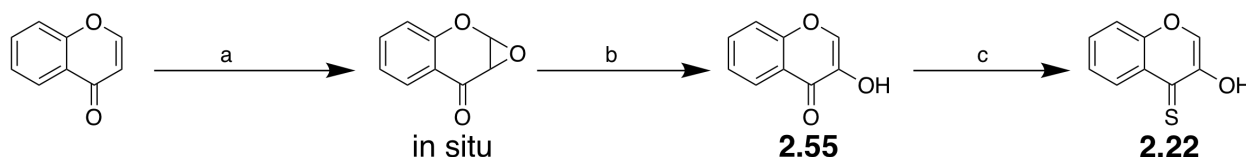
mmol, 46%) as a bright yellow solid. $^1\text{H NMR}$ (400 MHz, $\text{DMSO-}d_6$) δ : 8.79 (*br s*, 1H), 8.67 (*d*, $J = 8.0$ Hz, 1H), 8.06 (*d*, $J = 8.8$ Hz, 1H), 7.43 (*t*, $J = 8.0$ Hz, 1H), 7.55 (*t*, $J = 7.2$ Hz, 1H), 4.04 (*s*, 3H), 2.71 (*s*, 3H); ESI-MS(+): m/z 206.28 $[\text{M}+\text{H}]^+$.



Scheme 2.8. Route to **2.19**. Reagents and conditions: (a) P_4S_{10} , pyridine, 120 °C, 16 h, theoretical yield; (b) NaOH, MeOH, THF, 50 °C, 1 h, 38%.

Ethyl 4-thio-1,4-dihydroquinoline-3-carboxylate (2.54): To a solution of ethyl 4-oxo-1,4-dihydroquinoline-3-carboxylate (0.20 g, 0.92 mmol) in 10 mL pyridine, P_4S_{10} (0.51 g, 2.30 mmol) was added, and the reaction mixture was heated to reflux at 120 °C for 16 h. Then the reaction mixture was allowed to cool to room temperature and was concentrated under reduced pressure. The resulting residue was purified by column chromatography, using a gradient of 100% hexanes to 100% ethyl acetate, and then from 100% CH_2Cl_2 to 15% MeOH in CH_2Cl_2 . The desired product eluted in both 70% ethyl acetate in hexanes, as well as in 10% MeOH in CH_2Cl_2 . Fractions containing the desired product were concentrated under reduced pressure to obtain **2.54** (0.24 g, 1.01 mmol, theoretical yield) as a slightly impure, orange smelly solid. $^1\text{H NMR}$ (400 MHz, $\text{DMSO-}d_6$) δ : 8.71 (*dd*, $J_1 = 8.8$ Hz, $J_2 = 1.2$ Hz, 1H), 8.27 (*d*, $J = 6.0$ Hz, 1H), 7.78 – 7.74 (*m*, 1H), 7.68 (*d*, $J = 7.6$ Hz, 1H), 7.50 (*t*, $J = 7.2$ Hz, 1H), 4.25 (*q*, $J = 7.2$ Hz, 2H), 3.98 (*s*, 3H), 1.28 (*t*, $J = 7.2$ Hz, 3H); ESI-MS(+): m/z 234.23 $[\text{M}+\text{H}]^+$, 256.16 $[\text{M}+\text{Na}]^+$.

4-Thioxo-1,4-dihydroquinoline-3-carboxylic acid (2.19): To a solution of **2.54** (0.18 g, 0.56 mmol) in 5 mL THF, 6 mL of 1 M NaOH were added so that the organic and aqueous layers salted out. A small amount of MeOH was added to mix the resulting layers, and the reaction mixture was placed on a rotary evaporator to remove volatiles. The reaction mixture was heated at 50 °C for 1 h, while under reduced pressure. The reaction mixture was allowed to cool to room temperature and was acidified with HCl. The resulting precipitate was collected via vacuum filtration and washed with a small amount of cold DI water. The resulting crude solid was purified by column chromatography, using a gradient of 100% CH₂Cl₂ to 15% MeOH in CH₂Cl₂. The desired product eluted in 7-10% MeOH in CH₂Cl₂. Fractions containing the desired product were concentrated under reduced pressure to obtain **19** (0.07 g, 0.34 mmol, 38%) as a yellow solid. ¹HNMR (400 MHz, DMSO-*d*₆) δ : 9.24 (s, 1H), 8.92 (d, *J* = 8.0 Hz, 1H), 8.09 – 8.00 (m, 2H), 7.78 (t, *J* = 8.4 Hz, 1H), 4.22 (s, 1H); ESI-MS(-): *m/z* 205.02 [M-H]⁻.



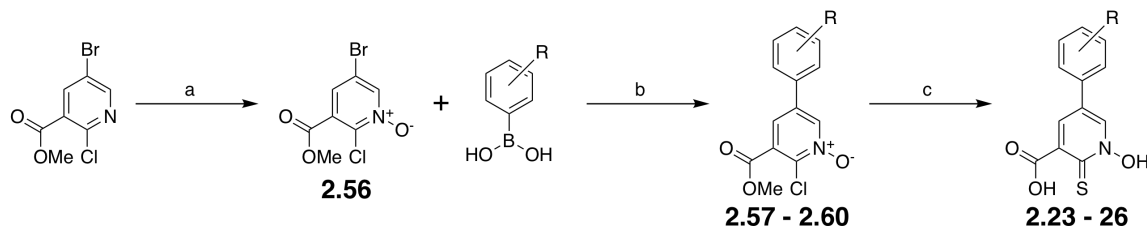
Scheme 2.9. Route to **2.22**. Reagents and conditions: (a) mCPBA, toluene, 110 °C, 3 h; (b) 1 M HCl, 100 °C, 1 h, 36% over two steps; P₄S₁₀, HMDO, TEA, THF, 25 °C, 16 h, 35%.

3-Hydroxy-4H-chromen-4-one (2.55): 4H-chromen-4-one (0.50 g, 3.42 mmol) and mCPBA (0.95 g, 4.11 mmol) were dissolved in toluene (20 ml) and were stirred at reflux for 3 hours to generate the epoxide intermediate. After removal of solvent under vacuum, the residue was taken up and heated to reflux in 1 M HCl (50 mL) for 1 hour to hydrolyze the epoxide ring. After cooling to room temperature, the acidic solution was extracted three times with ethyl acetate (35 mL). The combined organics were dried and concentrated, and the resultant oil was

purified by silica column chromatography in an ethyl acetate/hexanes system. The two isomers eluted similarly, but were resolved chromatographically. The desired isomer gives a positive (deep red) iron chloride stain whereas the undesired isomer did not stain with iron chloride. **2.55** (0.20 g, 1.23 mmol, 36%) was collected as a white crystalline solid. ^1H NMR (400 MHz, Acetone- d_6) δ : 8.25 – 8.11 (m, 2H), 7.78 (t, J = 8.7 Hz, 1H), 7.61 – 7.56 (d, J = 8.6 Hz, 1H), 7.46 (t, J = 8.1 Hz, 1H); ESI-MS(+): m/z 163.02 $[\text{M}+\text{H}]^+$.

3-Hydroxy-4H-chromene-4-thione (2.22): **2.55** (0.20 g, 1.23 mmol) was dissolved in THF (20 ml). 1,1,1,3,3,3-Hexamethyldisiloxane (0.87 mL, 4.1 mmol) was added to the stirring solution. P_4S_{10} was then added in one portion with one drop of TEA. The reaction stirred overnight at room temperature. Upon completion by TLC analysis, as indicated by a new spot that gave a positive (black) iron chloride stain, all solvent was removed under reduced pressure and the residue was purified by silica chromatography in an ethyl acetate/hexanes system to afford **2.22** (0.77 g, 0.43 mmol, 35%) as an orange solid. ^1H NMR (400 MHz, CDCl_3) δ : 8.59 (d, J = 8.2 Hz, 1H), 8.06 (s, 1H), 7.71 (t, J = 7.3 Hz, 1H), 7.56 (d, J = 8.5 Hz, 1H), 7.47 (t, J = 7.6 Hz, 1H); ESI-MS(+): m/z 179.61 $[\text{M}+\text{H}]^+$.

Route to Derivative Compounds 2.23 – 2.37



Scheme 2.10. Route to derivatives 2.23 – 2.26. Reagents and conditions: (a) TFA, H₂O₂, 80 °C, 3 h, 75%; (b) PdCl₂(dppf), S-Phos, K₃PO₄, 1,4-dioxanes, H₂O, 100 °C, 1 h, 41 – 53%; 1 M NaOH, NaSH, 25 – 80 °C, 4 h, 15 – 69%.

Methyl 5-bromo-2-chloro-1-methyl-1H-pyridine-3-carboxylate (2.56): Following general oxidation protocol B, from methyl 5-bromo-2-chloronicotinate (7.89 g, 31.5 mmol) in 60 mL trifluoroacetic acid with 20 mL 30% H₂O₂ heated at 80 °C for 3 h, 2.56 (6.3 g, 23.64 mmol, 75%) was obtained as a light yellow solid. ¹HNMR (400 MHz, Acetone-*d*₆) δ: 8.74 (d, *J*=2.0 Hz, 1H), 7.86 (d, *J*=2.4 Hz, 1H), 3.93 (s, 3H); ESI-MS(+): *m/z* 266.23 [M + H]⁺.

2-Chloro-3-(methoxycarbonyl)-5-phenylpyridine 1-oxide (2.57): Compound 2.56 (0.15 g, 0.56 mmol), S-Phos (0.023 g, 0.056 mmol), and phenylboronic acid (0.082 g, 0.675 mmol) were dissolved in 2 mL of 1,4-dioxane. Potassium carbonate (0.23 g, 1.69 mmol) was dissolved in 0.5 mL water and the aqueous was added to the solution containing the product. The reaction mixture was degassed under vacuum for 10 min, after which PdCl₂(dppf) (0.007 g, 0.028 mmol) was added. The reaction mixture was heated at 75°C for 16 h, and was then hot filtered through a thin pad of celite. The filtrate was concentrated under reduced pressure and the resulting residue was purified by column chromatography, using a gradient of 100% hexanes to 100% ethyl acetate. The desired product eluted in 70% ethyl acetate in hexanes. Fractions containing the desired product were concentrated under reduced pressure to obtain 2.57 (0.061 g, 0.231

mmol, 41%) as a yellow oil that solidified upon standing to a yellow solid. ¹HNMR (400 MHz, Acetone-*d*₆) δ : 8.77 (s, 1H), 7.94 (s, 1H), 7.79 (d, *J* = 8.4 Hz, 2H), 7.58 – 7.52 (m, 3H), 3.99 (s, 3H); ESI-MS(+): *m/z* 264.34 [M + H]⁺.

1-Hydroxy-5-phenyl-2-thioxo-1,2-dihydropyridine-3-carboxylic acid (2.23): Following general thionation protocol A, from **2.57** (0.056 g, 0.212 mmol), **2.23** (0.02 g, 0.081 mmol, 38%) was obtained as a yellow solid. ¹HNMR (400 MHz, Acetone-*d*₆) δ : 9.10 (d, *J* = 0.8 Hz, 1H), 8.69 (d, *J* = 1.6 Hz, 1H), 7.82 (d, *J* = 7.2 Hz, 2H), 7.55 (t, *J* = 7.6 Hz, 2H), 7.51 (t, *J* = 7.2 Hz, 1H); ESI-MS(-): *m/z* 246.10 [M - H]⁻.

2-Chloro-3-(methoxycarbonyl)-5-(*para*-methoxyphenyl)-pyridine 1-oxide (2.58): Following the above general cross-coupling protocol, from **2.56** (0.2 g, 0.751 mmol), **2.58** (0.1157 g, 0.394 mmol, 53%) was obtained as a white crystalline solid. ¹HNMR (400 MHz, Acetone-*d*₆) δ : 8.72 (s, 1H), 7.90 (s, 1H), 7.75 (d, *J* = 8.8 Hz, 2H), 7.10 (d, *J* = 8.4 Hz, 2H), 3.98 (s, 3H), 3.88 (s, 3H); ESI-MS(+): *m/z* 294.23 [M + H]⁺.

1-Hydroxy-5-(4-methoxyphenyl)-2-thioxo-1,2-dihydropyridine-3-carboxylic acid (24): Following general thionation protocol A, from **2.58** (0.090 g, 0.306 mmol), **24** (0.059 g, 0.213 mmol, 69%) was obtained as a yellow solid. ¹HNMR (400 MHz, Acetone-*d*₆) δ : 9.05 (s, 1H), 8.66 (s, 1H), 7.77 (d, *J* = 8.8 Hz, 2H), 7.11 (d, *J* = 8.8 Hz, 2H), 3.88 (s, 3H); ESI-MS(-): *m/z* 276.11 [M - H]⁻.

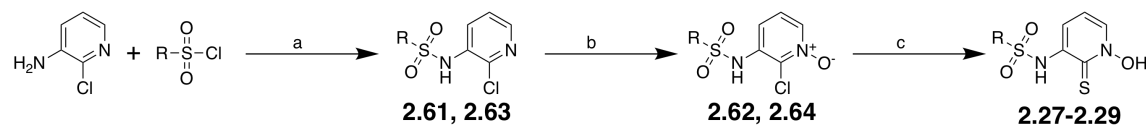
2-Chloro-3-(methoxycarbonyl)-5-(*meta*-methoxyphenyl)-pyridine 1-oxide (2.59): Following the above general cross-coupling protocol, from **2.56** (0.2 g, 0.751 mmol), **2.59** (0.1143 g, 0.389 mmol, 52%) was obtained as a white crystalline solid. ¹HNMR (400 MHz, Acetone-*d*₆) δ : 8.78 (s, 1H), 7.94 (s, 1H), 7.47 (t, *J* = 8.0 Hz, 1H), 7.35 (s, 2H), 7.08 (d, *J* = 8.0 Hz, 1H), 3.98 (s, 3H), 3.91 (s, 3H); ESI-MS(+): *m/z* 294.27 [M + H]⁺.

1-Hydroxy-5-(3-methoxyphenyl)-2-thioxo-1,2-dihydropyridine-3-carboxylic acid (25): Following general thionation protocol A, from **2.59** (0.090 g, 0.306 mmol), **25** (0.0226 g, 0.082 mmol, 27%) was obtained as a yellow solid. ¹HNMR (400 MHz, Acetone-*d*₆) δ : 9.09 (d, *J* = 2.0 Hz, 1H), 8.66 (d, *J* = 2.0 Hz, 1H), 7.46 (t, *J* = 8.0 Hz, 1H), 7.38 – 7.36 (m, 2H), 7.04 (d, *J* = 8.0 Hz, 1H), 3.91 (s, 3H); ESI-MS(-): *m/z* 276.18 [M - H]⁻.

2-Chloro-3-(methoxycarbonyl)-5-(*meta*-acetamidphenyl)-pyridine 1-oxide (2.60): Following the above general cross-coupling protocol, from **2.56** (0.4 g, 1.501 mmol), **2.60** (0.2178 g, 0.679 mmol, 45%) was obtained as a yellow solid. ¹HNMR (400 MHz, Acetone-*d*₆) δ : 10.11 (*br s*, 1H), 8.87 (d, *J* = 2.0 Hz, 1H), 7.92 (s, 1H), 7.88 (d, *J* = 2.0 Hz, 1H), 7.75 (d, *J* = 8.8 Hz, 2H), 7.66 (t, *J* = 2.8 Hz, 1H), 7.44 – 7.42 (m, 2H), 3.92 (s, 3H), 2.06 (s, 3H); ESI-MS(-): *m/z* 321.29 [M - H]⁻.

5-(3-Acetamidophenyl)-1-hydroxy-2-thioxo-1,2-dihydropyridine-3-carboxylic acid (2.26): Following general thionation protocol A, from **2.60** (0.20 g, 0.624 mmol), **26** (0.028 g, 0.093 mmol, 15%) was obtained as a yellow solid. ¹HNMR (400 MHz, Acetone-*d*₆) δ : 10.08 (*br s*,

1H), 8.97 (s, 1H), 7.92 (s, 1H), 8.26 (s, 1H), 7.64 (d, $J = 8.4$ Hz, 1H), 7.41 – 7.39 (m, 2H), 2.06 (s, 3H); ESI-MS(-): m/z 303.15 $[M - H]^-$.



Scheme 2.11. General route to derivatives **2.27 – 2.28**. Reagents and conditions: (a) 2-chloropyridin-3-amine, sulfonyl chloride, microwave irradiation, pyridine, 130 °C, 6 min, 91 – 92%; (b) mCPBA, CH_2Cl_2 , MeOH, 25 °C, 24 h, 56 – 74%; (c) NaSH, KI, H_2O , 100 °C, 8 h, 11 – 22%.

N-(2-chloropyridin-3-yl)benzenesulfonamide (2.61): Following the general sulfonamide cross-coupling procedure, 2-chloropyridin-3-amine (0.200 g, 1.56 mmol) and methanesulfonyl chloride (0.298 mL, 2.33 mmol) were dissolved in 2 mL dry pyridine and heated in the microwave reactor at 130°C for 3 min to obtain **2.61** (0.384 g, 1.43 mmol, 92%) as a white solid. ^1H NMR (400 MHz, $\text{DMSO}-d_6$) δ : 10.34 (*br s*, 1H), 8.21 – 8.19 (m, 1H), 7.85 – 7.82 (m, 1H), 7.72 – 7.69 (m, 4H), 7.65 – 7.54 (m, 2H), 7.41 – 7.38 (m, 1H); ESI-MS(+): m/z 269 $[M + H]^+$.

2-Chloro-3-(phenylsulfonamido)pyridine 1-oxide (2.62): Following the general oxidation protocol A, from **2.61** (0.350 g, 1.30 mmol) and mCPBA (0.670 g, 3.90 mmol) in 10 mL chloroform at 25 °C for 48 h **2.62** (0.274 g, 0.961 mmol, 74%) was obtained as a slightly impure pale yellow powdery solid. ^1H NMR (400 MHz, $\text{DMSO}-d_6$) δ : 8.25, (d, $J = 6.4$ Hz, 1H), 7.85-7.57 (m, 6H), 7.30 (t, $J = 7.2$ Hz, 1H), 7.21 (d, $J = 8.8$ Hz, 1H); ESI-MS(+): m/z 285 $[M + H]^+$.

N-(1-hydroxy-2-thioxo-1,2-dihydropyridin-3-yl)benzenesulfonamide (27): Using the following modified general thionation protocol B, to a solution of **2.62** (0.256 g, 0.899 mmol) in

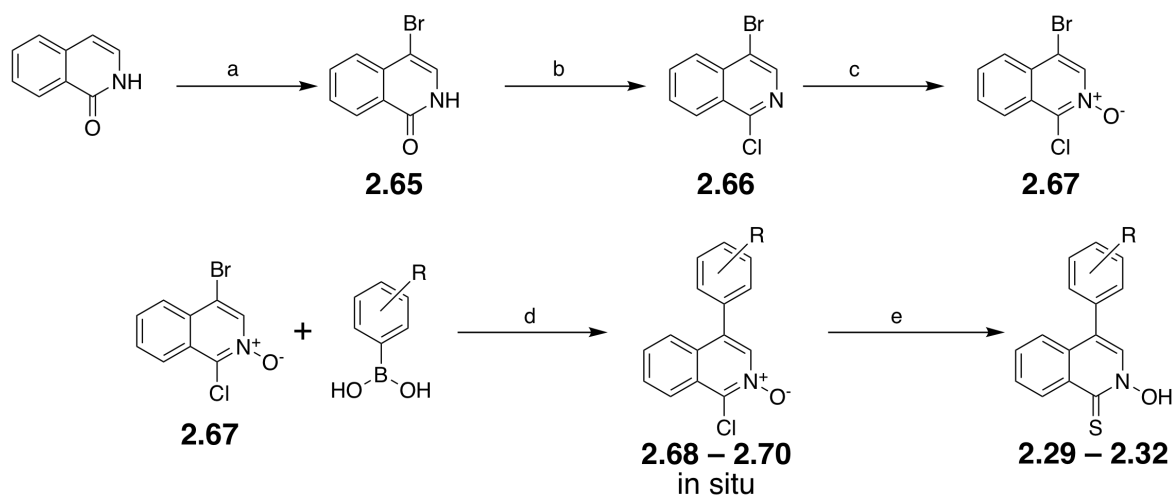
5 mL DI water with MeOH, 5 mL saturated sodium hydrogen sulfide solution (excess) was added. After heating the reaction mixture to reflux at 100 °C for 16 h, KI (0.448 g, 2.70 mmol) was added, and the reaction continued to heat at reflux at 100 °C for 16 h to obtain **27** (0.027 g, 0.095 mmol, 11%) as waxy white solid. ¹HNMR (400 MHz, Acetone-*d*₆) δ: 11.45 (*br s*, 1H), 8.66 (*br s*, 1H), 8.22 (d, *J* = 6.8 Hz, 1H), 7.95 (d, *J* = 8.4 Hz, 2H), 7.73 (d, *J* = 8.0 Hz, 1H), 7.67 (t, *J* = 7.6 Hz, 1H), 7.58 (t, *J* = 6.8 Hz, 2H), 7.01 (t, *J* = 6.8 Hz, 1H); ESI-MS(-): *m/z* 282.12 [M - H]⁻.

N-(2-chloropyridin-3-yl)-1-phenylmethanesulfonamide (2.63): Following the general sulfonamide cross-coupling procedure, 2-chloropyridin-3-amine (0.500 g, 3.89 mmol) and phenylmethanesulfonyl chloride (1.11g, 5.83 mmol) were dissolved in 2 mL dry pyridine and heated in the microwave reactor at 130°C for 13 min to obtain **2.63** (0.999 g, 3.53 mmol, 91%) as a dark yellow oil that solidifies upon standing to a light brown crystalline solid. ¹HNMR (400 MHz, DMSO-*d*₆) δ: 9.73 (*br s*, 1H), 8.16 (dd, *J*₁ = 4.4 Hz, *J*₂ = 1.6 Hz, 1H), 7.59 (dd, *J*₁ = 8.0 Hz, *J*₂ = 1.6 Hz, 1H), 7.40 – 7.30 (m, 6H), 4.58 (s, 2H); ESI-MS(+): *m/z* 283 [M + H]⁺.

2-chloro-3-((phenylmethyl)sulfonamido)pyridine 1-oxide (2.64): Following the general oxidation protocol A, from **2.63** (0.527 g, 1.30 mmol) in 10 mL of 1:1 CH₂Cl₂ and MeOH with mCPBA (0.680 g, 3.90 mmol) at 0-25 °C for 24, after which additional mCPBA (0.680 g, 3.90 mmol) was added, and the reaction was continued for another 24 h to obtain **2.64** (0.219 g, 0.732 mmol, 56%) as a slightly impure tan-yellow solid. ¹HNMR (400 MHz, DMSO-*d*₆) δ: 9.98 (s, 1H), 8.26 (d, *J* = 6.4 Hz, 1H), 7.38-7.33 (m, 5H), 7.26-7.23 (m, 2H), 4.62 (s, 2H); ESI-MS(+): *m/z* 299 [M + H]⁺.

N-(1-hydroxy-2-thioxo-1,2-dihydropyridin-3-yl)-1-phenylmethanesulfonamide (2.28):

Following the general thionation protocol B, from **2.64** (0.200 g, 0.670 mmol) with KI (0.333 g, 2.01 mmol), **2.28** (0.043 g, 0.133 mmol, 22%) was obtained as an off-white waxy solid. ¹HNMR (400 MHz, DMSO-*d*₆) δ : 8.87 (*br s*, 1H), 8.13 (d, *J* = 6.8 Hz, 1H), 7.29 (s, 6H), 6.77 (t, *J* = 7.2 Hz, 1H), 4.71 (s, 2H); ESI-MS(+): *m/z* 296.96 [M + H]⁺. ESI-MS(-): *m/z* 295.11 [M - H]⁻.



Scheme 2.12. General route to derivatives **2.29 – 2.32**. Reagents and conditions: (a) NBS, DMF, 25 °C, 1 h, 84%; (b) POCl₃, 100 °C, 1.5 h, 82%; (c) TFA, H₂O₂, 90 °C, 2 h, 46%; (d) phenyl boronic acid, PdCl₂(dppf), K₃PO₄, 1,4-dioxanes, H₂O, 100 °C, 1 h; (e) NaSH, 1 M NaOH, 25 – 80 °C, 4 h, 7 – 36% over two steps.

4-Bromoisoquinolin-1(2H)-one (2.65): To a solution of isoquinolin-1(2H)-one (4 g, 27.6 mmol) in 45 mL dry DMF NBS (4.90 g, 27.6 mmol) was added in one portion. The reaction mixture was placed under a nitrogen atmosphere and allowed to stir at room temperature for 1 h. Then the reaction mixture was diluted with 75 mL cold DI water to form a white precipitate. The resulting solid was collected via vacuum filtration and washed with a small amount of cold DI water to obtain **2.65** (5.193 g, 23.81 mmol, 84%) as an off-white solid in the form of fine

needle-like crystals. ¹HNMR (400 MHz, DMSO-*d*₆) δ : 11.59 (*br s*, 1H), 8.22 (d, *J* = 8.0 Hz, 1H), 8.85 (t, *J* = 8.0 Hz, 1H), 7.75 (d, *J* = 8.0 Hz, 1H), 7.59 (t, *J* = 7.6 Hz, 1H), 7.55 (d, *J* = 2.4 Hz, 1H);

4-Bromo-1-chloroisoquinoline (2.66): Compound **2.65** (2.1 g, 9.37 mmol) was dissolved in neat POCl₃ (20 mL, 215 mmol). The reaction mixture was placed under a nitrogen environment and heated to reflux at 100°C for 1.5 h. Then the reaction mixture was allowed to cool to room temperature and submerged in an ice bath. A small amount of MeOH was added to the cold reaction mixture, and cold 6 M NaOH was added to quench the reaction. The quenched reaction was extracted into ethyl acetate using 3×20 mL, and the combined organic layers were washed with brine. The organic was concentrated under reduced pressure and the resulting residue was purified by column chromatography, using a gradient of 100% hexanes to 100% ethyl acetate. The desired product eluted in 10% ethyl acetate in hexanes. Fractions containing the desired product were concentrated under reduced pressure to obtain **2.66** (1.875 g, 7.73 mmol, 82%) as white to light orange solid. ¹HNMR (400 MHz, Acetone-*d*₆) δ : 8.53 (s, 1H), 8.38 (d, *J* = 8.4 Hz, 1H), 8.23 (d, *J* = 8.4 Hz, 1H), 8.06 (t, *J* = 8.4 Hz, 1H), 7.94 (t, *J* = 7.2 Hz, 1H); ESI-MS(+): *m/z* 240.93 [M + H]⁺.

4-Bromo-1-chloro-2-N-oxideisoquinoline (2.67): To a solution of **2.66** (3.6 g, 14.85 mmol) in 45 mL trifluoroacetic acid, 15 mL of 30% H₂O₂ was added dropwise. The reaction mixture was heated to reflux at 90 °C for 2 h. Then the reaction mixture was concentrated under reduced pressure and the resulting crude was purified by column chromatography, using a gradient of 100% hexanes to 100% ethyl acetate. The desired product eluted slowly in 40% ethyl acetate in

hexanes. Fractions containing the desired product were concentrated under reduced pressure to obtain **2.67** (1.774 g, 6.86 mmol, 46%) in as a light peach solid. ¹HNMR (400 MHz, Acetone-*d*₆) δ : 8.62 (s, 1H), 8.12 (d, *J* = 4.0 Hz, 1H), 8.10 (d, *J* = 3.2 Hz, 1H), 7.87 (t, *J* = 7.2 Hz, 1H), 7.81 (t, *J* = 7.2 Hz, 1H); ESI-MS(+): *m/z* 258.26 [M + H]⁺.

2-Hydroxy-4-phenylisoquinoline-1(2*H*)-thione (2.29): This reaction was performed over two steps. Compound **2.67** (0.1 g, 0.387 mmol) and phenylboronic acid (0.052 g, 0.426 mmol) were dissolved in 2 mL 1,4-dioxane. Tribasic potassium phosphate (0.246 g, 1.161 mmol) was dissolved in 0.5 mL DI water and the aqueous was added to the solution containing the starting material. The reaction mixture was degassed under vacuum for 10 min, after which PdCl₂(dppf) (0.0067 g, 0.027 mmol) was added. The reaction mixture was heated at 100 °C for 30 min, and then hot filtered over a thin pad of celite. The filtrate was concentrated under reduced pressure and the resulting residue was purified by column chromatography, using a gradient of 100% hexanes to 100% ethyl acetate. The desired product eluted impure in 80% ethyl acetate in hexanes. Fractions containing the desired product were concentrated under reduced pressure to obtain impure **2.68** (0.0578 g, 0.226 mmol, 58%) as a light tan solid that was used immediately with no further purification. Then following the general thionation protocol A, from **2.68** (0.056 g, 0.219 mmol) at 80 °C for 3 h, **2.29** (0.025 g, 0.099 mmol, 26%) was obtained over two steps as a bright yellow solid. ¹HNMR (400 MHz, Acetone-*d*₆) δ : 12.07 (*br s*, 1H), 8.83 (d, *J* = 7.2 Hz, 1H), 8.18 (s, 1H), 7.83 – 7.77 (m, 4H), 7.58 (s, 5H); ESI-MS(+): *m/z* 252.28 [M + H]⁺.

2-Hydroxy-4-(4-methoxyphenyl)isoquinoline-1(2*H*)-thione (30): This reaction was performed over two steps. Compound **2.67** (0.15 g, 0.580 mmol), (4-methoxyphenyl)boronic acid (0.106 g,

0.696 mmol) and S-phos (0.024 g, 0.058 mmol) were dissolved in 2 mL 1,4-dioxane. Tribasic potassium phosphate (0.370 g, 1.741 mmol) was dissolved in 0.5 mL water and the aqueous was added to the solution containing the starting material. The reaction mixture was degassed under vacuum for 10 min after which PdCl₂(dppf) (0.0101 g, 0.041 mmol) was added. The reaction mixture was heated at 95 °C for 1 h, and then filtered through a thin celite pad. The filtrate was concentrated under reduced pressure and the resulting residue was purified by column chromatography, running gradient from 100% hexanes to 100% ethyl acetate. The desired product eluted impure in 70% ethyl acetate in hexanes. Fractions containing the desired product were concentrated under reduced pressure to obtain **2.69** (0.082 g, 0.287 mmol, 50%) as an impure, slightly oily tan solid that was used immediately with no further purification. Then following the general thionation protocol A, from **2.69** at 80 °C for 3 h, **2.30** (0.0432 g, 0.152, 26%) was obtained over two steps as a bright yellow solid. ¹HNMR (400 MHz, Acetone-*d*₆) δ: 12.07 (*br s*, 1H), 8.84 (d, *J* = 7.6 Hz, 1H), 8.15 (s, 1H), 7.85 – 7.78 (m, 3H), 7.51 (d, *J* = 7.6 Hz, 2H), 7.14 (d, *J* = 7.6 Hz, 2H), 3.91 (s, 3H); ESI-MS(-): *m/z* 282.32 [M - H]⁻, 314.28 [M + MeOH-H]⁻.

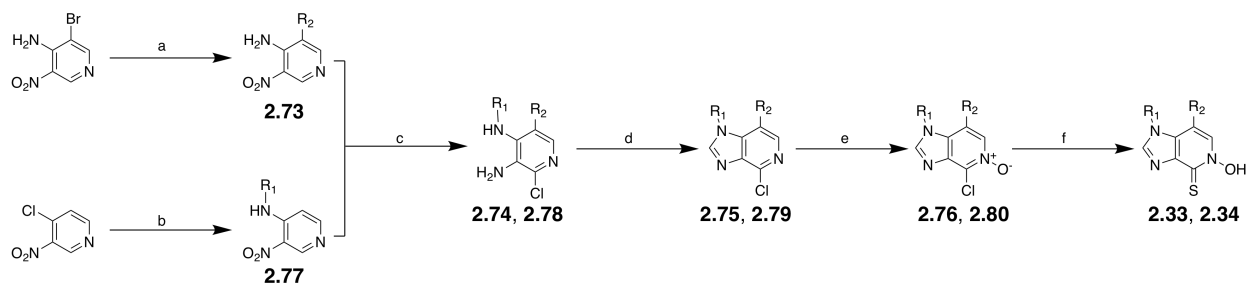
2-Hydroxy-4-(3-methoxyphenyl)isoquinoline-1(2H)-thione (2.31): This reaction was performed over two steps. Compound **2.67** (0.15 g, 0.580 mmol), (3-methoxyphenyl)boronic acid (0.106 g, 0.696 mmol), and S-phos (0.024 g, 0.058 mmol) were dissolved in 2 mL 1,4-dioxane. Potassium phosphate (0.370 g, 1.741 mmol) was dissolved in 0.5 mL water and the aqueous was added to the solution containing the starting material. The reaction mixture was degassed under vacuum for 10 min after which PdCl₂(dppf) (0.0101 g, 0.041 mmol) was added. The reaction mixture was heated at 100°C for 5 h, and was then filtered through a thin celite pad.

The filtrate was concentrated under reduced pressure and the resulting residue was purified by column chromatography, using a gradient of 100% hexanes to 100% ethyl acetate. The desired product eluted impure in 65% ethyl acetate in hexanes. Fractions containing the desired product were concentrated under reduced pressure to obtain **2.70** (0.0765 g, 0.268 mmol, 46%) as an impure, slightly oily pinkish solid that was used immediately with no additional purification. Then following the general thionation protocol A, from **2.70** at 80 °C for 3 h, **2.31** (0.0116 g, 0.041 mmol, 7%) was obtained over two steps as a bright yellow solid. ¹HNMR (400 MHz, Acetone-*d*₆) δ: 12.08 (*br s*, 1H), 8.83 (d, *J* = 8.0 Hz, 1H), 8.20 (s, 1H), 7.81 – 7.77 (m, 3H), 8.83 (t, *J* = 8.0, 1H), 7.49 (t, *J* = 8.0, 1H), 7.15 – 7.10 (m, 3H), 3.89 (s, 3H); ESI-MS(-): *m/z* 282.33 [M - H]⁻, 314.22 [M + MeOH-H]⁻.

1-Chloro-4-(thiophen-3-yl)isoquinoline (2.71): Using the following modified cross coupling protocol, **2.66** (0.35 g, 1.4 mmol), thiophen-3-ylboronic acid (0.18 g, 1.40 mmol), K₃PO₄ (0.92 g, 4.3 mmol), and PdCl₂(dppf) adduct (0.08 g, 0.10 mmol) were dissolved in 2 mL 1,4-dioxane with 1 mL water, and the reaction mixture was placed in the microwave reactor at 110 °C for 25 min to obtain **2.71** (0.18 g, 0.74 mmol, 53%) as a white solid. ¹HNMR (400 MHz, DMSO-*d*₆) δ: 8.37 (d, *J* = 8.4 Hz, 1H), 8.32 (s, 1H), 8.05 (d, *J* = 8.4 Hz, 1H), 7.93 (t, *J* = 6.8 Hz, 1H), 7.89 – 7.86 (m, 2H), 7.81 (dd, *J*₁ = 4.8 Hz, *J*₂ = 3.2 Hz, 1H), 7.42 (dd, *J*₁ = 5.2 Hz, *J*₂ = 1.2 Hz, 1H); ESI-MS(+): *m/z* 246 [M + H]⁺.

2-Hydroxy-4-(thiophen-3-yl)isoquinoline-1(2H)-thione (2.32): This reaction was performed over two steps. Following oxidation protocol A, from **2.71** (0.18 g, 0.74 mmol), the oxidation intermediate **2.72** (0.09 g, 0.36 mmol, 48%) was obtained as a very impure yellow oil that was

used immediately in the following step with no additional purification. Then **2.72** (0.09 g, 0.36 mmol) was thionated according to the general thionation protocol A at 0 °C for 3 h to obtain **2.32** (0.032 g, 0.13 mmol, 36%) as a pale yellow solid. ¹HNMR (400 MHz, Acetone-*d*₆) δ : 12.07 (*br s*, 1H), 8.82 (*d*, *J* = 8.0 Hz, 1H), 8.24 (*s*, 1H), 7.92 (*d*, *J* = 8.0 Hz, 1H), 7.84 (*t*, *J* = 6.8 Hz, 1H), 7.80 – 7.73 (*m*, 3H), 7.41 (*d*, *J* = 4.8 Hz, 1H); ESI-MS(-): *m/z* 258.19 [*M* - H]⁻.



Scheme 2.13. Route to derivatives **2.33** and **2.34**. Reagents and conditions: (a) 3-bromo-5-nitropyridin-4-amine, phenyl boronic acid, S-Phos, PdCl₂(dppf), K₃PO₄, 1,4-dioxanes, H₂O, 100 °C, 16 h, 70%; (b) 4-chloro-3-nitropyridine, aniline, 25 °C, 1 h, 22%; (c) SnCl₂, HCl, 90 °C, 3 h, 72 – 90%; (d) triethyl orthoformate, cat. HCl, 25 °C, 16 h, 77 – 100%; (e) TFA, H₂O₂, 90 °C, 3 h, 44 – 48 %; (f) NaSH, H₂O, 0 – 80 °C, 2 h, 45 – 60%.

3-Nitro-5-phenylpyridin-4-amine (2.73): To a suspension of 3-bromo-5-nitropyridin-4-amine (1.00 g, 4.59 mmol) and S-Phos (0.19 g, 0.46 mmol) in 20 mL 1,4-dioxane, 15 mL DMF was added to aid solubility. K₃PO₄ (2.92 g, 13.76 mmol) was dissolved in 4 mL DI water and the aqueous was added to the solution containing the starting material. The reaction mixture was degassed under vacuum for 10 min, after which PdCl₂(dppf)-CH₂Cl₂ adduct (0.057 g, 0.230 mmol) was added. The reaction mixture was heated at 100 °C for 16 h. Then the reaction mixture was allowed to cool to room temperature and filtered through a pad of celite. The filtrate was concentrated under reduced pressure and the resulting residue was purified by column chromatography, using a gradient of 100% hexanes to 100% ethyl acetate. The desired

product eluted in 60% ethyl acetate in hexanes. Fractions containing the desired product were concentrated under reduced pressure to obtain **2.73** (0.69 g, 3.22 mmol, 70%) as a bright yellow solid. ¹HNMR (400 MHz, DMSO-*d*₆) δ : 9.02 (s, 1H), 8.09 (s, 1H), 7.55-7.42 (m, 5H), 7.28 (br s, 2H); ESI-MS(+): *m/z* 216 [M+H]⁺.

2-Chloro-5-phenylpyridine-3,4-diamine (2.74): A solution of **2.73** (0.69 g, 3.21 mmol) in 10 mL 12 M HCl was pre-heated to 90°C. SnCl₂ (2.81 g, 14.8 mmol) was dissolved in an additional 5 mL of 12 M HCl, and the SnCl₂ solution was added dropwise to the solution containing the starting material. The reaction mixture was placed under a nitrogen atmosphere and was heated to reflux at 130 °C for 3 h. Then the reaction mixture was allowed to cool to room temperature and was neutralized with NaOH solution to pH 7. The neutralized mixture was extracted exhaustively into organic using 3:1 CH₂Cl₂/IPA. The combined organic layers were dried over magnesium sulfate, and the solids were filtered off and discarded. The filtrate was concentrated under reduced pressure and the resulting residue was purified by via column chromatography, using a gradient of 100% hexanes to 100% ethyl acetate. The desired product eluted in 72% ethyl acetate in hexanes. Fractions containing the desired product were concentrated under reduced pressure to obtain **2.74** (0.51 g, 2.31 mmol, 72%) as a white solid. ¹HNMR (400 MHz, DMSO-*d*₆) δ : 7.48-7.45 (m, 2H), 7.39-7.36 (m, 3H), 7.25 (s, 1H), 5.37 (s, 2H), 4.87 (s, 2H); ESI-MS(+): *m/z* 220 [M+H]⁺.

4-Chloro-7-phenyl-1H-imidazo[4,5-*c*]pyridine (2.75): To a suspension of **2.74** (0.25 g, 1.10 mmol) in triethyl orthoformate (15 mL, 90 mmol), a minimal amount of DMF was added to induce solubility. A catalytic amount of 12 M HCl was added to the solution containing the

starting material, and the reaction mixture was allowed to stir at room temperature for 1.5 h. The reaction mixture was concentrated under reduced pressure and the resulting residue was purified by column chromatography, using a gradient of 100% hexanes to 100% ethyl acetate, and then from 100% CH₂Cl₂ to 15% MeOH in CH₂Cl₂. The desired product eluted in 10% MeOH in CH₂Cl₂. Fractions containing the desired product were concentrated under reduced pressure to obtain **2.75** (0.30 g, 1.13 mmol, theoretical yield) as an HCl salt as a flaky white solid. ¹HNMR (400 MHz, DMSO-*d*₆) δ : 8.67 (s, 1H), 8.29 (s, 1H), 7.83 (d, *J* = 7.6 Hz, 2H), 7.54 (t, *J* = 7.6 Hz, 2H), 7.49-7.45 (m, 1H), 6.67 (*br s*, 1H); ESI-MS(+): *m/z* 230 [M+H]⁺.

4-Chloro-7-phenyl-1H-imidazo[4,5-c]pyridine 5-oxide (2.76): Following general oxidation protocol A, from **2.75** (0.30 g, 1.13 mmol), **2.76** (0.12 g, 0.50 mmol, 44%) was obtained as a slightly impure light brown crystalline solid. ¹HNMR (400 MHz, DMSO-*d*₆) δ : 8.56 (s, 1H), 8.49 (s, 1H), 7.56-7.49 (m, 4H), 7.43 (t, *J* = 7.6 Hz, 1H); ESI-MS(+): *m/z* 246 [M+H]⁺.

5-Hydroxy-7-phenyl-1,5-dihydro-4H-imidazo[4,5-c]pyridine-4-thione (2.33): Using the following modified general thionation protocol A, from **2.76** (0.10 g, 0.41 mmol) at 80 °C for 2 h and purification by column chromatography using a gradient of 100% CH₂Cl₂ to 15% MeOH in CH₂Cl₂ and recrystallization from IPA, **2.33** (0.045 g, 0.18 mmol, 45%) was obtained as an off white solid. ¹HNMR (400 MHz, DMSO-*d*₆) δ : 12.24 (*br s*, 1H), 8.42 (d, *J* = 7.2 Hz, 2H), 8.08 (d, *J* = 7.6 Hz, 2H), 7.47 (t, *J* = 7.2 Hz, 2H), 7.47 (t, *J* = 7.2 Hz, 1H); ESI-MS(+): *m/z* 244.17 [M + H]⁺; ESI-MS(-): *m/z* 242.21 [M - H]⁻.

3-Nitro-N-phenylpyridin-4-amine (2.77): 4-chloro-3-nitropyridine (0.50 g, 3.15 mmol) was dissolved in neat aniline (5.00 mL, 54.8 mmol), and the reaction mixture was allowed to stir at room temperature for 1 hr. An exotherm was noted to occur after 10 min. Upon reaction completion, as indicated by TLC, the reaction was taken up in ethyl acetate, washed with DI water to remove most of the aniline. The aqueous was back-extracted, and the combined organic layers were concentrated under reduced pressure. The resulting residue was purified by column chromatography, using a gradient of 100% hexanes to 100% ethyl acetate. The desired product eluted in 30% ethyl acetate in hexanes. Fractions containing the desired product were concentrated under reduced pressure to obtain **2.77** (0.15 g, 0.70 mmol, 22%) as a yellow solid. $^1\text{H NMR}$ (400 MHz, $\text{DMSO-}d_6$) δ : 9.83 (*br s*, 1H), 9.09 (d, $J = 2.8$ Hz, 1H), 8.23 (dd, $J_1 = 6.0$ Hz, $J_2 = 3.2$ Hz, 1H), 7.51-7.46 (m, 2H), 7.38-7.31 (m, 3H), 6.87 (dd, $J_1 = 6.0$ Hz, $J_2 = 2.8$ Hz, 1H); ESI-MS(+): m/z 216 $[\text{M}+\text{H}]^+$.

2-Chloro-N4-phenylpyridine-3,4-diamine (2.78): A solution of **2.77** (0.15 g, 0.70 mmol) in 5 mL of 12 M HCl was pre-heat to 90 °C. SnCl_2 (0.61 g, 3.2 mmol) was dissolved in 5 mL of 12 M HCl, and the SnCl_2 solution was added dropwise to the solution containing the starting material. The reaction mixture was placed under a nitrogen atmosphere and was heated to reflux at 120°C for 3 h. Then the reaction mixture was allowed to cool to room temperature and was neutralized with NaOH solution to pH 7. The neutralized solution was extracted into organic using ethyl acetate with a small amount of MeOH. The combined organic layers were washed with brine and dried over magnesium sulfate. The organic was concentrated under reduced pressure and the resulting residue was purified by column chromatography, using a gradient of 100% hexanes to 100% ethyl acetate. The desired product eluted in 53% ethyl acetate in

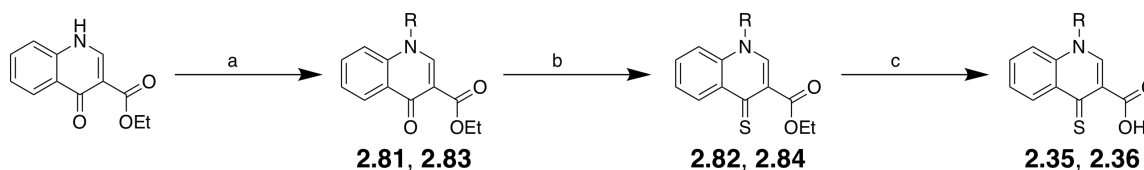
hexanes. Fractions containing the desired product were concentrated under reduced pressure to obtain **2.78** (0.14 g, 0.63 mmol, 90%) as a light yellow solid. ¹HNMR (400 MHz, DMSO-*d*₆) δ: 7.57 (d, *J* = 5.2 Hz, 1H), 7.34 (t, *J* = 8.4 Hz, 2H), 7.17 (d, *J* = 7.6 Hz, 2H), 7.07 (*br s*, 1H), 7.03 (t, *J* = 7.6 Hz, 1H), 7.00 (d, *J* = 5.2 Hz, 1H), 4.65 (*br s*, 2H); ESI-MS(+): *m/z* 220 [M+H]⁺.

4-Chloro-1-phenyl-1H-imidazo[4,5-c]pyridine (2.79): To a suspension of **2.78** (0.13 g, 0.57 mmol) in triethyl orthoformate (15 mL, 90 mmol), a small amount of DMF was added to induce solubility. A catalytic amount of 12 M HCl was added to the solution containing the starting material, and the reaction mixture was allowed to stir at room temperature for 16 h. The reaction mixture was concentrated under reduced pressure, and the resulting residue was purified by column chromatography, using a gradient of 100% CH₂Cl₂ to 15% MeOH in CH₂Cl₂. The desired product eluted in 5% MeOH in CH₂Cl₂. Fractions containing the desired product were concentrated under reduced pressure to obtain **2.79** (0.10 g, 0.57 mmol, 77%) as an off-white solid. ¹HNMR (400 MHz, DMSO-*d*₆) δ: 8.59 (s, 1H), 8.22 (d, *J* = 5.6 Hz, 1H), 7.75-7.68 (m, 4H), 7.63-7.58 (m, 2H); ESI-MS(+): *m/z* 230 [M+H]⁺.

4-Chloro-1-phenyl-1H-imidazo[4,5-c]pyridine 5-oxide (2.80): Following the general oxidation protocol A, from **2.79** (0.09 g, 0.39 mmol), **2.80** (0.046 g, 0.188 mmol, 48%) was obtained as a light orange oily solid. ¹HNMR (400 MHz, DMSO-*d*₆) δ: 8.69 (s, 1H), 8.37 (s, 1H), 7.78-7.58 (m, 6H); ESI-MS(+): *m/z* 246 [M+H]⁺.

5-hydroxy-1-phenyl-1,5-dihydro-4H-imidazo[4,5-c]pyridine-4-thione (2.34): Using the following modified version of thionation protocol A, from **2.80** (0.04 g, 0.16 mmol) at 0 °C for 1

h and purification by extraction of the filtrate with CH₂Cl₂ and column chromatography using a gradient of 100% hexanes to 100% ethyl acetate, **2.34** (0.024 g, 0.097 mmol, 60%) was obtained as an off white solid. ¹HNMR (400 MHz, DMSO-*d*₆) δ: 12.05 (*br s*, 1H), 8.63 (*s*, 1H), 8.29 (*d*, *J* = 7.2 Hz, 1H), 7.67-7.62 (*m*, 4H), 7.57-7.53 (*m*, 1H), 7.06 (*d*, *J* = 7.2 Hz, 1H); ESI-MS(+): *m/z* 244.17 [M + H]⁺. ESI-MS(-): *m/z* 242.11 [M - H]⁻.



Scheme 2.14. Route to derivatives **2.35** and **2.36**. Reagents and conditions: (a) ethyl 4-oxo-1,4-dihydroquinoline-3-carboxylate, alkyl halide, K₂CO₃, DMF, 80 °C, 16 h, 96 – 99%; (b) P₄S₁₀, pyridine, 120 °C, 16 h, theoretical yield; (c) NaOH, MeOH, THF, 50 °C, 1 h, 25 – 67%.

Ethyl 1-methyl-4-oxo-1,4-dihydroquinoline-3-carboxylate (2.81): To a solution of ethyl 4-oxo-1,4-dihydroquinoline-3-carboxylate (0.20 g, 0.92 mmol) in 15 mL dry DMF, potassium carbonate (0.25 g, 1.84 mmol) and methyl iodide (0.23 mL, 3.68 mmol) were sequentially added. The reaction mixture was heated at 80 °C for 16 h, after which potassium acetate (0.36 g, 3.68 mmol) was added to quench the excess methyl iodide at 80 °C for 1 h. Then the reaction mixture was cooled to room temperature and was concentrated under reduced pressure. The resulting residue was purified by column chromatography, using a gradient of 100% CH₂Cl₂ to 15% MeOH in CH₂Cl₂. The desired product eluted in two peaks: the first in 100% CH₂Cl₂, and the second in 15% MeOH in CH₂Cl₂. Fractions containing the desired product were concentrated under reduced pressure to obtain **2.81** (0.21 g, 0.91 mmol, 99%) as a yellow solid in long spindle crystals that were initially yellow, but turned pink over time. ¹HNMR (400 MHz, DMSO-*d*₆) δ: 8.66 (*s*, 1H), 8.22 (*d*, *J* = 8.0 Hz, 1H), 7.78 (*t*, *J* = 8.0 Hz, 1H), 7.71 (*d*, *J* = 8.4 Hz, 1H), 7.48 (*t*,

$J = 7.2$ Hz, 1H), 4.21 (q, $J = 7.2$ Hz, 2H), 3.91 (s, 3H), 1.27 (t, $J = 7.2$ Hz, 3H); ESI-MS(+): m/z 232.22 [M+H]⁺, 254.19 [M+Na]⁺.

Ethyl 1-methyl-4-thioxo-1,4-dihydroquinoline-3-carboxylate (2.82): Compound **2.81** (0.180 g, 0.78 mmol) and P₄S₁₀ (0.432 g, 1.95 mmol) were dissolved in 10 mL pyridine, and the reaction mixture was heated to reflux at 120 °C for 16 h. Then the reaction mixture was cooled to room temperature and concentrated under reduced pressure. The resulting residue was purified by column chromatography, using a gradient of 100% hexanes to 100% ethyl acetate, and then from 100% CH₂Cl₂ to 15% MeOH in CH₂Cl₂. The desired product eluted in both 70% ethyl acetate in hexanes, as well as in 10% MeOH in CH₂Cl₂. Fractions containing the desired product were concentrated under reduced pressure to obtain **2.82** (0.200 g, 0.809 mmol, theoretical yield) as a slightly impure, orange, slightly smelly solid. ¹HNMR (400 MHz, DMSO-*d*₆) δ : 8.81 (d, $J = 8.4$ Hz, 1H), 8.38 (s, 1H), 7.86 – 7.85 (m, 2H), 7.60 – 7.56 (m, 1H), 4.24 (q, $J = 7.2$ Hz, 2H), 1.29 (t, $J = 7.2$ Hz, 3H); ESI-MS(+): m/z 248.23 [M+H]⁺, 270.16 [M+Na]⁺.

1-Methyl-4-thioxo-1,4-dihydroquinoline-3-carboxylic acid (2.35): To a solution of **2.82** (0.18 g, 0.73 mmol) in 5 mL THF, 6 mL of 1 M NaOH were added so that the organic and aqueous layers salted out. A small amount of MeOH was added to mix the resulting layers, and the reaction mixture was placed on a rotary evaporator to remove volatiles. The reaction mixture was heated at 50 °C for 1 h, while under reduced pressure. The reaction mixture was allowed to cool to room temperature and was acidified with HCl. The resulting precipitate was collected via vacuum filtration and washed with a small amount of cold DI water. The resulting crude solid was purified by column chromatography, using a gradient of 100% CH₂Cl₂ to 15% MeOH in

CH₂Cl₂. The desired product eluted in 7-10% MeOH in CH₂Cl₂. Fractions containing the desired product were concentrated under reduced pressure to obtain **2.35** (0.040 g, 0.18 mmol, 25%) in 25 % yield as a yellow solid. ¹HNMR (400 MHz, DMSO-*d*₆) δ : 9.10 (s, 1H), 8.82 (d, *J* = 8.4 Hz, 1H), 7.96 – 7.89 (m, 2H), 7.72 (t, *J* = 8.0 Hz, 1H); ESI-MS(+): *m/z* 220.33 [M+H]⁺, 242.35 [M+Na]⁺.

Ethyl 1-benzyl-4-oxo-1,4-dihydroquinoline-3-carboxylate (2.83): To a solution of ethyl 4-oxo-1,4-dihydroquinoline-3-carboxylate (0.20 g, 0.92 mmol) in 15 mL dry DMF, potassium carbonate (0.25 g, 1.84 mmol) and benzyl bromide (0.44 mL, 3.68 mmol) were added sequentially. The reaction mixture was heated at 80 °C for 16 h. Then the reaction mixture was allowed to cool to room temperature, and was concentrated under reduced pressure. The resulting residue was and purified by column chromatography, using a gradient of 100% CH₂Cl₂ to 10% MeOH in CH₂Cl₂. The desired product eluted in two peaks: the first in 100% CH₂Cl₂, and the second in 10% MeOH in CH₂Cl₂. Fractions containing the desired product were concentrated under reduced pressure to obtain **2.83** (0.27 g, 0.88 mmol, 96%) as a light yellow, crystalline solid. ¹HNMR (400 MHz, DMSO-*d*₆) δ : 8.92 (s, 1H), 8.24 (dd, *J*₁ = 8.0 Hz, *J*₂ = 1.2 Hz, 1H), 7.67 – 7.60 (m, 2H), 7.43 – 7.22 (m, 6H), 5.68 (s, 2H), 4.23 (q, *J* = 7.2 Hz, 2H), 1.28 (t, *J* = 7.2 Hz, 3H); ESI-MS(+): *m/z* 308.36 [M+H]⁺, 330.39 [M+Na]⁺.

Ethyl 1-benzyl-4-thioxo-1,4-dihydroquinoline-3-carboxylate (2.84): Compound **2.83** (0.21 g, 0.67 mmol) and P₄S₁₀ (0.37 g, 1.67 mmol) were dissolved in 10 mL pyridine, and the reaction mixture was heated to reflux at 120 °C for 16 h. Then the reaction mixture was allowed to cool to room temperature and was concentrated under reduced pressure. The resulting residue was

purified by crude by column chromatography, using a gradient of 100% hexanes to 100% ethyl acetate, and then from 100% CH₂Cl₂ to 15% MeOH in CH₂Cl₂. The desired product eluted in both 70% ethyl acetate in hexanes to 100% ethyl acetate, as well as in 10% MeOH in CH₂Cl₂. Fractions containing the desired product were concentrated under reduced pressure to obtain **2.84** (0.20 g, 0.60 mmol, 90%) as an orange, slightly smelly solid. ¹HNMR (400 MHz, DMSO-*d*₆) δ : 8.81 (d, *J* = 8.0 Hz, 1H), 8.63 (d, *J* = 2.0 Hz, 1H), 7.78 – 7.70 (m, 2H), 7.51 (t, *J* = 8.0 Hz, 1H), 7.38 – 7.24 (m, 5H), 5.72 (s, 2H), 4.28 (dq, *J*₁ = 7.2 Hz, *J*₂ = 2.4 Hz, 2H), 1.30 (dt, *J*₁ = 7.2 Hz, *J*₂ = 2.4 Hz, 3H); ESI-MS(+): *m/z* 324.33 [M+H]⁺, 346.26 [M+Na]⁺.

1-Benzyl-4-thioxo-1,4-dihydroquinoline-3-carboxylic acid (2.36): To a solution of **2.84** (0.18 g, 0.56 mmol) in 5 mL THF, 6 mL of 1 M NaOH were added so that the organic and aqueous layers salted out. A small amount of MeOH was added to mix the resulting layers, and the reaction mixture was placed on a evaporator to remove volatiles. The reaction mixture was heated at 50 °C for 1 h, while under reduced pressure. The reaction mixture was allowed to cool to room temperature and was acidified with HCl. The resulting precipitate was collected via vacuum filtration and washed with a small amount of cold DI water. The resulting crude solid was purified by column chromatography, using a gradient of 100% CH₂Cl₂ to 15% MeOH in CH₂Cl₂. The desired product eluted in 7-10% MeOH in CH₂Cl₂. Fractions containing the desired product were concentrated under reduced pressure to obtain **2.36** (0.10 g, 0.34 mmol, 67%) as a yellow solid. ¹HNMR (400 MHz, DMSO-*d*₆) δ : 9.45 (s, 1H), 8.92 (dd, *J*₁ = 8.4 Hz, *J*₂ = 1.2 Hz, 1H), 7.97 (d, *J* = 8.8 Hz, 1H), 7.89 (dt, *J*₁ = 7.2 Hz, *J*₂ = 1.6 Hz, 1H), 7.70 (dt, *J*₁ = 7.2 Hz, *J*₂ = 1.2 Hz, 1H), 7.37 – 7.28 (m, 5H), 5.99 (s, 2H); ESI-MS(+): *m/z* 296.26 [M+H]⁺, 318.24 [M+Na]⁺.

IC₅₀ of Select Compounds

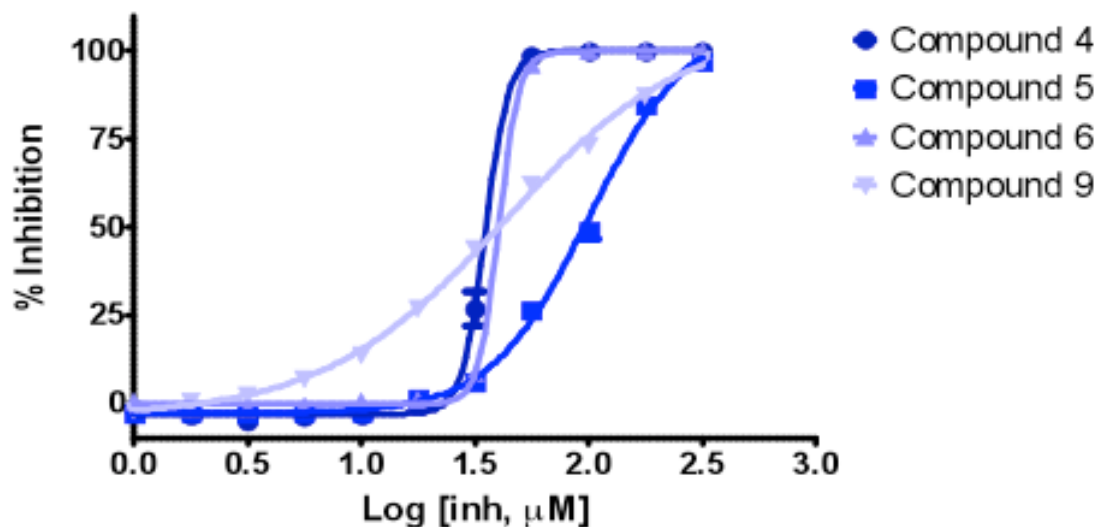


Figure 2.5. Dose-response curve of compounds **2.4**, **2.5**, **2.6**, and **2.9** against NDM-1. This plot was fit using Graphpad Prism, using four-variable response parameters to determine IC₅₀ values.

Preparation of Zn(Tp^{Ph,Me}) Complexes

Synthesis and Crystallization of Zn(Tp^{Ph,Me}) Model Complexes. Compound **2.9** (0.025 g, 0.15 mmol) and [Zn(Tp^{Ph,Me}) OH] (0.085 g, 0.15 mmol) were dissolved in 15 mL of CH₂Cl₂ with 10 mL MeOH. The reaction mixture was stirred overnight under a nitrogen atmosphere at room temperature. The resulting mixture was concentrated to dryness via rotary evaporation and dissolved in a minimal amount of benzene, approximately 5 mL. If benzene was not sufficient to dissolve the majority of solid, a minimal amount of methanol, up to 5 mL was added. The solution was filtered via vacuum filtration to remove any un-dissolved solids. The resulting filtrate was recrystallized using vapor diffusion with pentane; crystals typically formed within 2-3 days.

Single X-ray Diffraction Crystallography. Suitable crystals of $[\text{Zn}(\text{Tp}^{\text{Ph,Me}})]$ complexes were selected and placed on either a Bruker APEX-II Ultra diffractometer with a Mo-K α Microfocus Rotating Anode and a APEX-II CCD area detector or a Bruker Kappa diffractometer equipped with a Bruker X8 APEX II Mo sealed tube and a Bruker APEX-II CCD. The crystals were kept at 100 K using a liquid nitrogen cold stream during data collection. Diffraction data was integrated, scaled and merged within the APEXIII software suite (Bruker, 2017). Structure solution and refinement was performed within Olex2.⁵¹ Structure solution was performed using the ShelXT⁵² structure solution program using Direct Methods and the resulting structure was refined with the XL⁵³ refinement package using Least Squares minimization. The crystal data files of all complexes were deposited into the Cambridge Crystallographic Data Centre (CCDC) and assigned a number (Table 2.3). Crystallographic data collection and refinement information is listed in Table 2.3.

Table 2.3. Crystal data and structure refinement for [(Tp^{Ph,Me})Zn] model complexes.

Compound	Tp ^(Ph,Me) Zn(2.4)	Tp ^(Ph,Me) Zn(2.9)	Tp ^(Ph,Me) Zn(2.14)
Identification code	1843245	1843243	1843244
Empirical formula	C ₃₆ H ₃₅ BN ₈ O ₃ S ₂ Zn	C ₃₆ H ₃₂ BN ₉ OSZn	C ₃₄ H ₃₁ BN ₈ OSZn
Formula weight	768.02	714.94	675.91
Temperature/K	100.0	100.0	100.0
Crystal system	monoclinic	monoclinic	monoclinic
Space group	P2 ₁ /n	P2 ₁ /c	P2 ₁ /c
a/Å	14.511(2)	12.7513(9)	13.8778(9)
b/Å	16.314(3)	23.7763(17)	10.8790(7)
c/Å	16.703(3)	21.6147(16)	21.2351(14)
α/°	90	90	90
β/°	115.232(2)	90.351(2)	91.493(2)
γ/°	90	90	90
Volume/Å ³	3576.7(10)	6553.0(8)	3204.9(4)
Z	4	8	4
ρ _{calc} /cm ³	1.426	1.449	1.401
μ/mm ⁻¹	0.852	0.860	0.873
F(000)	1592.0	2960.0	1400.0
Crystal size/mm ³	0.25 × 0.2 × 0.06	0.35 × 0.35 × 0.18	0.3 × 0.08 × 0.03
Radiation	MoKα (λ = 0.71073)	MoKα (λ = 0.71073)	MoKα (λ = 0.71073)
2θ range for data collection/°	3.982 to 51.424	2.546 to 52.036	2.936 to 52.042
Index ranges	-17 ≤ h ≤ 15, -19 ≤ k ≤ 19, -20 ≤ l ≤ 20	-15 ≤ h ≤ 15, -29 ≤ k ≤ 29, -26 ≤ l ≤ 24	-17 ≤ h ≤ 17, -13 ≤ k ≤ 13, -24 ≤ l ≤ 26
Reflections collected	24862	77364	44326
Independent reflections	6819 [R _{int} = 0.0541, R _{sigma} = 0.0545]	12911 [R _{int} = 0.0475, R _{sigma} = 0.0339]	6321 [R _{int} = 0.0574, R _{sigma} = 0.0360]
Data/restraints/parameters	6819/0/464	12911/0/889	6321/0/418
Goodness-of-fit on F ²	1.023	1.025	0.849
Final R indexes [I ≥ 2σ (I)]	R ₁ = 0.0379, wR ₂ = 0.0794	R ₁ = 0.0322, wR ₂ = 0.0766	R ₁ = 0.0307, wR ₂ = 0.0970
Final R indexes [all data]	R ₁ = 0.0573, wR ₂ = 0.0871	R ₁ = 0.0491, wR ₂ = 0.0850	R ₁ = 0.0433, wR ₂ = 0.1108
Largest diff. peak/hole / e Å ⁻³	0.51/-0.40	0.34/-0.40	0.45/-0.41

2.6 Acknowledgements

Chapter 2, in large part, is a reprint of materials published in the following paper: Isosteres of Hydroxypyridinethione as Druglike Pharmacophores for Metalloenzyme Inhibition, Adamek, R.N.; Credille, C.V.; Dick, B.L.; Cohen, S.M.; *J. Biol. Inorg. Chem.* **2018**, *23*, 1129-1138. DOI: 10.1007/S00775-018-1593-1. The dissertation author was the primary researcher and the primary author for the reprinted data presented herein. Reprinted with permission from Journal of Biological Inorganic Chemistry. Copyright 2018 Springer Nature.

2.7 References

1. Holm, R. H.; Kennepohl, P.; Solomon, E. I., Structural and Functional Aspects of Metal Sites in Biology. *Chem. Rev.* **1996**, *96*, 2239-2314.
2. Andreini, C.; Bertini, I.; Cavallaro, G.; Holliday, G. L.; Thornton, J. M., Metal Ions in Biological Catalysis: from Enzyme Databases to General Principles. *J. Biol. Inorg. Chem.* **2008**, *13*, 1205-1218.
3. Waldron, K. J.; Rutherford, J. C.; Ford, D.; Robinson, N. J., Metalloproteins and Metal Sensing. *Nature* **2009**, *460* (7257), 823-30.
4. Yang, Y.; Hu, X. Q.; Li, Q. S.; Zhang, X. X.; Ruan, B. F.; Xu, J.; Liao, C. Z., Metalloprotein Inhibitors for the Treatment of Human Diseases. *Curr. Top. Med. Chem.* **2016**, *16*, 384-396.
5. Moellering, R. C., NDM-1 - A Cause for Worldwide Concern. *New Engl. J. Med.* **2010**, *363*, 2377-2379.
6. Ju, H.; Zhang, J.; Huang, B. S.; Kang, D. W.; Huang, B.; Liu, X. Y.; Zhan, P., Inhibitors of Influenza Virus Polymerase Acidic (PA) Endonuclease: Contemporary Developments and Perspectives. *J. Med. Chem.* **2017**, *60*, 3533-3551.
7. Agrawal, A.; Johnson, S. L.; Jacobsen, J. A.; Miller, M. T.; Chen, L. H.; Pellecchia, M.; Cohen, S. M., Chelator Fragment Libraries for Targeting Metalloproteinases. *Chemmedchem* **2010**, *5*, 195-199.
8. Kubec, R.; Krejcova, P.; Simek, P.; Vaclavik, L.; Hajslova, J.; Schraml, J., Precursors and Formation of Pyrithione and Other Pyridyl-Containing Sulfur Compounds in Drumstick Onion, *Allium stipitatum*. *J. Agr. Food Chem.* **2011**, *59*, 5763-5770.

9. Puerta, D. T.; Lewis, J. A.; Cohen, S. M., New Beginnings for Matrix Metalloproteinase Inhibitors: Identification of High-Affinity Zinc-Binding Groups. *J. Am. Chem. Soc.* **2004**, *126*, 8388-8389.
10. Dinning, A. J.; Al-Adham, I. S. I.; Eastwood, I. M.; Austin, P.; Collier, P. J., Pyrithione Biocides as Inhibitors of Bacterial ATP Synthesis. *J. Appl. Microbiol.* **1998**, *85*, 141-146.
11. Schwartz, J. R., Zinc Pyrithione: A Topical Antimicrobial With Complex Pharmaceutics. *J. Drugs Dermatol.* **2016**, *15*, 140-144.
12. Konstantinou, I. K.; Albanis, T. A., Worldwide Occurrence and Effects of Antifouling Paint Booster Biocides in the Aquatic Environment: A Review. *Environ. Int.* **2004**, *30*, 235-248.
13. Jakupec, M. A.; Galanski, M.; Arion, V. B.; Hartinger, C. G.; Keppler, B. K., Antitumour Metal Compounds: more than Theme and Variations. *Dalton T.* **2008**, (2), 183-194.
14. Summa, V.; Petrocchi, A.; Bonelli, F.; Crescenzi, B.; Donghi, M.; Ferrara, M.; Fiore, F.; Gardelli, C.; Paz, O. G.; Hazuda, D. J.; Jones, P.; Kinzel, O.; Laufer, R.; Monteagudo, E.; Muraglia, E.; Nizi, E.; Orvieto, F.; Pace, P.; Pescatore, G.; Scarpelli, R.; Stillmock, K.; Witmer, M. V.; Rowley, M., Discovery of Raltegravir, a Potent, Selective Orally Bioavailable HIV-Integrase Inhibitor for the Treatment of HIV-AIDS Infection. *J. Med. Chem.* **2008**, *51*, 5843-5855.
15. Gunthard, H. F.; Saag, M. S.; Benson, C. A.; del Rio, C.; Eron, J. J.; Gallant, J. E.; Hoy, J. F.; Mugavero, M. J.; Sax, P. E.; Thompson, M. A.; Gandhi, R. T.; Landovitz, R. J.; Smith, D. M.; Jacobsen, D. M.; Volberding, P. A., Antiretroviral Drugs for Treatment and Prevention of HIV Infection in Adults 2016 Recommendations of the International Antiviral Society-USA Panel. *Jama-J. Am. Med. Assoc.* **2016**, *316*, 191-210.
16. Cushman, D. W.; Ondetti, M. A., Design of Angiotensin Converting Enzyme Inhibitors. *Nat. Med.* **1999**, *5*, 1110-1112.
17. Pfeffer, M. A.; Braunwald, E.; Moye, L. A.; Basta, L.; Brown, E. J.; Cuddy, T. E.; Davis, B. R.; Geltman, E. M.; Goldman, S.; Flaker, G. C.; Klein, M.; Lamas, G. A.; Packer, M.; Rouleau, J.; Rouleau, J. L.; Rutherford, J.; Wertheimer, J. H.; Hawkins, C. M., Effect of Captopril on Mortality and Morbidity in Patients with Left-Ventricular Dysfunction after Myocardial-Infarction - Results of the Survival and Ventricular Enlargement Trial. *New Engl. J. Med.* **1992**, *327*, 669-677.
18. Lewis, E. J.; Hunsicker, L. G.; Bain, R. P.; Rohde, R. D., The Effect of Angiotensin-Converting Enzyme-Inhibition on Diabetic Nephropathy. *New Engl. J. Med.* **1993**, *329*, 1456-1462.
19. Baell, J.; Walters, M. A., Chemistry: Chemical Con Artists Foil Drug Discovery. *Nature* **2014**, *513*, 481-483.
20. Chen, Y.; Cohen, S. M., Investigating the Selectivity of Metalloenzyme Inhibitors in the Presence of Competing Metalloproteins. *Chemmedchem* **2015**, *10*, 1733-1738.

21. Day, J. A.; Cohen, S. M., Investigating the Selectivity of Metalloenzyme Inhibitors. *J. Med. Chem.* **2013**, *56*, 7997-8007.
22. Kinch, M. S.; Haynesworth, A.; Kinch, S. L.; Hoyer, D., An Overview of FDA-Approved New Molecular Entities: 1827-2013. *Drug discovery today* **2014**, *19*, 1033-1039.
23. Yang, Y.; Hu, X.-Q.; Li, Q.-S.; Zhang, X.-X.; Ruan, B.-F.; Xu, J.; Liao, C., Metalloprotein Inhibitors for the Treatment of Human Diseases. *Curr. Top. Med. Chem.* **2016**, *16*, 384-396.
24. Britten, C. D.; Rowinsky, E. K.; Soignet, S.; Patnaik, A.; Yao, S. L.; Deutsch, P.; Lee, Y.; Lobell, R. B.; Mazina, K. E.; McCreery, H.; Pezzuli, S.; Spriggs, D., A Phase I and Pharmacological Study of the Farnesyl Protein Transferase Inhibitor L-778,123 in Patients with Solid Malignancies. *Clin Cancer Res* **2001**, *7* (12), 3894-3903.
25. Sebti, S. M.; Hamilton, A. D., Farnesyltransferase and Geranylgeranyltransferase I Inhibitors and Cancer Therapy: Lessons from Mechanism and Bench-to-Bedside Translational Studies. *Oncogene* **2000**, *19* (56), 6584-6593.
26. Jones, R. A.; Katritzky, A. R., N-Oxides and Related Compounds .17. The Tautomerism of Mercapto-Pyridine and Acylamino-Pyridine 1-Oxides. *J. Chem. Soc.* **1960**, (Jul), 2937-2942.
27. Turley, P. A.; Fenn, R. J.; Ritter, J. C., Pyrithiones as Antifoulants: Environmental Chemistry and Preliminary Risk Assessment. *Biofouling* **2000**, *15*, 175-182.
28. Pearson, R. G., Hard and Soft Acids and Bases. *J. Am. Chem. Soc.* **1963**, *85*, 3533-3539.
29. Pearson, R. G., Hard and Soft Acids and Bases HSAB.1. Fundamental Principles. *J. Chem. Educ.* **1968**, *45* (9), 581-587.
30. Martin, D. P.; Cohen, S. M., Nucleophile Recognition as an Alternative Inhibition Mode for Benzoic Acid Based Carbonic Anhydrase Inhibitors. *Chem. Commun.* **2012**, *48*, 5259-5261.
31. Credille, C. V.; Chen, Y.; Cohen, S. M., Fragment-Based Identification of Influenza Endonuclease Inhibitors. *J. Med. Chem.* **2016**, *59*, 6444-6454.
32. Schonherr, D.; Wollatz, U.; Haznar-Garbacz, D.; Hanke, U.; Box, K. J.; Taylor, R.; Ruiz, R.; Beato, S.; Becker, D.; Weitschies, W., Characterisation of Selected Active Agents Regarding pK(a) Values, Solubility Concentrations and pH Profiles by SiriusT3. *Eur. J. Pharm. Biopharm.* **2015**, *92*, 155-170.
33. Slater, B.; McCormack, A.; Avdeef, A.; Comer, J. E. A., pH-Metric Log P .4. Comparison of Partition-Coefficients Determined by HPLC and Potentiometric Methods to Literature Values. *J. Pharm. Sci.* **1994**, *83*, 1280-1283.
34. Lipinski, C. A.; Lombardo, F.; Dominy, B. W.; Feeney, P. J., Experimental and computational approaches to estimate solubility and permeability in drug discovery and development settings. *Adv. Drug Deliver. Rev.* **2001**, *46*, 3-26.

35. Veber, D. F.; Johnson, S. R.; Cheng, H. Y.; Smith, B. R.; Ward, K. W.; Kopple, K. D., Molecular Properties that Influence the Oral Bioavailability of Drug Candidates. *J. Med. Chem.* **2002**, *45*, 2615-2623.
36. Clark, D. E.; Pickett, S. D., Computational methods for the prediction of 'drug-likeness'. *Drug discovery today* **2000**, *5*, 49-58.
37. Congreve, M.; Carr, R.; Murray, C.; Jhoti, H., A Rule of Three for Fragment-Based Lead Discovery? *Drug discovery today* **2003**, *8*, 876-877.
38. Lassalas, P.; Gay, B.; Lasfargeas, C.; James, M. J.; Tran, V.; Vijayendran, K. G.; Brunden, K. R.; Kozlowski, M. C.; Thomas, C. J.; Smith, A. B.; Huryn, D. M.; Ballatore, C., Structure Property Relationships of Carboxylic Acid Isosteres. *J. Med. Chem.* **2016**, *59*, 3183-3203.
39. Hughes, J. D.; Blagg, J.; Price, D. A.; Bailey, S.; DeCrescenzo, G. A.; Devraj, R. V.; Ellsworth, E.; Fobian, Y. M.; Gibbs, M. E.; Gilles, R. W.; Greene, N.; Huang, E.; Krieger-Burke, T.; Loesel, J.; Wager, T.; Whiteley, L.; Zhang, Y., Physicochemical drug properties associated with in vivo toxicological outcomes. *Bioorg. Med. Chem. Lett.* **2008**, *18*, 4872-4875.
40. Puerta, D. T.; Cohen, S. M., Examination of Novel Zinc-Binding Groups for Use in Matrix Metalloproteinase Inhibitors. *Inorg. Chem.* **2003**, *42*, 3423-3430.
41. Martin, D. P.; Blachly, P. G.; McCammon, J. A.; Cohen, S. M., Exploring the Influence of the Protein Environment on Metal-Binding Pharmacophores. *J. Med. Chem.* **2014**, *57*, 7126-7135.
42. Supuran, C. T.; Scozzafava, A.; Casini, A., Carbonic Anhydrase Inhibitors. *Med. Res. Rev.* **2003**, *23*, 146-189.
43. Overall, C. M.; Lopez-Otin, C., Strategies for MMP inhibition in cancer: Innovations for the post-trial era. *Nat. Rev. Cancer* **2002**, *2*, 657-672.
44. Scozzafava, A.; Owa, T.; Mastrolorenzo, A.; Supuran, C. T., Anticancer and antiviral sulfonamides. *Curr. Med. Chem.* **2003**, *10*, 925-953.
45. Rotondo, C. M.; Wright, G. D., Inhibitors of Metallo-Beta-Lactamases. *Curr Opin Microbiol* **2017**, *39*, 96-105.
46. Nordmann, P.; Poirel, L.; Walsh, T. R.; Livermore, D. M., The Emerging NDM Carbapenemases. *Trends Microbiol.* **2011**, *19* (12), 588-95.
47. Kim, Y.; Cunningham, M. A.; Mire, J.; Tesar, C.; Sacchettini, J.; Joachimiak, A., NDM-1, the Ultimate Promiscuous Enzyme: Substrate Recognition and Catalytic Mechanism. *FASEB J.* **2013**, *27* (5), 1917-27.

48. Thomas, P. W.; Zheng, M.; Wu, S. S.; Guo, H.; Liu, D. L.; Xu, D. G.; Fast, W., Characterization of Purified New Delhi Metallo-beta-lactamase-1. *Biochemistry-US* **2011**, *50* (46), 10102-10113.
49. Yuan, P.; Bartlam, M.; Lou, Z.; Chen, S.; Zhou, J.; He, X.; Lv, Z.; Ge, R.; Li, X.; Deng, T.; Fodor, E.; Rao, Z.; Liu, Y., Crystal Structure of an Avian Influenza Polymerase PA(N) Reveals an Endonuclease Active Site. *Nature* **2009**, *458*, 909-13.
50. Crepin, T.; Dias, A.; Palencia, A.; Swale, C.; Cusack, S.; Ruigrok, R. W. H., Mutational and Metal Binding Analysis of the Endonuclease Domain of the Influenza Virus Polymerase PA Subunit. *J. Virol.* **2010**, *84*, 9096-9104.
51. Dolomanov, O. V.; Bourhis, L. J.; Gildea, R. J.; Howard, J. A. K.; Puschmann, H., OLEX2: A Complete Structure Solution, Refinement and Analysis Program. *J. Appl. Crystallogr.* **2009**, *42*, 339-341.
52. Sheldrick, G., Crystal Structure Refinement with SHELXL. *Acta Crystallogr., Sect. C* **2015**, *71*, 3-8.
53. Sheldrick, G., A Short History of SHELX. *Acta Crystallogr., Sect. A* **2008**, *64*, 112-122.

Chapter 3: Isosteres of Hydroxypyridinethione as Inhibitors of Human Insulin Degrading Enzyme

3.1 Introduction

As described in Chapter 2, a library of elaborated hydroxypyridine thione (HOPTO) small molecules had been previously prepared. This library had been characterized to have a broad range of pharmacokinetic properties, making it a useful starting point for drug discovery efforts against disease relevant metalloenzymes. To advance this work to useful applications, this elaborated HOPTO library was screened against the human metalloenzyme Insulin-Degrading Enzyme (IDE) as a proof-of-concept of the application of the HOPTO scaffold as a therapeutic agent. Excitingly, this screen revealed 1,2-HOPTO and the advanced 3-methylsulfonamide-1,2-HOPTO to have good activity against the IDE disease target. Further efforts to perform structural activity relationship (SAR) studies on this 3-methylsulfonamide-1,2-HOPTO scaffold lead to the discovery of a novel IDE inhibitor, with strong potential to be useful as a readily available tool compound in future IDE studies.

IDE is a very large ~118 kDa metalloenzyme (Figure 3.1), and is classified as cryptidase type enzyme, as it uses a clamshell-like mechanism to engulf substrate peptides within its abnormally large active site of 13,000 Å³.¹ IDE is comprised of a positively charged N-domain linked to a negatively charged C-domain, with the catalytic Zn²⁺ motif nestled deep within the interior of the N-Domain, where the metal site is used to hydrolyze the various IDE peptide substrates.¹ To aid in substrate binding, IDE utilizes an exosite approximately 30 Å away from the catalytic site to anchor the N-terminus domain of the various IDE substrates and facilitate substrate unfolding.²⁻³ IDE has both open and closed conformational states, but preferentially exists in the open state for more rapid substrate capture.³ Mechanistically, IDE is believed to operate by first enveloping its peptide substrates, and upon complete enclosure of the substrate, hydrolysis occurs.²⁻³ In the case of insulin substrate, IDE is able to perform multiple peptide

cleavages without impacting the disulfide bonds that hold the hormone peptide together.² Upon cleavage of the substrate, IDE re-opens to release the hydrolyzed products, and the cycle begins anew.²⁻³ Considering the large size of IDE, and the energy it must take to open and close, there has been speculation as to whether IDE requires ATP to complete its mechanism. Studies on this matter showed that ATP only improved the activity of IDE against short peptides, and that ATP does not aid in degrading the larger IDE substrates such as insulin and amyloid- β .⁴⁻⁵

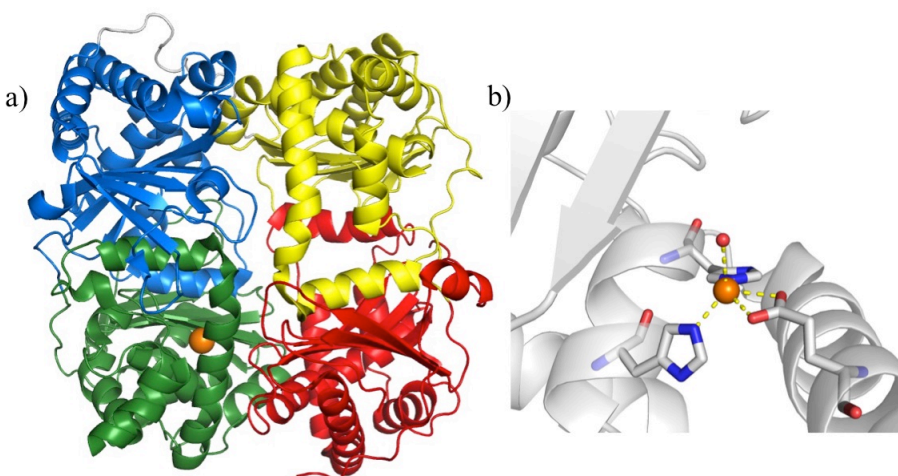


Figure 3.1. The structure of IDE. a) The entirety of IDE, with the N-Domain in blue and green, and the C-Domain in yellow and red, with the connecting hinge in white; b) Close-up of the buried catalytic Zn²⁺ and metal coordinating residues within the IDE active site, with Zn²⁺ shown as an orange sphere, water as a red sphere, and coordination bonds as yellow dashes.

At the time of its discovery, IDE was originally miscategorized as a Cys-dependent protease, as IDE was found to be inactivated by Cys-targeting inhibitors. It is now known that these Cys residues are utilized to maintain structural integrity,⁶ and that IDE instead belongs to the inverzinc family of metalloproteases. The catalytic Zn²⁺ necessary for enzymatic activity is coordinated by His111, His107, and Glu188, with an axial bound water to complete the tetrahedral coordination geometry of the metal center (Figure 3.1).¹

IDE is found across all domains of life, but within humans, misregulation of this mononuclear Zn^{2+} metalloenzyme has been implicated in both diabetes and neurodegeneration.⁴

⁷ While the biological roles of IDE are not yet fully understood, this metalloenzyme is known to be distributed throughout the body, and is found in both the intra- and extra-cellular domains.⁸ IDE functions to hydrolyze a broad range of hormonal peptides, yet paradoxically only hydrolyzes certain members of these disparate peptide families (Figure 3.2).¹ Chief among the known IDE substrates are insulin, glucagon, amylin, and amyloid- β .⁹⁻¹⁰ Of these amylin, insulin, and glucagon are relevant to the diabetes type 2 mellitus as amylin promotes satiety,¹¹ and insulin and glucagon work in tandem to down- and up-regulate blood glucose respectively.¹² Additionally, amyloid- β has been well established as a primary component of Alzheimer's Disease, making study of IDE of high relevance to AD pathogenesis.¹³⁻¹⁴

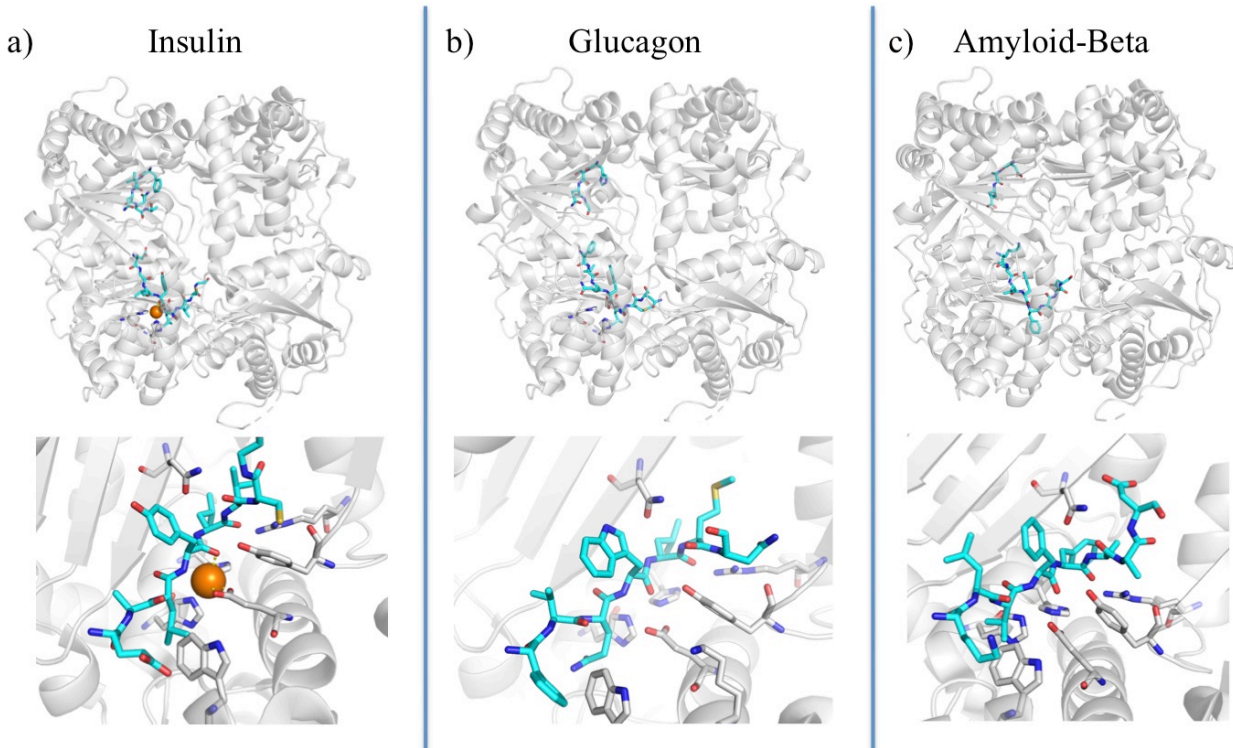


Figure 3.2. Demonstration of the paradoxical ability of IDE to bind and hydrolyze a broad range of substrates, as exemplified by Insulin (a), Glucagon (b), and amyloid- β (c).¹ The full structure of IDE bound to each substrate is shown on the top, with a close-up of the catalytic site below. For glucagon and amyloid- β , the apo-IDE was used so as to prevent substrate hydrolysis. PDB 2G54, 2G49, and 2G47 respectively.

Considering the relevance of IDE to various disease states, there has been great interest in developing substrate selective inhibitors of IDE,¹⁵ with particular emphasis on the development of tool compounds to tease out the different biological roles of IDE in relation to its various substrates. Among the more sought after-goals related to IDE are compounds that act as activators in respect to amyloid- β degradation, as a means to decrease levels of this AD progenitor protein.¹³⁻¹⁴ Additionally, there is particular interest in the discovery of compounds that inhibit insulin degradation, while retaining IDE activity against its other substrates. Such a strategy would be high relevance towards Type 2 Diabetes, as the resulting theoretical increased levels of insulin would serve to down-regulate blood glucose and prevent blood sugar spikes.^{4, 16-}

¹⁷ Conversely, selective inhibitors of either glucagon or amylin are presently not considered as useful from a disease treatment perspective, but would still see great value as tool compounds to aid in evaluating the biological roles of IDE. However, inhibition of IDE, let alone substrate selective, has remained a lofty goal. Of the reported IDE inhibitors, most are peptide based, and bind at an allosteric location dubbed the exo-site, far removed from the catalytic Zn^{2+} (Figure 3.3). There was recently one small molecule inhibitor reported that is both potent and selective for IDE inhibition of insulin hydrolysis, and is currently considered the best in class inhibitor (Figure 3.3);¹⁵ however, this compound has yet to be examined in cellular studies, so that its clinical efficacy has yet to be determined.

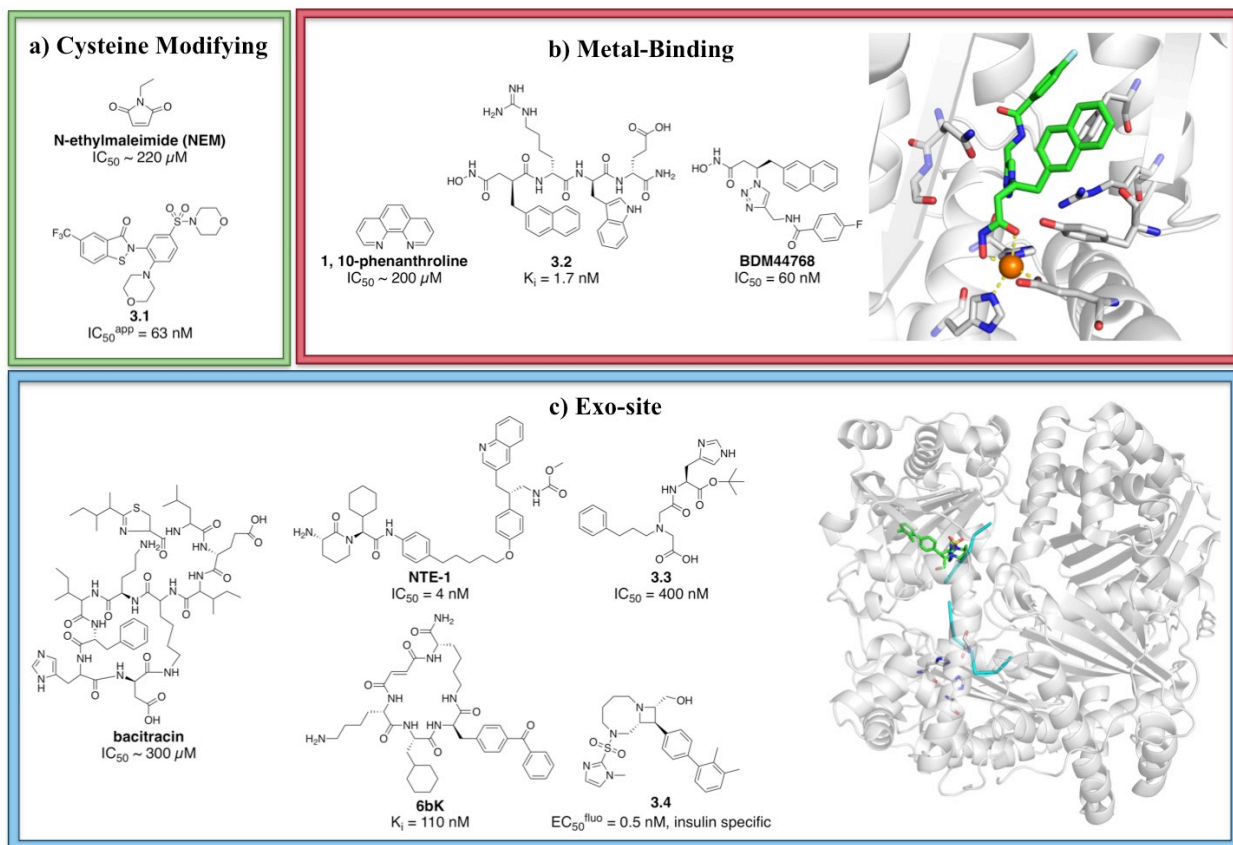


Figure 3.3. Structures and inhibition values of all reported IDE inhibitors.^{15, 18-25} a) Cysteine modifying IDE inhibitors. b) Metal-binding IDE inhibitors, with inset showing crystal structure of hydroxamate-based **3.2** coordinating to the active site Zn²⁺.¹⁸ c) Exo-site binding IDE inhibitors, with inset showing crystal structure of **3.4** bound to the IDE exo-site, with insulin co-crystallized in cyan.¹⁵

Metal-binding inhibitors of IDE have the potential to provide alternative avenues of IDE inhibition, but such classes of inhibitor have not been thoroughly explored against this disease target. There has been a dearth of metal-binding IDE inhibitors explored, with only two hydroxamic acid peptide compounds, and 1,4-phenanthroline reported (Figure 3.3).¹⁸⁻¹⁹ Hydroxamic acids are known to have potential issues with selectivity and metabolism into toxic by-products, and 1,4-phenanthroline is a known metal-stripping agent, which represents a poor strategy for metalloenzyme inhibition. To develop new inhibitors against IDE, an MBP library,

as described in Chapter 1, was screened for IDE inhibition against a set of biologically relevant IDE substrates, including insulin, glucagon, amylin, amyloid- β , as well as Substrate V. Substrate V is a synthetic fluorescent peptide, designed to recapitulate the structure of a shortened form of amyloid- β , and is therefore often included in IDE inhibitor screenings.²⁶ Screening of this MBP library lead to the discovery of 1,2-hydroxypyridine thione (1,2-HOPTO) as a fragment lead against IDE. Considering the efforts described in Chapter 2 towards elaboration of the HOPTO scaffold, it was decided to focus on screening this sublibrary against IDE. Excitingly, the 3-methylsulfonamide-1,2-HOPTO derivative displayed broad-spectrum activity against the various IDE substrates. As this compound features a relatively rapid and facile synthesis (see Experimental, Chapter 2), it has the potential to serve as a useful tool compound in future IDE studies.

3.2 Results and Discussion

Screening of the MBP Library

In an effort to broaden the scope of available MBP inhibitors for metalloenzymes, we have developed a ~350 component library of small molecules each bearing a unique metal-binding group.²⁷⁻²⁸ To identify MBPs with the potential for inhibitor development against IDE, this library was screened against IDE, testing for inhibition against the degradation of several key biological IDE substrates, including insulin, glucagon, amylin, and amyloid- β , as well as the synthetic Substrate V. Screening was conducted in a 96-wellplate format, with each compound initially tested at 200 μ M, yielding ~14 compounds with >50% inhibition at this concentration. Of these compounds, 1,2-HOPTO emerged as an early lead with an average $K_i = 86 \mu$ M against the evaluated substrates, and was selected for further SAR study.

Screening of Elaborated HOPTO Sublibrary

HOPTOs are a known class of powerful metal-ligands, particularly suited for Zn^{2+} binding based on hard-soft acid-base theory.²⁹⁻³⁰ They have been established to have bidentate-binding through a set of oxygen and sulfur donor atoms, where the sulfur has been demonstrated to exist predominately in the thione isomer.³¹ This preferred thione isomer is highly relevant, as free thiols have the propensity to cause off-target effects, whereas the sp^2 hybridized thione does not feature the same metabolic liabilities. In an effort to broaden the utility of HOPTOs as warheads for metalloenzyme inhibition, an expanded library of HOPTO derivatives was prepared and demonstrated to have druglike qualities while maintaining the core metal-binding capacities, as described in Chapter 2 of this thesis. As 1,2-HOPTO was an early lead for broad spectrum IDE inhibition, it was decided to employ this elaborated HOPTO sublibrary against IDE to better optimize the MBP warhead before pursuing furthering inhibitor elaboration. Screening of this elaborated HOPTO sublibrary revealed both 3-sulfonamide-1,2-HOPTO (**2.4**) and isoquinoline-1,2-HOPTO (**2.6**) to have improved inhibition activity at $K_i \sim 50 \mu\text{M}$ for both compounds. It was decided to pursue **2.4** for further use against IDE as **2.4** had better aqueous solubility compared to **2.6**.

Modeling of 2.4 in the IDE Active Site

The lead fragment **2.4** has been previously crystallized in a model Zinc hydrotris(3,5-phenylmethylpyrazolyl)borate $[(\text{Tp}^{\text{Ph,Me}})\text{Zn}(\mathbf{2.4})]$ complex, demonstrating a preferred Zn^{2+} metal-coordination through donor atoms of an axial thione and equatorial hydroxyl.³² Additionally, there have been previously reported crystal structures of hydroxamic acid based inhibitors of

IDE, showing that these compounds bind the IDE Zn^{2+} through axial carbonyl and equatorial hydroxyl.¹⁸ Considering the 1,2-HOPTO MBP core is a cyclized thione hydroxamic acid, the structure of hydroxamic acid **3.2** bound IDE was used to guide the modeling of **2.4** in the IDE active site. To prepare the in silico model, using Molecular Operating Environment (MOE), **2.4** from the crystal structure of $[(\text{Tp}^{\text{Ph,Me}})\text{Zn}(\mathbf{2.4})]$ was superposed over the hydroxamate of **3.2** bound the IDE Zn^{2+} by aligning the thione of **2.4** with the carbonyl of **3.2**, and the hydroxyl of **2.4** with the hydroxyl of **3.2**. This resulted in the model displayed in Figure 3.4, with compound **2.4** being predicted to bind IDE through the thione and hydroxyl donor atoms in a manner consistent with both the model $[(\text{Tp}^{\text{Ph,Me}})\text{Zn}(\mathbf{2.4})]$ and previous hydroxamic crystal structures.

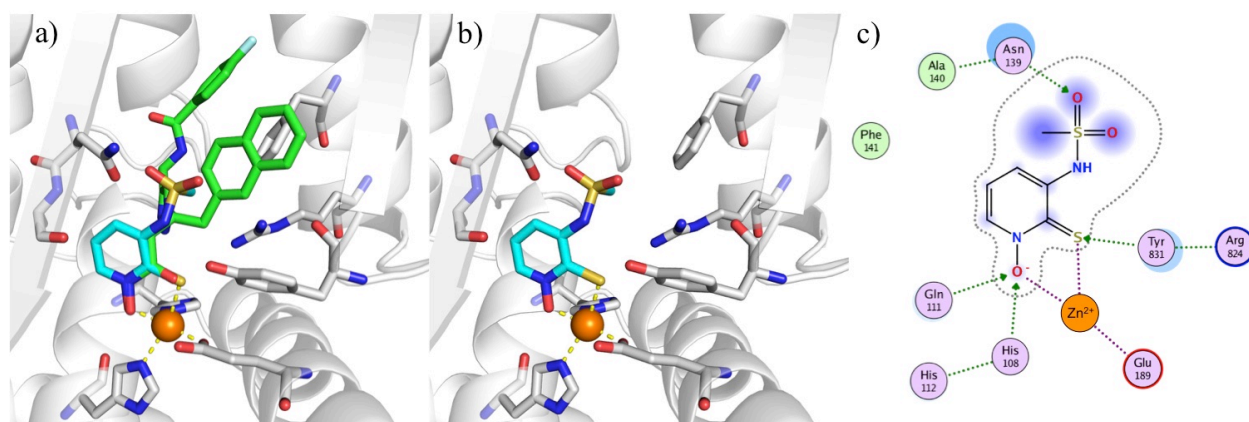
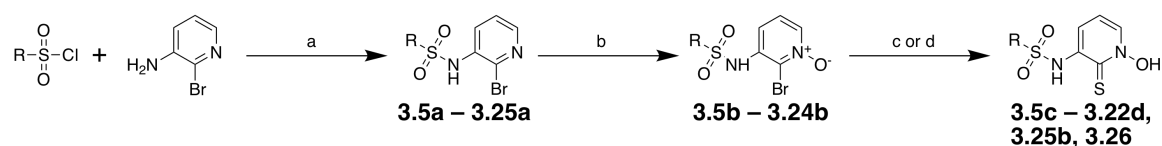


Figure 3.4. Model of **2.4** bound to the catalytic Zn^{2+} within the IDE active site. a) Superpose of **2.4** and **3.2**, which was used to create b) the center model of **2.4** bound to the Zn^{2+} in the IDE active site. c) A 2-D representation of the model, with Zn^{2+} in orange, coordination bonds as pink dashes, interactions as green arrows, and solvent exposed regions as blue spheres.

Synthesis and Elaboration of Sulfonamide HOPTO

To facilitate the use of these as sulfonamide derivatized HOPTOs as tool compounds, a readily adaptable and simple 3-step synthetic route amenable towards rapid derivatization was developed, as detailed in Scheme 3.1 below. Reacting the sulfonyl chloride of interest with the starting amine in a microwave reactor yielded the desired sulfonamide product. It was found that

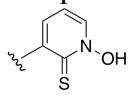
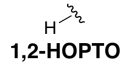
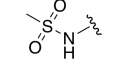
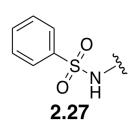
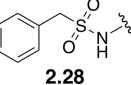
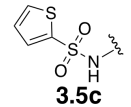
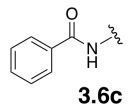
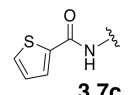
using excess amine relative to sulfonyl chloride aided in decreasing the amount of undesired disulfonamide product generated. This step is highly adaptable to a broad scope of both amine and sulfonyl chloride partners, as evidenced by the scope of sulfonamide HOPTOs prepared in this study. The subsequent step of oxidation using mCPBA achieves selective oxidation at the pyridinal nitrogen. It was also found that any disulfonamide product carried over into this step was easily separated by chromatographic methods. The final step of thionation was achieved by heating the oxidized product in a solution of freshly prepared saturated NaSH in the presence of KI. Quenching the reaction with HCl, and subsequent work-up of chromatography followed by recrystallization from IPA with varying amounts of H₂O yielded final HOPTO products. As a safety precaution, it is strongly recommended to use caution in quenching the NaSH solution with HCl, as highly toxic H₂S gas is released. This quench should be performed on ice and in a well-ventilated fume hood to ensure safety. In the case of the control compounds **3.25b** and **3.26**, thionation was instead achieved by heating the halogenated sulfonamide to reflux at 150 °C in DMF in the presence of excess thiourea. Finally, it is worth noting that the final HOPTO products were sometimes isolated as mixtures with the oxidized dimer through the sulfur atom. This dimer is easily reverted to back the active thione in the presence of DTT as a reductant (See Experimental Section 3.5, Figure 3.6). Considering IDE requires DTT in the assay buffer to ensure reduction of its 13 Cys residues, the DTT served the dual function of also ensuring the tested HOPTO species were in the active thione form.



Scheme 3.1. Synthesis of sulfonamide HOPTO derivatives. Reagents and conditions: a) sulfonyl chloride, pyridine, microwave irradiation, 120 °C, 15 min, 25 – 71%; b) mCPBA, CH₂Cl₂, MeOH, 25 – 35 °C, 16 – 72 h, 28 – 64%; c) sat. aq. NaSH, KI, MeOH, 50 – 100 °C, 4 – 16 h, 6 – 58%; d) thiourea, DMF, 150 °C, followed by 6 M HCl, 110 °C, 2 h, 22 – 40 %.

To further elaborate the lead **2.4**, it was decided to investigate the SAR of the sulfonamide moiety to explore other potential interactions within the active site. A precursory test of phenyl (**2.27**) and benzyl (**2.28**) derivatives showed some improvement relative to parent **2.4**, with **2.27** having an average $K_i = 21 \mu\text{M}$ against all of the tested substrates, and **2.28** having average $K_i = 33 \mu\text{M}$. Then utilizing an aromatic isostere replacement of the phenyl ring to a thiophene substituent yielded **5c** with a further improved average $K_i = 10 \mu\text{M}$.

Table 3.1. K_i values of parent HOPTO compounds against the various tested IDE substrates. Compounds **3.6c** and **3.7c** are included as amide variants of the sulfonamide.

Compound 	Insulin	Glucagon	Amylin	Amyloid- β	Substrate V	Average	Average without Substrate V
 1,2-HOPTO	-	-	-	-	-	86	-
 2.4	-	-	-	-	-	50	-
 2.27	19	9	28	13	36	21	17
 2.28	42	11	48	18	48	33	30
 3.5c	8	4	12	9	17	10	8
 3.6c	17	18	77	29	143	57	35
 3.7c	20	18	74	28	129	54	35

In addition, to validate the contribution of the sulfonamide to the overall activity of **3.5c**, amide controls **3.6c** and **3.7c** were prepared as respective analogs of **2.27** and **3.5c**. As shown in Table 3.1, **3.6c** had an average K_i of 57 μ M (35 μ M without substrate V) rendering **3.6c** ~2-3 times less active than **2.27**, and **3.7c** had an average K_i of 54 μ M (35 μ M without substrate V) making **3.7c** ~3 – 4 times less active than **3.5c**. As a whole, this data indicates that the sulfonamide moiety makes favorable interactions within the active site that are not achieved by the complementary amide derivatives.

Sulfonamide HOPTO SAR Analysis

In an effort to further improve the activity of the lead thiophene **3.5c**, **3.8c** – **3.22d** were synthesized (Scheme 3.1). The methyl derivative compounds **3.8c** – **3.11c**, were prepared to probe which positions would be amenable towards further elaboration. These methyl derivatives as a whole exhibited flat SAR with neither improvement nor loss in activity against IDE and the degradation of its substrates. Within the next set of tested alkyl substituents, cyclopropane **3.12c** had an average K_i of 39 μM , and showed higher levels of inhibition against degradation of glucagon and amylin with $K_i = 9 \mu\text{M}$ for each, and was slightly more sparing towards degradation of insulin and amyloid- β , with respective K_i values of 37 and 41 μM for these substrates. The other tested alkyl derivative, the bulky camphor **3.13c**, was slightly more on par with the thiophene, with an average K_i of 16 μM . Pyrazole derivatives **3.14c** and **3.15c** were prepared as analogues of the 5-member thiophene ring. Again, these showed somewhat flat SAR with average K_i values of 15 and 22 μM respectively. To explore alternate variations of the position of the thiophene, the 3-thiophene **3.16c** and alternate position 2-thiophene compounds **3.17c** and **3.18c** were prepared. Of these, **3.18c** was the most interesting, as although it had a higher average $K_i = 46 \mu\text{M}$, it was the most selective in this study towards sparing amylin degradation, making **3.18c** of potential interest as a tool compound in this regard.

To examine more lipophilic substituents, **3.19c** – **3.22d** were synthesized. The thiadiazole **3.21c** and 2-phenyl thiophene **3.22d** showed no improvement relative to **3.5c**, but the halogenated derivatives **3.19c** and **3.20c** showed improvement relative to the parent thiophene, with respective average K_i values of 9 and 7 μM , and averages of 9 and 5 μM when excluding the synthetic Substrate V. Between the halogenated derivatives, the brominated thiophene **3.20c** displayed slightly more broad-spectrum activity, with somewhat consistent inhibition levels

across the tested substrates, whereas the chlorinated thiophene **3.19c** displayed slightly more selectivity, with 11 times the activity against glucagon degradation than that of insulin.

Table 3.2. Inhibitory activity of thiophene sulfonamide derivatives against the IDE substrates.

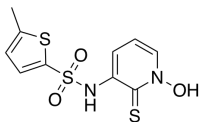
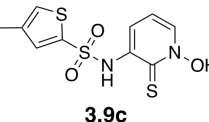
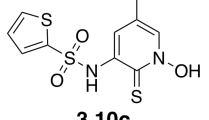
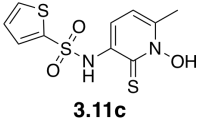
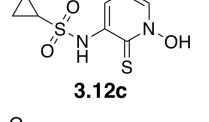
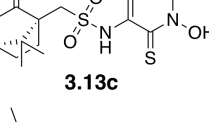
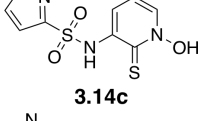
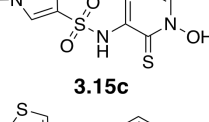
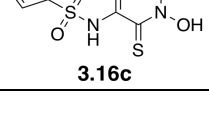
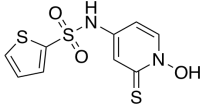
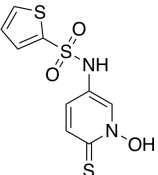
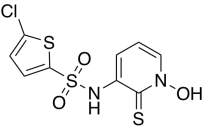
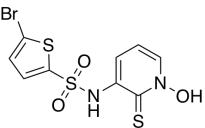
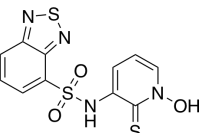
Compound	Insulin	Glucagon	Amylin	Amyloid- β	Substrate V	Average	Average without Substrate V
 3.8c	8	4	17	7	28	13	9
 3.9c	17	4	13	4	23	12	10
 3.10c	13	4	14	4	18	11	9
 3.11c	16	3	12	4	28	13	9
 3.12c	37	9	41	9	97	39	24
 3.13c	5	4	20	7	47	16	9
 3.14c	11	5	18	6	37	15	10
 3.15c	15	5	25	10	56	22	14
 3.16c	12	6	15	7	27	13	10

Table 3.2. Inhibitory activity of thiophene sulfonamide derivatives against the IDE substrates. (Continued)

Compound	Insulin	Glucagon	Amylin	Amyloid- β	Substrate V	Average	Average without Substrate V
 3.17c	6	11	39	10	30	19	16
 3.18c	20	10	105	11	86	46	36
 3.19c	22	2	7	3	13	9	9
 3.20c	7	2	8	3	14	7	5
 3.21c	19	4	12	7	31	15	11

3.3 Future Work

Validation of Metal-Binding Mechanism

To validate the mechanism of action as metal-binding at the active site Zn^{2+} , and ensure the compounds were not binding elsewhere, such as the exo-site, a set of four non-metal binding controls were prepared (Figure 3.5). Control compounds **3.23b** and **3.24b** were prepared as respective methyl and thiophene sulfonamide derivatives lacking the thione donor atom, and **3.25b** and **3.26**, were prepared as missing the complementary oxygen of the donor atom set. Together, these controls represent deletions of each of the donor atoms required for the bidentate

metal-coordination of the 1,2-HOPTO ligand, and neither should be capable of strong metal coordination. It is expected that none of these controls will have strong activity at 200 μM to inhibit degradation of any of the tested IDE substrates, a result which would indicate that the lead **2.4** and **3.5c** are likely binding as expected at the active site Zinc.

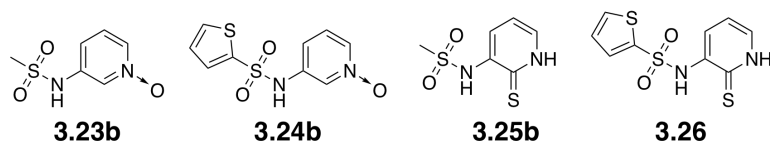


Figure 3.5. Prepared non-metal-binding IDE control compounds.

Protein Thermal Shift Assay

Protein thermal shift is a useful orthogonal method for confirmation of ligand binding to target protein. In this method, the protein of interest is steadily heated in the presence of a lipophilic-sensitive fluorescent dye, so that upon protein degradation, a fluorescent signal appears.³³⁻³⁵ Compounds that bind to a protein create favorable, stabilizing interactions, and thereby delay the onset of protein melt and degradation.³³⁻³⁵ By monitoring the change in protein melting point (ΔT_m) it is possible to confirm whether a ligand is bound to the protein of interest.³³⁻³⁵ As such a positive ΔT_m is indicative of protein stabilization and ligand binding, whereas a negative ΔT_m is indicative protein destabilization. It is worth noting though, that protein thermal shift is a qualitative technique, and the ΔT_m does not normally correlate to the overall inhibitory activity of ligand. Previous studies have shown that metal-binding hydroxamic acid IDE inhibitors induce a positive ΔT_m .³⁶ As detailed in the experimental section 3.5, incubation of **3.5c** with IDE yielded a $\Delta T_m = +1.97$ °C, confirming some degree of binding by these HOPTO ligands to IDE. It is worth noting that in our hands, DTT was included to both stabilize the IDE protein and reduce any HOPTO dimer, and the resulting stability caused a much higher IDE $T_m =$

79.68 °C than the previously reported $T_m = 48.61$ °C.³⁶ Future work will entail performing this thermal shift assay without excess DTT to replicate literature conditions.

Metalloenzyme Cross Screening and Selectivity

To demonstrate the selectivity of these lead thiophene sulfonamide HOPTO derivatives, **3.5c**, **3.19c**, and **3.20c** will be tested for activity against a set of relevant human metalloproteases. These will include the mononuclear Zn^{2+} carbonic anhydrase, MMP3, and MMP12, and dinuclear Mn^{2+} Arginase-1 (Arg1). Screening will be done at 10 μ M inhibitor, monitoring percent inhibition of these compounds against each metalloenzyme. It is expected that these compounds will have minimal activity against these metalloenzymes.

3.4 Conclusions

The goal of this work was to demonstrate the therapeutic applications of the elaborated HOPTO library, described in Chapter 2, as useful scaffolds for drug discovery efforts. To achieve that goal, IDE was selected as a proof-of-concept metalloenzyme target, as IDE relies on an active site Zn^{2+} for catalytic activity. Furthermore, IDE itself is a relevant target, as it is unusually able to hydrolyze a broad range of peptide substrates, making IDE inhibition of high importance towards conditions such as Type 2 Diabetes as well as Alzheimer's Disease. Screening the elaborated HOPTO library resulted in the discovery of 3-sulfonamide-1,2-HOPTO as a novel IDE inhibitor, with an average K_i of 50 μ M against the tested IDE substrates, and derivatization of the sulfonamide resulted in thiophene sulfonamide **3.5c**, with an average K_i of 10 μ M against the IDE substrates. Further SAR studies yielded halogen derivatives **3.19c** and **3.20c**, of which the bromine **3.20c** had broad spectrum activity against all of the tested IDE

substrates with $K_i = 5 \mu\text{M}$, and chlorine **3.19c** was 11 times more active against glucagon degradation than insulin degradation. Overall, these compounds represent a new class of metal-binding IDE inhibitors, and due to their rapid, facile syntheses, should be readily available and serve as highly useful tool compounds for future studies of IDE inhibition.

3.5 Experimental

General Synthetic Methods: Unless otherwise noted, all reagents and solvents were purchased from commercial suppliers and used with no additional purification. Microwave reactions were performed using a CEM Discover series S-class microwave reactor in pressure-sealed vessels. Silica gel column chromatography was performed using a CombiFlash Rf⁺ Teledyne ISCO system, using hexane, ethyl acetate, CH₂Cl₂ or MeOH as eluents. Separations were monitored via a Teledyne ISCO Rf⁺ PurIon ESI-MS detector with 1 Da resolution. ¹H NMR spectra were obtained using Varian 400 MHz and 500 MHz spectrometers at the Department of Chemistry and Biochemistry at UC San Diego. ¹H NMR data is reported in parts per million relative to the residual non-deuterated solvent signals, and spin multiplicities are given as s (singlet), *br s* (broad singlet), d (doublet), dd (doublet of doublets), t (triplet), dt (doublet of triplets), q (quartet), and m (multiplet). When available, coupling constants (J) are reported in hertz (Hz). The purity of compounds **3.5c** – **3.22d**, as well as **3.25b** and **3.26** were determined to be at least 90% by analytical HPLC analysis combined with elemental analysis. Standard resolution mass spectrometry was performed at either the UC San Diego Molecular Mass Spectrometry Facility or on the previously described Teledyne ISCO Rf⁺ PurIon ESI-MS detector. Compounds **2.4**, **2.27**, and **2.28** were prepared as previously reported in Chapter 2.

Generation of Sulfonyl Chloride

5-Phenylthiophene-2-sulfonyl chloride (3.22a): To a solution of DMF (0.87 mL, 11.2 mmol) cooled to 0 °C while under a nitrogen atmosphere, sulfonyl chloride (913 μ L, 11.2 mmol) was added dropwise, and the reaction was stirred for 15 min, until the mixture formed a white solid. Then 2-phenylthiophene (1.50 g, 9.36 mmol) was added in one portion, and the solids were heated as a melt at 100 °C for 45 min, noting that upon initial addition of the white thiophene, the solid mixture turned yellow, and upon heating, melt was observed to occur at 55 °C. Upon reaching 100 °C, the reaction mixture had turned from clear yellow to clear green. After heating at 100 °C for 45 min, upon reaction completion, the melt was cooled to 25 °C, diluted with ethyl acetate, and ice water was added. With a chilled separatory funnel, the product was extracted into organic using 2 \times 15 mL ethyl acetate, and the combined organic was washed with brine and dried over magnesium sulfate. The solids were filtered off and discarded, and the resulting filtrate was concentrated under reduced pressure to yield a blue liquid. The product was then purified by column chromatography, running an isocratic in gradient 100% hexanes. Like fractions of the desired product were combined and concentrated under reduced pressure, until there was a remaining volume of ~5 mL hexanes, containing a solid precipitate of the desired product. The precipitate was collected via vacuum filtration and washed with hexanes to obtain **3.22a** (1.25 g, 4.81 mmol, 51%) as a powdery solid that was pale yellow with a greenish tint in color. ¹HNMR (400 MHz, (CD₃)₂SO): 7.60 (d, *J* = 7.6, 2H), 7.39 (t, *J* = 7.6, 2H), 7.31 – 7.27 (m, 2H), 7.11 (d, *J* = 2.8, 1H).

Sulfonamide Coupling

General Sulfonamide Coupling Protocol: Unless otherwise noted, the following protocol was used for sulfonamide coupling. To a heat-gun dried microwave vessel equipped with stir bar and charged with a solution of starting amine (1.3 eq) in 2 mL dry pyridine, sulfonyl chloride (1.0 eq) was added in one portion. The mixture was placed in a microwave reactor and irradiated at 120 °C for 15 min. Upon cooling, the reaction mixture was diluted with 15 mL ethyl acetate, and washed with 2×15 mL 4 M HCl. The aqueous was back-extracted with an additional 15 mL ethyl acetate, and the combined organic was washed with brine, dried over magnesium sulfate, and the solids were filtered off and discarded. The filtrate was concentrated under reduced pressure, and the resulting crude was purified by column chromatography, running gradient from 100% hexanes to 100% ethyl acetate. The desired sulfonamide product typically eluted in 50% ethyl acetate in hexanes. Like fractions were combined and concentrated under reduced pressure to obtain the desired sulfonamide product that was used directly in the subsequent step. As previously noted, some coupling reactions resulted in an inseparable mix of sulfonamide and disulfonamide products. These mixtures were carried over directly into the next step with no additional purification.

N-(2-Bromopyridin-3-yl)thiophene-2-sulfonamide (3.5a): Following the general method for sulfonamide coupling, from 2-bromopyridin-3-amine (1.50 g, 8.67 mmol) and thiophene-2-sulfonyl chloride (1.27 g, 6.94 mmol), the desired product **3.5a** (1.53 g, 4.80 mmol, 55%) was obtained as a peach colored solid. ¹H NMR (400 MHz, DMSO-*d*₆): δ 10.41 (*br s*, 1H), 8.25 (d, *J* = 4.4, 1H), 7.97 (d, *J* = 5.2, 1H), 7.70 (d, *J* = 7.6, 1H), 7.49 – 7.44 (m, 2H), 7.16 (t, *J* = 4.4, 1H); ESI-MS(-): *m/z* 317.18 [M - H]⁻.

N-(2-Bromopyridin-3-yl)benzamide (3.6a): To a 0 °C solution of 2-bromopyridin-3-amine (0.600 g, 3.47 mmol) and pyridine (0.56 mL, 6.9 mmol) in 10 mL CH₂Cl₂, a mixture of benzoyl chloride (269 μL, 2.31 mmol) in 5 mL CH₂Cl₂ was added dropwise. The reaction mixture was allowed to slowly warm to 25 °C for 16 h, and was then diluted with an additional 15 mL CH₂Cl₂, and was washed with 20 mL 4 M HCl. The aqueous was back-extracted with 10 mL CH₂Cl₂, and the combined organic phase was washed with brine, dried over magnesium sulfate, and the solids were filtered off and discarded. The filtrate was concentrated under reduced pressure, and the resulting crude was purified by column chromatography, running gradient from 100% hexanes to 100% ethyl acetate. The desired product eluted in 50% ethyl acetate in hexanes. Like fractions were combined and concentrated under reduced pressure to obtain **3.6a** (0.549 g, 1.98 mmol, 86 %) as a clear oil that solidified upon standing. ¹H NMR (400 MHz, DMSO-*d*₆): δ 10.10 (*br s*, 1H), 8.30 (dd, *J*₁ = 4.4, *J*₂ = 1.2, 1H), 8.01 (d, *J* = 7.2, 3H), 7.65 – 7.47 (m, 4H); ESI-MS(+): *m/z* 277.12 [M + H]⁺.

N-(2-Bromopyridin-3-yl)thiophene-2-carboxamide (3.7a): Following the same protocol used in **3.6a**, from 2-bromopyridin-3-amine (0.600 g, 3.47 mmol), pyridine (0.56 mL, 6.9 mmol), and thiophene-2-carbonyl chloride (247 μL, 2.31 mmol), the desired **3.7a** (0.536 g, 1.89 mmol, 82%) was obtained as a clear oil that solidified upon standing. ¹H NMR (400 MHz, DMSO-*d*₆): δ 10.23 (*br s*, 1H), 8.30 (d, *J* = 4.8, 1H), 8.02 (d, *J* = 3.6, 1H), 7.96 (d, *J* = 7.6, 1H), 7.90 (d, *J* = 5.2, 1H), 7.51 (dd, *J*₁ = 7.6, *J*₂ = 0.8, 1H), 7.25 (t, *J* = 5.2, 1H); ESI-MS(+): *m/z* 283.11 [M + H]⁺.

N-(2-Bromopyridin-3-yl)-5-methylthiophene-2-sulfonamide (3.8a): Following the general method for sulfonamide coupling, from 2-bromopyridin-3-amine (0.600 g, 3.47 mmol) and 5-methylthiophene-2-sulfonyl chloride (608 μ L, 4.51 mmol), the desired product **3.8a** (0.380 g, 1.14 mmol, 33%) was obtained as a light yellow oil that solidified upon standing. ^1H NMR (400 MHz, DMSO- d_6): δ 10.31 (*br s*, 1H), 8.24 (dd, $J_1 = 4.8$, $J_2 = 1.6$, 1H), 7.68 (dd, $J_1 = 7.6$, $J_2 = 1.6$, 1H), 7.45 (dd, $J_1 = 8.0$, $J_2 = 4.8$, 1H), 7.30 (d, $J = 3.6$, 1H), 6.87 (dd, $J_1 = 4.0$, $J_2 = 1.2$, 1H), 2.48 (s, 3H); ESI-MS(+): m/z 333.10 [M + H] $^+$.

N-(2-Bromopyridin-3-yl)-4-methylthiophene-2-sulfonamide (3.9a): Following the general method for sulfonamide coupling, from 2-bromopyridin-3-amine (0.484 g, 2.80 mmol) and 4-methylthiophene-2-sulfonyl chloride (0.500 g, 2.54 mmol), the desired product **3.9a** (0.560 g, 1.68 mmol, 66%) was obtained as a slightly impure white solid that was used directly in the next step without any additional purification. ^1H NMR (400 MHz, DMSO- d_6): δ 10.39 (*br s*, 1H), 8.24 (dd, $J_1 = 4.4$, $J_2 = 1.2$, 1H), 7.67 (dd, $J_1 = 8.0$, $J_2 = 1.2$, 1H), 7.55 – 7.54 (m, 2H), 7.45 (dd, $J_1 = 7.6$, $J_2 = 4.4$, 1H), 7.35 (s, 1H), 2.19 (s, 3H); ESI-MS(-): m/z 333.15 [M - H].

N-(2-Bromo-5-methylpyridin-3-yl)thiophene-2-sulfonamide (3.10a): Following the general method for sulfonamide coupling, from 2-bromo-5-methylpyridin-3-amine (0.500 g, 2.67 mmol) and thiophene-2-sulfonyl chloride (0.635 g, 3.48 mmol), the desired product **3.10a** (0.513 g, 1.20 mmol, 43%) was obtained as a white solid contaminated with approximately 25% disulfonamide product. The product was used directly in the next step without any additional purification. ^1H NMR (400 MHz, DMSO- d_6): δ 10.31 (*br s*, 1H), 8.10 (s, 1H), 7.96 (d, $J = 5.2$, 1H), 7.52 (s, 1H), 7.48 (d, $J = 3.6$, 1H), 7.16 (t, $J = 4.8$, 1H), 2.25 (s, 3H); ESI-MS(+): m/z 331.29 [M + H] $^+$.

N-(2-Bromo-6-methylpyridin-3-yl)thiophene-2-sulfonamide (3.11a): Following the general method for sulfonamide coupling, from 2-bromo-6-methylpyridin-3-amine (0.500 g, 2.67 mmol) and thiophene-2-sulfonyl chloride (0.635 g, 3.48 mmol), the desired product **3.11a** (0.746 g, 1.90 mmol, 71%) was obtained as a white solid contaminated with approximately 15% disulfonamide product. The product was used directly in the next step without any additional purification. ¹H NMR (400 MHz, DMSO-*d*₆): δ 10.25 (*br s*, 1H), 7.96 (d, *J* = 4.8, 1H), 7.53 (d, *J* = 8.0, 1H), 7.45 (d, *J* = 3.6, 1H), 7.30 (d, *J* = 7.6, 1H), 7.15 (t, *J* = 4.8, 1H), 2.41 (s, 3H); ESI-MS(-): *m/z* 331.26 [M - H]⁻.

N-(2-Bromopyridin-3-yl)cyclopropanesulfonamide (3.12a): Following the general method for sulfonamide coupling, from 2-bromopyridin-3-amine (0.750 g, 4.34 mmol) and cyclopropanesulfonyl chloride (662 μ L, 6.50 mmol), the desired product **3.12a** (0.850 g, 3.07 mmol, 71%) was obtained as a light yellow solid. ¹H NMR (400 MHz, DMSO-*d*₆): δ 9.70 (*br s*, 1H), 8.26 (dt, *J*₁ = 4.4, *J*₂ = 1.6, 1H), 7.84 (dt, *J*₁ = 8.0, *J*₂ = 1.6, 1H), 7.46 (qd, *J*₁ = 4.4, *J*₂ = 1.6, 1H), 2.77 – 2.70 (m, 1H), 1.01 – 0.96 (m, 2H), 0.90 – 0.86 (m, 2H); ESI-MS(+): *m/z* 279.12 [M + H]⁺.

N-(2-Chloropyridin-3-yl)-1-((1R,4S)-7,7-dimethyl-2-oxobicyclo[2.2.1]heptan-1-yl)methanesulfonamide (3.13a): Following the general method for sulfonamide coupling, from 2-chloropyridin-3-amine (0.350 g, 2.02 mmol) and ((1R,4S)-7,7-dimethyl-2-oxobicyclo[2.2.1]heptan-1-yl)methanesulfonyl chloride (0.650 g, 2.59 mmol), the desired product **3.13a** (0.382 g, 1.11 mmol, 43%) was obtained as a pale yellow solid. ¹H NMR (400

MHz, DMSO- d_6): δ 9.79 (*br s*, 1H), 8.25 (d, $J = 4.8$, 1H), 7.95 (d, $J = 8.0$, 1H), 7.47 (dd, $J_1 = 8.0$, $J_2 = 4.8$, 1H), 3.50 (d, $J = 14.8$, 1H), 3.15 (d, $J = 14.8$, 1H), 2.38 – 2.29 (m, 2H), 2.06 (t, $J = 4.4$, 1H), 1.97 – 1.91 (m, 2H), 1.59 – 1.52 (m, 1H), 1.43 – 1.37 (m, 1H), 1.01 (s, 3H), 0.79 (s, 3H); ESI-MS(+): m/z 343.31 [M + H]⁺.

N-(2-Bromopyridin-3-yl)-1-methyl-1H-pyrazole-3-sulfonamide (3.14a): Following the general method for sulfonamide coupling, from 2-bromopyridin-3-amine (0.500 g, 2.89 mmol) and 1-methyl-1H-pyrazole-3-sulfonyl chloride (0.475 g, 2.63 mmol), the desired product **3.14a** (0.354 g, 1.12 mmol, 43%) was obtained as a pale tan oil that solidified upon standing. ¹H NMR (400 MHz, DMSO- d_6): δ 10.18 (*br s*, 1H), 8.21 (dd, $J_1 = 4.8$, $J_2 = 1.6$, 1H), 7.88 (d, $J = 2.0$, 1H), 7.72 (dd, $J_1 = 8.0$, $J_2 = 1.6$, 1H), 7.42 (dd, $J_1 = 8.0$, $J_2 = 4.8$, 1H), 6.57 (d, $J = 2.4$, 1H), 3.91 (s, 3H); ESI-MS(+): m/z 317.25 [M + H]⁺.

N-(2-bromopyridin-3-yl)-1-methyl-1H-pyrazole-4-sulfonamide (3.15a): Following the general method for sulfonamide coupling, from 2-bromopyridin-3-amine (0.500 g, 2.89 mmol) and 1-methyl-1H-pyrazole-4-sulfonyl chloride (0.626 g, 3.47 mmol), the desired product **3.15a** (0.611 g, 1.93 mmol, 67%) was obtained as a clear oil that solidified upon standing to a white solid. ¹H NMR (400 MHz, DMSO- d_6): δ 9.97 (*br s*, 1H), 8.23 (s, 1H), 8.21 (dd, $J_1 = 4.8$, $J_2 = 1.6$, 1H), 7.69 (s, 1H), 7.67 (d, $J = 1.6$, 1H), 7.42 (dd, $J_1 = 8.0$, $J_2 = 4.8$, 1H), 3.85 (s, 3H); ESI-MS(-): m/z 315.20 [M - H]⁻.

N-(2-Bromopyridin-3-yl)thiophene-3-sulfonamide (3.16a): Following the general method for sulfonamide coupling, from 2-bromopyridin-3-amine (0.600 g, 3.47 mmol) and thiophene-3-

sulfonyl chloride (823 mg, 4.51 mmol), the desired product **3.16a** (0.583 g, 1.83 mmol, 53%) was obtained as a light brown oil that solidified upon standing. ¹H NMR (400 MHz, DMSO-*d*₆): δ 10.17 (*br s*, 1H), 8.22 – 8.21 (m, 1H), 8.12 – 8.11 (m, 1H), 7.76 – 7.74 (m, 1H), 7.64 – 7.61 (m, 1H), 7.44 – 7.40 (m, 1H), 7.28 – 7.26 (m, 1H); ESI-MS(-): *m/z* 317.19 [M - H]⁻.

N-(2-Bromopyridin-4-yl)thiophene-2-sulfonamide (3.17a): Following the general method for sulfonamide coupling, from 2-bromopyridin-4-amine (0.750 g, 4.34 mmol) and thiophene-2-sulfonyl chloride (1.19 g, 6.50 mmol), the desired product **3.17a** (1.37 g, 4.29 mmol, 55%) was obtained as a pale yellow oil that solidified upon standing to a white solid. ¹H NMR (400 MHz, DMSO-*d*₆): δ 11.57 (*br s*, 1H), 8.19 (d, *J* = 6.0, 1H), 8.01 (dd, *J*₁ = 4.8, *J*₂ = 1.2, 1H), 7.79 (dd, *J*₁ = 3.6, *J*₂ = 1.2, 1H), 7.24 (d, *J* = 2.0, 1H), 7.20 – 7.16 (m, 2H); ESI-MS(+): *m/z* 321.13 [M + H]⁺.

N-(6-Bromopyridin-3-yl)thiophene-2-sulfonamide (3.18a): Following the general method for sulfonamide coupling, from 6-bromopyridin-3-amine (0.750 g, 4.34 mmol) and thiophene-2-sulfonyl chloride (1.19 g, 6.50 mmol), the desired product **3.18a** (1.38 g, 4.29 mmol) was obtained in theoretical yield as a pale yellow solid contaminated with approximately 50% disulfonamide product. The product was used directly in the next step without any additional purification. ¹H NMR (400 MHz, DMSO-*d*₆): δ 10.87 (*br s*, 1H), 8.26 (dd, *J*₁ = 4.8, *J*₂ = 1.2, 1H), 8.12 (d, *J* = 2.8, 1H), 7.95 (dd, *J*₁ = 5.2, *J*₂ = 1.2, 1H), 7.79 (dd, *J*₁ = 4.0, *J*₂ = 1.6, 1H), 7.62 – 7.57 (m, 2H), 7.30 (t, *J* = 5.2, 1H); ESI-MS(+): *m/z* 321.15 [M + H]⁺.

N-(2-Bromopyridin-3-yl)-5-chlorothiophene-2-sulfonamide (3.19a): Following the general method for sulfonamide coupling, from 2-bromopyridin-3-amine (3.00 g, 17.3 mmol) and 5-chlorothiophene-2-sulfonyl chloride (1.86 mL, 13.9 mmol), the desired product **3.19a** (2.27 g, 6.41 mmol, 37%) was obtained as a light tan solid contaminated with approximately 10% disulfonamide product. The product was used directly in the next step without any additional purification. $^1\text{H NMR}$ (400 MHz, $\text{DMSO-}d_6$): δ 10.65 (*br s*, 1H), 8.28 (dd, $J_1 = 4.4$, $J_2 = 1.2$, 1H), 7.71 (dd, $J_1 = 8.0$, $J_2 = 1.6$, 1H), 7.48 (dd, $J_1 = 8.0$, $J_2 = 4.8$, 1H), 7.37 (d, $J = 4.0$, 1H), 7.25 (d, $J = 4.0$, 1H); ESI-MS(-): m/z 353.09 [M - H] $^-$.

5-Bromo-N-(2-bromopyridin-3-yl)thiophene-2-sulfonamide (3.20a): Following the general method for sulfonamide coupling, from 2-bromopyridin-3-amine (1.00 g, 5.78 mmol) and 5-bromothiophene-2-sulfonyl chloride (1.21 g, 4.62 mmol), the desired product **3.20a** (1.41 g, 3.54 mmol, 61%) was obtained as a pale yellow solid contaminated with approximately 20% disulfonamide product. The product was used directly in the next step without any additional purification. $^1\text{H NMR}$ (400 MHz, $\text{DMSO-}d_6$): δ 10.64 (*br s*, 1H), 8.28 (d, $J = 4.4$, 1H), 7.72 – 7.68 (m, 2H), 7.51 – 7.46 (m, 2H); ESI-MS(-): m/z 397.03 [M - H] $^-$.

N-(2-bromopyridin-3-yl)benzo[c][1,2,5]thiadiazole-4-sulfonamide (3.21a): Following the general method for sulfonamide coupling, from 2-bromopyridin-3-amine (0.350 g, 2.02 mmol) and benzo[c][1,2,5]thiadiazole-4-sulfonyl chloride (0.380 g, 1.62 mmol), the desired product **3.21a** (0.382 g, 1.03 mmol, 51%) was obtained as a cream colored solid. $^1\text{H NMR}$ (400 MHz, $\text{DMSO-}d_6$): δ 10.49 (*br s*, 1H), 8.41 (d, $J = 8.8$, 1H), 8.21 (dd, $J_1 = 4.8$, $J_2 = 1.6$, 1H), 8.13 (d, J

= 6.8, 1H), 7.84 – 7.76 (m, 2H), 7.43 (dd, $J_1 = 8.0$, $J_2 = 4.8$, 1H); ESI-MS(+): m/z 373.16 [M + H]⁺.

N-(2-Chloropyridin-3-yl)-1-((1R,4S)-7,7-dimethyl-2-oxobicyclo[2.2.1]heptan-1-

yl)methanesulfonamide (3.22b): Following the general method for sulfonamide coupling, from 2-bromopyridin-3-amine (1.08 g, 6.23 mmol) and **3.22a** (1.24 g, 4.79 mmol), the desired product **3.22b** (1.13 g, 2.85 mmol, 60%) was obtained as a fluffy bright white solid. ¹H NMR (400 MHz, DMSO-*d*₆): δ 10.53 (*br s*, 1H), 8.28 – 8.26 (m, 1H), 7.75 – 7.70 (m, 3H), 7.56 (d, $J = 2.4$, 1H), 7.48 – 7.39 (m, 5H); ESI-MS(+): m/z 393.23 [M + H]⁺.

N-(Pyridin-3-yl)methanesulfonamide (3.23a): To a 0 °C solution of pyridin-3-amine (1.00 g, 10.6 mmol) in 2 mL of 1:1 CH₂Cl₂/pyridine, a solution of methanesulfonyl chloride (987 μ L, 12.7 mmol) in 1 mL CH₂Cl₂ was added dropwise, and the reaction mixture was allowed to warm to 25 °C for 16 h. Then the reaction mixture was diluted with 20 mL ethyl acetate and washed with 2×20 mL DI water. The aqueous was extracted with 20 mL ethyl acetate, and the combined organic washes were washed with brine, and concentrated under reduced pressure. The resulting crude solid was purified by column chromatography, running gradient from 100% hexanes to 100% ethyl acetate. The desired product eluted slowly in 100% ethyl acetate. Like fractions were combined and concentrated under reduced pressure to obtain **3.23a** (0.618 g, 3.59 mmol, 34%) as a white solid. ¹H NMR (400 MHz, DMSO-*d*₆): δ 10.00 (*br s*, 1H), 8.42 (s, 1H), 8.31 (d, $J = 4.8$, 1H), 7.61 (dd, $J_1 = 8.4$, $J_2 = 0.8$, 1H), 7.36 (dd, $J_1 = 8.0$, $J_2 = 4.8$, 1H), 3.04 (s, 3H); ESI-MS(-): m/z 171.22 [M - H]⁻.

N-(Pyridin-3-yl)thiophene-2-sulfonamide (3.24a): Following the same protocol used in **3.23a**, from pyridin-3-amine (1.00 g, 10.6 mmol) and thiophene-2-sulfonyl chloride (1.94 g, 10.6 mmol), the desired **3.24a** (1.953 g, 8.13 mmol, 77%) was obtained as a white solid. ¹H NMR (400 MHz, DMSO-*d*₆): δ 10.69 (*br s*, 1H), 8.29 (d, *J* = 4.8, 2H), 7.92 (d, *J* = 4.8, 1H), 7.57 – 7.53 (m, 2H), 7.32 (dd, *J*₁ = 8.0, *J*₂ = 4.8, 1H), 7.12 (t, *J* = 3.6, 1H); ESI-MS(-): *m/z* 239.24 [M - H]⁻.

N-(2-bromopyridin-3-yl)methanesulfonamide (3.25a): Following the general method for sulfonamide coupling, from 2-bromopyridin-3-amine (1.08 g, 6.23 mmol) and methanesulfonyl chloride (645 μL, 8.33 mmol), the desired product **3.25a** (0.510 g, 2.05 mmol, 25%) was obtained as a pale yellow liquid contaminated with approximately 50% disulfonamide product. The product was used directly in the next step without any additional purification. ¹H NMR (400 MHz, DMSO-*d*₆): δ 9.66 (*br s*, 1H), 8.23 (d, *J* = 8.0, 1H), 7.83 (d, *J* = 7.6, 1H), 7.48 – 7.45 (m, 1H), 3.11 (s, 3H); ESI-MS(-): *m/z* 249 [M - H]⁻.

Oxidation

General Oxidation Coupling Protocol: Unless otherwise noted, the following protocol was used. To a solution of sulfonamide in 20 mL 1:1 CH₂Cl₂/MeOH, a solution of mCPBA (5 eq.) in 10 mL 1:1 CH₂Cl₂/MeOH was added in one portion. The reaction mixture was then heated at 35 °C for 72 h. Upon completion, the reaction mixture was concentrated under reduced pressure and the resulting crude was purified by column chromatography, running gradient first from 100% hexanes to 100% ethyl acetate, and then from 100% CH₂Cl₂ to 15% MeOH in CH₂Cl₂. The desired products typically eluted in 8 – 10 % MeOH in CH₂Cl₂. Like fractions were

combined and concentrated under reduced pressure to obtain the desired oxidized product that was used directly in the subsequent step

2-Bromo-3-(thiophene-2-sulfonamido)pyridine 1-oxide (3.5b): Following the general method for oxidation, from **3.5a** (1.50 g, 4.70 mmol) and mCPBA (6.32 g, 77.0% Wt, 28.2 mmol), at 25 °C for 16 h, the desired product **3.5b** (0.742 g, 2.21 mmol, 55%) was obtained as a light yellow solid. ¹H NMR (400 MHz, DMSO-*d*₆): δ 10.61 (*br s*, 1H), 8.35 (d, *J* = 6.8, 1H), 7.99 (d, *J* = 4.8, 1H), 7.55 (d, *J* = 3.6, 1H), 7.39 (t, *J* = 6.8, 1H), 7.21 – 7.16 (m, 2H); ESI-MS(-): *m/z* 333.11 [M - H]⁻.

3-Benzamido-2-bromopyridine 1-oxide (3.6b): Following the general method for oxidation, from **3.6a** (0.540 g, 1.95 mmol) and mCPBA (2.18 g, 77.0% Wt, 9.74 mmol), at 35 °C for 16 h, the desired product **3.6b** (0.169 g, 0.577 mmol, 30%) was obtained as an off-white solid. ¹H NMR (400 MHz, DMSO-*d*₆): δ 10.34 (*br s*, 1H), 8.42 (d, *J* = 6.4, 1H), 7.98 (d, *J* = 7.2, 1H), 7.64 (t, *J* = 7.2, 1H), 7.58 – 7.52 (m, 2H), 7.46 (t, *J* = 6.4, 1H); ESI-MS(+): *m/z* 293.05 [M + H]⁺.

2-bromo-3-(thiophene-2-carboxamido)pyridine 1-oxide (3.7b): Following the general method for oxidation, from **3.7a** (0.530 g, 1.87 mmol) and mCPBA (2.10 g, 77.0% Wt, 9.36 mmol), at 35 °C for 16 h, the desired product **3.7b** (0.358 g, 1.20 mmol, 64%) was obtained as a yellow oil that solidified upon standing. ¹H NMR (400 MHz, DMSO-*d*₆): δ 10.38 (*br s*, 1H), 8.42 (dd, *J*₁ = 6.0, *J*₂ = 1.6, 1H), 8.01 (dd, *J*₁ = 2.8, *J*₂ = 0.8, 1H), 7.92 (dd, *J*₁ = 4.8, *J*₂ = 0.8, 1H), 7.51 – 7.46 (m, 2H), 7.25 (dt, *J*₁ = 3.6, *J*₂ = 1.2, 1H); ESI-MS(+): *m/z* 299.02 [M + H]⁺.

2-Bromo-3-((5-methylthiophene)-2-sulfonamido)pyridine 1-oxide (3.8b): Following the general method for oxidation, from **3.8a** (0.380 g, 1.28 mmol) and mCPBA (1.28 g, 77.0% Wt, 5.70 mmol), at 25 °C for 67 h, the desired product **3.8b** (0.202 g, 0.578 mmol, 51%) was obtained as an off-white solid. ¹H NMR (400 MHz, DMSO-*d*₆): δ 10.52 (*br s*, 1H), 8.35 (d, *J* = 6.4, 1H), 7.40 – 7.37 (m, 2H), 7.21 (d, *J* = 8.0, 1H), 6.88 (d, *J* = 3.2, 1H), 2.48 (s, 3H); ESI-MS(-): *m/z* 347.16 [M - H]⁻.

2-Bromo-3-((4-methylthiophene)-2-sulfonamido)pyridine 1-oxide (3.9b): Following the general method for oxidation, from **3.9a** (0.560 g, 1.68 mmol) and mCPBA (1.88 g, 77.0% Wt, 8.40 mmol), at 25 °C for 72 h, the desired product **3.9b** (0.192 g, 0.550 mmol, 33%) was obtained as a yellow solid. ¹H NMR (400 MHz, DMSO-*d*₆): δ 10.56 (*br s*, 1H), 8.35 (d, *J* = 6.4, 1H), 7.58 (s, 1H), 7.42 (s, 1H), 7.38 (t, *J* = 6.4, 1H), 7.19 (d, *J* = 8.4, 1H), 2.20 (s, 3H); ESI-MS(-): *m/z* 349.10 [M - H]⁻.

2-Bromo-5-methyl-3-(thiophene-2-sulfonamido)pyridine 1-oxide (3.10b): Following the general method for oxidation, from **3.10a** (0.500 g, 1.13 mmol) and mCPBA (1.68 g, 77.0% Wt, 7.50 mmol), at 30 °C for 16 h, the desired product **3.10b** (0.101 g, 0.289 mmol, 26%) was obtained as a pale yellow solid. ¹H NMR (400 MHz, DMSO-*d*₆): δ 10.53 (*br s*, 1H), 8.29 (s, 1H), 7.98 (d, *J* = 5.2, 1H), 7.55 (d, *J* = 4.0, 1H), 7.16 (t, *J* = 4.0, 1H), 7.01 (s, 1H), 2.20 (s, 3H); ESI-MS(+): *m/z* 349.11 [M + H]⁺.

2-Bromo-6-methyl-3-(thiophene-2-sulfonamido)pyridine 1-oxide (3.11b): Following the general method for oxidation, from **3.11a** (0.730 g, 1.86 mmol) and mCPBA (5.87 g, 77.0% Wt, 2.45 mmol), at 30 °C for 20 h, the desired product **3.11b** (0.216 g, 0.289 mmol, 33%) was obtained as a white solid. ¹H NMR (400 MHz, DMSO-*d*₆): δ 10.50 (*br s*, 1H), 7.98 (d, *J* = 4.8, 1H), 7.52 (d, *J* = 3.6, 1H), 7.46 (d, *J* = 8.4, 1H), 7.16 (t, *J* = 8.8, 1H), 7.11 (d, *J* = 8.4, 1H), 2.37 (s, 3H); ESI-MS(+): *m/z* 349.14 [M + H]⁺.

2-Bromo-3-(cyclopropanesulfonamido)pyridine 1-oxide (3.12b): Following the general method for oxidation, from **3.12a** (0.890 g, 3.13 mmol) and mCPBA (3.60 g, 77.0% Wt, 16.1 mmol), at 30 °C for 16 h, the desired product **3.12b** (0.470 g, 0.160 mmol, 50%) was obtained as a white solid. ¹H NMR (400 MHz, DMSO-*d*₆): δ 9.87 (*br s*, 1H), 8.36 (dd, *J*₁ = 5.2, *J*₂ = 2.4, 1H), 7.42 – 7.37 (m, 2H), 2.81 – 2.75 (m, 1H), 1.03 – 0.98 (m, 2H), 0.97 – 0.91 (m, 2H); ESI-MS(+): *m/z* 295.14 [M + H]⁺.

2-Chloro-3-(((1R,4S)-7,7-dimethyl-2-oxobicyclo[2.2.1]heptan-1-yl)methyl)sulfonamido)pyridine 1-oxide (3.13b): Following the general method for oxidation, from **3.13a** (0.380 g, 1.11 mmol) and mCPBA (1.24 g, 77.0% Wt, 5.54 mmol), at 40 °C for 4 d, the desired product **3.13b** (0.241 g, 0.672 mmol, 61%) was obtained as a yellow oil that solidified upon standing. ¹H NMR (400 MHz, DMSO-*d*₆): δ 7.98 (d, *J* = 6.4, 1H), 7.42 (d, *J* = 8.4, 1H), 7.19 (t, *J* = 8.0, 1H), 3.37 (d, *J* = 5.6, 1H), 2.95 (d, *J* = 14.8, 1H), 2.52 – 2.46 (m, 1H), 2.33 – 2.27 (m, 1H), 2.01 (t, *J* = 4.0, 1H), 1.90 – 1.86 (m, 2H), 1.53 – 1.46 (m, 1H), 1.39 – 1.33 (m, 1H), 1.00 (s, 3H), 0.76 (s, 3H); ESI-MS(+): *m/z* 357.31 [M + H]⁺.

2-Bromo-3-((1-methyl-1H-pyrazole)-3-sulfonamido)pyridine 1-oxide (3.14b): Following the general method for oxidation, from **3.14a** (0.350 g, 1.10 mmol) and mCPBA (1.24 g, 77.0% Wt, 5.52 mmol), at 30 °C for 72 h, the desired product **3.14b** (0.166 g, 0.498 mmol, 45%) was obtained as a yellow solid. ¹H NMR (400 MHz, DMSO-*d*₆): δ 10.40 (*br s*, 1H), 8.33 (d, *J* = 6.4, 1H), 7.90 (s, 1H), 7.36 (d, *J* = 1.2, 1H), 7.25 (d, *J* = 8.4, 1H), 6.61 (s, 1H), 3.91 (s, 3H); ESI-MS(+): *m/z* 333.14 [M + H]⁺.

2-Bromo-3-((1-methyl-1H-pyrazole)-3-sulfonamido)pyridine 1-oxide (3.15b): Following the general method for oxidation, from **3.15a** (0.600 g, 1.89 mmol) and mCPBA (2.12 g, 77.0% Wt, 9.46 mmol), at 30 °C for 16 h, the desired product **3.15b** (0.212 g, 0.636 mmol, 34%) was obtained as an off-white solid. ¹H NMR (400 MHz, DMSO-*d*₆): δ 10.18 (*br s*, 1H), 8.31 (dd, *J*₁ = 6.4, *J*₂ = 1.2, 1H), 8.28 (s, 1H), 7.74 (s, 1H), 7.36 (t, *J* = 6.8, 1H), 7.20 (dd, *J*₁ = 8.4, *J*₂ = 0.8, 1H), 3.85 (s, 3H); ESI-MS(+): *m/z* 331.17 [M + H]⁺.

2-Bromo-3-(thiophene-3-sulfonamido)pyridine 1-oxide (3.16b): Following the general method for oxidation, from **3.16a** (0.580 g, 1.82 mmol) and mCPBA (2.04 g, 77.0% Wt, 9.09 mmol), at 25 °C for 67 h, the desired product **3.16b** (0.256 g, 0.763 mmol, 42%) was obtained as an off-white solid. ¹H NMR (400 MHz, DMSO-*d*₆): δ 10.61 (*br s*, 1H), 8.35 (d, *J* = 6.8, 1H), 7.99 (d, *J* = 4.8, 1H), 7.55 (d, *J* = 3.6, 1H), 7.39 (t, *J* = 6.8, 1H), 7.21 – 7.16 (m, 2H); ESI-MS(-): *m/z* 333.22 [M - H]⁻.

2-Bromo-4-(thiophene-2-sulfonamido)pyridine 1-oxide (3.17b): Following the general method for oxidation, from **3.17a** (1.00 g, 3.13 mmol) and mCPBA (2.11 g, 77.0% Wt, 9.40

mmol), at 35 °C for 16 h, the desired product **3.17b** (0.298 g, 0.889 mmol, 28%) was obtained as a white solid. ¹H NMR (400 MHz, DMSO-*d*₆): δ 11.30 (*br s*, 1H), 8.31 (d, *J* = 7.2, 1H), 7.98 (d, *J* = 4.8, 1H), 7.70 (d, *J* = 3.6, 1H), 7.44 (d, *J* = 2.8, 1H), 7.19 – 7.14 (m, 2H); ESI-MS(+): *m/z* 335.10 [M + H]⁺.

2-Bromo-4-(thiophene-2-sulfonamido)pyridine 1-oxide (3.18b): Following the general method for oxidation, from **3.18a** (1.00 g, 3.13 mmol) and mCPBA (2.11 g, 77.0% Wt, 9.40 mmol), at 35 °C for 16 h, the desired product **3.18b** (0.323 g, 0.964 mmol, 31%) was obtained as a white solid. ¹H NMR (400 MHz, DMSO-*d*₆): δ 11.09 (*br s*, 1H), 8.13 (d, *J* = 2.0, 1H), 7.99 (dd, *J*₁ = 4.8, *J*₂ = 1.6, 1H), 7.81 (d, *J* = 8.8, 1H), 7.68 (dd, *J*₁ = 4.0, *J*₂ = 1.2, 1H), 7.17 (dd, *J*₁ = 5.2, *J*₂ = 4.0, 1H), 7.04 (dd, *J*₁ = 8.8, *J*₂ = 2.0, 1H); ESI-MS(+): *m/z* 335.08 [M + H]⁺.

2-Bromo-3-((5-chlorothiophene)-2-sulfonamido)pyridine 1-oxide (3.19b): Following the general method for oxidation, from **3.19a** (1.80 g, 1.86 mmol) and mCPBA (6.84 g, 77.0% Wt, 5.09 mmol), at 35 °C for 48 h, the desired product **3.19b** (0.876 g, 2.37 mmol, 47%) was obtained as a yellow-tan solid. ¹H NMR (400 MHz, DMSO-*d*₆): δ 10.85 (*br s*, 1H), 8.39 (dd, *J*₁ = 6.4, *J*₂ = 0.8, 1H), 7.44 (d, *J* = 4.0, 1H), 7.40 (t, *J* = 6.4, 1H), 7.25 (d, *J* = 4.0, 1H), 7.22 (dd, *J*₁ = 8.4, *J*₂ = 0.8, 1H); ESI-MS(-): *m/z* 369.12 [M - H]⁻.

2-Bromo-3-((5-chlorothiophene)-2-sulfonamido)pyridine 1-oxide (3.20b): Following the general method for oxidation, from **3.20a** (1.40 g, 3.52 mmol) and mCPBA (3.94 g, 77.0% Wt, 17.6 mmol), at 35 °C for 6 d, the desired product **3.20b** (0.497 g, 1.20 mmol, 34%) was obtained

as a tan solid. $^1\text{H NMR}$ (400 MHz, $\text{DMSO-}d_6$): δ 10.81 (*br s*, 1H), 8.37 (d, $J = 6.4$, 1H), 7.42 – 7.39 (m, 2H), 7.34 (d, $J = 4.0$, 1H), 7.21 (d, $J = 8.4$, 1H); ESI-MS(-): m/z 413.02 [$\text{M} - \text{H}$] $^-$.

3-(Benzo[c][1,2,5]thiadiazole-4-sulfonamido)-2-bromopyridine 1-oxide (3.21b): Following the general method for oxidation, from **3.21a** (0.350 g, 0.943 mmol) and mCPBA (1.06 g, 77.0% Wt, 4.71 mmol), at 30 °C for 5 d, the desired product **3.21b** (0.147 g, 0.380 mmol, 40%) was obtained as a tan solid. $^1\text{H NMR}$ (400 MHz, $\text{DMSO-}d_6$): δ 8.26 (d, $J = 8.8$, 1H), 8.08 (d, $J = 7.2$, 1H), 7.94 – 7.92 (m, 1H), 7.60 (t, $J = 6.8$, 1H), 7.17 (d, $J = 8.4$, 1H), 7.10 – 7.06 (m, 1H); ESI-MS(+): m/z 389.11 [$\text{M} + \text{H}$] $^+$.

2-Bromo-3-((5-phenylthiophene)-2-sulfonamido)pyridine 1-oxide (3.22c): Following the general method for oxidation, from **3.22b** (1.05 g, 2.66 mmol) and mCPBA (2.98 g, 77.0% Wt, 13.3 mmol), at 35 °C for 16 h, the desired product **3.22c** (0.590 g, 1.43 mmol, 54%) was obtained as a pale yellow solid. $^1\text{H NMR}$ (400 MHz, $\text{DMSO-}d_6$): δ 10.73 (*br s*, 1H), 8.36 (d, $J = 6.4$, 1H), 7.71 (d, $J = 7.6$, 2H), 7.57 – 7.54 (m, 2H), 7.47 – 7.39 (m, 4H), 7.25 (d, $J = 8.4$, 1H); ESI-MS(+): m/z 409.17 [$\text{M} + \text{H}$] $^+$.

3-(methylsulfonamido)pyridine 1-oxide (3.23b): Following the general method for oxidation, from **3.23a** (0.400 g, 2.32 mmol) and mCPBA (2.60 g, 77.0% Wt, 11.6 mmol), at 35 °C for 16 h, the final product was obtained as an impure solid, which was then recrystallized from 7:3 IPA to CH_2Cl_2 to yield **3.23b** (0.240 g, 1.28 mmol, 55%) as cream colored crystals. $^1\text{H NMR}$ (400 MHz, $\text{DMSO-}d_6$): δ 10.28 (*br s*, 1H), 8.03 (s, 1H), 7.97 (d, $J = 6.0$, 1H), 7.36 (t, $J = 6.8$, 1H),

7.15 (d, $J = 8.4$, 1H), 3.13 (s, 3H); HRMS (ESI-TOF): m/z calcd for $C_6H_7N_2O_3S^-$: 187.0183 [M-H]⁻; found: 187.0182.

3-(methylsulfonamido)pyridine 1-oxide (3.24b): Following the general method for oxidation, from **3.24a** (0.500 g, 2.08 mmol) and mCPBA (2.33 g, 77.0% Wt, 10.4 mmol), at 35 °C for 16 h, the final product was obtained as an impure solid, which was then recrystallized from 1:1 MeOH to CH_2Cl_2 to yield **3.24b** (0.221 g, 0.862 mmol, 41%) as creamy yellow colored crystals. ¹H NMR (400 MHz, DMSO- d_6): δ 11.01 (*br s*, 1H), 7.99 – 7.95 (m, 2H), 7.95 (s, 1H), 7.67 – 7.66 (m, 1H), 7.33 (t, $J = 7.6$, 1H), 7.18 – 7.16 (m, 1H), 7.12 (d, $J = 8.4$, 1H); HRMS (ESI-TOF): m/z calcd for $C_9H_7N_2O_3S_2^-$: 254.9904 [M-H]⁻; found: 254.9904.

Thionation

General Thionation Protocol: The starting material and 1.5 equivalents of KI were dissolved in 5 mL DI water with a minimal amount of MeOH to dissolve as needed. Then 5 mL of saturated freshly prepared sodium hydrogen sulfide solution (excess) was added to the solution containing the starting material. The reaction mixture was then heated at 50 – 100 °C for 3 – 16 h. Upon reaction completion as indicated by TLC, the reaction mixture was cooled to 0 °C, and slowly quenched with 6 M HCl. CAUTION: The neutralization of NaSH using acid generates H₂S gas, which is both highly flammable and highly toxic by inhalation; only perform neutralization in well-vented fume hood. After waiting ~5 min to allow the resultant H₂S gas to evolve and disperse, the resulting mixture was extracted into organic using 3×15 mL ethyl acetate. The combined organic was washed with aqueous 1 M Na₂S₂O₃, until the aqueous went from cloudy to clear. Then the organic was washed with brine, dried over magnesium sulfate,

and the solids were filtered off and discarded. The filtrate was concentrated under reduced pressure, and the remaining residue was then purified by column chromatography, using a gradient of 100% hexanes to 100% CH₂Cl₂, and then to 15% MeOH in CH₂Cl₂. The desired product typically eluted around 80% CH₂Cl₂ in hexanes. When necessary, the collected product was recrystallized from 7:3 IPA to water. The crystals were collected via vacuum filtration and rinsed with a small amount of cold IPA to obtain the desired final products.

N-(1-Hydroxy-2-thioxo-1,2-dihydropyridin-3-yl)thiophene-2-sulfonamide (3.5c): Following the above general thionation protocol, from **3.5b** (0.500 g, 1.49 mmol) with KI (0.371 g, 2.24 mmol) in 5 mL saturated NaSH solution (excess) at 100 °C for 8 h, **3.5c** (0.160 g, 0.555 mmol, 37%) was obtained as a pale yellow solid. ¹H NMR (400 MHz, DMSO-*d*₆): δ 9.50 (*br s*, 1H), 8.17 (d, *J* = 6.8, 1H), 7.98 (d, *J* = 4.8, 1H), 7.72 (d, *J* = 4.0, 1H), 7.59 (d, *J* = 8.0, 1H), 7.14 (t, *J* = 4.8, 1H), 6.88 (d, *J* = 7.6, 1H); ¹³C NMR (500 MHz, DMSO-*d*₆): δ 164.3, 138.6, 137.3, 135.4, 134.3, 134.0, 128.4, 119.4, 112.8; HRMS (ESI-TOF): *m/z* calcd for [C₉H₇N₂O₃S₃]⁻: 286.9624 [M-H]⁻; found: 286.9626.

N-(1-Hydroxy-2-thioxo-1,2-dihydropyridin-3-yl)benzamide (3.6c): Following the above general thionation protocol, from **3.6b** (0.160 g, 0.546 mmol) with KI (0.136 g, 0.819 mmol) in 5 mL saturated NaSH solution (excess) at 40 °C for 16 h, **3.6c** (0.065 g, 0.260 mmol, 48%) was obtained as an off white solid. ¹H NMR (400 MHz, DMSO-*d*₆): δ 10.55 (*br s*, 1H), 8.55 (d, *J* = 7.6, 1H), 8.21 (d, *J* = 7.2, 1H), 7.96 (d, *J* = 7.6, 2H), 7.69 – 7.60 (m, 3H), 6.98 (t, *J* = 7.6, 1H); ¹³C NMR (500 MHz, DMSO-*d*₆): δ 165.2, 163.4, 138.7, 134.1, 133.1, 132.6, 129.7, 127.5,

119.1, 113.4; HRMS (ESI-TOF): m/z calcd for $[C_{12}H_9N_2O_2S]^-$: 245.0390 $[M-H]^-$; found: 245.0391.

N-(1-Hydroxy-2-thioxo-1,2-dihydropyridin-3-yl)thiophene-2-carboxamide (3.7c):

Following the above general thionation protocol, from **3.7b** (0.350 g, 1.17 mmol) with KI (0.291 g, 1.76 mmol) in 5 mL saturated NaSH solution (excess) at 40 °C for 16 h, **3.7c** (0.130 g, 0.515 mmol, 44%) was obtained as a grey solid. 1H NMR (400 MHz, DMSO- d_6): δ 10.42 (*br s*, 1H), 8.41 (d, $J = 7.6$, 1H), 8.21 (d, $J = 6.8$, 1H), 7.96 (d, $J = 4.8$, 1H), 7.82 (d, $J = 3.2$, 1H), 7.27 (t, $J = 3.6$, 1H), 6.96 (t, $J = 6.8$, 1H); ^{13}C NMR (500 MHz, DMSO- d_6): δ 163.3, 160.0, 138.7, 138.4, 133.5, 132.6, 130.0, 129.2, 119.3, 113.3; HRMS (ESI-TOF): m/z calcd for $[C_{10}H_7N_2O_2S_2]^-$: 250.9954 $[M-H]^-$; found: 250.9957.

N-(1-Hydroxy-2-thioxo-1,2-dihydropyridin-3-yl)-5-methylthiophene-2-sulfonamide (3.8c):

Following the above general thionation protocol, from **3.8b** (0.200 g, 0.573 mmol) with KI (0.143 g, 0.859 mmol) in 5 mL saturated NaSH solution (excess) at 100 °C for 8 h, **3.8c** (0.058 g, 0.18 mmol, 33%), was obtained as a pale yellow solid. 1H NMR (400 MHz, DMSO- d_6): δ 9.44 (*br s*, 1H), 8.17 (d, $J = 6.8$, 1H), 7.58 – 7.56 (m, 2H), 6.90 – 6.87 (m, 2H), 2.45 (s, 3H); ^{13}C NMR (500 MHz, DMSO- d_6): δ 164.0, 149.7, 137.4, 135.3, 134.8, 133.9, 127.0, 118.7, 112.9, 15.6; HRMS (ESI-TOF): m/z calcd for $[C_{10}H_9N_2O_3S_3]^-$: 300.9781 $[M-H]^-$; found: 300.9780.

N-(1-Hydroxy-2-thioxo-1,2-dihydropyridin-3-yl)-4-methylthiophene-2-sulfonamide (3.9c):

Following the above general thionation protocol, from **3.9b** (0.190 g, 0.544 mmol) with KI (0.135 g, 0.816 mmol) in 5 mL saturated NaSH solution (excess) at 100 °C for 5 h, **3.9c** (0.070 g,

0.230 mmol, 43%) was obtained as a pale yellow solid. ^1H NMR (400 MHz, DMSO- d_6): δ 9.47 (*br s*, 1H), 8.17 (dd, $J_1 = 6.8$, $J_2 = 1.2$, 1H), 7.58 – 7.56 (m, 3H), 6.89 (t, $J = 8.0$, 1H), 2.16 (s, 3H); ^{13}C NMR (500 MHz, DMSO- d_6): δ 166.5, 153.3, 148.23, 139.3, 138.6, 134.9, 132.7, 129.7, 124.4, 15.5; HRMS (ESI-TOF): m/z calcd for $[\text{C}_{10}\text{H}_9\text{N}_2\text{O}_3\text{S}_3]^-$: 300.9781 $[\text{M-H}]^-$; found: 300.9778.

N-(1-Hydroxy-5-methyl-2-thioxo-1,2-dihydropyridin-3-yl)thiophene-2-sulfonamide (3.10c):

Following the above general thionation protocol, from **3.10b** (0.100 g, 0.286 mmol) with KI (0.071 g, 0.430 mmol) in 3 mL saturated NaSH solution (excess) at 75 °C for 3 h, **3.10c** (0.0057 g, 0.019 mmol, 7%) was obtained as a very pale yellow solid. ^1H NMR (400 MHz, Acetone- d_6): δ 8.65 (*br s*, 1H), 8.17 (s, 1H), 7.92 (d, $J = 4.8$, 1H), 7.77 (d, $J = 4.0$, 1H), 7.63 (s, 1H), 7.16 (t, $J = 4.0$, 1H), 2.34 (s, 3H); HRMS (ESI-TOF): m/z calcd for $[\text{C}_{10}\text{H}_9\text{N}_2\text{O}_3\text{S}_3]^-$: 300.9781 $[\text{M-H}]^-$; found: 300.9779.

N-(1-Hydroxy-5-methyl-2-thioxo-1,2-dihydropyridin-3-yl)thiophene-2-sulfonamide (3.11c):

Following the above general thionation protocol, from **3.11b** (0.210 g, 0.601 mmol) with KI (0.150 g, 0.902 mmol) in 3 mL saturated NaSH solution (excess) at 75 °C for 3 h, **3.11c** (0.011 g, 0.036 mmol, 6%) was obtained as a pale yellow solid. ^1H NMR (400 MHz, DMSO- d_6): δ 12.49 (*br s*, 1H), 9.35 (*br s*, 1H), 7.95 (d, $J = 4.8$, 1H), 7.68 (d, $J = 4.0$, 1H), 7.55 (d, $J = 8.0$, 1H), 7.12 (t, $J = 4.0$, 1H), 6.85 (d, $J = 8.0$, 1H), 2.41 (s, 3H); HRMS (ESI-TOF): m/z calcd for $[\text{C}_{10}\text{H}_9\text{N}_2\text{O}_3\text{S}_3]^-$: 300.9781 $[\text{M-H}]^-$; found: 300.9778.

N-(1-Hydroxy-2-thioxo-1,2-dihydropyridin-3-yl)cyclopropanesulfonamide (3.12c):

Following the above general thionation protocol, from **3.12b** (0.460 g, 0.157 mmol) with KI (0.391 g, 2.35 mmol) in 5 mL saturated NaSH solution (excess) at 100 °C for 8 h, **3.12c** (0.132 g, 0.534 mmol, 34%) was obtained as a pale yellow solid. ¹H NMR (400 MHz, DMSO-*d*₆): δ 8.94 (*br s*, 1H), 8.22 (dd, *J*₁ = 6.8, *J*₂ = 1.2, 1H), 7.58 (dd, *J*₁ = 7.6, *J*₂ = 0.8, 1H), 6.90 (t, *J* = 7.6, 1H), 2.87 – 2.81 (m, 1H), 1.05 – 0.95 (m, 4H); ¹³C NMR (500 MHz, DMSO-*d*₆): δ 153.2, 147.9, 135.3, 133.1, 123.9, 30.9, 5.9; HRMS (ESI-TOF): *m/z* calcd for [C₈H₉N₂O₃S₂]⁻: 245.0060 [M-H]⁻; found: 245.0061.

1-((1R,4S)-7,7-Dimethyl-2-oxobicyclo[2.2.1]heptan-1-yl)-N-(1-hydroxy-2-thioxo-1,2-

dihydropyridin-3-yl)methanesulfonamide (3.13c): Following the above general thionation protocol, from **3.13b** (0.240 g, 0.669 mmol) with KI (0.167 g, 1.00 mmol) in 5 mL saturated NaSH solution (excess) at 80 °C for 6 h, **3.13c** (0.011 g, 0.031 mmol, 5%) was obtained as a dark grey solid. ¹H NMR (400 MHz, DMSO-*d*₆): δ 11.63 (*br s*, 1H), 8.45 (*br s*, 1H), 8.31 (d, *J* = 6.4, 1H), 7.81 (d, *J* = 7.6, 1H), 7.11 (t, *J* = 7.2, 1H), 3.66 (d, *J* = 15.2, 1H), 3.30 (d, *J* = 10.8, 1H), 2.46 – 2.34 (m, 2H), 2.15 – 2.13 (m, 1H), 1.94 (d, *J* = 18.4, 2H), 1.82 – 1.75 (m, 1H), 1.53 – 1.47 (m, 1H), 1.09 (s, 3H), 0.87 (s, 3H); HRMS (ESI-TOF): *m/z* calcd for [C₁₅H₁₉N₂O₄S₂]⁻: 355.0792 [M-H]⁻; found: 355.0789.

N-(1-Hydroxy-2-thioxo-1,2-dihydropyridin-3-yl)-1-methyl-1H-pyrazole-3-sulfonamide

(3.14c): Following the above general thionation protocol, from **3.14b** (0.166 g, 0.498 mmol) with KI (0.124 g, 0.747 mmol) in 5 mL saturated NaSH solution (excess) at 100 °C for 5 h, **3.14c** (0.047 g, 0.17 mmol, 33%) was obtained as a light grey solid. ¹H NMR (400 MHz, DMSO-*d*₆):

δ 9.35 (*br s*, 1H), 8.14 (d, $J = 6.8$, 1H), 7.88 (d, $J = 1.6$, 1H), 7.54 (d, $J = 7.6$, 1H), 6.87 (t, $J = 7.6$, 1H), 6.78 (d, $J = 1.6$, 1H), 3.87 (s, 3H); ^{13}C NMR (500 MHz, DMSO- d_6): δ 152.7, 149.5, 147.7, 134.2, 133.8, 133.2, 124.2, 107.3, 25.9; HRMS (ESI-TOF): m/z calcd for $[\text{C}_9\text{H}_9\text{N}_4\text{O}_3\text{S}_2]^-$: 285.0122 [M-H] $^-$; found: 285.0122.

N-(1-Hydroxy-2-thioxo-1,2-dihydropyridin-3-yl)-1-methyl-1H-pyrazole-4-sulfonamide

(3.15c): Following the above general thionation protocol, from **3.15b** (0.210 g, 0.630 mmol) with KI (0.157 g, 0.945 mmol) in 5 mL saturated NaSH solution (excess) at 100 °C for 5 h, **3.15c** (0.057 g, 0.20 mmol, 32%) was obtained as a dark grey solid. ^1H NMR (400 MHz, DMSO- d_6): δ 9.24 (*br s*, 1H), 8.14 (d, $J = 6.8$, 1H), 8.44 (s, 1H), 8.14 (d, $J = 6.8$, 1H), 7.85 (s, 1H), 7.53 (d, $J = 8.0$, 1H), 6.86 (t, $J = 7.6$, 1H), 3.82 (s, 3H); ^{13}C NMR (500 MHz, DMSO- d_6): δ 163.6, 138.8, 137.7, 133.9, 133.3, 119.9, 117.8, 113.0, 25.9; HRMS (ESI-TOF): m/z calcd for $[\text{C}_9\text{H}_9\text{N}_4\text{O}_3\text{S}_2]^-$: 285.0122 [M-H] $^-$; found: 285.0121.

N-(1-Hydroxy-2-thioxo-1,2-dihydropyridin-3-yl)thiophene-3-sulfonamide **(3.16c):**

Following the above general thionation protocol, from **3.16b** (0.250 g, 0.746 mmol) with KI (0.186 g, 1.12 mmol) in 5 mL saturated NaSH solution (excess) at 100 °C for 8 h, **3.16c** (0.053 g, 0.18 mmol, 25%) was obtained as a pale yellow solid. ^1H NMR (400 MHz, DMSO- d_6): δ 9.36 (*br s*, 1H), 8.40 – 8.39 (m, 1H), 8.14 (d, $J = 6.8$, 1H), 7.73 – 7.71 (m, 1H), 7.54 (d, $J = 8.0$, 1H), 7.35 (d, $J = 5.2$, 1H), 6.84 (t, $J = 8.0$, 1H); ^{13}C NMR (500 MHz, DMSO- d_6): δ 153.2, 148.1, 147.8, 139.2, 132.6, 130.2, 125.6, 124.2, 119.7; HRMS (ESI-TOF): m/z calcd for $[\text{C}_9\text{H}_7\text{N}_2\text{O}_3\text{S}_3]^-$: 286.9624 [M-H] $^-$; found: 286.9623.

N-(1-Hydroxy-2-thioxo-1,2-dihydropyridin-4-yl)thiophene-2-sulfonamide (3.17c):

Following the above general thionation protocol, from **3.17b** (0.290 g, 0.865 mmol) with KI (0.215 g, 2.30 mmol) in 5 mL saturated NaSH solution (excess) at 100 °C for 8 h, **3.17c** (0.083 g, 0.288 mmol, 33%) was obtained as a very pale yellow solid. ¹H NMR (400 MHz, DMSO-*d*₆): δ 11.95 (*br s*, 1H), 11.44 (*br s*, 1H), 8.25 (dd, *J*₁ = 7.2, *J*₂ = 3.6, 1H), 8.04 – 8.02 (m, 1H), 7.76 – 7.74 (m, 1H), 7.22 – 7.18 (m, 2H), 6.64 – 6.62 (m, 1H); HRMS (ESI-TOF): *m/z* calcd for [C₉H₇N₂O₃S₃]⁻: 286.9624 [M-H]⁻; found: 286.9627.

N-(1-Hydroxy-6-thioxo-1,6-dihydropyridin-3-yl)thiophene-2-sulfonamide (3.18c):

Following the above general thionation protocol, from **3.18b** (0.310 g, 0.925 mmol) with KI (0.230 g, 2.39 mmol) in 5 mL saturated NaSH solution (excess) at 100 °C for 8 h, **3.18c** (0.028 g, 0.097 mmol, 10%) was obtained as a pale yellow solid. ¹H NMR (400 MHz, Acetone-*d*₆): δ 8.31 (dd, *J*₁ = 2.4, *J*₂ = 0.4, 1H), 7.93 (dd, *J*₁ = 4.8, *J*₂ = 1.2, 1H), 7.64 (dd, *J*₁ = 3.6, *J*₂ = 1.2, 1H), 7.58 (dd, *J*₁ = 9.2, *J*₂ = 0.4, 1H), 7.33 (dd, *J*₁ = 9.2, *J*₂ = 2.4, 1H), 7.19 (dd, *J*₁ = 5.2, *J*₂ = 4.0, 1H); ¹³C NMR (500 MHz, DMSO-*d*₆): δ 167.0, 139.0, 134.8, 133.7, 133.6, 129.5, 129.4, 128.5, 125.8; HRMS (ESI-TOF): *m/z* calcd for [C₉H₇N₂O₃S₃]⁻: 286.9624 [M-H]⁻; found: 286.9626.

5-Chloro-N-(1-hydroxy-2-thioxo-1,2-dihydropyridin-3-yl)thiophene-2-sulfonamide (3.19c):

Following the above general thionation protocol, from **3.19b** (0.300 g, 0.812 mmol) with KI (0.202 g, 1.22 mmol) in 5 mL saturated NaSH solution (excess) at 65 °C for 16 h, **3.19c** (0.152 g, 0.471 mmol, 58%) was obtained as a pale yellow solid. ¹H NMR (400 MHz, DMSO-*d*₆): δ 9.64 (*br s*, 1H), 8.23 (dd, *J*₁ = 6.8, *J*₂ = 0.8, 1H), 7.62 – 7.57 (m, 2H), 7.23 (d, *J* = 4.0, 1H), 6.89 (t, *J* =

7.2, 1H); ^{13}C NMR (500 MHz, DMSO- d_6): δ 164.7, 137.2, 136.9, 134.5, 134.2, 128.7, 121.0, 112.8; HRMS (ESI-TOF): m/z calcd for $[\text{C}_9\text{H}_6\text{ClN}_2\text{O}_3\text{S}_3]^-$: 320.9235 $[\text{M}-\text{H}]^-$; found: 320.9234.

5-Bromo-N-(1-hydroxy-2-thioxo-1,2-dihydropyridin-3-yl)thiophene-2-sulfonamide (3.20c):

Following the above general thionation protocol, from **3.20b** (0.300 g, 0.724 mmol) with KI (0.180 g, 1.09 mmol) in 5 mL saturated NaSH solution (excess) at 75 °C for 17 h, **3.20c** (0.050 g, 0.14 mmol, 19%) was obtained as a pale yellow solid. ^1H NMR (400 MHz, DMSO- d_6): δ 9.62 (*br s*, 1H), 8.22 (d, $J = 6.8$, 1H), 7.59 – 7.56 (m, 2H), 7.32 (d, $J = 3.6$, 1H), 6.89 (t, $J = 7.2$, 1H); ^{13}C NMR (500 MHz, DMSO- d_6): δ 164.6, 139.7, 137.0, 134.9, 134.4, 132.1, 121.0, 120.8, 112.8; HRMS (ESI-TOF): m/z calcd for $[\text{C}_9\text{H}_6\text{BrN}_2\text{O}_3\text{S}_3]^-$: 364.8729 $[\text{M}-\text{H}]^-$; found: 364.8728.

N-(1-Hydroxy-2-thioxo-1,2-dihydropyridin-3-yl)benzo[*c*][1,2,5]thiadiazole-4-sulfonamide

(3.21c): Following the above general thionation protocol, from **3.21b** (0.150 g, 0.387 mmol) with KI (0.0965 g, 0.581 mmol) in 5 mL saturated NaSH solution (excess) at 75 °C for 17 h, **3.21c** (0.018 g, 0.053 mmol, 14%) was obtained as a deep yellow solid. ^1H NMR (400 MHz, DMSO- d_6): δ 9.73 (*br s*, 1H), 8.40 (d, $J = 8.8$, 1H), 8.32 (d, $J = 7.2$, 1H), 8.06 (d, $J = 6.8$, 1H), 7.84 (t, $J = 6.8$, 1H), 7.56 (d, $J = 8.0$, 1H), 6.78 (t, $J = 6.8$, 1H); HRMS (ESI-TOF): m/z calcd for $[\text{C}_{11}\text{H}_7\text{N}_4\text{O}_3\text{S}_3]^-$: 338.9686 $[\text{M}-\text{H}]^-$; found: 338.9683.

N-(1-Hydroxy-2-thioxo-1,2-dihydropyridin-3-yl)-5-phenylthiophene-2-sulfonamide (3.22d):

Following the above general thionation protocol, from **3.22c** (0.400 g, 0.973 mmol) with KI (0.242 g, 1.46 mmol) in 5 mL saturated NaSH solution (excess) at 60 °C for 16 h, **3.22d** (0.153 g, 0.420 mmol, 43%) was obtained as a light yellow solid. ^1H NMR (400 MHz, DMSO- d_6): δ

9.58 (*br s*, 1H), 8.19 (d, $J = 7.2$, 1H), 7.74 (d, $J = 3.6$, 1H), 7.70 – 7.66 (m, 2H), 7.62 (d, $J = 8.0$, 1H), 7.55 (d, $J = 4.0$, 1H), 7.51 – 7.39 (m, 4H), 6.90 (t, $J = 7.6$, 1H); ^{13}C NMR (500 MHz, DMSO- d_6): δ 150.3, 147.5, 136.1, 133.6, 129.8, 129.7, 129.6, 129.1, 128.5, 128.4, 126.8, 126.5, 125.8, 125.7, 123.9, 113.2.

N-(2-Thioxo-1,2-dihydropyridin-3-yl)methanesulfonamide (3.25b): To a solution of **3.25a** (0.500 g, 50% Wt, 0.996 mmol) in 15 mL DMF, thiourea (1.82 g, 23.9 mmol) was added in one portion, and the reaction was placed under argon and heated to reflux at 150 °C for 12 h, after which the reaction mixture had changed color to dark brown. Then the reaction was cooled to 110 °C, and 6 M HCl (15 mL, 90 mmol) was added in one portion; the reaction was heated at 110°C for an additional 2 h. Then the reaction mixture was cooled to 25 °C, diluted with 50 mL brine, and extracted into organic using 3×15 mL ethyl acetate. The combined organic was washed with an additional 15 mL brine, dried over magnesium sulfate, and the solids were filtered off and discarded. The filtrate was concentrated under reduced pressure, and the resulting crude was purified by column chromatography, running gradient from 100% hexanes to 100% ethyl acetate, and then from 100% CH₂Cl₂ to 15% MeOH in CH₂Cl₂. The desired product eluted in 85% ethyl acetate in hexanes. Like fractions of the desired product were combined and concentrated under reduced pressure. The resulting solid was recrystallized from 3:1 ethyl acetate to hexanes, and the solid was collected via vacuum filtration and washed with hexanes to obtain **3.25b** (0.081 g, 0.40 mmol, 40 %) as a pale yellow solid. ^1H NMR (400 MHz, DMSO- d_6): δ 8.71 (*br s*, 1H), 7.61 – 7.58 (m, 2H), 6.90 (t, $J = 6.8$, 1H), 3.16 (s, 3H); HRMS (ESI-TOF): m/z calcd for C₆H₉N₂O₂S₂⁺: 205.0100 [M+H]⁺; found: 205.0103.

N-(2-Thioxo-1,2-dihydropyridin-3-yl)thiophene-2-sulfonamide (3.26): Following the same protocol used in **3.25b**, from **3.5a** (0.500 g, 1.57 mmol) and thiourea (1.43 g, 18.8 mmol) the desired **3.26** (0.094 g, 0.35 mmol, 22%) was obtained as a deep yellow solid. ^1H NMR (400 MHz, DMSO- d_6): δ 9.27 (*br s*, 1H), 7.98 (d, $J = 4.8$, 1H), 7.73 (d, $J = 0.8$, 1H), 7.65 (d, $J = 7.6$, 1H), 7.57 (d, $J = 6.0$, 1H), 7.16 – 7.15 (m, 1H), 6.88 (d, $J = 7.6$, 1H); ^{13}C NMR (500 MHz, DMSO- d_6): δ 168.3, 138.6, 136.4, 135.3, 134.3, 133.8, 128.4, 122.6, 114.2; HRMS (ESI-TOF): m/z calcd for $\text{C}_9\text{H}_7\text{N}_2\text{O}_2\text{S}_3^-$: 270.9675 [M-H] $^-$; found: 270.9675.

DTT in IDE Assay

The prepared elaborated HOPTOs were found to partially form dimers through the thione, as identified by LCMS (Figure 3.5a), where the peak at 8.25 min correlates the mass of the dimer with ESI-MS(+) = m/z 574.89 [M + H] $^+$, and the peak at 9.64 min matches the mass of **5c** at ESI-MS(+) = m/z 289.07 [M + H] $^+$. The addition of 0.5 mM DTT in the HPLC trace was found to dramatically reduce the size of the dimer peak (Figure 3.5b), with relative percent peak area of the dimer shrinking from 14.4% to 5.5%.

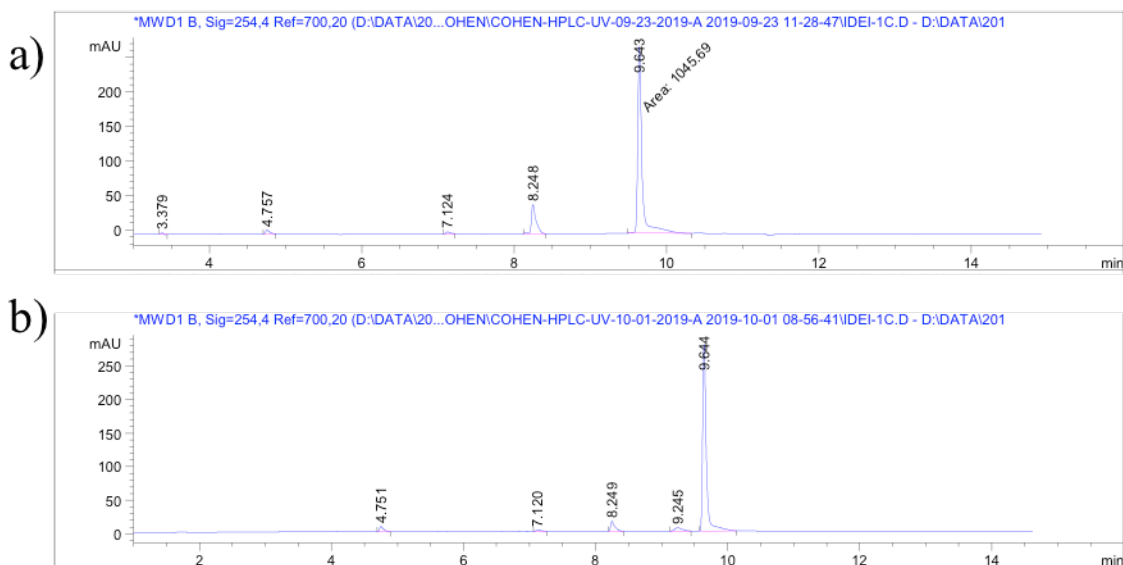


Figure 3.6. a) The HPLC trace of **5c** in 1:4MeOH to water with no additives. The peak at 8.25 min correlates to the dimer, whereas the peak at 9.64 min is **5c**; b) The HPLC trace of **5c** in 1:4MeOH to water with 0.5 mM DTT. The presence of DTT reduces the dimer peak.

Protein Thermal Shift Assay

To each well of a 96-well 0.2 mL optical MicroAmp (ThermoFisher) thermocycler plate was added 9.5 μ L of buffer (ThermoFisher Thermal Shift buffer with 0.5 mM DTT), 4 μ L of IDE in buffer (0.5 mg/mL), 4 μ L of ligand in buffer (1 mM), and 2.5 μ L of SYPRO orange Thermal Shift dye (ThermoFisher) in buffer, so that each well contained a final concentration of 0.1 mg/mL and 200 μ M ligand. The thermocycler plate wells were sealed prior to analysis, and the plate was then heated in a thermocycler from 25 to 99 $^{\circ}$ C at a ramp rate of 0.05 $^{\circ}$ C/sec. All thermal shift measurement was taken in six replicates, monitoring fluorescence using the ROX filter channel with ex = 580 nm and em = 623 nm. Finally, the fluorescence signal was fitted to a first derivative curve to identify T_m .

3.6 Acknowledgements

Chapter 3, in part, is currently being prepared for submission for publication of the material. Adamek, R.N.; Suire, C.; Leissring, M.; Cohen, S.M. The dissertation author was the primary researcher and the primary author for the reprinted data presented herein.

3.7 References

1. Shen, Y.; Joachimiak, A.; Rosner, M. R.; Tang, W. J., Structures of Human Insulin-Degrading Enzyme Reveal a New Substrate Recognition Mechanism. *Nature* **2006**, *443*, 870-4.
2. Manolopoulou, M.; Guo, Q.; Malito, E.; Schilling, A. B.; Tang, W. J., Molecular Basis of Catalytic Chamber-Assisted Unfolding and Cleavage of Human Insulin by Human Insulin-Degrading Enzyme. *J. Biol. Chem.* **2009**, *284*, 14177-88.
3. McCord, L. A.; Liang, W. G.; Dowdell, E.; Kalas, V.; Hoey, R. J.; Koide, A.; Koide, S.; Tang, W. J., Conformational States and Recognition of Amyloidogenic Peptides of Human Insulin-Degrading Enzyme. *Proc. Natl. Acad. Sci. U. S. A.* **2013**, *110*, 13827-32.
4. Tang, W. J., Targeting Insulin-Degrading Enzyme to Treat Type 2 Diabetes Mellitus. *Trends. Endocrinol. Metab.* **2016**, *27*, 24-34.
5. Song, E. S.; Juliano, M. A.; Juliano, L.; Fried, M. G.; Wagner, S. L.; Hersh, L. B., ATP Effects on Insulin-Degrading Enzyme are Mediated Primarily Through its Triphosphate Moiety. *J. Biol. Chem.* **2004**, *279*, 54216-20.
6. Di Costanzo, L.; Moulin, M.; Haertlein, M.; Meilleur, F.; Christianson, D. W., Expression, Purification, Assay, and Crystal Structure of Perdeuterated Human Arginase I. *Arch. Biochem. Biophys.* **2007**, *465*, 82-9.
7. Hersh, L. B., The Insulysin (Insulin Degrading Enzyme) Enigma. *Cell. Mol. Life Sci.* **2006**, *63*, 2432-4.
8. Tundo, G. R.; Sbardella, D.; Ciaccio, C.; Grasso, G.; Gioia, M.; Coletta, A.; Polticelli, F.; Di Pierro, D.; Milardi, D.; Van Endert, P.; Marini, S.; Coletta, M., Multiple Functions of Insulin-Degrading Enzyme: A Metabolic Crosslight? *Crit. Rev. Biochem. Mol. Biol.* **2017**, *52*, 554-582.
9. Duckworth, W. C.; Kitabchi, A. E., Insulin and Glucagon Degradation by the Same Enzyme. *Diabetes* **1974**, *23*, 536-43.
10. Farris, W.; Mansourian, S.; Chang, Y.; Lindsley, L.; Eckman, E. A.; Frosch, M. P.; Eckman, C. B.; Tanzi, R. E.; Selkoe, D. J.; Guenette, S., Insulin-Degrading Enzyme Regulates the Levels of Insulin, Amyloid Beta-Protein, and the Beta-Amyloid Precursor Protein Intracellular Domain in Vivo. *Proc. Natl. Acad. Sci. U. S. A.* **2003**, *100*, 4162-7.

11. Hayes, M. R.; Mietlicki-Baase, E. G.; Kanoski, S. E.; De Jonghe, B. C., Incretins and Amylin: Neuroendocrine Communication between the Gut, Pancreas, and Brain in Control of Food Intake and Blood Glucose. *Annu. Rev. Nutr.* **2014**, *34*, 237-60.
12. Jiang, G.; Zhang, B. B., Glucagon and Regulation of Glucose Metabolism. *Am. J. Physiol. Endocrinol. Metab.* **2003**, *284*, E671-8.
13. Kurochkin, I. V.; Guarnera, E.; Berezovsky, I. N., Insulin-Degrading Enzyme in the Fight against Alzheimer's Disease. *Trends Pharmacol. Sci.* **2018**, *39*, 49-58.
14. Malito, E.; Hulse, R. E.; Tang, W. J., Amyloid Beta-Degrading Cryptidases: Insulin Degrading Enzyme, Presequence Peptidase, and Peprilysin. *Cell. Mol. Life. Sci.* **2008**, *65*, 2574-85.
15. Maianti, J. P.; Tan, G. A.; Vetere, A.; Welsh, A. J.; Wagner, B. K.; Seeliger, M. A.; Liu, D. R., Substrate-Selective Inhibitors that Reprogram the Activity of Insulin-Degrading Enzyme. *Nat. Chem. Biol.* **2019**, *15*, 565-574.
16. Duckworth, W. C.; Bennett, R. G.; Hamel, F. G., Insulin Degradation: Progress and Potential. *Endocr. Rev.* **1998**, *19*, 608-24.
17. Costes, S.; Butler, P. C., Insulin-Degrading Enzyme Inhibition, a Novel Therapy for Type 2 Diabetes? *Cell Metab.* **2014**, *20*, 201-3.
18. Leissring, M. A.; Malito, E.; Hedouin, S.; Reinstatler, L.; Sahara, T.; Abdul-Hay, S. O.; Choudhry, S.; Maharvi, G. M.; Fauq, A. H.; Huzarska, M.; May, P. S.; Choi, S.; Logan, T. P.; Turk, B. E.; Cantley, L. C.; Manolopoulou, M.; Tang, W. J.; Stein, R. L.; Cuny, G. D.; Selkoe, D. J., Designed Inhibitors of Insulin-Degrading Enzyme Regulate the Catabolism and Activity of Insulin. *PLoS One* **2010**, *5*, e10504.
19. Deprez-Poulain, R.; Hennuyer, N.; Bosc, D.; Liang, W. G.; Enee, E.; Marechal, X.; Charton, J.; Totobenazara, J.; Berte, G.; Jahklal, J.; Verdet, T.; Dumont, J.; Dassonneville, S.; Woitrain, E.; Gauriot, M.; Paquet, C.; Duplan, I.; Hermant, P.; Cantrelle, F. X.; Sevin, E.; Culot, M.; Landry, V.; Herledan, A.; Piveteau, C.; Lippens, G.; Leroux, F.; Tang, W. J.; van Endert, P.; Staels, B.; Deprez, B., Catalytic Site Inhibition of Insulin-Degrading Enzyme by a Small Molecule Induces Glucose Intolerance in Mice. *Nat. Commun.* **2015**, *6*, 8250.
20. Durham, T. B.; Toth, J. L.; Klimkowski, V. J.; Cao, J. X.; Siesky, A. M.; Alexander-Chacko, J.; Wu, G. Y.; Dixon, J. T.; McGee, J. E.; Wang, Y.; Guo, S. Y.; Cavitt, R. N.; Schindler, J.; Thibodeaux, S. J.; Calvert, N. A.; Coghlan, M. J.; Sindelar, D. K.; Christe, M.; Kiselyov, V. V.; Michael, M. D.; Sloop, K. W., Dual Exosite-binding Inhibitors of Insulin-degrading Enzyme Challenge Its Role as the Primary Mediator of Insulin Clearance in Vivo. *J. Biol. Chem.* **2015**, *290*, 20044-59.
21. Charton, J.; Gauriot, M.; Totobenazara, J.; Hennuyer, N.; Dumont, J.; Bosc, D.; Marechal, X.; Elbakali, J.; Herledan, A.; Wen, X.; Ronco, C.; Gras-Masse, H.; Heninot, A.; Pottiez, V.; Landry, V.; Staels, B.; Liang, W. G.; Leroux, F.; Tang, W. J.; Deprez, B.; Deprez-Poulain, R., Structure-Activity Relationships of Imidazole-Derived 2-[N-carbamoylmethyl-

alkylamino]acetic acids, Dual Binders of Human Insulin-Degrading Enzyme. *Eur. J. Med. Chem.* **2015**, *90*, 547-67.

22. Abdul-Hay, S. O.; Bannister, T. D.; Wang, H.; Cameron, M. D.; Caulfield, T. R.; Masson, A.; Bertrand, J.; Howard, E. A.; McGuire, M. P.; Crisafulli, U.; Rosenberry, T. R.; Topper, C. L.; Thompson, C. R.; Schurer, S. C.; Madoux, F.; Hodder, P.; Leissring, M. A., Selective Targeting of Extracellular Insulin-Degrading Enzyme by Quasi-Irreversible Thiol-Modifying Inhibitors. *ACS Chem. Biol.* **2015**, *10* (12), 2716-24.

23. Maianti, J. P.; McFedries, A.; Foda, Z. H.; Kleiner, R. E.; Du, X. Q.; Leissring, M. A.; Tang, W. J.; Charron, M. J.; Seeliger, M. A.; Saghatelian, A.; Liu, D. R., Anti-Diabetic Activity of Insulin-Degrading Enzyme Inhibitors Mediated by Multiple Hormones. *Nature* **2014**, *511*, 94-8.

24. Roth, R. A., Bacitracin: An Inhibitor of the Insulin Degrading Activity of Glutathione-Insulin Transhydrogenase. *Biochem. Biophys. Res. Commun.* **1981**, *98*, 431-8.

25. Neant-Fery, M.; Garcia-Ordonez, R. D.; Logan, T. P.; Selkoe, D. J.; Li, L.; Reinstatler, L.; Leissring, M. A., Molecular Basis for the Thiol Sensitivity of Insulin-Degrading Enzyme. *Proc. Natl. Acad. Sci. U. S. A.* **2008**, *105*, 9582-7.

26. Liu, Z.; Zhu, H.; Fang, G. G.; Walsh, K.; Mwamburi, M.; Wolozin, B.; Abdul-Hay, S. O.; Ikezu, T.; Leissring, M. A.; Qiu, W. Q., Characterization of Insulin Degrading Enzyme and Other Amyloid-Beta Degrading Proteases in Human Serum: A Role in Alzheimer's Disease? *J. Alzheimers Dis.* **2012**, *29*, 329-40.

27. Agrawal, A.; Johnson, S. L.; Jacobsen, J. A.; Miller, M. T.; Chen, L. H.; Pellecchia, M.; Cohen, S. M., Chelator Fragment Libraries for Targeting Metalloproteinases. *Chemmedchem* **2010**, *5*, 195-199.

28. Jacobsen, J. A.; Fullagar, J. L.; Miller, M. T.; Cohen, S. M., Identifying Chelators for Metalloprotein Inhibitors Using a Fragment-Based Approach. *J. Med. Chem.* **2011**, *54*, 591-602.

29. Pearson, R. G., Hard and Soft Acids and Bases. *J. Am. Chem. Soc.* **1963**, *85*, 3533-3539.

30. Pearson, R. G., Hard and Soft Acids and Bases HSAB.1. Fundamental Principles. *J. Chem. Educ.* **1968**, *45* (9), 581-587.

31. Jones, R. A.; Katritzky, A. R., N-Oxides and Related Compounds .17. The Tautomerism of Mercapto-Pyridine and Acylamino-Pyridine 1-Oxides. *J. Chem. Soc.* **1960**, (Jul), 2937-2942.

32. Adamek, R. N.; Credille, C. V.; Dick, B. L.; Cohen, S. M., Isosteres of Hydroxypyridinethione as Drug-like Pharmacophores for Metalloenzyme Inhibition. *J. Biol. Inorg. Chem.* **2018**, *23*, 1129-1138.

33. Semisotnov, G. V.; Rodionova, N. A.; Razgulyaev, O. I.; Uversky, V. N.; Gripas, A. F.; Gilmanshin, R. I., Study of the "Molten Globule" Intermediate State in Protein Folding by a Hydrophobic Fluorescent Probe. *Biopolymers* **1991**, *31*, 119-28.

34. Pantoliano, M. W.; Petrella, E. C.; Kwasnoski, J. D.; Lobanov, V. S.; Myslik, J.; Graf, E.; Carver, T.; Asel, E.; Springer, B. A.; Lane, P.; Salemme, F. R., High-Density Miniaturized Thermal Shift Assays as a General Strategy for Drug Discovery. *J. Biomol. Screening* **2001**, *6*, 429-40.
35. Lo, M. C.; Aulabaugh, A.; Jin, G.; Cowling, R.; Bard, J.; Malamas, M.; Ellestad, G., Evaluation of Fluorescence-Based Thermal Shift Assays for Hit Identification in Drug Discovery. *Anal. Biochem.* **2004**, *332*, 153-9.
36. Herledan, A.; Andres, M.; Lejeune-Dodge, A.; Leroux, F.; Biela, A.; Piveteau, C.; Warengem, S.; Couturier, C.; Deprez, B.; Deprez-Poulain, R., Drug Target Engagement Using Coupled Cellular Thermal Shift Assay-Acoustic Reverse-Phase Protein Array. *SLAS Discovery* **2020**, *25*, 207-214.

Chapter 4: MBP Isoosteres as Inhibitors of Metallo- β -Lactamase

4.1 Introduction

As described in Chapter 1, since medicinal chemistry can be informally translated as “healing black earth magic” it is rather fitting that many ancient cultures utilized a medical technique of treating open wounds with dirt or moldy bread as a means to prevent infection. It would be discovered many centuries later that this seemingly dubious practice was actually taking advantage of native sources of antibiotics, as soil bacteria and fungal spores are known to produce some of the most powerful antibiotics used to date. Indeed, since the class of β -lactams was discovered by Alexander Fleming in 1928, they have gone on to become the singularly most successful and commonly prescribed class of antibiotics.¹ Their powerful anti-bacterial activity stems from their ability to block peptidoglycan synthesis through inhibition of the unique bacterial transpeptidase enzyme, which disrupts and weakens the cell wall, eventually leading to cellular lysis and death (Figure 4.1).² The β -lactam bond serves as a mimic of the transpeptidase native substrate, D-Ala-D-Ala, so that binding and subsequent opening of the β -lactam results in covalent binding to the transpeptidase, blocking the active site from further interactions.

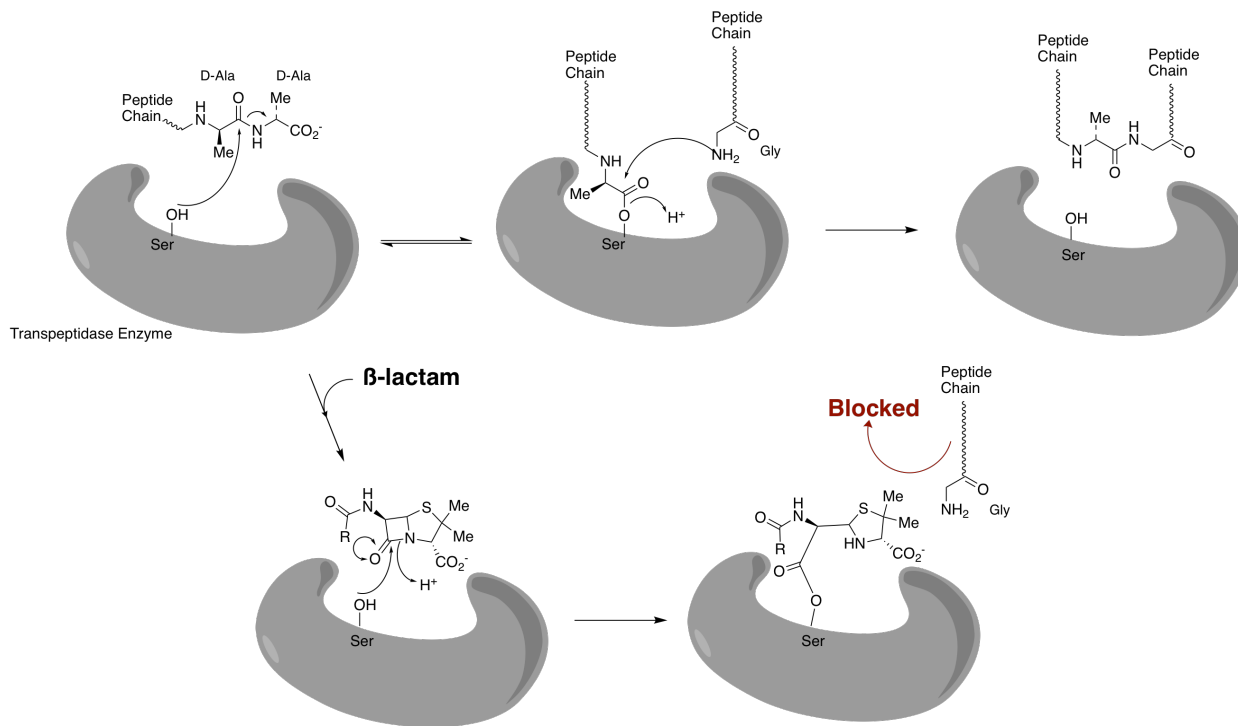


Figure 4.1. The mechanism of β -lactam inhibition of transpeptidase enzyme. The upper portion displays the normal action of transpeptidase cross-linking, whereas the bottom pathway displays the mechanism of covalent inhibition by a generic β -lactam. Adapted from Patrick.¹

Unfortunately, the overuse of these antibiotics has created a natural selection pressure for bacteria to adapt and develop resistance mechanisms to these β -lactam drugs.³ Some of these resistance mechanisms include efflux pumps, mutations of target proteins, and most problematic, the emergence of β -lactamase enzymes.⁴ β -Lactamases confer bacterial resistance through the premature hydrolysis of the β -lactam bond that is crucial for the activity of these drugs.⁴ The β -lactamases are classified according to the Ambler system, where classes A, C, and D rely on an active site serine residue to accomplish their hydrolytic activity.³ In particular, class A has a preference for penicillins, C prefers cephalosporins, and D prefers oxacillins.³ Class B is unique among the β -lactamases in that these consist of metallo- β -lactamases (MBLs) that rely on one or more active site Zn^{2+} ions to achieve β -lactam cleavage. Of the MBLs, New Delhi Metallo- β -Lactamase-1 (NDM-1), Verona Integrase Metallo- β -Lactamase-2 (VIM-2), and Imipenemase-1

(IMP-1), and have been the most prevalent in terms of posing a threat to human health.⁵ NDM-1 is generally regarded as the MBL of greatest concern, as it is the most easily communicable and has been shown to be capable of hydrolyzing all clinically relevant β -lactams,⁶ including the carbapenems, which are used as a last resort therapeutic against resistant infections. Therefore, the remainder of this section will focus on NDM-1 (unless otherwise stated) as it is the most pertinent and well studied of the MBLs.

NDM-1 is thought to have originated within the *Xanthomonas/Pseudoxanthomonas* species of rice plant pathogenic bacteria,⁷ but it has since been documented in multiple members of the Enterobacteriaceae family, the Acinetobacter family, and as well as the Pseudomonas family.⁸ NDM-1 was first reported in 2008 in a Swedish patient visiting New Delhi,⁹ and has since been documented worldwide, with most NDM-1 infections predominately located in India.¹⁰ NDM-1 infections are typically spread through nosocomial hospital acquisition, community acquisition – which also requires an environmental reservoir, as well as through personal travel.⁸ NDM-1 is easily communicable between different bacteria populations as it is carried on bla_{NDM-1} ,⁹ a plasmid capable of horizontal gene transfer. In addition to conferring β -lactam resistance, the bla_{NDM-1} plasmid is also known to encode resistance to many other common antibiotics, including aminoglycosides, fluoroquinolones, macrolides, and sulfonamides, so that NDM-1 bearing infections are often difficult to treat as they display pan-antibiotic resistance.^{11,12} In light of rapid transmission and widespread resistance to conventional antibiotic treatments, NDM-1 harboring pathogens have been labeled as “superbugs” and are widely considered to be of grave concern towards human health.¹³

Typical of other MBLs, NDM-1 relies on two active site Zn^{2+} ions to achieve β -lactam hydrolysis, shown in Figure 4.2 below. Within the active site, Zn_1^{2+} is bound by His122, His120,

and His189 while Zn_2^{2+} is bound by a Cys208, His250, Asp124 triad, and the two metals are bridged by a hydroxyl anion.¹⁴ The Zn_1^{2+} is coordinated in a tetrahedral geometry, whereas Zn_2^{2+} is coordinated in a distorted tetrahedral geometry. Additionally, Zn_1^{2+} is considered to be tightly bound with an unknown K_d , but the Zn_2^{2+} is more weakly coordinated with a $K_d = 2 \mu M$.¹⁵ These Zn^{2+} ions are located in the active site of NDM-1, which consists of a long, shallow, solvent-exposed groove¹⁶ with a large β -hairpin loop that is believed to close during substrate binding and catalysis; this loop is largest in NDM-1 compared to other MBLs, such as VIM-2 and IMP-1.¹⁷ In addition, the active site of NDM-1 is larger and more flexible than these other MBLs, which allows NDM-1 to accommodate such a broad range of substrates, including the carbapenems.¹⁸

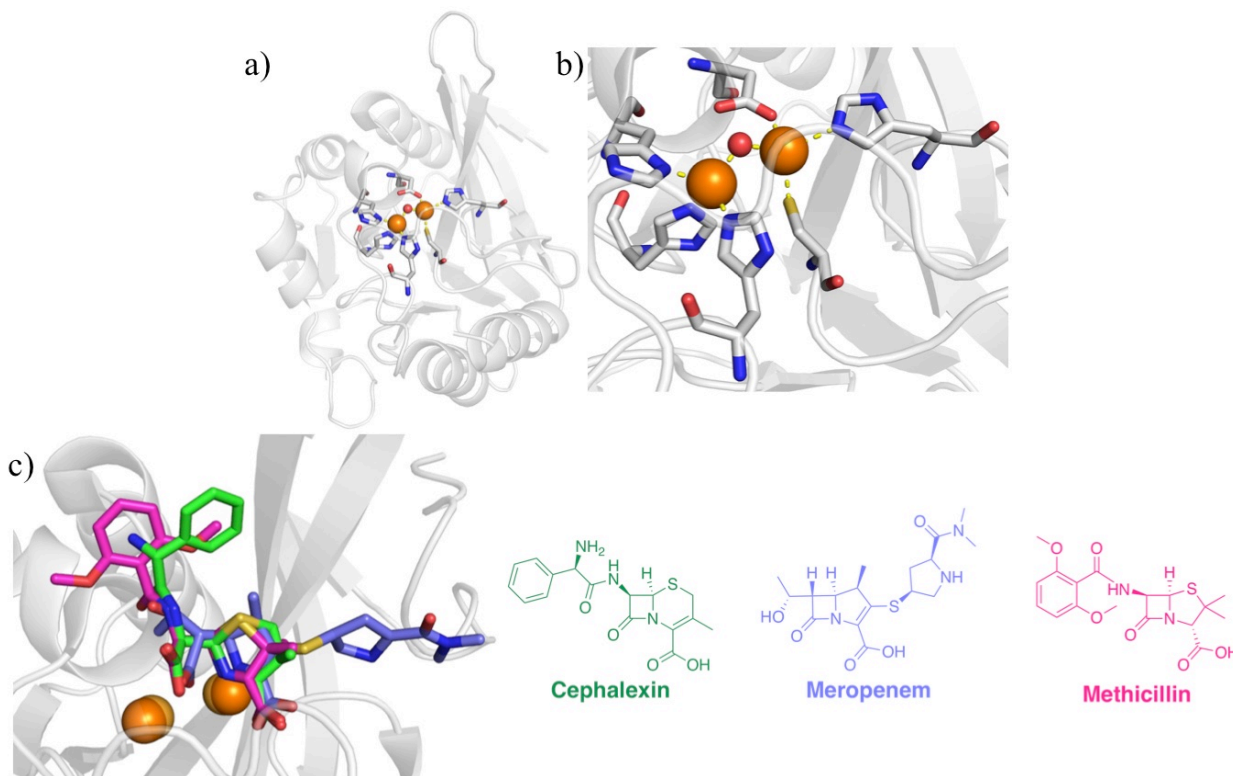


Figure 4.2. a) Full structure of NDM-1 (PDB 3SPU).¹⁹ b) Close-up of the NDM-1 active site (PDB 3SPU).¹⁹ c) Demonstration of the broad-spectrum activity of NDM-1 showing the overlaid hydrolysis products of three different classes of β -lactam (PDB 4RL2, 4EYL, and 4EY2).²⁰⁻²¹

During the mechanism of β -lactam cleavage, as shown in Figure 4.3 below, the β -lactam substrate briefly coordinates over the Zn^{2+} ions, which polarizes the molecule, making it more electrophilic and susceptible to nucleophilic attack. Meanwhile, the intrinsic Lewis acidity of the active site Zn^{2+} ions lowers the pK_a of the bridging hydroxyl,²² making it more nucleophilic and effectively catalyzing insertion of the hydroxyl into the carbonyl, thus cleaving the β -lactam bond.

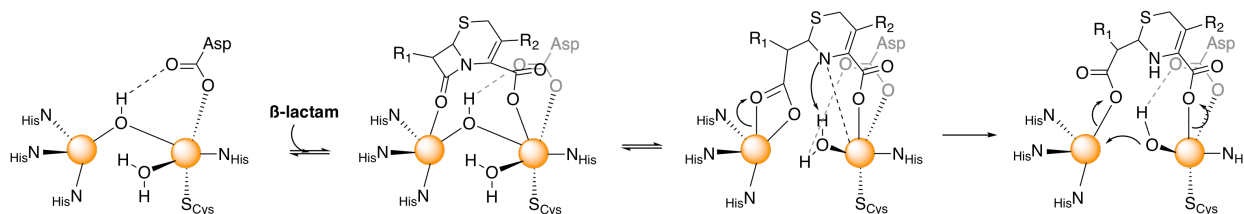


Figure 4.3. The proposed mechanism of β -lactam hydrolysis within the NDM-1 active site. Adapted from Yang et al.²²

Currently, there are no FDA approved drugs against NDM-1 or any other MBL. However, a class of cyclic boronates were reported by Burns et. al.²³ and have been shown to have strong efficacy against both serine and metallo classes of β -lactamase.²⁴ Of these, taniborbactam (VNRX-5133) is currently in advanced clinical trials (Figure 4.4).²⁵⁻²⁶ NDM-1 bearing infections have been historically been treated through the administration of nitrofurantoin²⁷ or by reserve antibiotics such as colistin, in the hopes of exploiting any antibiotic resistance not covered by the powerful bla_{NDM-1} cassette.²⁸ These treatments are not expected to be viable long-term solutions as growing resistance these therapeutics has already been reported; in particular with the recent development of MCR-1 for colistin resistance.²⁹ Therefore, there is

a large interest in developing NDM-1 inhibitors that prevent the premature hydrolysis of β -lactams, thereby restoring the activity of these antibiotics.

Unfortunately, NDM-1 has been a difficult target for rational inhibitor development; mainly due to the before mentioned flexibility and lack of specificity within the active site. Aside from the Zn^{2+} ions, there are very few molecular features to make the strong interactions necessary for highly active inhibitors.⁵ As such, the vast majority of the inhibitor development against NDM-1 has focused on the incorporation of some form of MBP in an effort to directly target the Zn^{2+} ions that are responsible for the catalytic activity of this metalloenzyme.⁵ A selection of these inhibitors are shown in Figure 4.4 below; a more thorough review of metal-binding MBL inhibitors is presented in Chen/Adamek et al.³⁰

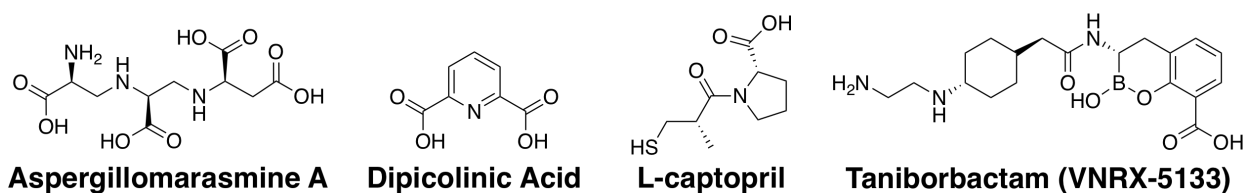


Figure 4.4. A representative selection of previously reported NDM-1 inhibitors.^{25-26, 31-33}

4.2 Hydroxyquinoline-Based Inhibitors of NDM-1

In an effort to identify and develop new MBP inhibitors of NDM-1, an MBP fragment library described in Chapter 1 was screened against NDM-1. This screen used the β -lactam chromacef as a chromophoric substrate, so that substrate hydrolysis by NDM-1 causes an increase of absorbance at 442 nm that can be monitored using a standard plate reader in a high-throughput format. The MBP library was screened at 200 μ M for NDM-1 inhibition, which would be indicated by no increase in absorbance at 442 nm. The details of this screen are reported in Experimental Section 4.4. From this MBP library screen, two lead scaffolds emerged

against NDM-1, derivatized 8-hydroxyquinoline (8-hydroxyquinoline), and derivatives of 1-hydroxypyridine-2-thione (1,2-HOPTO), of which the latter is discussed in Section 4.3. Among the 8-hydroxyquinoline family, 5-chloro-8-hydroxyquinoline (**4.3**) and 2-carboxy-8-hydroxyquinoline (**4.4**) demonstrated particularly good activity, with $IC_{50} = 27 \mu\text{M}$ and $IC_{50} = 2.9 \mu\text{M}$, respectively (Figure 4.5). From a preliminary SAR analysis, both **4.3** and **4.4** were substantially more potent MBPs than the related 8-hydroxyquinoline fragments **4.1** and **4.2**. While **4.1** is capable of inhibition through metal binding, the addition of the 5-chloro in **4.3** significantly increases the activity of the fragment, potentially due to the electron-withdrawing nature of chlorine facilitating deprotonation of the hydroxyl moiety. This strong increase in activity from the simple addition of a 5-chloro substituent emphasizes the importance of optimizing the MBP. Additionally, **4.4** was found to more active than either **4.1** or **4.2**, which represent the parent halves of the two chelating groups present in **4.4**. The potential of **4.4** to coordinate in a bidentate manner to both of the active site Zn^{2+} ions likely explains this boost in potency.

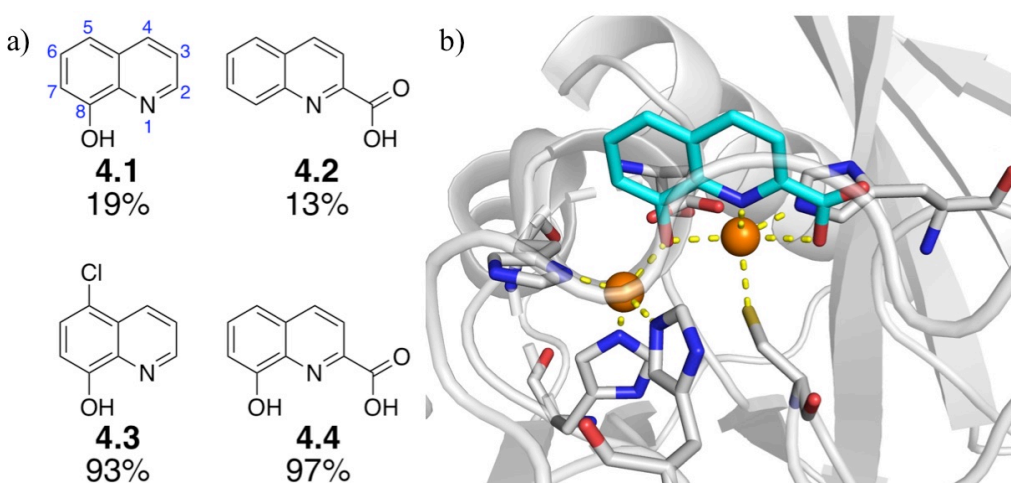


Figure 4.5. a) Percent inhibition of hit 8-hydroxyquinoline fragments against NDM-1 at 200 μM . Quinoline scaffold numbering is shown on **4.1** in blue. b) Proposed model of **4.4** bound to the NDM-1 active site (3SPU).

Several classes of metal-binding inhibitors have been reported against NDM-1, predominantly thiol and carboxylic acid based MBPs, whereas 8-hydroxyquinoline based inhibitors have yet to be reported, making this 8-hydroxyquinoline a novel scaffold for further exploration against NDM-1. As **4.3** and **4.4** were both viable fragment hits for further development, in addition to being comprised the same core 8-hydroxyquinoline pharmacophore, it was decided to have inhibitor development focus on a fragment merge of the moieties present in both scaffolds, followed by fragment elaboration of this new lead. To aid discovery efforts, a representative model of **4.4** bound to the NDM-1 active site was prepared (Figure 4.5b). Based on this modeling, it is predicted that **4.4** binds with the hydroxyl group coordinating in a bridging fashion between the Zn^{2+} ions, replacing the native bound water. Whether the remaining donor atoms from the pyridine and carboxylate groups preferably coordinate Zn_1 or Zn_2 is unclear, but it is proposed that Zn_2 is the more probable site, as this ion is natively in a distorted tetrahedron configuration, which would allow for easier coordination of the ligand as opposed the tetrahedral coordination sphere of Zn_1 . In favor of this assignment, hydrolyzed substrate and reported crystal structures of carboxylic acid containing MBL inhibitors all display coordination to Zn_2 , furthering the hypothesis that **4.4** is predominately bound to Zn_2 .³⁰ With this model in hand, it was decided to elaborate the merged scaffolds of **4.3** and **4.4** at the 2- and 7- positions of 8-hydroxyquinoline (see Figure 4.5a for 8-hydroxyquinoline numbering), as this design strategy would probe for potential interactions along either side of the active site channel; these regions of interest for derivatization are highlighted in Figure 4.6 below. Additionally, a small set of derivatives at the 5- position was prepared with the intentions of probing for possible interactions with β -hairpin loop when it closes over the active site during catalysis.

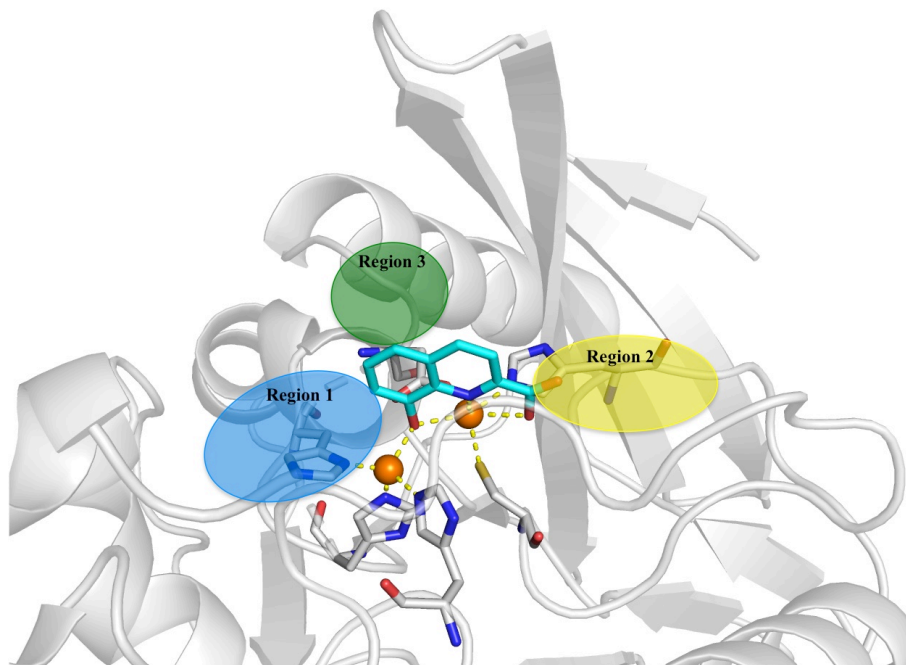
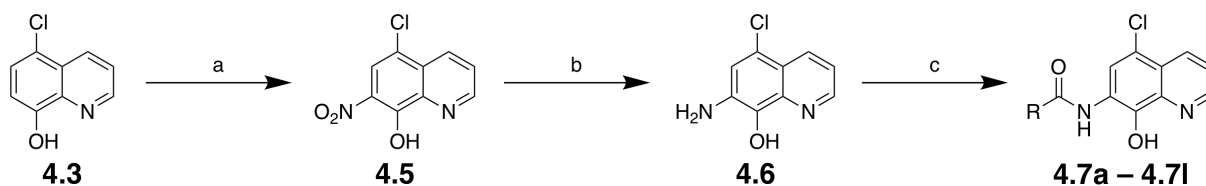


Figure 4.6. Regions of interest for exploration of the 8-hydroxyquinoline scaffold.

4.2.1 7-Derivatized 8-hydroxyquinolines

To prepare 8-hydroxyquinoline derivatives modified at the 7-position, it was decided to use amide coupling to attach and rapidly explore a broad scope of substituents. These compounds were prepared as illustrated in Scheme 4.1, starting from treating 5-chloro-8-hydroxyquinoline with equivalent amounts of nitric acid to afford selective nitration at the 7-position. Then, selective reduction was achieved by stirring the resulting product **4.5** with 1.5 eq of a 1:1 molar solution of sodium dithionite and potassium carbonate to reduce the nitro to an amine without removal of the halogen. Finally, amide coupling was achieved by combining the amine **4.6** with various acid chlorides to prepare a range of substituents. Upon completion of the amide coupling reaction, the reaction mixture was stirred in 1 M NaOH for 2 h to hydrolyze any incidental coupling to the free hydroxyl. Subsequent reaction work-up and chromatography yielded final products with amide-linked substituents at the 7-position.

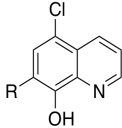


Scheme 4.1 Synthesis of 7-derivatized 8-hydroxyquinolines. Reagents and conditions: a) 5-chloro-8-hydroxyquinoline, conc. HNO₃, conc. H₂SO₄, 0 °C, 1 h, 57%; b) Na₂S₂O₄, K₂CO₃, MeOH and H₂O, 25 °C, 10 min, 67%; c) acid chloride, TEA, CH₂Cl₂, 25 °C, 15 min, then 1 M NaOH, 25 °C, 1 h, 11 – 54%.

Screening results of the 7-position sublibrary against NDM-1 are displayed in Table 4.1 below. While some library members displayed overall better activity than parent **4.3** (27 μM), none had significantly better activity than **4.4** (2.9 μM). Notably, **4.6** and **4.7a** were prepared as controls of small substituents, and had respective IC₅₀ values of 2.7 and 2.2 μM, which were improvements from **4.3**, and on par with **4.4**. Compounds with phenyl substituents and varying linker chain lengths of n = 0, 1, and 2 were prepared as **4.7b – 4.7d**; of these, the benzyl derivative with n = 1 had the best activity with an IC₅₀ = 3.1 μM, whereas the phenyl n = 0 had IC₅₀ > 10 μM, and the ethylene linker n = 2 had IC₅₀ = 9.3 μM. Attempts at performing an isosteric replacement of the aromatic phenyl to a thiophene moiety in **4.7k** and **4.7l** produced conflicting trends, where the n = 0 thiophene **4.7k** had an IC₅₀ = 1.3 μM (the best of the 8-hydroxyquinoline derivatives prepared in this study), and the methylene spacer n = 1 thiophene **4.7l** had slightly worse activity at IC₅₀ = 10.3 μM. To explore the effects of lipophilic bulk, compounds **4.7e – 4.7j** were prepared. Of these, the only trend that emerged was a slight preference for placement of lipophilic bulk, where bulk placed *meta* to the amide linker had better activity than bulk placed *para* to the amide linker, as exemplified by the 1-naphthamide **4.7f** IC₅₀ = 2.5 μM compared to 2-naphthamide **4.7e** IC₅₀ = 28 μM, and again with the *m*-chloro **4.7j** having an IC₅₀ = 9.1 μM compared to the *p*-chloro **4.7h** having an IC₅₀ >30 μM. As none of

these prepared derivatives at the 7-position had significantly improved activity relative to **4.4**, it was decided not to pursue further derivatives at that position. It is entirely possible that including a carboxylic acid at the 2-position would further improved inhibitor activity, but that synthesis would represent future work for this study.

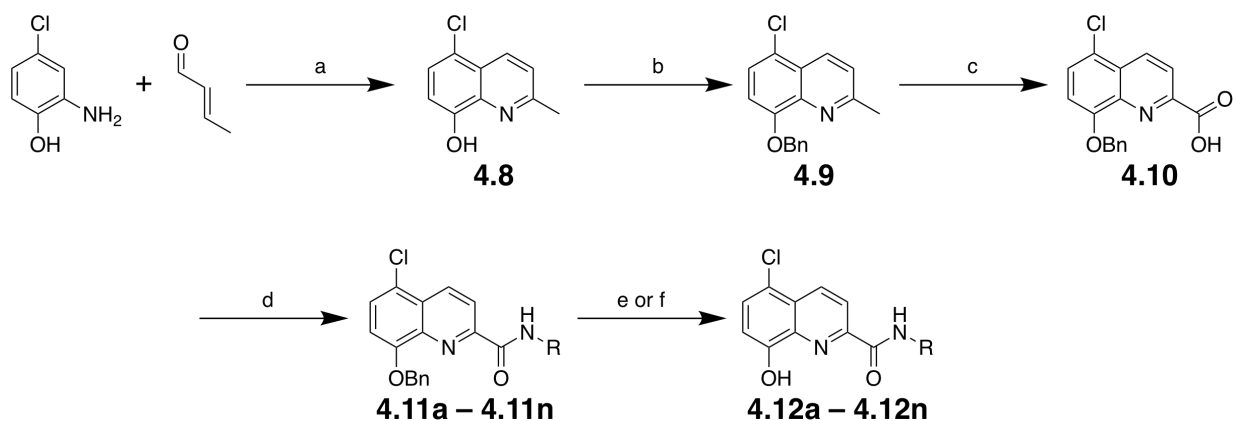
Table 4.1. Summary of IC₅₀ values of 8-hydroxyquinoline derivatized at the 7-position.

					
Compound	R	IC ₅₀ (μM)	Compound	R	IC ₅₀ (μM)
4.6		2.7	4.7g		> 30
4.7a		2.2	4.7h		> 30
4.7b		> 10	4.7i		> 30
4.7c		3.1	4.7j		9.1
4.7d		9.3	4.7k		1.3
4.7e		28	4.7l		10.3
4.7f		2.5	-	-	-

4.2.2 2-Derivatized 8-hydroxyquinolines

To prepare 2-position 8-hydroxyquinoline derivatives, it was decided to elaborate by building off the 2-carboxylic acid, as this position was more readily available to derivatization

compared to the 3- and 4-positions. The synthetic route is shown in Scheme 4.2. Starting from 2-amino-4-chlorophenol and crotonaldehyde, cyclization through a Doebner-Miller Von Skrappe reaction yielded the desired quinoline **4.8** with a methyl handle installed at the 2-position. Then benzyl protection followed by oxidation using selenium dioxide yielded the necessary carboxylic acid handle in **4.10**. Then, amide coupling using HOBt and EDC to attach various substituents yielded a small library of amide derivatives. Finally, benzyl deprotection was achieved with either strong acid or boron trichloride to yield final products.

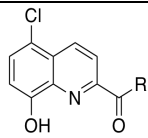
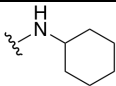
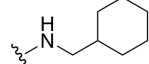
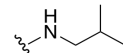
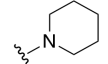
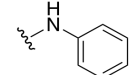
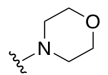
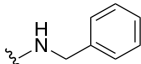
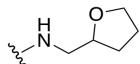
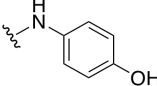
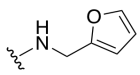
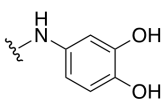
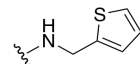


Scheme 4.2. Synthesis of 2-derivatized 8-hydroxyquinolines. Reagents and conditions: a) 2-amino-4-chlorophenol, crotonaldehyde, toluene and 6 M HCl, 70 °C, 16 h, 40%; b) benzyl bromide, K₂CO₃, DMF, 80 °C, 1.5 h, theoretical yield; c) SeO₂, pyridine, 115 °C, 2 h, 97%; d) amine, HOBt, EDC, TEA, 60 °C, 12 h, 17 – 72%; e) 5:5:1 12 M HCl to glacial acetic acid to TFA, 70 °C, 16 h, 19 – 81%; f) BCl₃, CH₂Cl₂, 0 °C, 1 h, 34 – 100%.

Screening results of the 2-position sublibrary against NDM-1 are displayed in Table 4.2 below. As a whole, these compounds essentially had no activity against NDM-1, with nearly all tested compounds having IC₅₀ >50 μM. It is possible that this loss in activity was due to the choice of elaborating from the carboxylic acid, as this blocked off the carboxylic acid from participating in metal-binding. As this 8-hydroxyquinoline class is dependent on the metal-binding interactions for the primary source of binding activity, it is possible that derivatizing

from the carboxylic acid occluded that necessary interaction. However, two compounds maintained some activity against NDM-1, compounds **4.12g** with a catechol substituent, and **4.12i** with a cyclohexyl ring substituent. These compounds have respective IC₅₀ values of 7.8 and 5.2 μM, and it is not clear why these out of the other 2-position derivatives maintained activity against NDM-1.

Table 4.2. Summary of IC₅₀ values of 8-hydroxyquinoline derivatized at the 2-position.

					
Compound	R	IC ₅₀ (μM)	Compound	R	IC ₅₀ (μM)
4.12a		2.8	4.12h		> 50
4.12b		> 50	4.12i		5.2
4.12c		> 50	4.12j		> 50
4.12d		> 50	4.12k		> 50
4.12e		> 50	4.12l		> 50
4.12f		> 50	4.12m		> 50
4.12g		7.8	4.12n		> 50

Additionally compound **4.12a** was prepared as a merge of the moieties present in **4.4** and **4.5**. This compound had an IC₅₀ = 2.8 μM, and did not have improved activity from the parent lead compounds. However, **4.12a**, along with **4.6**, **4.7c**, **4.7k**, **4.7l**, **4.12f**, and **4.12k** were evaluated (in collaboration with Dr. Michael Crowder, Miami U. Ohio) in a time-kill cell assay

for resensitization of NDM-1 expressing *E. coli* to β -lactam antibiotics. Of these, **4.6**, **4.7c**, **4.7k**, **4.7l**, and **4.12f** all precipitated from solution and resultantly had no β -lactam resensitization; **4.12k**, while being soluble, also displayed no resensitization. Of the compounds tested, only **4.12a** was found to restore the antibacterial activity of imipenem (Figure 4.7). In this study, NDM-1 expressing *E. coli* displayed resistance to 4 $\mu\text{g/mL}$ imipenem as evidenced by no decrease in the OD relative to controls, and cells treated with only **4.12a** at 100 $\mu\text{g/mL}$ displayed some cytotoxicity with an OD of 0.46. Then treatment with both 4 $\mu\text{g/mL}$ imipenem and 100 $\mu\text{g/mL}$ **4.12a** resulted in no bacterial growth, indicating resensitization of the NDM-1 expressing bacteria to β -lactam antibiotics.

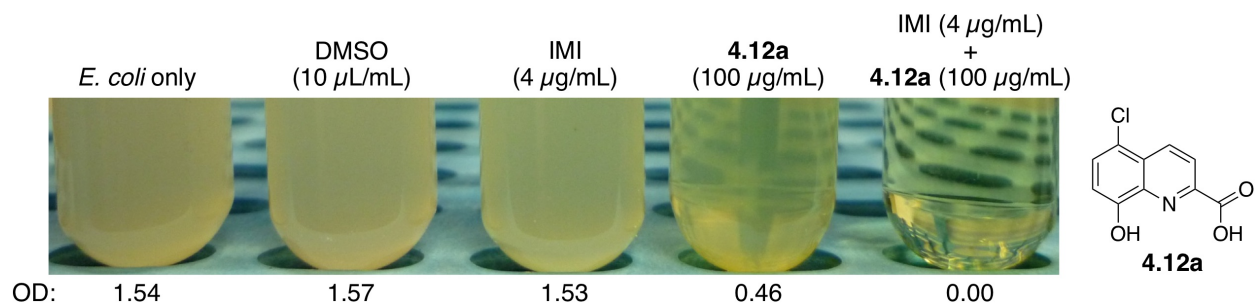
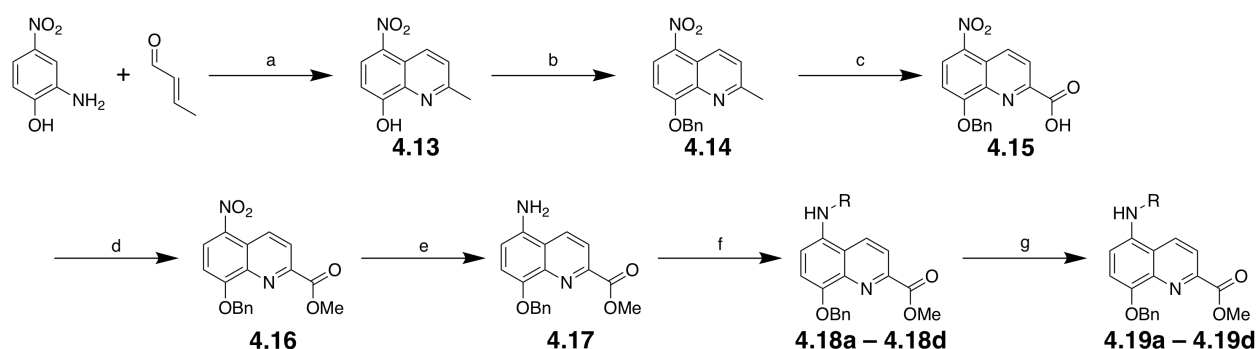


Figure 4.7. Time-kill cell assay of **4.12a** against NDM-1 expressing *E. coli* grown for 24 hours, with the optical density displayed below each test tube.

4.2.3 5-Derivatized 8-hydroxyquinolines

Finally, a sublibrary of 8-hydroxyquinoline derivatives from the 5-position were prepared to probe for potential interactions with the flexible active site loop. The route to these compounds is displayed below in Scheme 4.3. Combining 2-amino-4-nitrophenol with crotonaldehyde in a Doebner Miller von Skraupp cyclization yielded quinoline **4.13**. The resulting product was then benzyl protected, followed by oxidation of the 2-Me to a carboxylic acid using selenium dioxide to yield **4.15**. After methyl ester protection of **4.15**, the nitro- group

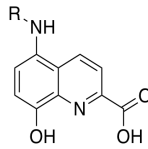
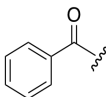
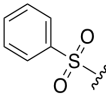
was reduced to an amine through hydrogenation. Unfortunately, this reaction was found to be low yielding, and alternative reduction conditions, such as using zinc dust or sodium dithionite, failed to produce the desired product. Then the scaffold was derivatized through either amide or sulfonamide coupling, giving products **4.18a** – **4.18b**. Finally, deprotection by stirring in base to achieve de-esterification, followed by reacting with boron trichloride afforded final products **4.19a** – **4.19b**.



Scheme 4.3. Synthesis of 5-derivatized 8-hydroxyquinolines. Reagents and conditions: a) 2-amino-4-nitrophenol, crotonaldehyde, toluene and 6M HCl, 70 °C, 16 h, 42%; b) benzyl bromide, K₂CO₃, DMF, 65 °C, 6 h, 66%; c) SeO₂, pyridine, 115 °C, 2 h, 91%; d) MeOH, cat. H₂SO₄, 110 °C 72 h, 81%; e) 5% w/w Pd/C, 1 atm H₂, 25 °C, 48 h, 14%; f) acid/sulfonyl chloride, CH₂Cl₂, TEA, 0 °C, 2 h, 52 – 85%; 1 M NaOH, 25 °C, 1 h, then BCl₃, CH₂Cl₂, 0 °C, 4 h, 4 – 40%.

The results of screening **4.19a** – **4.19b** against NDM-1 are summarized in Table 4.3. These compounds displayed flat SAR with essentially no improvement in activity against NDM-1 relative to the parent **4.4**. Of these compounds, the amide variants **4.19a** and **4.19b** had respective IC₅₀ values of 2.7 μM and 9.3 μM, were slightly less active than the respective sulfonamide counterparts **4.19c** and **4.19d**, which had respective IC₅₀ values of 1.4 μM and 1.5 μM. Considering these derivatives at the 5-position featured little change in inhibitory activity against NDM-1, it was decided not to pursue the scaffold for further development against NDM-1.

Table 4.3. Summary of IC₅₀ values of 8-hydroxyquinoline derivatized at the 5-position.

					
Compound	R	IC ₅₀ (μM)	Compound	R	IC ₅₀ (μM)
4.19a		2.7	4.19c		> 30
4.19b		2.2	4.19d		> 30

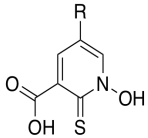
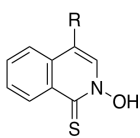
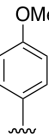
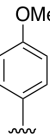
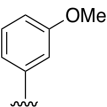
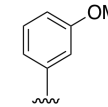
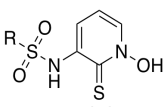
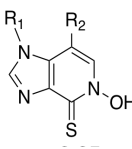
4.2.3 Conclusions on 8-Hydroxyquinoline as a Scaffold for NDM-1 Inhibition

The 5-chloro-8-hydroxyquinoline and 2-carboxy-8-hydroxyquinoline scaffolds emerged as early leads against NDM-1 with respective IC₅₀ values of 27 μM and 2.9 μM. To pursue these compounds against NDM-1, it was decided to merge the moieties present in **4.3** and **4.4**, and elaborate from the 7- and 2-positions to probe along the channel for potential interactions, as well as at the 5-position for interactions with the β-hairpin loop. Sublibraries bearing derivatives at each of these positions were prepared, as detailed above. Unfortunately, none of the prepared derivatives had improvement from the lead MBP scaffolds. It is unclear why there was no improvement in inhibitory activity despite elaboration of the 8-hydroxyquinoline scaffolds; it is possible that these elaborations made no additional interactions with the active site, resulting in no increase in inhibition. Still, compound **4.12a** showed some promise with its ability to restore the activity of imipenem against NDM-1 bearing *E. coli* bacteria. With the potency of **4.12a** in mind, it is possible that alternate elaboration strategies on the 8-hydroxyquinoline scaffold may result in more potent inhibitors of NDM-1.

4.3 Hydroxypyridine Thione-Based Inhibitors of NDM-1

In addition to the previously described 8-hydroxyquinoline scaffold, 1-hydroxypyridiene-2-thione (1,2-HOPTO) also emerged as a lead, displaying 69% inhibition against NDM-1 at 200 μM . As the elaborated 1,2-HOPTO library had been previously prepared and characterized as described in Chapter 2, it was screened against NDM-1 at 200 μM , with the results provided in Table 2.2. From this screen, compounds **2.4**, **2.5**, **2.6**, **2.9**, **2.11**, **2.17**, and **2.21** all displayed >90% inhibition at 200 μM . Considering multiple HOPTO scaffolds displayed inhibitory activity against NDM-1, and that in Chapter 2, several derivatives of these scaffolds had been previously prepared, it was decided to also screen these prepared derivatives against NDM-1. As a result, compounds **2.23** – **2.35** were also tested against NDM-1, with the results displayed below in Table 4.4.

Table 4.4 IC₅₀ values of 1,2-HOPTO based compounds tested against NDM-1.

						
Compound	R	IC ₅₀ (μM)	Compound	R	IC ₅₀ (μM) ^a	
2.2	H	0.77	2.6	H	1.2	
2.23		2.1	2.30		0.24	
2.24		1.7	2.31		0.28	
2.25		5.9	2.32		0.25	
						
Compound	R	IC ₅₀ (μM)	Compound	R ₁	R ₂	IC ₅₀ (μM)
2.4		13.6	2.9	H	H	46.2
2.27		7.5	2.34	H		26.6
-	-	-	2.35		H	15.9

^aThese IC₅₀ values were found to vary depending on assay conditions, as further detailed in section 4.3a.

Starting with **2.2**, which had an IC₅₀ = 0.77 μM, the aromatic derivatives **2.23** – **2.25** were found to have decreased activity in the range of IC₅₀ = 1.7 – 5.9 μM. However, performing the same substitutions on the 2-hydroxyisoquinoline-1-thione scaffold resulted in an improvement in IC₅₀ values from the parent **2.6** having an IC₅₀ = 1.2 μM, and the derivative compounds **2.30** – **32** all having IC₅₀ values near 0.24 μM. It is worth noting however, that these 2-

hydroxyisoquinoline-1-thione based inhibitors were found to have varying IC_{50} values depending on the assay conditions used, as detailed in section 4.3a, but the overall trend of improvement in the inhibition activity of **2.30 – 32** relative to parent **2.6** remained consistent.

To verify that **2.6** and its derivatives were acting through a metal-binding mechanism and not stripping the Zn^{2+} from the active site, both relative tryptophan fluorescence and equilibrium dialysis were performed in collaboration with Dr. Crowder, with the results displayed in Figure 4.8 below. For the relative tryptophan fluorescence assay, it was decided to take advantage of Trp93, as this residue is located directly adjacent to the active site, so that a metal-binding inhibitor would be positioned in close proximity to this residue. As shown in Figure 4.8a, both **2.6** and **2.31** caused a decrease in tryptophan fluorescence, indicating that they likely bind in the NDM-1 active site. As a control, EDTA was included as it acts through a metal-stripping mechanism; and therefore should not, and did not, cause a decrease in tryptophan fluorescence. L-Captopril was also included as a control as it has been verified to bind NDM-1 by coordinating with a free thiol bound μ between the active site Zn^{2+} ions; however, it did not cause a decrease in tryptophan fluorescence, likely because the molecule has no aromatic groups capable of absorbing at 348 nm. To ensure the prepared HOPTOs were not stripping the metals from the NDM-1 active site, equilibrium dialysis was performed. As shown in Figure 4.8b, compounds **2.6** and **2.31**, as well as the L-captopril control, did not cause significant decrease of Zn^{2+} levels, even at 16 times higher inhibitor concentration to enzyme concentration. For a control, EDTA was included as a metal stripping agent, and as expected, caused a significant loss of NDM-1 Zn^{2+} content. This data, as a whole, suggests that these 1,2-HOPTO compounds induce NDM-1 inhibition through a metal-binding mechanism, and not through metal-stripping.

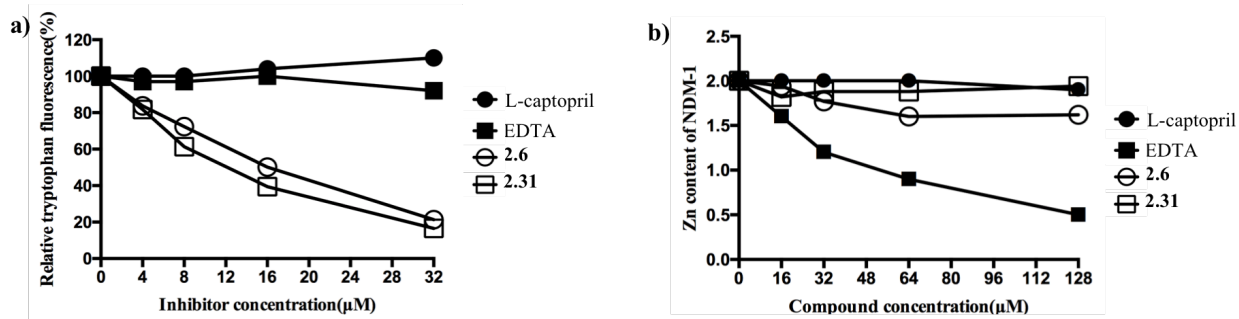


Figure 4.8. a) Relative tryptophan fluorescence of **2.6** and **2.31** binding NDM-1, with L-captopril and EDTA as controls. **2.6** and **2.31** display binding as indicated by the decrease in relative tryptophan fluorescence intensity at 348 nm; b) Equilibrium dialysis of the Zn²⁺ content of NDM-1 (8 μM) with **2.6** and **2.31** as inhibitors. L-captopril was included as a non-metal stripping control, and EDTA as a metal-stripping control.

While **2.6** and its derivatives were found to be good inhibitors of NDM-1, they were found to have poor aqueous solubility. Therefore, it was decided to prepare scaffolds **2.4** and **2.9** as more aqueous soluble isosteres of **2.2** and **2.6**, respectively. Sulfonamide compound **2.4** had an IC₅₀ = 13.6 μM, and the phenyl sulfonamide derivative **2.30** showed slight improvement with an IC₅₀ of 7.5 μM. Then, the deazapurine HOPTO **2.9** had an IC₅₀ of 46.2 μM, and its phenyl derivatives had **2.34** and **2.35** had respective IC₅₀ values of 26.6 and 15.9 μM. Both of these derivatives displayed slightly better activity against NDM-1 than the parent **2.9**. Considering both **2.34** and **2.35** vary only by the position of the attached phenyl ring substituent, and that **2.35** had better activity, it is likely that the position of the phenyl ring in **2.35** is preferred over **2.34**. However, once again, none of these HOPTO derivatives displayed sub-micromolar potency against NDM-1.

Although no cellular studies testing for β-lactam resensitization were performed on these prepared HOPTO compounds, it is highly likely they would have displayed good cellular efficacy, as a paper was released by Sham et. al. detailing the use of 6-carboxy-1,2-HOPTO (**2.3**) based inhibitors against the MBL VIM-2.³⁴ This study discussed the use of **2.3** and its

derivatives against VIM-2, showing that this HOPTO scaffold was able to inhibit VIM-2, showed low human cell cytotoxicity, and was able to resensitize VIM-2 expressing *E. coli* to the antibiotic amoxicillin. In light of how other HOPTO scaffolds had better activity against NDM-1 than **2.3**, it is probable that they would have also displayed similar cellular efficacy.

4.3.1 NDM-1 Assay Screening of 1,2-HOPTO Derivatives

Over the course of this study, the NDM-1 screening assay underwent many iterations. The earliest assays were performed using the previously chromacef substrate, which produces a colorimetric output of absorbance at 442 nm upon hydrolysis by NDM-1. This assay was eventually disfavored due to the high amounts of substrate necessary to generate a readable signal, that is, the chromacef assay could not be performed in a 96-well plate, and instead required the use of cuvettes to monitor readout, which dramatically reduced any HTS capabilities. Additional limitations to the original chromacef assay include the high K_{cat} , so that the high substrate turnover rate limits the assay to only reading the first 15 s of the assay, which is an inherently small window to monitor. Finally, the high substrate demands of the chromacef assay out compete many of the comparatively weaker binding inhibitors, potentially making lead discovery difficult.

In order to address the above chromacef assay limitations, the screening method was switched to the commercially available fluorescent fluorocillin green substrate, which must undergo two β -lactam hydrolysis events to generate the active fluorophore. While this change to the fluorescent fluorocillin green addressed the previous chromacef substrate limitations, this fluorocillin green substrate was also found to be problematic. Using fluorocillin green, inhibitor scaffolds were often found to display ‘activation’ of the NDM-1 enzyme, where within the dose-

response curve, some points at the base of the dose-response curve with smaller concentrations of inhibitor were found to dramatically increase the enzymatic activity by ~70% as shown in Figure 4.9a. Fortunately, it was found that the addition of 1% DMSO to the assay buffer and was able to partially mitigate this observed ‘activation’ and provide consistent assay readouts when the enzyme concentration was kept at 100 pM (Figure 4.9b).

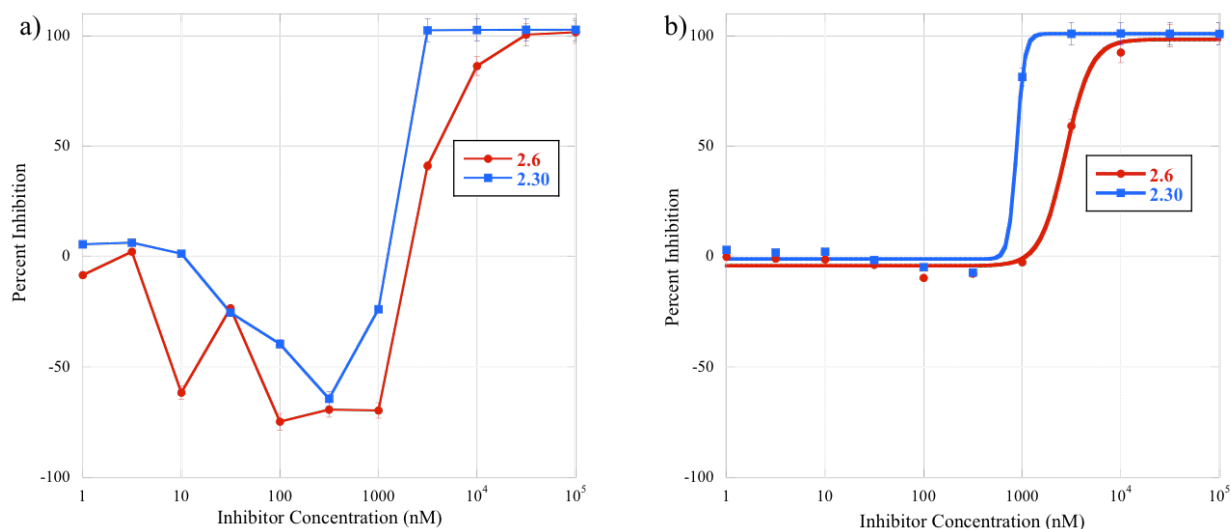


Figure 4.9. Effects of DMSO on NDM-1 fluorocillin green assay. a) Dose-response curves for **2.6** (red) and **2.30** (blue) with no additives in the assay buffer, resulting in enzyme activation at low concentrations of inhibitor; b) Dose-response curves for **2.6** (red) and **2.30** (blue) with 1% DMSO in the assay buffer, demonstrating correction of the previously observed enzyme activation.

Unfortunately, adding 1% DMSO to correct the enzyme activation was discouraged by UT Austin collaborator Dr. Thomas, who found that at even lower enzyme concentrations of 50 pM, the concentration of DMSO no longer affected enzymatic activity (Figure 4.10a-b). Instead, Dr. Thomas found that at these lower enzyme concentrations, the inclusion of excess Zn²⁺ was able to correct the enzyme ‘activation’ (Figure 4.10c). It is possible that the excess Zn²⁺ corrects the activation by stabilizing the metalloenzyme, as the Zn₂ site is known to be more labile with

a K_d of approximately $2 \mu\text{M}$,¹⁵ so that the inclusion of extra Zn^{2+} helps to prevent metal dissociation, thereby stabilizing and the enzyme. Under these modified assay conditions of 0.5 nM NDM-1 enzyme, it was found that for the HOPTO scaffolds, it was necessary to add $5.0 \mu\text{M}$ Zn to correct and eliminate the enzyme ‘activation’ (Figure 4.10c). Unfortunately, these high levels of Zinc also titrate away available inhibitor, resulting in an apparent reduced activity for the HOPTO scaffold against NDM-1. A summary of various NDM-1 assay conditions is presented in Table 4.5 below.

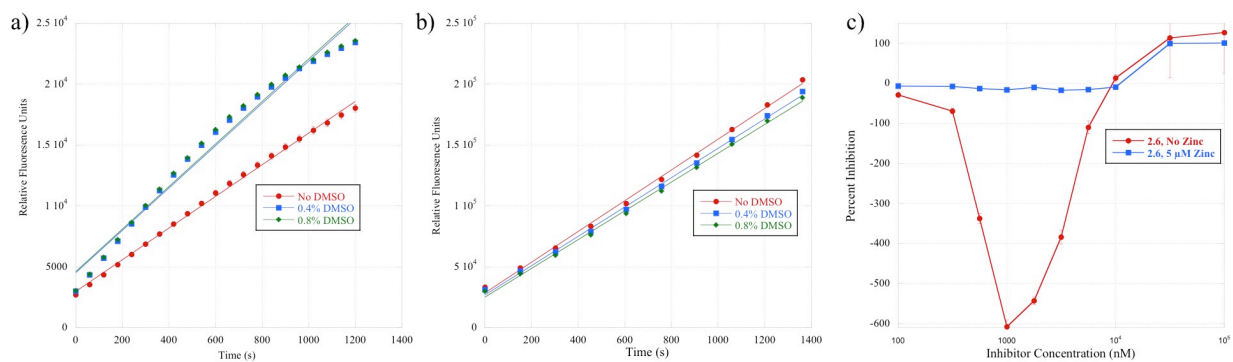


Figure 4.10. a) Graph of NDM-1 activity over time, measured in relative fluorescence units, at 100 pM enzyme, where the inclusion of DMSO increases the rate of enzyme activity. b) Graph of NDM-1 activity over time, measured in relative fluorescence units, at 50 pM enzyme, where the inclusion of DMSO no longer affects the rate of enzyme activity. c) Dose-response curves for **2.6** with no additives in the assay buffer (red) resulting in enzyme activation at low concentrations of inhibitor, and with $5 \mu\text{M}$ Zn^{2+} (blue) demonstrating correction of the previously observed enzyme activation.

Table 4.5. Summary of HOPTO IC₅₀ values under different assay conditions.

Compound	100 pM enzyme 1% DMSO, No Zinc	50 pM enzyme 5 μ M Zinc, No DMSO	Collaborator Values 50 pM enzyme No Zinc, No DMSO
2.2	9.24 μ M ^a	NA	0.77 μ M
2.23	9.35 μ M ^a	NA	2.1 μ M
2.4	NA	13.6 μ M	NA
2.27	NA	7.5 μ M	NA
2.6	2.1 μ M	16.3 μ M	1.2 μ M
2.30	0.90 μ M	20.8 μ M	0.24 μ M
2.9	33.7 μ M	46.2 μ M	NA
2.34	NA	26.6 μ M	NA
2.35	NA	15.9 μ M	NA

^aThese conditions had no additional DMSO.

4.3.2 Conclusions on 1,2-HOPTO Based NDM-1 Inhibitors

The 1,2-HOPTO scaffold initially showed strong potential for inhibitor development against NDM-1. From the preliminary screen, 7 compounds displayed greater than 90% inhibition against NDM-1 at 200 μ M. Then elaborated derivatives of these scaffolds were tested against NDM-1, with derivatives of 2-hydroxyisoquinoline-1-thione showing the best activity against NDM-1. To ensure these compounds were acting through a metal binding mechanism, both relative tryptophan fluorescence and equilibrium dialysis were performed, showing that both **2.6** and **2.31** were binding at the active site and not removing Zn²⁺ from the metalloenzyme. Then to improve the aqueous solubility of these 2-hydroxyisoquinoline-1-thione based compounds, isosteric replacement was done, switching to a deazapurine scaffold. While this change resulted in improved water solubility, these compounds were less active than the 2-hydroxyisoquinoline-1-thione based inhibitors. Unfortunately, further progress on developing the HOPTO scaffold was stalled due to an inability to achieve reproducible and predictive assays with these compounds. This resulted in an inability to consistently and reliably reproduce inhibition constants, which greatly stymied the progression of developing HOPTO based NDM-1

inhibitors. If the HOPTO scaffold is to be further pursued against NDM-1, it may be prudent to rely on orthogonal methods to in vitro enzymatic screening; as such, techniques such as thermal shift analysis or phenotypic screening against NDM-1 expressing bacteria would be more reliable methods of screening for efficacious results.

4.4 Conclusions

The goal of this work was to utilize MBP compounds against NDM-1, and through hit-to-lead rational drug development, prepare compounds capable of resensitizing NDM-1 bearing bacteria to conventional β -lactam antibiotics. To this end, screening of the MBP library revealed both the 8-hydroxyquinoline and 1,2-HOPTO MBP scaffolds to have strong inhibition against NDM-1. Efforts to elaborate and further derivatize the 8-hydroxyquinoline scaffold failed to produce compounds with better activity than the parent scaffold. However, compound **4.12a** was tested against NDM-1 expressing *E. coli*, and was found to restore the activity of the β -lactam imipenem; evidencing the capacity for this scaffold to still have therapeutic potential. It is possible that other elaborations besides the ones detailed here may result in 8-hydroxyquinoline based inhibitors of NDM-1.

Regarding 1,2-HOPTO based inhibitors of NDM-1, 2-hydroxyisoquinoline-1-thione based compounds were found to be the most potent of the scaffolds tested. These were determined to act through a metal-binding mechanism and not metal-stripping, as verified by a combination of relative tryptophan fluorescence and equilibrium dialysis. Unfortunately, due to difficulties with inconsistent assay methods, these HOPTO based inhibitors could not be further pursued. That is, not to say that this work was entirely unsuccessful, but that these HOPTO

compounds still have the potential to be useful against NDM-1 bearing bacterial should these in vitro enzymatic assay difficulties be addressed in future work.

4.5 Experimental

Synthetic Methods

Unless otherwise noted, all reagents and solvents were purchased from commercial suppliers and used with no additional purification. Silica gel column chromatography was performed using a CombiFlash Rf⁺ Teledyne ISCO system, using hexane, ethyl acetate, CH₂Cl₂ or MeOH as eluents. Reverse phase separations utilized a C18-column on the same instrument with a 0.1% formic acid in water and acetonitrile as eluents. Separations were monitored via a Teledyne ISCO RF⁺ PurIon ESI-MS detector with 1 Da resolution. ¹H NMR spectra were obtained using Varian 400 MHz spectrometers at the Department of Chemistry and Biochemistry at UC San Diego. ¹H NMR data is reported in parts per million relative to the residual non-deuterated solvent signals, and spin multiplicities are given as s (singlet), *br* s (broad singlet), d (doublet), dd (doublet of doublets), t (triplet), dt (doublet of triplets), q (quartet), and m (multiplet). When available, coupling constants (J) are reported in hertz (Hz). The purity of prepared final compounds was determined to be at least 90% by ¹H NMR analysis. Standard resolution mass spectrometry was performed at either the UC San Diego Molecular Mass Spectrometry Facility or on the previously described Teledyne ISCO RF⁺ PurIon ESI-MS detector. The elaborated HOPTO compounds and their derivatives were prepared as previously reported in Chapter 2.

Synthesis of 7-position 8-hydroxyquinoline Derivatives

5-Chloro-7-nitro-8-hydroxyquinoline (4.5): A solution of 5-chloro-8-hydroxyquinoline (18.0 g, 100 mmol) in 100 mL concentrated sulfuric acid was cooled to 0 °C. To this solution, concentrated nitric acid (7.79 ml, 120 mmol) was slowly added in 20 aliquots of 400 μ L each over the course of 30 min. The reaction mixture was allowed to stir at 0 °C for an additional 30 min, and upon completion, was poured over 200 mL ice. After neutralization with NaOH, the product precipitated out of solution and was collected via vacuum filtration to obtain **4.5** (12.9 g, 57.2 mmol, 57%) as a light orange solid. $^1\text{H NMR}$ (400 MHz, $\text{DMSO-}d_6$): δ 9.11 – 9.09 (dd, $J_1 = 4.0$, $J_2 = 1.2$, 1H), 8.64 – 8.61 (dd, $J_1 = 8.4$, $J_2 = 1.2$, 1H), 8.22 (s, 1H), 7.97 – 7.94 (dd, $J_1 = 8.8$, $J_2 = 4.4$, 1H).

5-Chloro-7-amino-8-hydroxyquinoline (4.6): To a solution of $\text{Na}_2\text{S}_2\text{O}_4$ (7.75 g, 44.5 mmol) and K_2CO_3 (6.15 g, 44.5 mmol) in 100 mL of 1:1 MeOH to H_2O , **4.5** (2.0 g, 8.9 mmol) was added in one portion. The reaction mixture was stirred at 25 °C for 10 min, until complete, as indicated by TLC. Upon completion, the reaction mixture was concentrated under reduced pressure, until all solvents were removed. The resulting crude was taken up in acetone, gently heated at 60 °C for 15 min, and then hot filtered to remove salts. The filtrate was concentrated under reduced pressure to obtain **4.6** (1.17 g, 6.00 mmol, 67%) as a black solid. $^1\text{H NMR}$ (400 MHz, $\text{DMSO-}d_6$): δ 9.35 (*br*, 1H), 8.72 (d, $J = 3.2$, 1H), 8.23 (d, $J = 8.4$, 1H), 7.29 (d, $J = 4.0$, 1H), 2.28 (s, 1H), 5.31 (s, 2H, NH_2); ESI-MS(+): m/z 195 $[\text{M} + \text{H}]^+$.

General Acid Chloride Coupling Procedure: Unless otherwise noted, the following protocol was used for acid chloride mediated amide coupling. To a solution of **4.6** and TEA (2.2 eq) in 10

CH₂Cl₂, a solution of acid chloride (2.2 eq.) in 2 mL CH₂Cl₂ was added dropwise. The reaction mixture was stirred at 25 °C for 15 min, and upon reaction completion, was concentrated under reduced pressure. Then the crude was taken up in 20 mL MeOH with 10 mL 1 M NaOH, and stirred at 25 °C for 1 h. The solution was concentrated under reduced pressure to remove volatiles, and was then neutralized with 1 M HCl. The product was then extracted into organic using 3×15 mL ethyl acetate, and the combined organic was washed with brine, dried over magnesium sulfate, and the solids were filtered off and discarded. The filtrate was concentrated under reduced pressure, and the resulting crude was purified by column chromatography, running gradient from 100% CH₂Cl₂ to 10% MeOH in CH₂Cl₂. Like fractions containing the desired product were combined and concentrated under reduced pressure to obtain final products.

5-Chloro-7-acetamide-8-hydroxyquinoline (4.7a): A solution of **4.6** (0.100 g, 0.514 mmol) in 5 mL acetic anhydride (excess) was stirred for 5 min at 25 °C. Upon reaction completion, 5 mL H₂O was added, and the reaction mixture was stirred at 25 °C for another 5 min. Then 4 mL 1 M NaOH was added in one portion, and reaction solution was stirred 25 °C for 1 h. Then the solution was neutralized with HCl, and extracted into organic with 3×15 mL ethyl acetate. The combined organic was washed with brine, dried over magnesium sulfate, filter and the solids were filtered off and discarded. The filtrate was concentrated under reduced pressure, and the resulting crude was recrystallized from methanol to obtain **4.7a** (0.030 g, 0.13 mmol, 25%) as an off-white fluffy solid. ¹H NMR (400 MHz, DMSO-*d*₆): δ 9.69 (s, 1H), 8.92 (d, *J* = 2.8, 1H), 8.43 (d, *J* = 8.0, 1H), 8.36 (s, 1H), 7.64 (dd, *J*₁ = 7.6, *J*₂ = 3.6, 1H), 2.14 (s, 3H); ESI-MS(-): *m/z* 235.13 [M - H]⁻.

5-Chloro-7-benzamide-8-hydroxyquinoline (4.7b): A solution of benzoyl chloride (0.18 mL, 1.5 mmol) in 2 mL CH₂Cl₂ was added dropwise to a solution of **4.6** (0.10 g, 0.51 mmol), and TEA (0.215 mL, 1.54 mmol) in 10 mL CH₂Cl₂. The reaction mixture was stirred at 25 °C for 15 min, and upon reaction completion, was quenched with saturated sodium bicarbonate. Then the aqueous and organic layers were separated, and the organic was washed with brine and dried over magnesium sulfate. The solids were filtered off and discarded, and the filtrate was concentrated under reduced pressure. The resulting crude was recrystallize from ethanol to obtain **4.7b** (0.077 g, 37 mmol, 37%) as a yellow-green powder. ¹H NMR (400 MHz, DMSO-*d*₆): δ 10.23 (s, 1H), 9.02 (d, *J* = 3.2, 1H), 8.70 (d, *J* = 8.4, 1H), 8.22 (s, 1H), 8.07 (d, *J* = 7.2, 2H), 7.82 (dd, *J*₁ = 8.4, *J*₂ = 4.4, 1H), 7.62 (m, 1H), 7.55 (m, 2H); ESI-MS(+): *m/z* 299 [M + H]⁺.

5-Chloro-7-phenylacetamide-8-hydroxyquinoline (4.7c): From **4.6** (0.100 g, 0.514 mmol), **4.7c** (0.021 g, 0.067 mmol, 13%) was obtained as a dark black solid. ¹H NMR (400 MHz, DMSO-*d*₆): δ .86 (s, 1H), 8.92 (d, *J* = 2.8, 1H), 8.44 (d, *J* = 8.4, 1H), 8.37 (s, 1H), 7.63 (dd, *J*₁ = 8.4, *J*₂ = 4.0, 1H), 7.38 – 7.30 (m, 4H), 7.24 (m, 1H), 3.82 (s, 2H); ESI-MS(+): *m/z* 313 [M + H]⁺.

5-Chloro-7-cinnmoylamide-8-hydroxyquinoline (4.7d): From **4.6** (0.100 g, 0.514 mmol), **4.7d** (0.027 g, 0.082 mmol, 16%) was obtained as an off-white solid. ¹H NMR (400 MHz, DMSO-*d*₆): δ 9.68 (s, 1H), 8.91 (d, *J* = 1.6, 1H), 8.43 (d, *J* = 8.4, 1H), 8.37 (s, 1H), 7.62 (dd, *J*₁ = 8.4, *J*₂ = 2.8, 1H), 2.29 – 7.26 (m, 4H), 7.19 – 7.16 (m, 1H), 2.92 (t, *J* = 6.4, 2H), 2.78 (t, *J* = 7.6, 2H); ESI-MS(+): *m/z* 327.11 [M + H]⁺.

5-Chloro-7-(2-naphthylamide)-8-hydroxyquinoline (4.7e): From **4.6** (0.100 g, 0.514 mmol), **4.7e** (0.096 g, 0.28 mmol, 54%) was obtained as an off-white solid. ^1H NMR (400 MHz, DMSO- d_6): δ 10.11 (*br s*, 1H), 8.97 (d, $J = 2.8$, 1H), 8.68 (s, 1H), 8.51 (d, $J = 8.4$, 1H), 8.10 – 8.01 (m, 4H), 7.70 (dd, $J_1 = 8.4$, $J_2 = 4.0$, 1H), 7.64 (t, $J = 6.4$, 2H).

5-Chloro-7-(1-naphthylamide)-8-hydroxyquinoline (4.7f): From **4.6** (0.200 g, 1.03 mmol), **4.7f** (0.040 g, 0.12 mmol, 11%) was obtained as an off-white solid. ^1H NMR (400 MHz, DMSO- d_6): δ 10.12 (*br*, 1H), 8.96 (s, 1H), 8.51 (d, $J = 8.0$, 1H), 8.35 – 8.31 (m, 2H), 8.08 (d, $J = 8.0$, 1H), 8.02 (d, $J = 7.6$, 1H), 7.85 (d, $J = 6.8$, 1H), 7.70 (s, 1H), 7.63 – 7.58 (m, 3H).

5-Chloro-7-(p-toluamide)-8-hydroxyquinoline (4.7g): From **4.6** (0.100 g, 0.514 mmol), **4.7g** (0.070 g, 0.22 mmol, 44%) was obtained as an off-white solid. ^1H NMR (400 MHz, DMSO- d_6): δ 9.82 (*br s*, 1H), 8.94 (d, $J = 2.8$, 1H), 8.48 (d, $J = 9.2$, 1H), 8.16 (s, 1H), 7.92 (d, $J = 7.6$, 2H), 7.67 (dd, $J_1 = 8.4$, $J_2 = 4.0$, 1H), 7.34 (d, $J = 7.6$, 2H), 2.38 (s, 3H).

5-Chloro-7-(p-chlorobenzylamide)-8-hydroxyquinoline (4.7h): From **4.6** (0.100 g, 0.514 mmol), **4.7h** (0.045 g, 0.14 mmol, 27%) was obtained as an off-white solid. ^1H NMR (400 MHz, DMSO- d_6): δ 10.06 (*br s*, 1H), 8.96 (s, 1H), 8.49 (d, $J = 7.2$, 1H), 8.09 (s, 1H), 8.03 (d, $J = 7.6$, 2H), 7.70 (s, 1H), 7.61 (d, $J = 7.6$, 2H).

5-Chloro-7-(p-bromobenzylamide)-8-hydroxyquinoline (4.7i): From **4.6** (0.100 g, 0.514 mmol), **4.7i** (0.090 g, 0.24 mmol, 47%) was obtained as an off-white solid. ^1H NMR (400 MHz,

DMSO-*d*₆): δ 10.05 (*br s*, 1H), 8.96 (d, $J = 2.8$, 1H), 8.49 (d, $J = 8.4$, 1H), 8.09 (s, 1H), 7.96 (d, $J = 7.2$, 2H), 7.75 (d, $J = 7.6$, 2H), 7.70 (dd, $J_1 = 8.0$, $J_2 = 4.4$, 1H).

5-Chloro-7-(*m*-chlorobenzylamide)-8-hydroxyquinoline (4.7j): From **4.6** (0.100 g, 0.514 mmol), **4.7j** (0.073 g, 0.22 mmol, 43%) was obtained as an off-white solid. ¹H NMR (400 MHz, DMSO-*d*₆): δ 8.95 (d, $J = 3.2$, 1H), 8.49 (d, $J = 8.4$, 1H), 8.05 (s, 2H), 7.96 (d, $J = 6.8$, 1H), 7.68 (m, 2H), 7.57 (m, 1H).

5-Chloro-7-thiophenylamide-8-hydroxyquinoline (4.7k): From **4.6** (0.100 g, 0.514 mmol), **4.7k** (0.057 g, 0.19 mmol, 36%) was obtained as an off-white solid. ¹H NMR (400 MHz, DMSO-*d*₆): δ 8.94 (d, $J = 2.8$, 1H), 8.48 (d, $J = 9.2$, 1H), 8.07 (s, 1H), 8.03 (s, 1H), 7.86 (d, $J = 4.4$, 1H), 7.68 (dd, $J_1 = 8.4$, $J_2 = 3.2$, 1H), 7.22 (t, $J = 4.0$, 1H); ESI-MS(-): m/z 303.18 [M - H]⁻.

5-Chloro-7-thiopheneacetamide-8-hydroxyquinoline (4.7l): From **4.6** (0.100 g, 0.514 mmol), **4.7l** (0.027 g, 0.085 mmol, 11%) was obtained as an off-white solid. ¹H NMR (400 MHz, DMSO-*d*₆): δ 9.90 (s, 1H), 8.93 (d, $J = 2.8$, 1H), 8.44 (d, $J = 8.4$, 1H), 8.39 (s, 1H), 7.64 (dd, $J_1 = 8.8$, $J_2 = 4.0$, 1H), 7.39 (d, $J = 5.2$, 1H), 7.01-6.97 (m, 2H), 4.06 (s, 1H).

Synthesis of 2-position 8-hydroxyquinoline Derivatives

2-Methyl-5-chloro-8-hydroxyquinoline (4.8): A solution of 2-amino-4-chlorophenol (6.00 g, 41.8 mmol) in 60 mL toluene with 20 mL 6 M HCl was pre-heated to 70 °C for 5 min. Then crotonaldehyde (4.15 mL, 50.1 mmol) was added in one portion, and the reaction was heated at 70 °C for 16 h while open to air. Upon completion, the reaction was cooled to 25 °C, and the

organic layer was separated and discarded. The acidic solution was neutralized with NaOH to pH 7, and was then extracted into organic with 3×20 mL ethyl acetate. The combined organic was washed with brine, dried over magnesium sulfate, and the solids were filtered off and discarded. The filtrate was concentrated under reduced pressure, yielding a brown, sticky crude, which was then purified by column chromatography, running elution gradient from 100% hexanes to 100% ethyl acetate. The desired product eluted in 40% ethyl acetate in hexanes. Like fractions were combined and concentrated under reduced pressure to obtain **4.8** (3.27 g, 16.9 mmol, 40%) as a brown oil that solidified upon standing to a tan solid. ¹H NMR (400 MHz, DMSO-*d*₆): δ 9.75 (*br s*, 1H), 8.31 (d, *J* = 8.8, 1H), 7.54 (d, *J* = 8.8, 1H), 7.47 (d, *J* = 8.4, 1H), 7.02 (d, *J* = 8.4, 1H), 2.69 (s, 3H); ESI-MS(+): *m/z* 194 [M + H]⁺.

2-methyl-5-chloro-8-benzyloxyquinoline (4.9): To a solution of **4.8** (3.00 g, 15.5 mmol) and K₂CO₃ (4.50 g, 32.5 mmol) in 70 mL DMF, benzyl bromide (2.03 mL, 17.04 mmol) was added dropwise. The reaction was then heated at 80 °C for 90 min. Upon reaction completion, the reaction mixture was concentrated under reduced pressure. The resulting crude was taken up in 30 mL ethyl acetate, washed with water and then brine, and dried over magnesium sulfate. The solids were filtered off and discarded, and the filtrate was concentrated under reduced pressure to obtain **4.9** (5.50 g, 19.4 mmol, theoretical yield) as an off-white solid. ¹H NMR (400 MHz, CD₃OD): δ 8.47 – 8.41 (m, 1H), 7.56 – 7.29 (m, 7H), 7.14 – 7.09 (m, 1H), 5.38 (s, 2H); ESI-MS(+): *m/z* 284 [M + H]⁺, 306 [M + Na]⁺.

2-carboxyl-5-chloro-8-benzyloxyquinoline (4.10): To a solution of **4.9** (4.40 g, 0.705 mmol) in 70 mL pyridine, SeO₂ (0.235 g, 2.12 mmol) was added. The reaction mixture was heated to

reflux at 115 °C for 2 h, and upon completion, the solution was hot filtered to remove the reduced selenium salts. The filtrate was concentrated under reduced pressure, and taken up in water to precipitate product, and was heated at 100 °C for 30 min to dissolve excess selenium. The suspension was hot filtered to collect **4.10** (4.86 g, 15.5 mmol, 97%) as a light tan solid. ¹H NMR (400 MHz, CD₃OD): δ 8.74 (d, *J* = 9.2, 1H), 8.33 (d, *J* = 9.2, 1H), 7.79 (d, *J* = 8.4, 1H), 7.58 (d, *J* = 6.4, 2H), 7.41 – 7.31 (m, 4H), 5.42, (s, 2H); ESI-MS(-): *m/z* 312.18 [M - H]⁻.

General amide coupling procedure: To a solution of **4.10** (0.20 g, 0.64 mmol) and TEA (0.107 mL, 0.956 mmol) in 4 mL dry DMF, HOBT (0.117 g, 0.956 mmol), and EDC (1.22 g, 6.37 mmol) were sequentially added. The reaction mixture was allowed to activate at 25 °C for 30 min, then the amine (1.5 eq.) was added in one portion. The reaction mixture was then heated at 60 °C for 12 h. Upon completion, the reaction mixture was concentrated under reduced pressure, taken up in ethyl acetate and wash with saturated NaHCO₃ followed by brine, and dried over magnesium sulfate. The solids were filtered off and discarded, and the filtrate was concentrated under reduced pressure. The resulting crude was taken up in a solution of 2% ethyl acetate in hexanes to precipitate out pure amide-coupled product, which was subsequently collected by vacuum filtration and washed with hexanes to obtain the desired product.

2-diethylamide-5-chloro-8-benzyloxyquinoline (4.11b): From **4.10** (0.15 g, 0.48 mmol), **4.11b** (0.093 g, 0.25 mmol, 53%), was obtained as a light tan oil that solidified upon standing. ¹H NMR (400 MHz, Acetone-*d*₆): δ 8.63 (d, *J* = 8.8, 1H), 7.93 (d, *J* = 8.4, 1H), 7.68 (d, *J* = 8.4, 1H), 7.58 (d, *J* = 7.2, 2H), 7.42-7.32 (m, 4H), 5.37 (s, 2H), 3.55 (q, *J*₁ = 6.8, *J*₂ = 7.2, 2H), 3.50 (q, *J*₁ = 6.8, *J*₂ = 7.2, 2H), 1.24 (d, *J* = 6.8, 6H).

2-isobutylamide-5-chloro-8-benzyloxyquinoline (4.11c): From **4.10** (0.20 g, 0.64 mmol), **4.11c** (0.115 g, 0.312 mmol, 49%) was obtained as a light tan solid. $^1\text{H NMR}$ (400 MHz, Acetone- d_6): δ 8.67 (d, $J = 8.4$, 1H), 8.51 (t, $J = 5.6$, 1H), 8.27 (d, $J = 8.8$, 1H), 7.75 (d, $J = 8.4$, 1H), 7.58 (d, $J = 7.2$, 2H), 7.41 – 7.34 (m, 4H), 5.39 (s, 2H), 3.23 (t, $J = 6.4$, 2H), 1.89 – 1.82 (m, 1H); ESI-MS(+): m/z 369.13 $[\text{M} + \text{H}]^+$, 391.11 $[\text{M} + \text{Na}]^+$.

2-phenylamide-5-chloro-8-benzyloxyquinoline (4.11d): From **4.10** (0.15 g, 0.48 mmol), **4.11d** (0.032 g, 0.083 mmol, 17%) was obtained as a light tan solid. $^1\text{H NMR}$ (400 MHz, Acetone- d_6): δ 10.56 (*br s*, 1H, NH), 8.74 (d, $J = 8.8$, 1H), 8.36 (d, $J = 8.8$, 1H), 7.83 (d, $J = 8.4$, 1H), 7.77 (d, $J = 7.6$, 2H), 7.65 (d, $J = 7.2$, 2H), 7.43 – 7.36 (m, 6H), 7.16 (t, $J = 7.2$, 1H), 5.44 (s, 2H); ESI-MS(+): m/z 389.09 $[\text{M} + \text{H}]^+$, 411.05 $[\text{M} + \text{Na}]^+$.

2-benzylamide-5-chloro-8-benzyloxyquinoline (4.11e): From **4.10** (0.20 g, 0.64 mmol), **4.11e** (0.063 g, 0.16 mmol, 25%) was obtained as a light tan solid. $^1\text{H NMR}$ (400 MHz, Acetone- d_6): δ 8.86 (*br s*, 1H), 8.75 (d, $J = 8.4$, 1H), 8.43 (d, $J = 8.8$, 1H), 7.72 (d, $J = 8.4$, 1H), 7.55 (dd, $J_1 = 7.6$, $J_2 = 2.4$, 2H), 7.43 (d, $J = 7.2$, 2H), 7.38 – 7.27 (m, 10H), 5.41 (s, 2H), 4.70 (d, $J = 6.0$, 2H).

2-(*p*-phenolamide)-5-chloro-8-benzyloxyquinoline (4.11f): From **4.10** (0.150 g, 0.478 mmol), **4.11f** (0.132 g, 0.326 mmol, 68%) was obtained as a dark brown solid. $^1\text{H NMR}$ (400 MHz, Acetone- d_6): δ 10.30 (s, 1H), 8.80 (d, $J = 8.8$, 1H), 8.45 (d, $J = 8.8$, 1H), 8.36 (*br s*, 1H, OH), 7.77 (d, $J = 8.4$, 1H), 7.72 (d, $J = 7.6$, 2H), 7.67 (d, $J = 8.8$, 2H), 7.49 (t, $J = 7.2$, 2H), 7.43-7.41 (m, 2H), 6.91 (d, $J = 8.8$, 2H), 5.49 (s, 2H).

2-piperenylamide-5-chloro-8-benzyloxyquinoline (4.11g): From **4.10** (0.20 g, 0.64 mmol), **4.11g** (0.151 g, 0.394 mmol, 63%) was obtained as a light tan solid. ¹H NMR (400 MHz, CD₃OD): δ 8.63 (d, $J = 8.4$, 1H), 7.90 (d, $J = 8.8$, 1H), 7.67 (m, 4H), 5.38 (s, 2H), 3.70 (d, $J = 35.6$, 4H), 1.67 (s, 6H); ESI-MS(+): m/z 381.6 [M + H]⁺, 403.11 [M + Na]⁺.

2-cyclohexylamide-5-chloro-8-benzyloxyquinoline (4.11h): From **4.10** (0.200 g, 0.637 mmol), **4.11h** (0.153 g, 0.387 mmol, 61%) was obtained as a light tan solid. ¹H NMR (400 MHz, Acetone-*d*₆): δ 8.74 (m, 1H), 8.40 (d, $J = 4.4$, 1H), 8.38 (d, $J = 4.4$, 1H), 7.77-7.73 (m, 1H), 7.67 (s, 2H), 7.49-7.44 (m, 2H), 7.41-7.38 (m, 2H), 5.40 (d, $J = 3.2$, 2H), 3.96 (*br s*, 1H), 1.98 (s, 2H), 1.75 (s, 2H), 1.63 (s, 1H), 1.49-1.35 (m, 4H), 1.23-1.19 (m, 1H); ESI-MS(+): m/z 395.15 [M + H]⁺, 417.13 [M + Na]⁺.

2-acetylcyclohexylamide-5-chloro-8-benzyloxyquinoline (4.11i): From **4.10** (0.150 g, 0.478 mmol), **4.11i** (0.080 g, 0.20 mmol, 41%) was obtained as a light tan solid. ¹H NMR (400 MHz, Acetone-*d*₆): δ 8.74 (d, $J = 8.8$, 1H), 8.46 (*br s*, 1H, *NH*), 8.39 (d, $J = 8.8$, 1H), 7.74 (d, $J = 8.4$, 1H), 7.65 (d, $J = 7.6$, 2H), 7.47-7.36 (m, 4H), 5.43 (s, 2H), 3.34 (t, $J = 6.8$, 2H), 1.83-1.57 (m, 8H), 1.32-1.01 (m, 7H); ESI-MS(+): m/z 409.15 [M + H]⁺, 431.12 [M + Na]⁺.

2-piperonamide-5-chloro-8-benzyloxyquinoline (4.11j): From **4.10** (0.150 g, 0.478 mmol), **4.11j** (0.122 g, 0.251 mmol, 52%) was obtained as a light tan solid. ¹H NMR (400 MHz, Acetone-*d*₆): δ 8.78 (*br s*, 1H, *NH*), 8.75 (d, $J = 8.8$, 1H), 8.42 (d, $J = 8.4$, 1H), 7.72 (d, $J = 8.4$, 1H), 7.55 (d, $J = 6.4$, 2H), 7.36-7.33 (m, 4H), 6.97 (s, 1H), 6.92 (d, $J = 8.0$, 1H), 6.82 (d, $J = 8.0$,

1H), 5.90 (s, 2H), 5.41 (s, 2H), 4.59 (d, $J = 6.4$, 2H); ESI-MS(+): m/z 447.07 $[M + H]^+$, 469.07 $[M + Na]^+$.

2-morpholinoamide-5-chloro-8-benzyloxyquinoline (4.11k): From **4.10** (0.150 g, 0.478 mmol), **4.11k** (0.100 g, 0.261 mmol) was obtained as a light tan solid. 1H NMR (400 MHz, Acetone- d_6): δ 8.66 (d, $J = 8.8$, 1H), 8.01 (d, $J = 8.8$, 1H), 7.72 (d, $J = 8.4$, 1H), 7.61 (d, $J = 6.8$, 2H), 7.46 – 7.36 (m, 4H), 5.38 (s, 2H), 3.92 (t, $J = 4.4$, 2H), 3.78 – 3.73 (m, 4H), 3.63 (t, $J = 4.8$, 2H).

2-tetrahydrofurfurylamide-5-chloro-8-benzyloxyquinoline (4.11l): From **4.10** (0.150 g, 0.478 mmol), **4.11l** (0.090 g, 0.23 mmol, 47%) was obtained as a light tan solid. 1H NMR (400 MHz, Acetone- d_6): δ 8.75 (d, $J = 8.8$, 1H), 8.54 (*br s*, 1H), 7.76 (d, $J = 8.4$, 1H), 7.66 (d, $J = 7.6$, 1H), 7.48-7.35 (m, 4H), 5.44 (s, 2H), 4.12 – 4.06 (m, 1H), 3.86 – 3.81 (m, 1H), 3.73 – 3.62 (m, 2H), 3.53-3.47 (m, 1H), 1.92 – 1.86 (m, 1H), 1.70 – 1.63 (m, 1H); ESI-MS(+): m/z 397.16 $[M + H]^+$, 419.11 $[M + Na]^+$.

2-furfurylacetylamide-5-chloro-8-benzyloxyquinoline (4.11m): From **4.10** (0.150 g, 0.478 mmol), **4.11m** (0.135 g, 0.344 mmol, 72%) was obtained as a light tan solid. 1H NMR (400 MHz, Acetone- d_6): δ 8.75 (d, $J = 8.8$, 1H), 8.73 (*br s*, 1H, *NH*), 8.41 (d, $J = 8.8$, 1H), 7.73 (d, $J = 8.4$, 1H), 7.59 (d, $J = 7.2$, 2H), 7.51 (s, 1H), 7.41 – 7.34 (m, 4H), 6.42 – 6.41 (m, 1H), 6.37 (dd, $J_1 = 3.2$, $J_2 = 0.8$, 1H), 5.43 (s, 2H), 4.69 (d, $J = 6.0$, 2H); ESI-MS(+): m/z 393.02 $[M + H]^+$, 415.06 $[M + Na]^+$.

2-thiophenylacetamide-5-chloro-8-benzyloxyquinoline (4.11n): From **4.10** (0.200 g, 0.637 mmol), **4.11n** (0.142 g, 0.637 mmol, 55%) was obtained as a light tan solid. ^1H NMR (400 MHz, Acetone- d_6): δ 8.87 (*br s*, 1H), 8.76 (d, $J = 8.8$, 1H), 8.43 (d, $J = 8.8$, 1H), 7.74 (d, $J = 8.8$, 1H), 7.57 (d, $J = 7.2$, 2H), 7.39 – 7.33 (m, 4H), 7.14 (d, $J = 2.4$, 1H), 7.01 (dd, $J_1 = 5.2$, $J_2 = 3.6$, 1H), 5.43 (s, 2H), 4.88 (d, $J = 6.4$, 2H).

General Acid Deprotection Procedure A: The benzyl protected hydroxyquinoline was taken up in 11 mL of a 5:5:1 solution of glacial acetic acid to 12 M HCl to TFA, and heated at 70 °C for 60 h. Upon reaction completion, the reaction mixture was concentrated under reduced pressure, and the resulting crude was purified by column chromatography, running gradient from 100% hexanes to 100% ethyl acetate. The desired products typically eluted from 40-60% ethyl acetate in hexanes. Like fractions were combined and concentrated under reduced pressure to obtain final products.

General BCl_3 Deprotection Procedure: In a flame-dried flask, the benzyl protected hydroxyquinoline in 5 mL dry CH_2Cl_2 and the solution was cooled to 0 °C. Then and add 1 M boron trichloride in CH_2Cl_2 (3 eq.) was added dropwise. The reaction mixture was allowed to react at 0 °C for 30 min, and was then warmed to 25 °C for 30 min. Upon completion, the reaction was carefully quenched with MeOH. Then the solution was concentrated under reduced pressure and the resulting crude was purified by column chromatography, running gradient from 100% hexanes to 100% ethyl acetate. The desired products typically eluted around 40-60% ethyl acetate in hexanes. Like fractions were combined and concentrated under reduced pressure to obtain final products.

2-Carboxy-5-chloro-8-hydroxyquinoline (4.12a): Following General Deprotection Procedure A, from **4.10** (0.200 g, 0.637 mmol), **4.12a** (0.028 g, 0.13 mmol, 19%) was obtained as a bright yellow solid. ^1H NMR (400 MHz, CD_3OD): δ 8.67 (d, $J = 8.8$, 1H), 8.28 (d, $J = 8.4$, 1H), 7.65 (d, $J = 8.4$, 1H), 7.12 (d, $J = 8.0$, 1H); ESI-MS(-): m/z 222.02 $[\text{M} - \text{H}]^-$.

2-Diethylamide-5-chloro-8-hydroxyquinoline (4.12b): Following General Deprotection Procedure B, from **4.11b** (0.086 g, 0.23 mmol), **4.12b** (0.065 g, 0.23 mmol, 100%) was obtained as a light tan solid. ^1H NMR (400 MHz, Acetone- d_6): δ 8.96 (s, 1H), 8.63 (d, $J = 8.4$, 1H), 7.81 (d, $J = 8.8$, 1H), 7.65 (d, $J = 8.4$, 1H), 7.18 (d, $J = 8.0$, 1H), 3.60 (q, $J = 7.2$, 2H), 3.38 (q, $J = 7.2$, 2H), 1.26 (t, $J = 7.2$, 3H), 1.16 (t, $J = 7.2$, 3H); ESI-MS(-): m/z 277.20 $[\text{M} - \text{H}]^-$.

2-Isobutylamide-5-chloro-8-hydroxyquinoline (4.12c): Following General Deprotection Procedure A, from **4.11c** (0.125 g, 0.317 mmol), **4.12c** (0.061 g, 0.22 mmol, 81%) was obtained as a light yellow-tan solid. ^1H NMR (400 MHz, Acetone- d_6): δ 9.48 (*br s*, 1H), 9.25 (*br s*, 1H), 8.74 (d, $J = 8.8$, 1H), 8.44 (d, $J = 8.8$, 1H), 7.70 (d, $J = 8.4$, 1H), 7.20 (d, $J = 8.4$, 1H), 3.31 (t, $J = 6.8$, 2H), 1.99-1.92 (m, 1H), 0.96 (d, $J = 6.8$, 6H); ESI-MS(+): m/z 279.17 $[\text{M} + \text{H}]^+$, 301.11 $[\text{M} + \text{Na}]^+$.

2-Phenylamide-5-chloro-8-hydroxyquinoline (4.12d): Following General Deprotection Procedure B, from **4.11d** (0.064 g, 0.17 mmol), **4.12d** (0.027 g, 0.090 mmol, 55%) was obtained as a light tan solid. ^1H NMR (400 MHz, Acetone- d_6): δ 10.77 (*br s*, 1H, *OH*), 9.61 (*br s*, 1H,

NH), 8.81 (d, $J = 8.8$, 1H), 8.54 (d, $J = 8.8$, 1H), 7.93 (d, $J = 8.4$, 2H), 7.75 (d, $J = 8.4$, 1H), 7.42 (t, $J = 8.0$, 2H), 7.25 (d, $J = 8.4$, 1H), 7.17 (d, $J = 7.6$, 1H); ESI-MS(-): m/z 297.15 [M - H]⁻.

2-Benzylamide-5-chloro-8-benzyloxyquinoline (4.12e): Following General Deprotection Procedure B, from **4.11e** (0.060 g, 0.15 mmol), **4.12e** (0.047 g, 0.15 mmol, 100%) was obtained as a light tan solid. ¹H NMR (400 MHz, Acetone-*d*₆): δ 9.68 (*br s*, 1H, OH), 9.51 (*br s*, 1H, NH), 8.75 (d, $J = 8.8$, 1H), 8.47 (d, $J = 8.4$, 1H), 7.70 (d, $J = 8.4$, 1H), 7.41-7.26 (m, 5H), 7.19 (d, $J = 8.4$, 1H), 4.72 (d, $J = 6.4$, 2H); ESI-MS(-): m/z 311.16 [M - H]⁻.

2-(*p*-Phenolamide)-5-chloro-8-hydroxyquinoline (4.12f): Following General Deprotection Procedure B, from **4.11f** (0.127 g, 0.313 mmol), **4.12f** (0.062 g, 0.20 mmol, 63%) was obtained as a light tan solid. ¹H NMR (400 MHz, Acetone-*d*₆): δ 6.64 (*br s*, 1H), 9.60 (*br s*, 1H), 8.78 (d, $J = 8.8$, 1H), 8.52 (d, $J = 8.8$, 1H), 8.32 (*br s*, 1H), 7.23 (d, $J = 8.0$, 1H), 6.88 (d, $J = 8.8$, 2H); ESI-MS(-): m/z 313.13 [M - H]⁻.

2-Catecholamide-5-chloro-8-hydroxyquinoline (4.12g): Following General Deprotection Procedure B, from **4.11g** (0.115 g, 0.257 mmol), **4.12g** (0.077 g, 0.22 mmol) was obtained as a light tan solid. ¹H NMR (400 MHz, Acetone-*d*₆): δ 5.52 (*br s*, 1H), 8.75 (d, $J = 8.8$, 1H), 8.47 (d, $J = 8.8$, 1H), 7.91 (*br s*, 1H), 7.70 (d, $J = 8.4$, 1H), 7.19 (d, $J = 8.4$, 1H), 6.88 (s, 1H), 6.77 (d, $J = 8.0$, 1H), 6.72 (d, $J = 8.4$, 1H), 7.75 (d, $J = 6.4$, 2H); ESI-MS(-): m/z 342.98.15 [M - H]⁻.

2-Cyclohexylamide-5-chloro-8-hydroxyquinoline (4.12h): Following General Deprotection Procedure A, from **4.11h** (0.125 g, 0.317 mmol), **4.12h** (0.055 g, 0.18 mmol, 57%) was obtained

as a light yellow-tan solid; ^1H NMR (400 MHz, Acetone- d_6): δ 9.35 (*br s*, 1H, *OH*), 8.08 (*br s*, 1H, *NH*), 8.74 (d, $J = 8.8$, 1H), 8.45 (d, $J = 8.8$, 1H), 7.70 (d, $J = 8.4$, 1H), 7.19 (d, $J = 8.0$, 1H), 3.96 (s, 1H), 1.99 (s, 2H), 1.80 (s, 2H), 1.69 (d, $J = 12.8$, 1H), 1.46-1.35 (m, 4H), 1.21 (*br s*, 1H); ESI-MS(+): m/z 305.19 $[\text{M} + \text{H}]^+$, 327.15 $[\text{M} + \text{Na}]^+$.

2-Acetylcyclohexylamide-5-chloro-8-hydroxyquinoline (4.12i): Following General Deprotection Procedure B, from **4.11i** (0.080 g, 0.21 mmol), **4.12i** (0.035 g, 0.11 mmol, 53%) was obtained as a light tan solid. ^1H NMR (400 MHz, Acetone- d_6): δ 9.48 (*br s*, 1H), 9.22 (*br s*, 1H), 8.74 (d, $J = 8.8$, 1H), 8.44 (d, $J = 8.8$, 1H), 7.70 (d, $J = 8.4$, 1H), 7.20 (d, $J = 8.4$, 1H), 3.32 (t, $J = 6.4$, 2H), 1.81-1.63 (m, 7H), 1.28-0.97, (m, 6H); ESI-MS(+): m/z 319.30 $[\text{M} + \text{H}]^+$, 341.17 $[\text{M} + \text{Na}]^+$.

2-Piperenalamide-5-chloro-8-hydroxyquinoline (4.12j): Following General Deprotection Procedure A, from **4.11j** (0.115 g, 0.302 mmol), **4.12j** (0.021 g, 0.073 mmol, 24%) was obtained as a light yellow/tan solid. ^1H NMR (400 MHz, Acetone- d_6): δ 8.96 (*br s*, 1H), 8.66 (d, $J = 8.8$, 1H), 7.81 (d, $J = 8.4$, 1H), 7.66 (d, $J = 8.4$, 1H), 7.19 (d, $J = 8.0$, 1H), 3.74 (t, $J = 5.6$, 2H), 3.42 (t, $J = 5.6$, 2H), 1.69 (*br s*, 4H), 1.56 (s, 2H); ESI-MS(+): m/z 291.21 $[\text{M} + \text{H}]^+$, 313.11 $[\text{M} + \text{Na}]^+$.

2-Morpholinoamide-5-chloro-8-hydroxyquinoline (4.12k): Following General Deprotection Procedure B, from **4.11k** (0.097 g, 0.25 mmol), **4.12k** (0.043 g, 0.15 mmol, 58%) was obtained as a light tan solid. ^1H NMR (400 MHz, Acetone- d_6): δ 8.98 (*br s*, 1H, *OH*), 8.67 (d, $J = 8.8$,

1H), 7.88 (d, $J = 8.8$, 1H), 7.68 (d, $J = 8.4$, 1H), 7.20 (d, $J = 8.4$, 1H), 3.77 (s, 4H), 3.63 (dd, $J_1 = 16.4$, $J_2 = 4.8$, 4H); ESI-MS(+): m/z 293.25 $[M + H]^+$.

2-Tetrahydrofurfurylamide-5-chloro-8-hydroxyquinoline (4.12l): Following General Deprotection Procedure B, from **4.11l** (0.085 g, 0.21 mmol), **4.12l** (0.022 g, 0.072 mmol, 34%) was obtained as a bright yellow solid. ^1H NMR (400 MHz, Acetone- d_6): δ 9.64 (*br s*, 1H), 9.22 (s, 1H), 8.71 (d, $J = 8.8$, 1H), 8.42 (d, $J = 8.8$, 1H), 7.69 (d, $J = 8.0$, 1H), 7.18 (d, $J = 8.4$, 1H), 4.09 – 4.02 (m, 1H), 3.82 (q, $J_1 = 7.2$, $J_2 = 6.8$, 1H), 3.69 – 3.57 (m, 2H), 3.51 – 3.44 (m, 1H), 2.02 – 1.80 (m, 3H), 1.70 – 1.61 (m, 1H); ESI-MS(-): m/z 305.15 $[M - H]^-$.

2-Acetylfurfurylamide-5-chloro-8-benzyloxyquinoline (4.12m): Following General Deprotection Procedure B, from **4.11m** (0.087 g, 0.22 mmol), **4.12m** (0.049 g, 0.16 mmol, 73%) was obtained as a bright yellow solid. ^1H NMR (400 MHz, Acetone- d_6): δ 9.57 (*br s*, 1H, *NH*), 9.52 (*br s*, 1H, *OH*), 8.75 (d, $J = 8.8$, 1H), 8.44 (d, $J = 8.8$, 1H), 7.71 (d, $J = 8.4$, 1H), 7.48 (d, $J = 1.2$, 1H), 7.19 (d, $J = 8.0$, 1H), 6.37 (dd, $J_1 = 2.8$, $J_2 = 2.0$, 1H), 6.33 (d, $J = 2.4$, 1H), 4.69 (d, $J = 6.0$, 2H); ESI-MS(-): m/z 301.12 $[M - H]^-$.

2-Thiophenylacetylamide-5-chloro-8-hydroxyquinoline (4.12n): Following General Deprotection Procedure B, from **4.11n** (0.125 g, 0.306 mmol), **4.12n** (0.087 g, 0.27 mmol) was obtained as a light tan solid. ^1H NMR (400 MHz, Acetone- d_6): δ 9.73 (*br s*, 1H), 9.49 (s, 1H, *NH*), 8.77 (d, $J = 8.8$, 1H), 8.47 (d, $J = 8.8$, 1H), 7.71 (d, $J = 8.0$, 1H), 7.33 (dd, $J_1 = 5.2$, $J_2 = 1.2$, 1H), 7.20 (d, $J = 8.0$, 1H), 7.09 (d, $J = 2.4$, 1H), 6.96 (dd, $J_1 = 4.8$, $J_2 = 3.6$, 1H), 4.88 (d, $J = 6.0$, 1H); ESI-MS(+): m/z 318.95 $[M + H]^+$, 341.02 $[M + \text{Na}]^+$.

Synthesis of 5-position 8-hydroxyquinoline Derivatives

2-Methyl-5-nitro-8-hydroxyquinoline (4.13): A solution of 2-amino-4-nitrophenol (3.00 g, 19.5 mmol) in 60 mL toluene with 20 mL 6 M HCl was pre-heated to 70 °C for 5 min. Then crotonaldehyde (2.4 mL, 29.2 mmol) was added in one portion, and the reaction was heated at 70 °C for 16 h while open to air. Upon completion, the reaction was cooled to 25 °C, and the organic layer was separated and discarded. The acidic solution was neutralized with NaOH to pH 7, and was then extracted into organic with 3×20 mL ethyl acetate. The combined organic was washed with brine, dried over magnesium sulfate, and the solids were filtered off and discarded. The filtrate was concentrated under reduced pressure, yielding a red-brown, sticky crude, which was then purified by column chromatography, running elution gradient from 100% hexanes to 50% ethyl acetate in hexanes. The desired product eluted in 20% ethyl acetate in hexanes. Like fractions were combined and concentrated under reduced pressure to obtain **4.13** (3.30 g, 16.2 mmol, 42%) as a very bright orange-red solid. ¹H NMR (400 MHz, Acetone-*d*₆): δ 9.10 (d, *J* = 8.8, 1H), 8.52 (d, *J* = 8.8, 1H), 7.77 (d, *J* = 9.2, 1H), 7.22 (d, *J* = 8.8, 1H), 2.76 (s, 3H); ESI-MS(-): *m/z* 203.24 [M - H]⁻.

2-Methyl-5-nitro-8-benzyloxyquinoline (4.14): To a solution of **4.13** (3.50 g, 17.1 mmol) and K₂CO₃ (7.11 g, 51.4 mmol) in 30 mL DMF, benzyl bromide (5.10 mL, 42.9 mmol) was added dropwise. The reaction was then heated at 65 °C for 6 h. Upon reaction completion, the reaction mixture was concentrated under reduced pressure. The resulting crude was taken up in 30 mL ethyl acetate, washed with water and then brine, and dried over magnesium sulfate. The solids were filtered off and discarded, and the filtrate was concentrated under reduced pressure. The

resulting crude was purified by column chromatography, running gradient from 100% hexanes to 50% ethyl acetate in hexanes. The desired product eluted in 20% ethyl acetate in hexanes. Like fractions were combined and concentrated under reduced pressure to obtain **4.14** (3.30 g, 11.2 mmol, 66%) as a light yellow solid. ¹H NMR (400 MHz, Acetone-*d*₆): δ 8.94 (d, *J* = 9.2, 1H), 8.40 (d, *J* = 9.2, 1H), 7.66 (d, *J* = 9.2, 1H), 7.62 (d, *J* = 7.6, 2H), 7.46 – 7.33 (m, 4H), 5.50 (s, 2H), 2.71 (s, 3H); ESI-MS(+): *m/z* 295.05 [M + H]⁺.

2-Carboxyl-5-nitro-8-benzoxyquinoline (4.15): To a solution of **4.14** (3.40 g, 11.6 mmol) in 75 mL pyridine, SeO₂ (3.85 g, 34.7 mmol) was added. The reaction mixture was heated to reflux at 115 °C for 2 h, and upon completion, the solution was hot filtered to remove the reduced selenium salts. The filtrate was concentrated under reduced pressure, and taken up in water to precipitate product, and was heated at 100 °C for 30 min to dissolve excess selenium. The suspension was hot filtered to collect **4.15** (3.40 g, 10.5 mmol, 91%) as a light tan solid. ¹H NMR (400 MHz, Acetone-*d*₆): δ 9.38 (d, *J* = 9.2, 1H), 8.68 (d, *J* = 9.2, 1H), 8.50 (d, *J* = 9.2, 1H), 7.64 (d, *J* = 7.6, 2H), 7.55 (d, *J* = 8.8, 1H), 7.44-7.37 (m, 3H), 5.63, (s, 2H); ESI-MS(-): *m/z* 323.04 [M - H]⁻.

2-Methylester-5-nitro-8-benzoxyquinoline (4.16): To a solution of **4.15** (3.40 g, 10.5 mmol) in 300 mL MeOH, a catalytic H₂SO₄ was added, and the reaction mixture was heat to reflux at 110 °C for 72 h. Upon completion, the reaction was cooled to 25 °C, and concentrate under reduced pressure to remove volatiles. The resulting crude was taken up in a small amount of MeOH to precipitate the desired product. The solid was collected via vacuum filtration and rinsed with a small amount of MeOH to obtain **4.16** (2.89 g, 8.54 mmol, 81%) as a pale yellow powdery solid.

^1H NMR (400 MHz, Acetone- d_6): δ 9.30 (d, $J = 9.2$, 1H), 8.64 (d, $J = 8.8$, 1H), 8.43 (d, $J = 8.8$, 1H), 7.65 (d, $J = 7.2$, 2H), 7.51 (d, $J = 8.8$, 1H), 7.45 – 7.35 (m, 3H), 5.63, (s, 2H), 4.01 (s, 3H).

2-Methylester-5-amino-8-benzyloxyquinoline (4.17): A solution of **4.16** (2.0 g, 5.9 mmol) in 100 mL MeOH was degassed under vacuum, and then 5% w/w Pd/C (0.32 g, 0.29 mmol) was added in one portion. The reaction mixture was placed under a hydrogen atmosphere at 1 atm, and reacted at 25 °C for 48 h. Upon completion, the reaction mixture was filtered through a thin pad of celite, and the filtrate was concentrated under reduced pressure. The resulting crude was taken up in 20 mL ethyl acetate and washed with 1 M NaOH. Upon back-extraction, the combined organic was washed with brine, and dried over magnesium sulfate. The solids were filtered off and discarded, and the filtrate was concentrate under reduced pressure. The resulting crude was purified by column chromatography, running gradient from 100% hexanes to 100% ethyl acetate in hexanes. The desired product eluted in 50% ethyl acetate in hexanes. Like fractions were combined and concentrated under reduced pressure to obtain **4.17** (0.260 g, 0.843 mmol, 14%) as a red-tan solid. ^1H NMR (400 MHz, Acetone- d_6): δ 8.65 (d, $J = 8.8$, 1H), 8.07 (d, $J = 8.8$, 1H), 7.66 (d, $J = 7.6$, 2H), 7.38 (t, $J = 8.0$, 2H), 7.30 (t, $J = 7.2$, 1H), 7.18 (d, $J = 8.0$, 1H), 6.87 (d, $J = 8.0$, 1H), 5.34 (s, 2H), 5.17 (*br s*, 2H), 3.99 (s, 3H); ESI-MS(+): m/z 331.05 [$\text{M} + \text{Na}]^+$.

General amide and sulfonamide coupling procedure: A solution of **4.17** and TEA (0.68 eq) in 5 mL CH_2Cl_2 was cooled to 0 °C. Then a separate solution of either acid chloride or sulfonyl chloride (1.2 eq) in 2 mL CH_2Cl_2 was added dropwise to reaction. The reaction was allowed to warm slowly to 25 °C for 4 h. Upon completion, the reaction mixture was washed with 1 M

NaOH. Upon back-extraction, the combined organic layers were washed with brine, and dried over magnesium sulfate. The solids were filtered off and discarded, and the filtrate was concentrated under reduced pressure. The resulting crude was purified by column chromatography, running gradient from 100% hexanes to 100% ethyl acetate. The desired product typically eluted in 40 – 50% ethyl acetate in hexanes. Like fractions were combined and concentrated under reduced pressure to obtain the desired product.

2-Methyl ester-5-methylamide-8-benzyloxyquinoline (4.18a): Following the above general amide and sulfonamide coupling procedure, from **4.17** (0.062 g, 0.20 mmol) and acetic anhydride (0.023 mL, 0.24 mmol), **4.18a** (0.060 g, 0.17 mmol, 85%) was obtained as a tan solid. ¹H NMR (400 MHz, Acetone-*d*₆): δ 8.47 (d, *J* = 8.8, 1H), 8.21 (d, *J* = 8.8, 1H), 7.59-7.55 (m, 3H), 7.39-7.25 (m, 4H), 5.43 (s, 2H), 4.03 (s, 3H), 2.25 (s, 3H).

2-Methylester-5-benzamide-8-benzyloxyquinoline (4.18b): Following the above general amide and sulfonamide coupling procedure, from **4.17** (0.35 g, 0.11 mmol) and benzoyl chloride (0.016 mL, 0.14 mmol), **4.18b** (0.033 g, 0.080 mmol, 70%) was obtained as a tan solid. ¹H NMR (400 MHz, Acetone-*d*₆): δ 9.70 (*br s*, 1H), 8.61 (d, *J* = 8.8, 1H), 8.18 (d, *J* = 8.8, 1H), 8.14 (d, *J* = 7.2, 2H), 7.63 (t, *J* = 8.0, 1H), 7.67 – 7.55 (m, 5H), 7.44 – 7.33 (m, 4H), 5.51 (s, 2H), 3.99 (s, 3H).

2-Methyl ester-5-methylsulfonamide-8-benzyloxyquinoline (4.18c): Following the above general amide and sulfonamide coupling procedure, from **4.17** (0.050 g, 0.16 mmol) and methylsulfonic anhydride (0.056 mL, 0.32 mmol), **4.18c** (0.033 g, 0.085 mmol, 52%) was

obtained as a tan solid. ^1H NMR (400 MHz, Acetone- d_6): δ 8.91 (d, $J = 8.8$, 1H), 8.61 (*br s*, 1H), 8.26 (d, $J = 8.8$, 1H), 7.75 (d, $J = 8.4$, 1H), 7.63 (d, $J = 7.6$, 2H), 7.47 – 7.38 (m, 4H), 5.49 (s, 2H), 3.05 (s, 3H), 2.96 (s, 3H); ESI-MS(-): m/z 432.99 [$\text{M} - \text{H}$] $^-$.

2-Methyl ester-5-di-benzenesulfonamide-8-benzyloxyquinoline (4.18d): Following the above general amide and sulfonamide coupling procedure, from **4.17** (0.065 g, 0.21 mmol) and benzenesulfonyl chloride (0.054 mL, 0.42 mmol), **4.18d** (0.096 g, 0.16 mmol, 77%) was obtained as a tan solid. ^1H NMR (400 MHz, Acetone- d_6): δ 8.02 (t, $J = 7.1$, 1H), 7.96 (dd, $J_1 = 8.7$ $J_2 = 5.4$, 1H), 7.92 – 7.80 (m, 1H), 7.67 (d, $J = 7.5$, 1H), 7.46 (d, $J = 7.5$, 1H), 7.38 (dd, $J_1 = 13.5$ $J_2 = 5.2$, 1H), 7.33 – 7.27 (m, 1H), 5.52 (d, $J = 5.3$, 1H), 4.01 (t, $J = 16.8$, 1H); ESI-MS(+): m/z 611.00 [$\text{M} + \text{Na}$] $^+$.

General Deprotection Procedure: To a solution of the starting 5-derivatized quinoline in 2 mL THF, 15 mL 1 M NaOH was added, and the reaction was stirred at 25 °C overnight for 16 h. Then the reaction mixture was neutralized with HCl, and concentrate under reduced pressure. The resulting solid was recrystallized from MeOH to obtain the intermediate carboxylic acid. This intermediate was placed in a flame-dried flask, taken up in 7 mL chloroform, and the solution was cooled to 0 °C. Then 1 mL of 1 M BCl_3 in CH_2Cl_2 (excess), was added dropwise and the reaction mixture was stirred at 0 °C for 30 min, then at 25 °C for 30 min. Upon reaction completion, the solution was carefully quenched with MeOH and concentrated under reduced pressure to obtain a crude solid. The crude was purified by reverse phase chromatography, running gradient from 100% water to 100% acetonitrile. Like fractions containing the desired product were combined and concentrated under reduced pressure to obtain final products.

2-Carboxy-5-methylamide-8-benzyloxyquinoline (4.19a): From the above general deprotection procedure, from **4.18a** (0.062 g, 0.20 mmol), **4.19a** (0.010 g, 0.041 mmol, 24%) was obtained as a tan solid. ¹H NMR (400 MHz, Acetone-*d*₆): δ 9.58 (*br s*, 1H), 9.22 (*br s*, 1H), 8.70 (d, *J* = 8.8, 1H), 8.25 (d, *J* = 8.8, 1H), 7.79 (d, *J* = 8.4, 1H), 7.63 (d, *J* = 7.2, 2H), 2.23 (s, 3H); ESI-MS(+): *m/z* 247.16 [M + H]⁺.

2-Carboxy-5-benzamide-8-hydroxyquinoline (4.19b): From the above general deprotection procedure, from **4.18b** (0.030 g, 0.073 mmol), **4.19b** (0.0053 g, 0.017 mmol, 24%) was obtained as a tan solid. ¹H NMR (400 MHz, Acetone-*d*₆): δ 8.40 (d, *J* = 5.6, 1H), 8.22 (d, *J* = 6.4, 1H), 8.07 (d, *J* = 7.2, 2H), 7.65 – 7.54 (m, 4H), 7.18 (d, *J* = 6.4, 1H).

2-Carboxy-5-methylsulfonamide-8-benzyloxyquinoline (4.19c): From the above general deprotection procedure, from **4.18c** (0.032 g, 0.083 mmol), **4.19c** (0.010 g, 0.035 mmol, 4%) was obtained as a tan solid. ¹H NMR (400 MHz, Acetone-*d*₆): δ 8.99 (s, 1H), 8.54 (*br s*, 1H), 8.34 (s, 1H), 7.80 (s, 1H), 7.28 (s, 1H), 3.05 (s, 3H); ESI-MS(-): *m/z* 281.05 [M - H]⁻.

2-Carboxy-5-benzenesulfonamide-8-benzyloxyquinoline (4.19d): From the above general deprotection procedure, from **4.18d** (0.045 g, 0.58 mmol), **4.19d** (0.011 g, 0.041 mmol, 40%) was obtained as a tan solid. ¹H NMR (400 MHz, Acetone-*d*₆): δ 8.73 (d, *J* = 6.8, 1H), 8.21 (d, *J* = 7.2, 1H), 7.69 (d, *J* = 6.8, 2H), 7.63 (t, *J* = 6.0, 1H), 7.51 (t, *J* = 6.4, 2H), 7.25 (d, *J* = 6.4, 1H), 7.15 (d, *J* = 6.4, 1H); ESI-MS(-): *m/z* 432.99 [M - H]⁻.

Assays against NDM-1

Colorimetric substrate assay protocol: NDM-1 was supplied as a gift from David Tierney. The assay was performed in triplicate in clear cuvettes. Each cuvette contained a total volume of 1,000 μ L including buffer (50 mM HEPES, 2 mM CHAPS, 5 μ M Zn-SO₄, pH 7.0), NDM-1 (8.0 nM), inhibitor (200 μ M), and chromacef substrate (3 μ M). The enzyme and inhibitor were initially incubated together for 20 min at room temperature, after which the reaction was initiated by substrate addition. Upon substrate addition, the change in absorbance was monitored for 15 s at 442 nm. The negative control contained no inhibitor and was arbitrarily set as 100% enzyme activity. IC₅₀ values were determined by incubating various concentrations of inhibitor with the enzyme using the aforementioned conditions, and dose response curves were generated, fitted, and analyzed using GraphPad Prism graphing software using four-variable response parameters.

Fluorescent substrate assay protocol: NDM-1 was supplied as a gift from David Tierney, and the Fluorocillin Green substrate was purchased from ThermoFisher. The assay was performed in a Costar black 96-well plate. Each well contained a total volume of 100 μ L including buffer (50 mM HEPES, 2 mM CHAPS, 5 μ M Zn-SO₄, pH 7.0), NDM-1 (100 pM), inhibitor (200 μ M), and fluorocillin green substrate (87 nM). The enzyme and inhibitor were initially incubated together for 20 min at room temperature, after which the reaction was initiated by substrate addition. The change in fluorescence was monitored for 20 min with excitation at 485 nm and reading emission at 528 nm. The negative control wells contained no inhibitor and were arbitrarily set as 100% enzyme activity. IC₅₀ values were determined by incubating various concentrations of inhibitor with the enzyme using the aforementioned conditions, and dose response curves were

generated, fitted, and analyzed using GraphPad Prism graphing software using four-variable response parameters.

Relative Tryptophan Fluorescence Assay: NDM-1 (final concentration 2 μM) in 2 mL of 50 mM HEPES at pH 7.5, was mixed with inhibitors at concentrations from 4 to 32 μM . After incubation for 30 min, fluorescence emission spectra of NDM-1 samples were obtained on a Perkin Elmer Luminescence spectrometer (Model LS-55), with an excitation wavelength of 280 nm and an emission spectrum from 300 to 400 nm. The relative tryptophan fluorescence intensity (at 348 nm) was calculated setting the intensity of HEPES buffer 0% and NDM-1 containing no inhibitors at 100%. L-Tryptophan (2 μM) was used in place of NDM-1 as a control.

4.6 Acknowledgements

Chapters 4, is, in part, a reprint of materials published in the following paper: Targeting Metalloenzymes for Therapeutic Intervention, Chen, Y.A.;* Adamek, R.N.;* Dick, B.L.; Credille, C.V.; Morrison, C.N.; Cohen, S.M.; *Chem. Rev.* **2018**, *118*, ASAP article. DOI: 10.1021/ACS.CHEMREV.8B00201. The dissertation author was the primary researcher and the primary author for the reprinted data presented herein. The dissertation author thanks the remaining co-authors for their contributions. Reprinted with permission from Chemical Reviews. Copyright 2018 American Chemical Society.

*These authors contributed equally to this work

4.7 References

1. Patrick, G. L., *An Introduction to Medicinal Chemistry*. 4 ed.; Oxford: 2009.
2. Lee, W.; McDonough, M. A.; Kotra, L.; Li, Z. H.; Silvaggi, N. R.; Takeda, Y.; Kelly, J. A.; Mobashery, S., A 1.2-A Snapshot of the Final Step of Bacterial Cell Wall Biosynthesis. *Proc. Natl. Acad. Sci. U. S. A.* **2001**, *98*, 1427-31.
3. Drawz, S. M.; Bonomo, R. A., Three Decades of Beta-Lactamase Inhibitors. *Clin. Microbiol. Rev.* **2010**, *23*, 160-201.
4. Fisher, J. F.; Meroueh, S. O.; Mobashery, S., Bacterial Resistance to Beta-Lactam Antibiotics: Compelling Opportunism, Compelling Opportunity. *Chem. Rev.* **2005**, *105*, 395-424.
5. Rotondo, C. M.; Wright, G. D., Inhibitors of Metallo-Beta-Lactamases. *Curr Opin Microbiol* **2017**, *39*, 96-105.
6. Nordmann, P.; Poirel, L.; Walsh, T. R.; Livermore, D. M., The Emerging NDM Carbapenemases. *Trends Microbiol.* **2011**, *19*, 588-95.
7. Sekizuka, T.; Matsui, M.; Yamane, K.; Takeuchi, F.; Ohnishi, M.; Hishinuma, A.; Arakawa, Y.; Kuroda, M., Complete Sequencing of the bla(NDM-1)-Positive IncA/C Plasmid from Escherichia coli ST38 Isolate Suggests a Possible Origin from Plant Pathogens. *PLoS One* **2011**, *6*, e25334.
8. Wailan, A. M.; Paterson, D. L., The Spread and Acquisition of NDM-1: A Multifactorial Problem. *Expert Rev. Anti-Infect. Ther.* **2014**, *12*, 91-115.
9. Yong, D.; Toleman, M. A.; Giske, C. G.; Cho, H. S.; Sundman, K.; Lee, K.; Walsh, T. R., Characterization of a New Metallo-Beta-Lactamase Gene, bla(NDM-1), and a Novel Erythromycin Esterase Gene Carried on a Unique Genetic Structure in Klebsiella pneumoniae Sequence Type 14 from India. *Antimicrob. Agents Chemother.* **2009**, *53*, 5046-54.
10. Berrazeg, M.; Diene, S.; Medjahed, L.; Parola, P.; Drissi, M.; Raoult, D.; Rolain, J., New Delhi Metallo-Beta-Lactamase Around the World: An eReview using Google Maps. *Euro. Surveill.* **2014**, *19*.
11. Woodford, N.; Turton, J. F.; Livermore, D. M., Multiresistant Gram-Negative Bacteria: The Role of High-Risk Clones in the Dissemination of Antibiotic Resistance. *FEMS Microbiol. Rev.* **2011**, *35*, 736-55.
12. Walsh, T. R., Emerging Carbapenemases: A Global Perspective. *Int. J. Antimicrob. Agents* **2010**, *36 Suppl 3*, S8-14.
13. Moellering, R. C., Jr., NDM-1--A Cause for Worldwide Concern. *N. Engl. J. Med.* **2010**, *363*, 2377-9.

14. Kim, Y.; Cunningham, M. A.; Mire, J.; Tesar, C.; Sacchettini, J.; Joachimiak, A., NDM-1, the Ultimate Promiscuous Enzyme: Substrate Recognition and Catalytic Mechanism. *FASEB J.* **2013**, *27*, 1917-27.
15. Thomas, P. W.; Zheng, M.; Wu, S. S.; Guo, H.; Liu, D. L.; Xu, D. G.; Fast, W., Characterization of Purified New Delhi Metallo-beta-lactamase-1. *Biochemistry-U.S.* **2011**, *50*, 10102-10113.
16. Zhang, H.; Hao, Q., Crystal Structure of NDM-1 Reveals a Common Beta-Lactam Hydrolysis Mechanism. *FASEB J.* **2011**, *25*, 2574-82.
17. Aitha, M.; Moller, A. J.; Sahu, I. D.; Horitani, M.; Tierney, D. L.; Crowder, M. W., Investigating the Position of the Hairpin Loop in New Delhi Metallo-Beta-Lactamase, NDM-1, during Catalysis and Inhibitor Binding. *J. Inorg. Biochem.* **2016**, *156*, 35-9.
18. Palzkill, T., Metallo-Beta-Lactamase Structure and Function. *Ann. N. Y. Acad. Sci.* **2013**, *1277*, 91-104.
19. King, D.; Strynadka, N., Crystal Structure of New Delhi metallo-Beta-Lactamase Reveals Molecular Basis for Antibiotic Resistance. *Protein Sci.* **2011**, *20*, 1484-91.
20. Feng, H.; Ding, J. J.; Zhu, D. Y.; Liu, X. H.; Xu, X. Y.; Zhang, Y.; Zang, S. S.; Wang, D. C.; Liu, W., Structural and Mechanistic Insights into NDM-1 Catalyzed Hydrolysis of Cephalosporins. *J Am Chem Soc* **2014**, *136*, 14694-14697.
21. King, D. T.; Worrall, L. J.; Gruninger, R.; Strynadka, N. C. J., New Delhi Metallo-beta-Lactamase: Structural Insights into beta-Lactam Recognition and Inhibition. *J Am Chem Soc* **2012**, *134*, 11362-11365.
22. Yang, H.; Aitha, M.; Marts, A. R.; Hetrick, A.; Bennett, B.; Crowder, M. W.; Tierney, D. L., Spectroscopic and Mechanistic Studies of Heterodimetallic Forms of Metallo-Beta-Lactamase NDM-1. *J Am Chem Soc* **2014**, *136*, 7273-85.
23. Burns, C. J.; Goswami, R.; Jackson, R. W.; Lessen, T.; Li, W.; Pevear, D.; Tirunahari, P. K.; Xu, H. BETA-LACTAMASE INHIBITORS. WO2010130708A1, 2010.
24. Brem, J.; Cain, R.; Cahill, S.; McDonough, M. A.; Clifton, I. J.; Jimenez-Castellanos, J. C.; Avison, M. B.; Spencer, J.; Fishwick, C. W.; Schofield, C. J., Structural Basis of Metallo-Beta-Lactamase, Serine-Beta-Lactamase and Penicillin-Binding Protein Inhibition by Cyclic Boronates. *Nat. Commun.* **2016**, *7*, 12406.
25. Krajnc, A.; Lang, P. A.; Panduwawala, T. D.; Brem, J.; Schofield, C. J., Will Morphing Boron-Based Inhibitors Beat the Beta-Lactamases? *Curr. Opin. Chem. Biol.* **2019**, *50*, 101-110.
26. Liu, B.; Trout, R. E. L.; Chu, G. H.; McGarry, D.; Jackson, R. W.; Hamrick, J. C.; Daigle, D. M.; Cusick, S. M.; Pozzi, C.; De Luca, F.; Benvenuti, M.; Mangani, S.; Docquier, J. D.; Weiss, W. J.; Pevear, D. C.; Xerri, L.; Burns, C. J., Discovery of Taniborbactam (VNRX-

5133): A Broad-Spectrum Serine- and Metallo-beta-lactamase Inhibitor for Carbapenem-Resistant Bacterial Infections. *J. Med. Chem.* **2020**, *63*, 2789-2801.

27. Rogers, B. A.; Sidjabat, H. E.; Silvey, A.; Anderson, T. L.; Perera, S.; Li, J.; Paterson, D. L., Treatment Options for New Delhi Metallo-Beta-Lactamase-Harboring Enterobacteriaceae. *Microb. Drug Resist.* **2013**, *19*, 100-3.

28. Garonzik, S. M.; Li, J.; Thamlikitkul, V.; Paterson, D. L.; Shoham, S.; Jacob, J.; Silveira, F. P.; Forrest, A.; Nation, R. L., Population Pharmacokinetics of Colistin Methanesulfonate and formed Colistin in ritically Ill Patients from a Multicenter Study Provide Dosing Suggestions for Various Categories of Patients. *Antimicrob. Agents Chemother.* **2011**, *55*, 3284-94.

29. Liu, Y. Y.; Wang, Y.; Walsh, T. R.; Yi, L. X.; Zhang, R.; Spencer, J.; Doi, Y.; Tian, G. B.; Dong, B. L.; Huang, X. H.; Yu, L. F.; Gu, D. X.; Ren, H. W.; Chen, X. J.; Lv, L. C.; He, D. D.; Zhou, H. W.; Liang, Z. S.; Liu, J. H.; Shen, J. Z., Emergence of Plasmid-Mediated Colistin Resistance Mechanism MCR-1 in Animals and Human Beings in China: A Microbiological and Molecular Biological Study. *Lancet Infect Dis* **2016**, *16*, 161-168.

30. Chen, A. Y.; Adamek, R. N.; Dick, B. L.; Credille, C. V.; Morrison, C. N.; Cohen, S. M., Targeting Metalloenzymes for Therapeutic Intervention. *Chem. Rev.* **2019**, *119*, 1323-1455.

31. King, A. M.; Reid-Yu, S. A.; Wang, W.; King, D. T.; De Pascale, G.; Strynadka, N. C.; Walsh, T. R.; Coombes, B. K.; Wright, G. D., Aspergillomarasmine A Overcomes Metallo-Beta-Lactamase Antibiotic Resistance. *Nature* **2014**, *510*, 503-6.

32. Brem, J.; van Berkel, S. S.; Zollman, D.; Lee, S. Y.; Gileadi, O.; McHugh, P. J.; Walsh, T. R.; McDonough, M. A.; Schofield, C. J., Structural Basis of Metallo-beta-Lactamase Inhibition by Captopril Stereoisomers. *Antimicrob. Agents Chemother.* **2016**, *60*, 142-50.

33. Chen, A. Y.; Thomas, P. W.; Stewart, A. C.; Bergstrom, A.; Cheng, Z.; Miller, C.; Bethel, C. R.; Marshall, S. H.; Credille, C. V.; Riley, C. L.; Page, R. C.; Bonomo, R. A.; Crowder, M. W.; Tierney, D. L.; Fast, W.; Cohen, S. M., Dipicolinic Acid Derivatives as Inhibitors of New Delhi Metallo-beta-lactamase-1. *J. Med. Chem.* **2017**, *60*, 7267-7283.

34. Shin, W. S.; Bergstrom, A.; Bonomo, R. A.; Crowder, M. W.; Muthyala, R.; Sham, Y. Y., Discovery of 1-Hydroxypyridine-2(1H)-thione-6-carboxylic Acid as a First-in-Class Low-Cytotoxic Nanomolar Metallo beta-Lactamase Inhibitor. *ChemMedChem* **2017**, *12*, 845-849.

Chapter 5: MBPs as Inhibitors of Human Arginase 1

5.1 Introduction to Arginase-1

In 1904, Kossel and Dakin reported the discovery of an enzyme isolated from canine liver that was capable of hydrolyzing the amino acid L-Arg.¹⁻² This enzyme would later come to be known as Arginase, and remains the oldest known example of a manganese dependent metalloenzyme. It is now known that Arginase is distributed across all domains of life, and plays a crucial role in completing the last step of the urea cycle by hydrolyzing the amino acid L-Arg into L-ornithine and urea. There are two Arginase isoforms, Arg1, which is primarily found in the cellular cytosol, and Arg2, which is localized in the mitochondria. Within the human body, Arg1 is primarily localized in the liver due to its role in the urea cycle, but is distributed at lower concentrations throughout the body, as Arg1 activity has also been established to play a role in maintaining body homeostasis, particularly in regard to regulating immune function. The isoforms share overall 58% sequence homology,³ but essentially 100% homology at the active site, which includes the catalytic Mn^{2+} ions.^{2,4} The remainder of this chapter shall be devoted to Arg1, unless otherwise noted.

Arg1 is a homotrimeric metalloenzyme, with each subunit bearing the same dinuclear Mn^{2+} active site (Figure 5.1a). The Arg1 active site is comprised of a narrow channel 15 Å deep by 9 Å across, with the catalytic Mn^{2+} ions at the base of the pocket, and an amino acid recognition motif present at the entrance of the pocket (Figure 5.1b).⁵ The Mn^{2+} ions, which are responsible for substrate hydrolysis, are ~3.3 Å apart from each other. Each Mn^{2+} ion is coordinated to one His and two Asp residues, with an additional two Asp residues bridging between the Mn^{2+} ions.⁶ Mn^{2+}_A is coordinated in square pyramidal geometry and Mn^{2+}_B is coordinated in distorted octahedral geometry.⁷ The coordination sphere of each Mn^{2+} ion is

completed by a bridging hydroxyl that is inserted in the guanidine moiety during L-arginine hydrolysis, as depicted below in Figure 5.1 c and d.

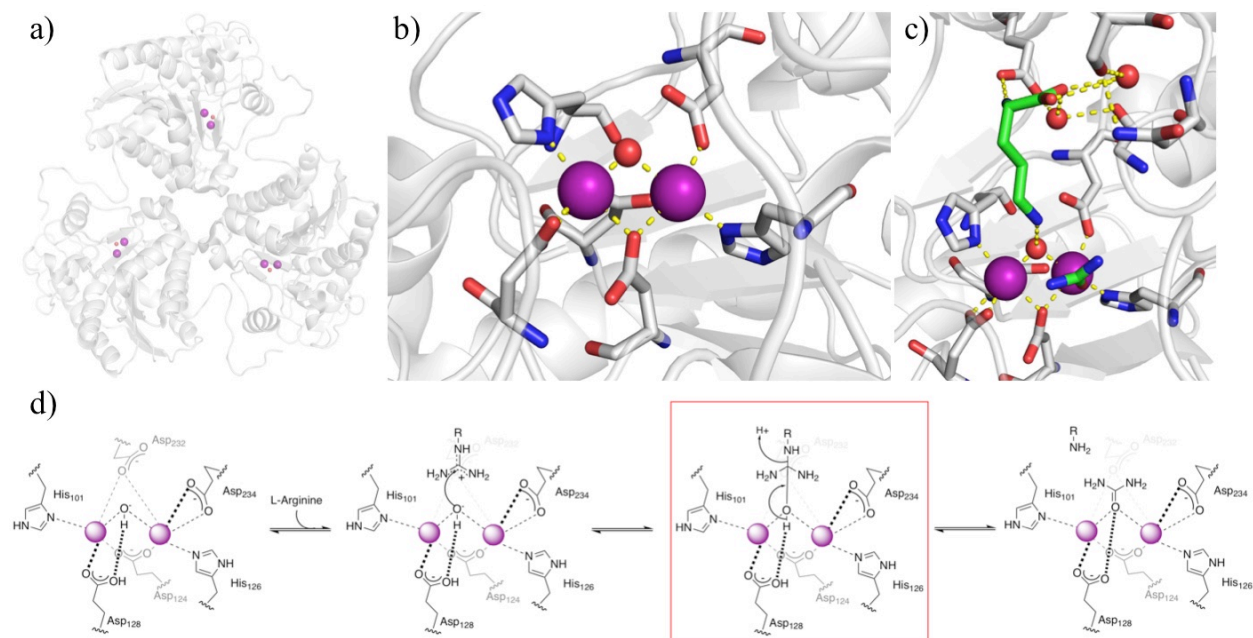


Figure 5.1. Structure of human Arg1 (PDB 1HQG).⁸ a) Full structure of the Arg1 homotrimer; b) close up of the Arg1 active site; c) structure of the hydrolyzed substrate, L-ornithine and urea, bound to the Arg1 active site; d) mechanism of Arg1 mediated L-arginine hydrolysis. The transition state intermediate is boxed in red.

Arg1 is known to be misregulated in a plethora of disease states, including heart disease, neurodegeneration, erectile dysfunction, and cancer, of which the latter utilizes Arg1 to inhibit T-cell proliferation and activity.⁹⁻¹⁰ T-cells are unable to produce their own L-arginine, and require an extracellular source to maintain activity. As such, Arg1 is used to regulate the immune system through the hydrolysis of L-arginine in order to control and turn down T-cell activity and proliferation after an immune response.¹¹ Cancerous tumors take advantage of this native functionality, and actively recruit Myeloid Derived Suppressor Cells (MDSCs) to up-regulate Arg1 production within the cancer tumor.¹² This creates a microenvironment devoid of L-arginine within the tumor, so that T-cells are unable to function and proliferate in close proximity

to the tumor, allowing the cancer to escape destruction by the native immune functions.¹²⁻¹³ Inhibition of Arg1 results in a restoration of T-cell levels of proliferation, and thereby increases native inhibition of tumors.¹⁴ While it is unlikely that an Arg1 inhibitor alone would be sufficient to completely restore immunity against cancer tumors, it would greatly increase it, so that an Arg1 inhibitor has strong potential to be used in combination therapies.

In regards to cancer treatment, the field of cancer immunotherapy has recently enjoyed a place of prominence in developing new and novel treatments.¹⁵ Many cell-based therapies and immune checkpoint blockades have all recently attained FDA approval and are now in clinical use.¹⁵⁻¹⁷ It is worth noting that all of these treatments can be considered as biologics, and to date, there are no small-molecule drugs with FDA-approval in cancer immunotherapy. This is especially surprising, considering small molecules are typically far easier to prepare and advance through clinical trials. To meet this need, Arg1 has been recognized as a likely enzyme target for small molecule inhibition in order to elicit a native immune response in the treatment of cancerous tumors,¹⁶⁻¹⁷ thereby furthering the importance in developing new inhibitors of Arg1.

Arg1 activity has also recently gained attention as a potential target in the treatment of Alzheimer's Disease (AD). AD is a severely debilitating neurodegenerative disease, typically of the elderly, that is characterized by the slow onset of loss of memory, critical thinking, and reasoning skills. As the overexpression of β -amyloid peptide plaques in AD have long been associated with toxicity and interference with brain function, decades of research and drug development efforts have been focused on targeting the amyloid pathology. Unfortunately, targeting the key enzymes in this pathway have proven to be unsuccessful, and resulted in toxicity-linked failure in human clinical trials that failed to produce the desired outcomes.¹⁸⁻²⁰ This has motivated efforts to test new hypotheses for treating AD. One such hypothesis is the role of L-

arginine metabolism, which is well-known to aid in neuroprotection and has been found to be misregulated resulting in reduced levels of this amino acid in the AD brain.²¹⁻²⁴ As Arg1 is the primary enzyme responsible for L-arginine hydrolysis, Arg1 inhibition is proposed as a strategy for restoring L-arginine levels in the AD brain to combat the effects of AD.^{22, 25-26}

The relationship of Arg1 overexpression to cancer has been well documented, and similar trends have been recently emerging in AD. L-arginine misregulation has been found to be a characteristic of the AD brain,^{21, 23-24} and recent studies have linked these L-arginine devoid regions with an immunosuppressive environment in the AD brain.²² Furthermore, these and other works have shown that Arg1 production and gene expression is upregulated in the same areas impacted by AD, implicating Arg1 action of L-arginine hydrolysis in connection to AD pathogenesis. Additionally, it has been shown in rodent models that interruption of Arg1 activity alleviates the symptoms of AD; furthering Arg1 as a candidate for the development of small molecule inhibitors to treat AD.^{22, 25-26}

Considering that Arg1 is the oldest known human Mn^{2+} metalloenzyme, it has historically been difficult to target, and currently has no FDA approved inhibitors. However, the approach of targeting Arg1 in relation to cancer immunotherapy, has recently started to bear fruit, as Calithera (now owned by Incyte) already has a boronic acid based small molecule inhibitor in Phase II clinical trials explicitly for this purpose. Beyond this clinical trial, the development of Arg1 inhibitors has been rather sparse, with boronic acid based inhibitors featuring predominantly in the field (Figure 5.2). 6-Aminohexaboronic acid (ABH) was the first discovered boronic acid inhibitor of Arg1,²⁷ with a modest IC_{50} value of 1.45 μM ,²⁸ and remains as the lead scaffold for Arg1 inhibitor development. It acts as a transition state mimic (see boxed transition state, Figure 1.5d), where the Arg1 attaches a nucleophilic hydroxyl, creating an un-

cleavable boronate that then remains trapped in the active site. Outside of the boronic acids, nor-N-omega-hydroxy-L-arginine (nor-NOHA) is a single-carbon deletion of N-omega-hydroxy-L-arginine (NOHA), the body's native Arg1 inhibitor. While nor-NOHA has reasonable activity against Arg1 ($IC_{50} = 1.2 \mu\text{M}$), it has a poor half-life in vivo that curtails its potential for drug development. Apart from the boronic acid warhead inhibitors, there has been no exploration of alternate metal-binding groups against Arg1. Therefore, a MBP approach represents an appealing strategy, as this inhibitor class has yet to be employed against Arg1.

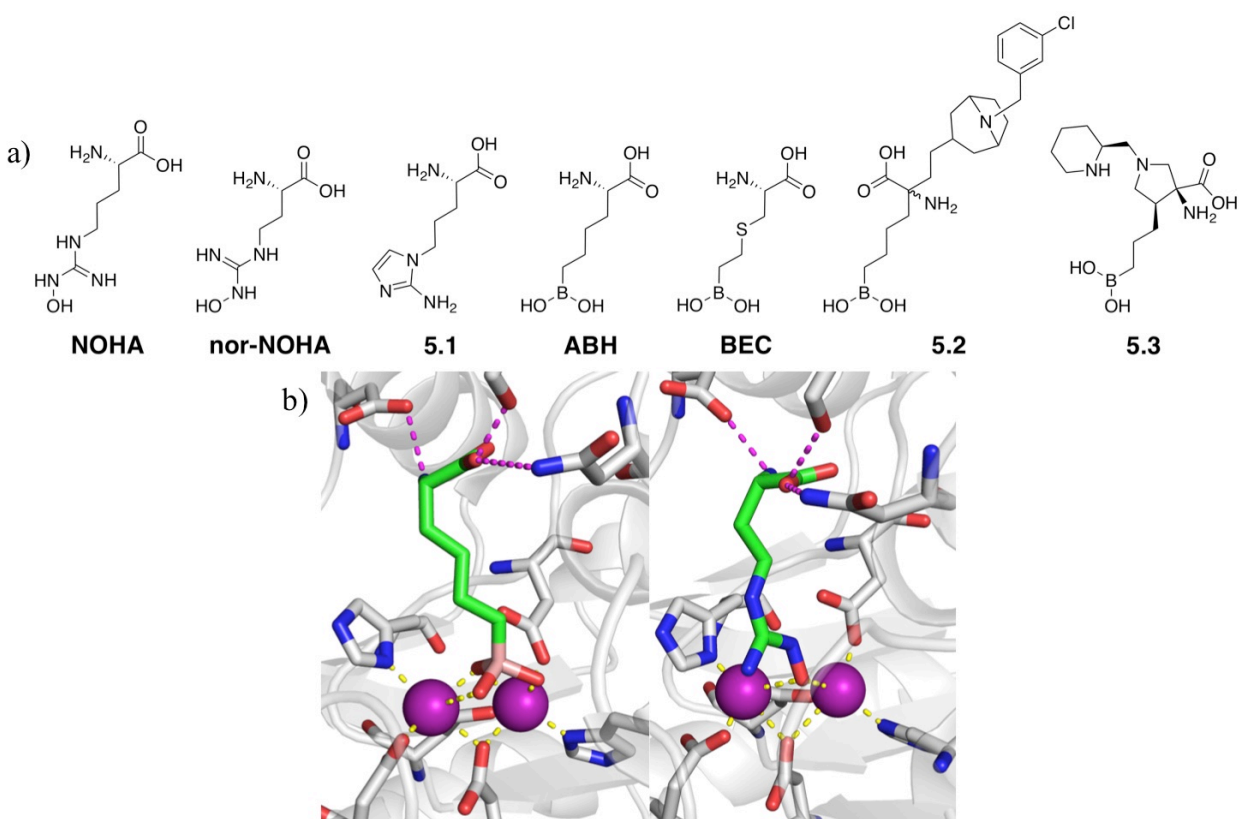


Figure 5.2. a) Summary of noteworthy Arg1 inhibitors; b) Crystal structures of lead Arg1 inhibitors, with important hydrogen bonds shown as magenta dashes. *Left:* Structure of ABH bound to the active site (PDB 2AEB).⁵ *Right:* Structure of nor-NOHA bound to the active site (PDB: 1HQH).⁸

5.2 Assay Protocol and Screening Results

In order to develop new, metal-binding inhibitors of Arg1, the MBP library as described in Chapter 1 was screened against human Arg1. This assay screen was from the protocol previously reported by Han and Viola,²⁹ as shown in Figure 5.3a, where upon hydrolysis by Arg1, the thioarginine substrate produces a free thiol that reacts with Ellman's Reagent as a developer to produce a colorimetric output at 412 nm.²⁹ To further optimize the Arg1 assay, the pH of the assay buffer was lowered from 9.0 to 8.5, because although Arg1 is reported to have maximum activity at pH 9.0,^{2, 30} this pH was experimentally determined to cause thioarginine substrate hydrolysis. Instead, pH 8.5 was chosen as this was experimentally found to offer a good balance between substrate stability and enzymatic activity. In addition, excess Mn²⁺ was included in the assay buffer to ensure the metal sites of Arg1 were fully occupied, as well as to preclude a metal-stripping mechanism of action for the metal-binding inhibitors. To validate these Arg1 assay conditions, the known Arg1 inhibitor nor-NOHA was used as a positive control, resulting in an experimental IC₅₀ value of 2.4±0.1 μM, closely matching the literature value IC₅₀ = 1.2 μM.^{8, 31} The entire MBP library was screened against Arg1 at a fragment concentration of 200 μM following the this modified Arg1 assay protocol, with the summary of these results shown in Figure 5.3b.

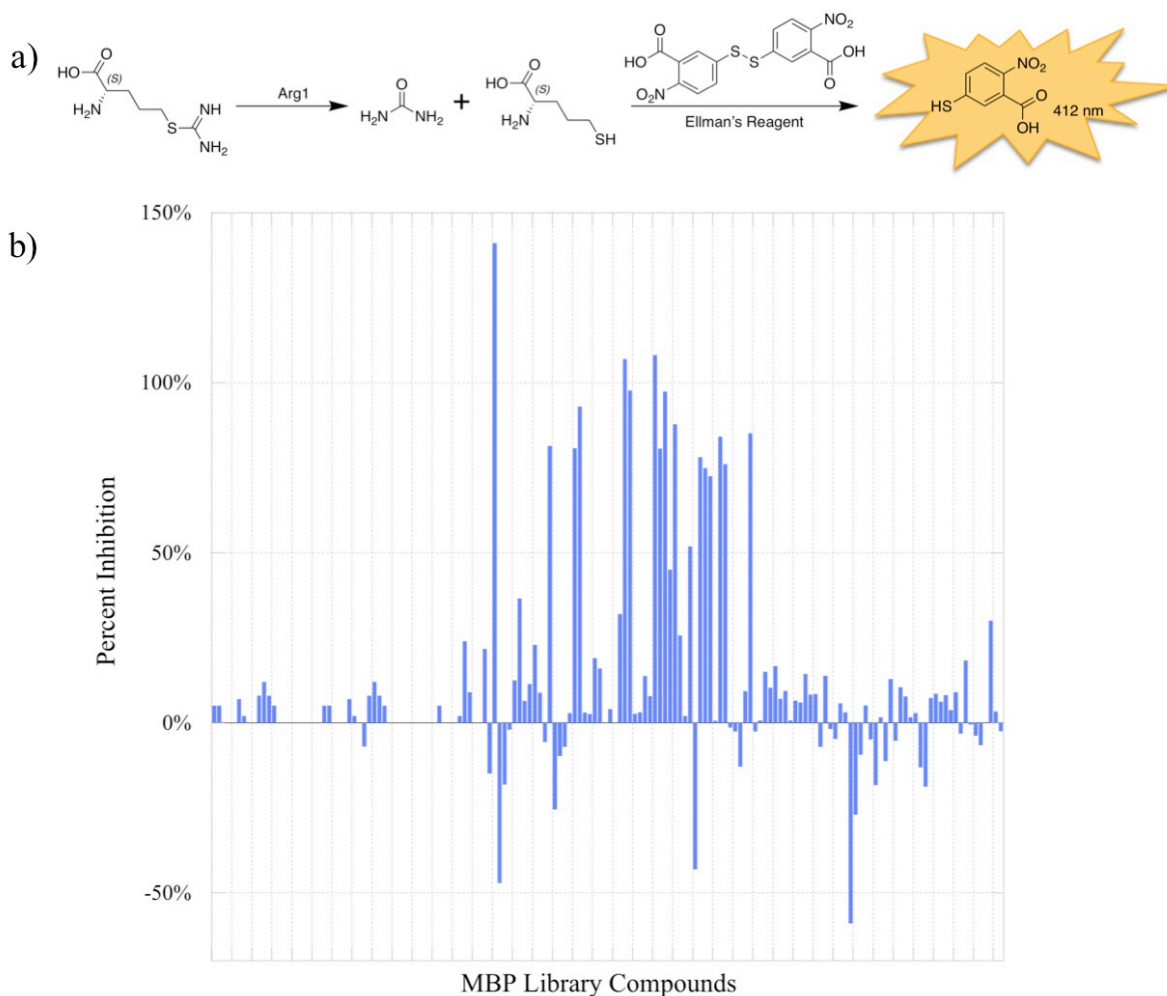


Figure 5.3. a) Mechanism of the Arg1 assay, where the thioarginine substrate is hydrolyzed by Arg1 to produce a free thiol that reacts with Ellman's Reagent, generating the chromophore 5-mercapto-2-nitrobenzoic acid (shown in gold starburst), which is monitored at 412 nm; b) Results of screening the MBP library against Arg1 at 200 μM .

From this MBP library screen, ~25 fragment hits were identified as having greater than 50% inhibition at a concentration of 200 μM . Of these hits, three inhibitor class emerged, catechol (**5.4**) gave an $\text{IC}_{50} = 24.0 \pm 7.7 \mu\text{M}$, oxazoline (**5.5**) $\text{IC}_{50} = 21.1 \pm 7.2 \mu\text{M}$, and phenol hydroxamic acid (**5.6**) with $\text{IC}_{50} = 52.8 \pm 8.5 \mu\text{M}$ (Figure 5.4). It is well worth noting that none of these MBP scaffolds have been previously reported as inhibitors of Arg1, making all of these novel scaffolds to explore as Arg1 inhibitors. Furthermore, it is readily observed that these

scaffolds all have a common motif of a phenol positioned next to another metal-binding group. It is likely that all of these lead scaffolds act through a metal-binding mechanism, with the phenol serving as a mimic of the native-bound hydroxyl, and the remaining donor atoms coordinated to either Mn_A or Mn_B. Considering the extremely tight steric constraints of the Arg1 active site, it is more likely that the remaining donor atoms coordinate to Mn_A, as crystallography shows slightly more available space around this metal ion. With this in mind, a proposed model of the mode of binding for each of these MBP warheads were prepared, and are displayed in Figure 5.4. As **5.6** contains three potential metal-binding donor atoms, it is possible that this molecule is also capable of binding both Mn²⁺, with the carbonyl of the hydroxamic acid as a bridging ligand between the Mn²⁺ ions. This alternate potential binding mode is displayed in Figure 5.4.

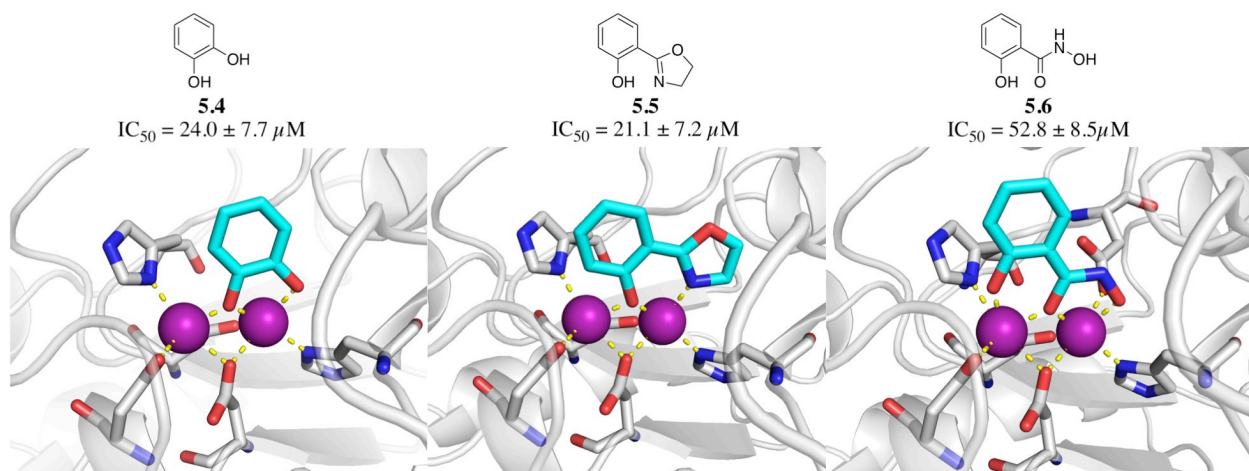


Figure 5.4. Structures and IC₅₀ values of identified lead MBP scaffolds for Arg1 inhibition. A proposed model of the mode of binding is shown beneath each MBP. Models were prepared using the structure PDB 3K2V.

5.3 MBP Inhibitor Development against Arg1

Considering MBP fragments **5.4** – **5.6** all showed good activity against Arg1, it was decided to pursue all of these scaffolds simultaneously to maximize MBP warhead diversity against Arg1. The general plan for inhibitor design against Arg1 is shown in Figure 5.5. This inhibitor development plan was designed around the active site constraints of Arg1 described above: 15 Å deep by 9 Å across, with the major active site feature being the catalytic Mn^{2+} at the bottom of the channel, and an amino acid recognition motif at the entrance. Therefore, the inhibitor design was decided to focus on first optimizing each of the MBP warheads for the best interactions at the base of the pocket, and the inclusion of an amino acid moiety to take advantage of the amino acid recognition motif. Further enhancing the appeal of this strategy, all of the previously reported Arg1 inhibitors have been based off similar design, with a metal-interaction group linked to an amino acid, as shown in Figure 5.2a. This general plan of inhibitor design was used for all of the catechol, oxazoline, and hydroxamic acid MBP scaffolds.

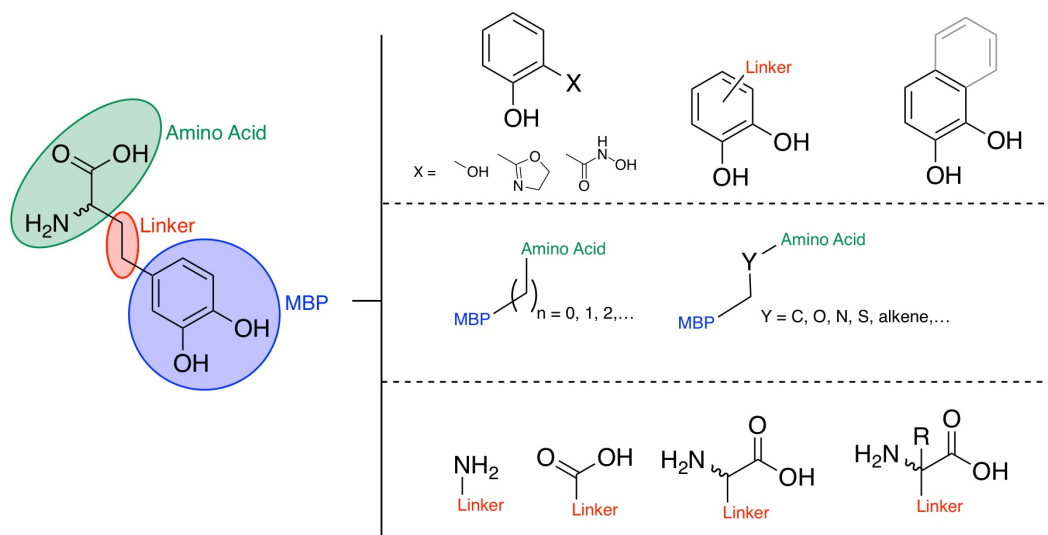


Figure 5.5. General plan for inhibitor design against Arg1, using a generic example of a catechol-based compound on the left.

5.3.1 Catechol based inhibitors of Arg1

From the initial MBP library screen, the catechol family of MBPs emerged with the strongest representation, with the parent catechol **5.4** having an IC_{50} value of $24.0 \pm 7.7 \mu\text{M}$, and 1,2-naphthylcatechol **5.7** having an even better IC_{50} value of $6.8 \pm 1.8 \mu\text{M}$ (Figure 5.6). As catechol compounds have the potential for inhibition through redox mechanisms, it is encouraging that **5.22** (Figure 5.6), the sulfonamide catechol isostere, also showed reasonable activity with 43% inhibition at $200 \mu\text{M}$. **5.22**, like catechol, has two deprotonatable donor atoms and binds through a 5-member metal-coordinate ring, but should not be capable of redox activity as it lacks the catechol moiety. Additionally, **5.18** – **5.20** all have carboxylic acids, which act as strong electron-withdrawing groups, and would greatly reduce, if not eliminate, their potential for redox chemistry; altogether indicating that these catechol based compounds are likely acting through a metal-binding mechanism and not through unspecific redox reactivity. To explore and optimize the catechol MBP warhead against Arg1, a set of various catechol isosteres and analogues were prepared, including both various heterocycles and R-groups, as shown in Figure 5.6 below.

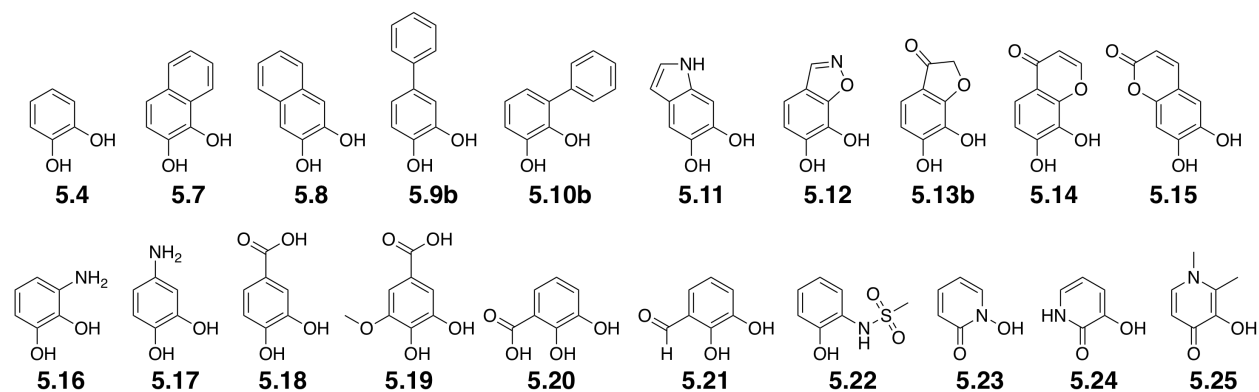
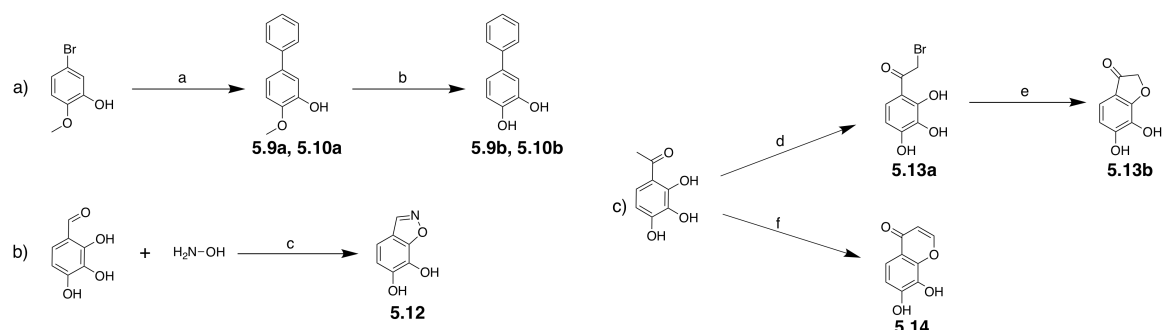


Figure 5.6. Summary of catechol analogues and isosteres tested against Arg1.

To achieve this diversity within the catechol scaffolds, catechols were prepared by either deprotecting commercially available methyl-ether protected catechols using boron tribromide, or by using various cyclization methods to form catechol containing bicyclic systems, shown in Scheme 5.1. To prepare **5.9b** and **5.10b**, Suzuki cross coupling was used to generate the biphenyl system, and then boron tribromide was used to deprotect the methyl ether, giving the desired catechol compounds. This same boron tribromide deprotection method was also used to deprotect 3- and 4-aminoveratrol to respectively yield **5.16** and **5.17**. Then, to form the various bicyclic systems, cyclizing 2,3,4-trihydroxybenzaldehyde with hydroxylamine gave the benzoisoxazole product **5.28**. Alternatively, reacting 2',3',4'-trihydroxyacetophenone with copper (II) bromide resulted in bromination adjacent the ketone to produce intermediate **5.13a**, which was then subjected to an intramolecular cyclization by heating in base to give benzofuran product **5.13b**. Finally, the same 2',3',4'-trihydroxyacetophenone was cyclized with *N,N*-dimethylformamide dimethyl acetal HCl by heating to reflux in toluene for 4 h to yield catechol **5.14**. The remaining catechol analogues used in this study were commercially purchased and tested with no additional purification.



Scheme 5.1. Synthetic methods for used preparing various catechol-based MBPs, where a) represents a general method of ester deprotection using **5.9b** as a representative example, and b) and c) are specific examples. Reagents and conditions: (a) phenyl boronic acid, S-Phos, potassium phosphate, PdCl₂(dppf)-CH₂Cl₂, 1,4-dioxane, H₂O, 85 °C, 1 h, 91-96%; (b) BBr₃, CH₂Cl₂, 0 – 25 °C, 50-95%; (c) potassium carbonate, ethanol, 100 °C, 2 h, 39%; (d) CuBr₂, ethyl acetate, chloroform, 70 °C, 16 h, 36%; (e) potassium carbonate, isopropanol, 100 °C, 20 h, 24%; (f) N,N'-dimethylformamide dimethyl acetal HCl, toluene, 100 °C, 4 h, 10%.

Upon preparing this library of catechol analogues, they were screened against Arg1, with the results displayed Table 5.1. It is worth noting that none of hydroxypyridinones (HOPOs) **5.23 – 5.25** emerged as hits against Arg1, with all having near 0% inhibition against Arg1 at 200 μM. This is especially surprising considering the catechol family featured so prominently among the Arg1 MBP hits. A likely explanation for this disparity in activity between these similar MBP scaffolds is that Arg1 features a rather basic active site with an optimal pH of 9.0, leaving Arg1 with a preference for the harder Lewis acid hydroxyl ligands of the catechol compared to the softer carbonyl donor atoms in present in the HOPOs. The other noteworthy trend within these catechols was a preference for preferred location of lipophilic substituents, where bulky groups placed *ortho*- to the catechol moiety were preferred over bulky groups placed *para*- to the catechol moiety. This was exemplified by 1,2-naphthyl catechol **5.7** having a lower IC₅₀ of 6.8±1.8 μM compared to the 2,3-naphthyl catechol **5.8** IC₅₀ of 41.2±4.0 μM, again with the 2,3-biphenyl catechol **5.10b** having a lower IC₅₀ of 15.6±7.9 μM compared to the 3,4-biphenyl catechol **5.9b** IC₅₀ of 27.5±7.9 μM, and finally again with the coumarin catechol **5.14** having a lower IC₅₀ of 58±24.0 μM compared to the IC₅₀ of **5.15** at ~100 μM. Overall, the

catechol scaffold demonstrated a tolerance of derivatization, with a few, namely 2,3-biphenyl catechol **5.10b** and 1,2-naphthyl catechol **5.7** demonstrating improvement relative to the parent scaffold, and themselves being candidates for future elaboration strategies.

Table 5.1. Results of screening the prepared catechol derivatives against Arg1.

Compound	IC ₅₀ (μM)	Compound	IC ₅₀ (μM)
5.4 (catechol)	24.0 ± 7.7	5.16	~320
5.7	6.8 ± 1.8	5.17	152.1 ± 0.5
5.8	41.2 ± 4.0	5.18	31.9 ± 21.5
5.9b	27.5 ± 6.0	5.19	19.0 ± 13.6
5.10b	15.6 ± 7.9	5.20	29.8 ± 15.1
5.11	>100	5.21	29.8 ± 19.0
5.12	>100	5.22	43% ^a
5.13b	~150	5.23	0% ^a
5.14	57.6 ± 24.0	5.24	0% ^a
5.15	~100	5.25	0% ^a

^aPercent Arg1 inhibition at a fragment concentration of 200 μM.

5.3.2 Oxazoline based inhibitors of Arg1.

Oxazoline compound **5.5** was also chosen for further elaboration, as this scaffold has been infrequently found as a metalloenzyme hit within our own metalloenzyme screens. Furthermore, searching the PDB shows that there are no reported crystal structures of this ligand being used as an enzyme inhibitor, making **5.5** an uncommon starting point for inhibitor development. Indeed, the only other known instance of this type of scaffold being used in metalloenzyme inhibitor development was in work recently submitted to *ChemMedChem* detailing the use of the isostere scaffold imidazoline (compound **5.26**) against ADA. In regards to Arg1, the novel oxazoline ring is likely the source of the good activity of **5.5** against Arg1. The oxazoline binds as a cyclized imine, but the resonant nature imparts a partial negative charge on the nitrogen, improving its H-bond accepting capacity, and making it a harder donor atom

ligand.³² As such, this would again demonstrate the Arg1 preference for harder donating atoms on the MBP. To explore and optimize the oxazoline MBP warhead against Arg1, a set of various oxazoline isosteres and analogues were prepared, including both various bicyclic systems and R groups, as shown in Figure 5.7 below.

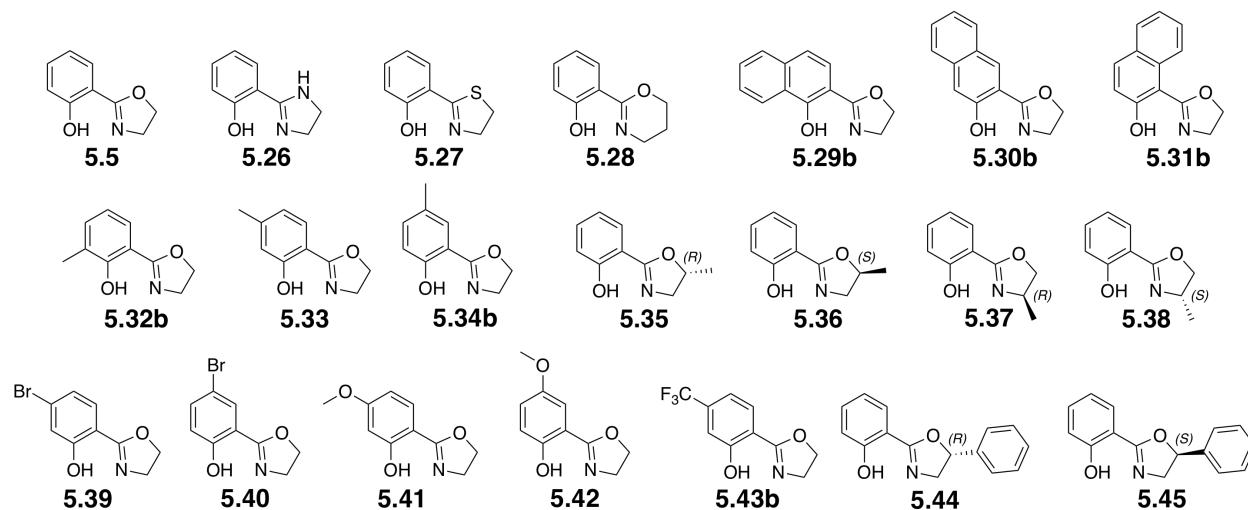
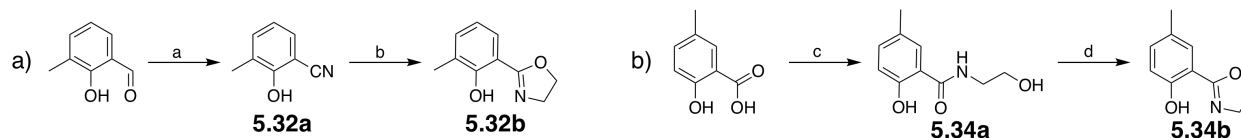


Figure 5.7. Summary of the various oxazoline analogues and isosteres tested against Arg1.

A series of oxazoline based derivatives were prepared to probe for potential interactions and likely sites for derivatization on the MBP scaffold. These compounds were synthesized following the protocol shown in Scheme 5.2. Derivatized oxazolines were prepared by cyclizing pre-functionalized 2-nitrile phenols with ethanolamine by heating to 110 °C in the presence of catalytic amounts of zinc chloride to generate the desired products. To install the desired stereochemistry in compounds **5.35** – **5.38**, the ethanolamine was substituted respectively with (*R*)-1-aminopropan-2-ol, (*S*)-1-aminopropan-2-ol, (*S*)-2-aminopropan-1-ol or (*R*)-2-aminopropan-1-ol to attain cyclization with the desired stereochemistry pre-installed. When the requisite starting 2-nitrilephenol compounds were unavailable, the desired oxazolines were instead prepared by reacting ethanolamine with salicylic acid derivatives to generate

ethanolamine-amides, which were then cyclized into the desired oxazoline products by adding thionyl chloride and stirring at room temperature overnight.



Scheme 5.2. General method for oxazoline synthesis by: a) cyclizing ethanolamine or aminopropanol with an aromatic nitrile (**5.32b** as a representative example), or b) by cyclizing amide-coupled ethanolamine (**5.34b** as a representative example). Reagents and conditions: (a) potassium acetate, hydroxylamine hydrochloride, formic acid, 100 °C, 24 h, 57% yield; (b) ZnCl₂, ethanolamine, toluene, 130 °C, 24 h, 75% yield; (c) ethanolamine, triethylamine, T3P, tetrahydrofuran, ethyl acetate, 70 °C, 16 h, 24% yield; (d) SOCl₂, CH₂Cl₂, 0 °C, 16 h, 80% yield.

The oxazoline derivatives were tested against Arg1, with the results displayed in Table 5.2. The parent compound **5.5** maintained the best activity with an IC₅₀ value of 20 μM. All attempts to pursue isosteres of the oxazoline ring moiety resulted in a drastic loss of activity, as exemplified in **5.26** – **5.28**. For **5.26**, it is logical that the imidazole ring resulted in a loss of activity, as the resonance between the two nitrogen atoms would pull electron density from the coordinating nitrogen, resulting in a weaker donor atom. Similarly, the sulfazoline **5.27** was expected to have a loss of activity as the change from oxygen to sulfur would electronically again make the nitrogen a softer donating atom.³² Finally, the ring-expansion in **5.28** also caused a dramatic loss of binding activity, perhaps because the geometry of the six-member ring is no longer ideally aligned for metal-coordination. Considering **5.26** – **5.28**, it appears as though perturbations to the oxazoline ring in **5.5** are not tolerated for Arg1 inhibition.

Table 5.2. Results of screening the prepared oxazoline derivatives against Arg1.

Compound	IC ₅₀ (μM)	Compound	IC ₅₀ (μM)
5.5	21.1 ± 7.2	5.36	68.6 ± 16.4
5.26	~300	5.37	>300
5.27	>300	5.38	>300
5.28	>300	5.39	33% ^a
5.29b	~200	5.40	43% ^a
5.30b	>300	5.41	52% ^a
5.31b	>300	5.42	81% ^a
5.32b	>300	5.43b	44% ^a
5.33	88.4 ± 29.7	5.44	0% ^a
5.34b	77.1 ± 20.1	5.45	0% ^a
5.35	52.7 ± 16.2	-	-

^aPercent Arg1 inhibition at a fragment concentration of 100 μM.

Compounds **5.29b** – **5.38** were designed to probe the steric interactions of **5.5** to determine the optimal site for further derivatization. None of these compounds had improved activity from the parent scaffold **5.5**, but the dramatic loss of inhibition activity in **5.32b**, **5.37**, and **5.38** indicate that these positions did not tolerate substitution. While **5.33** – **5.37** all had less activity than **5.5**, these compounds still displayed IC₅₀ values in the <100 μM range, indicating these sites may be tolerated for further elaboration. Indeed, it is worth noting that the methyl groups in **5.33** – **5.37** were tolerated but the methyl groups in **5.32b**, **5.37**, and **5.38** were not. This suggests that the methyl groups in **5.32b**, **5.37**, and **5.38** may be more physically constrained, and are potentially causing steric clashing with the confined Arg1 active site, whereas the methyl groups in **5.33** – **5.37** may be pointing into the free, unoccupied space of the Arg1 active site channel. To further probe and determine whether these positions were amenable to derivatization, compounds **5.39** – **5.45** were prepared. Of these, only **5.44** and **5.45** displayed no activity at 100 μM, indicating that bulky substituents off the oxazoline ring are not tolerated. Otherwise, **5.39** – **5.43** all maintained some activity at 100 μM of inhibitor, helping to cross verify that these remaining positions are amenable to further elaboration.

5.3.3 Hydroxamic acid based inhibitors of Arg1.

The hydroxamic acid compound **5.6** was selected for further elaboration against Arg1 as this MBP displayed a good IC_{50} value of $52.8 \pm 8.5 \mu\text{M}$. While the hydroxamic acid warhead is commonly employed against metalloenzymes, as noted in Chapter 1, this specific phenol hydroxamic acid MBP surprisingly has yet to be explored against Arg1. However, it is worth noting that the phenol in **5.6** is likely just as important for metal coordination as the hydroxamic acid, as deletion of the phenol in **5.55** resulted in an increased IC_{50} value to $\sim 200 \mu\text{M}$. To explore and optimize the hydroxamic acid MBP warhead against Arg1, a set of various hydroxamic acid isosteres and analogues were prepared, as shown in Figure 5.8 below.

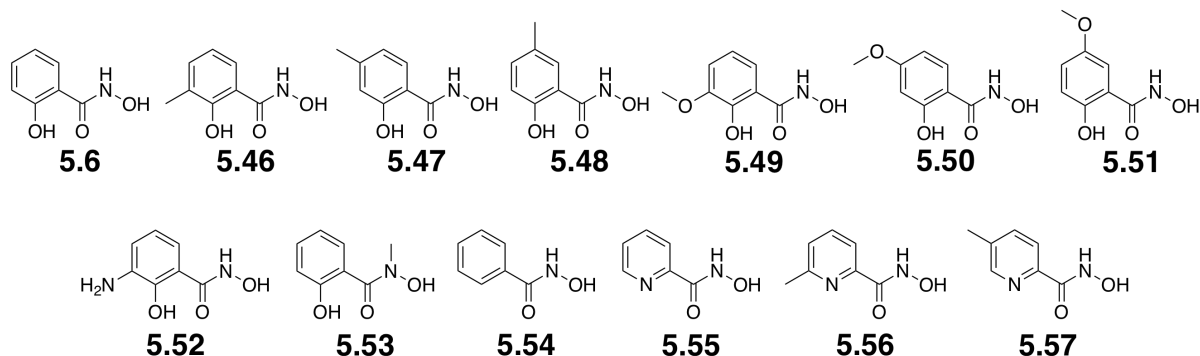
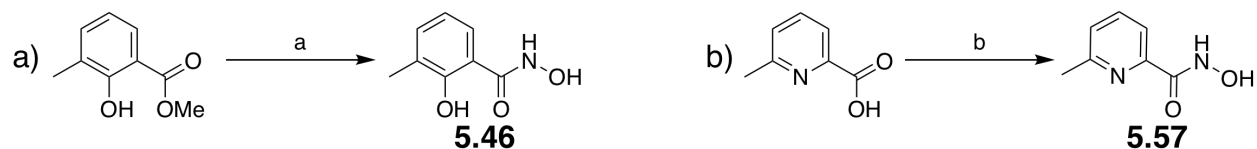


Figure 5.8. Summary of the various hydroxamic acid analogues and isosteres tested against Arg1.

The hydroxamic acid compounds used in this study were prepared as described in Scheme 5.3. Starting from pre-functionalized methyl salicylate, hydroxylamine hydrochloride in the presence of excess KOH was used to perform a nucleophilic addition-substitution reaction, thereby converting the methyl ester to a hydroxamic acid. In the case of **5.54**, methylhydroxylamine was used in place of the hydroxamic acid. To prepare **5.56** – **5.58**, the pre-functionalized picolinic acids were treated with thionyl chloride to generate an in situ acid

chloride, which was then reacted with hydroxylamine hydrochloride to produce the hydroxamic acid products.



Scheme 5.3. General method for hydroxamic synthesis by: a) performing a nucleophilic addition-substitution using hydroxylamine hydrochloride (**5.46** as a representative example), or b) by using acid chloride mediated nucleophilic attack (**5.57** as a representative example). Reagents and conditions: (a) hydroxylamine hydrochloride, KOH, MeOH, 70 °C, 5 h, 30 – 80% yield; (b) hydroxylamine hydrochloride, thionyl chloride, chloroform, 0 °C, 16 h, 30 – 80% yield.

The hydroxamic acid compounds were screened against Arg1, with the results displayed in Table 5.3. Compounds **5.46** – **5.48** were synthesized as methyl substituents to probe for optimal locations for further elaboration off the MBP. Of these, **5.46** was roughly on par with the parent MBP with an IC_{50} value of $47.6 \pm 7.0 \mu\text{M}$, whereas both **5.47** and **5.48** showed slight improvement relative to the parent **5.6**, with IC_{50} values of 41.4 ± 5.7 and $37.0 \pm 16.6 \mu\text{M}$, respectively. To confirm that these positions were amenable towards derivatization, methyl ether analogues **5.49** – **5.51** were prepared, and demonstrated maintenance of inhibitor activity against Arg1, with all compounds showing 72-81% Arg1 inhibition at 100 μM . To determine whether polar substituents would be tolerated, amine compound **5.52** was prepared, and as this compound did not display any inhibition at 100 μM , polar substituents were not further pursued. Finally, **5.55** – **5.57** were prepared to investigate replacement of the metal-coordinating hydroxyl with a heterocyclic nitrogen atom. While these compounds all displayed inhibitory activity against Arg1 at 100 μM , experimentally, they were found to produce inconsistent IC_{50} curves and were

not further pursued. Overall, the phenol hydroxamic acid scaffold demonstrated that it is well suited towards further inhibitor development.

Table 5.3. Results of screening the prepared hydroxamic acid derivatives against Arg1.

Compound	Percent Inhibition ^a	Compound	Percent Inhibition ^a
5.6	73% (IC ₅₀ = 52.8 ± 8.5 μM)	5.52	0%
5.46	100% (IC ₅₀ = 47.6 ± 7.0 μM)	5.53	0%
5.47	99% (IC ₅₀ = 41.4 ± 5.7 μM)	5.54	IC ₅₀ ~ 200 μM
5.48	81% (IC ₅₀ = 37.0 ± 16.6 μM)	5.55	81%
5.49	80%	5.56	20%
5.50	81%	5.57	77%
5.51	72%	-	-

^aPercent Arg1 inhibition at a fragment concentration of 100 μM

5.3.4 Unnatural amino acid MBP inhibitors of Arg1.

Finally, to merge the amino acid group with the MBP warheads, a set of unnatural amino acid MBPs was prepared, as shown in Figure 5.9. To generate diversity within the set of compounds, different linker lengths between amino acid and MBP were used, as well as different linker attachment positions. Additionally, terminal amine groups and terminal carboxylic acid groups were tested as a way to piece apart the individual contributions of each portion of the amino acid moiety. Unnatural amino acid oxazoline MBPs were not tested as they were found to be synthetically challenging and resistant to protecting group strategies. Additionally, an extended linker version of levodopa (Figure 5.9) was not prepared, as this compound was found to readily undergo cyclization and form a bicyclic system with itself.

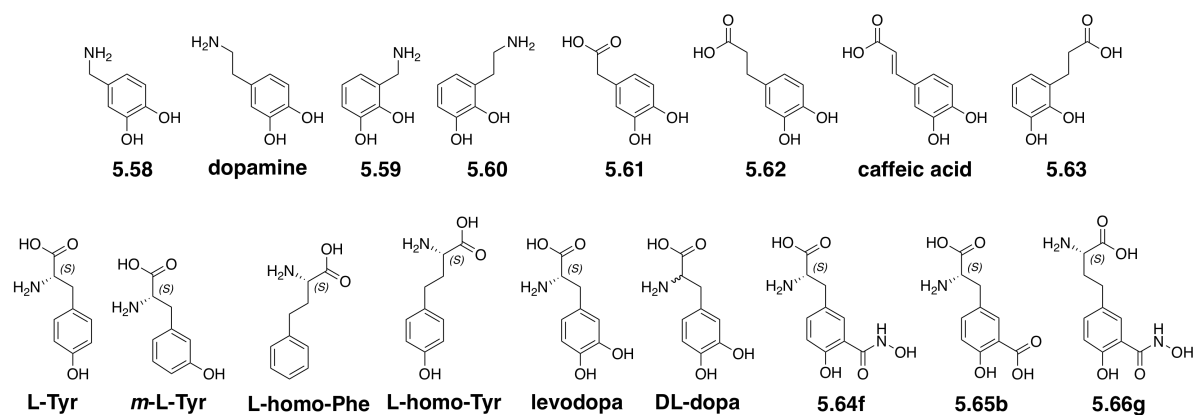
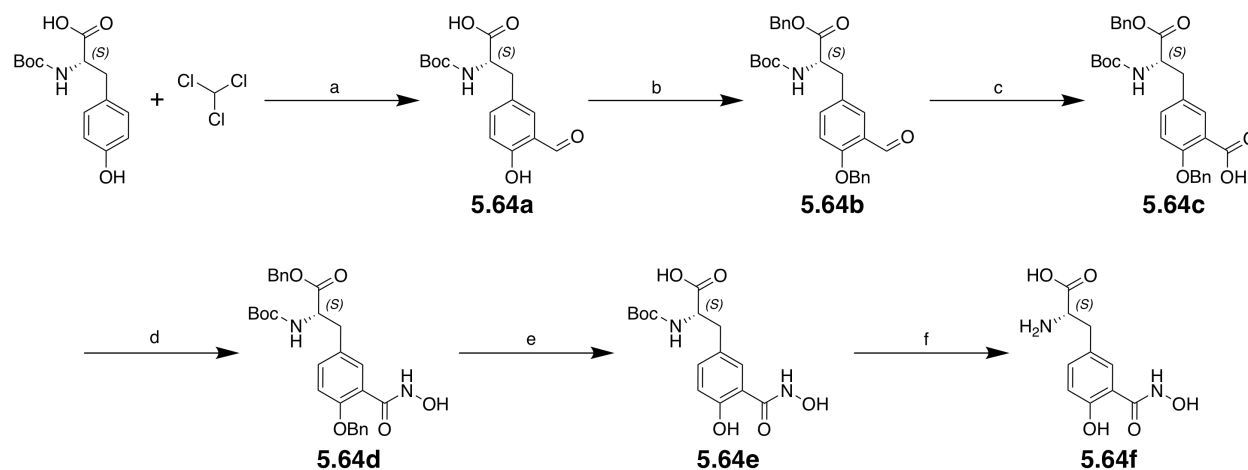


Figure 5.9. Summary of the various unnatural amino acid MBPs tested against Arg1.

To prepare these unnatural amino acid MBPs the synthetic procedures in Scheme 5.4 were used. This route was selected as it already had the amino acid moiety installed, and gave key intermediate **5.64c**, which allowed for selective functionalization and preparation of the hydroxamic acid, without affecting any of the other functional groups. Other methods of merging the MBP and amino acid, such as olefination and Friedel Crafts alkylation as well as acylation, were found to be unsuccessful. Starting from boc-protected L-tyrosine, a Reimer-Tiemann reaction was used to install a formyl group ortho to the phenol, giving product **5.64a**. The product was then benzyl protected at the carboxylic acid and phenol by stirring in two equivalents of benzyl bromide. Oxidation of the aldehyde to carboxylic acid was achieved by using potassium permanganate under Masamune oxidation conditions, giving intermediate **5.64c**. Then, the carboxylic acid was converted to hydroxamic acid by using thionyl chloride to generate an in situ acid chloride, which was then reacted with hydroxylamine hydrochloride to give the desired hydroxamic acid compound **5.64d**. Finally, deprotection was done over two steps, first by hydrogenation over Pd/C to remove the benzyl groups, and then by stirring with trifluoroacetic acid to remove the boc group. Work-up via reverse phase column chromatography gave the desired final product. To prepare salicylic acid compound **5.65b**, the

exact same protocol was used, while omitting the hydroxamic acid formation step, and to prepare the extended linker compound **5.66g**, boc-protected homo-L-tyrosine was used as the starting material in place of L-tyrosine.



Scheme 5.4. General method for unnatural amino acid MBP synthesis, using **5.64f** as a representative example. Reagents and conditions: (a) chloroform, sodium hydroxide, H_2O , 75°C , 5 h, 27% yield; (b) benzyl bromide, potassium carbonate, DMF, 25°C , 16 h, 72% yield; (c) potassium permanganate, potassium phosphate buffer, pH 8, *t*-butanol, 25°C , 3 h, 50% yield; (d) thionyl chloride, hydroxylamine hydrochloride, triethyl amine, THF, H_2O , 25°C , 2 h, 55% yield; (e) 10% Pd/C, H_2 gas, 1 atm, MeOH, 25°C , 2 h, 90% yield; (f) trifluoroacetic acid, CH_2Cl_2 , 25°C , 1.5 h, 63% yield.

These unnatural amino acid MBPs were screened against Arg1, with the results listed in Table 5.4. Of these, none had significantly improved activity relative to the parent MBP, but one compound, levodopa, displayed inhibition close with the parent catechol with an IC_{50} of $27.8 \pm 10.3 \mu\text{M}$. The separate amine and carboxylic acid portions of the amino acid in levodopa, dopamine and **5.62** respectively, both had decreased activity relative to levodopa, indicating the whole component of the amino acid has a synergistic effect. Additionally, DL-dopa, the racemic mixture of dextrodopa and levodopa had a slightly increased activity of $\sim 50 \mu\text{M}$, indicating that the L-isomer is preferred, as the presence of the D-isomer decreased the inhibitory activity.

Levodopa is the natural precursor to dopamine, and has already attained FDA approval for the treatment of Parkinson's Disease. As such, it is highly exciting that Levodopa displayed good affinity for Arg1, as repurposing already known drugs is a popular method of lead discovery. Certainly, cellular studies on the efficacy of Levodopa against Arg1 bearing cancers are strongly merited, and represent work to be done in future studies.

Table 5.4. Results of screening the prepared unnatural amino acid MBPs against Arg1.

Compound	IC ₅₀ (μM)	Compound	IC ₅₀ (μM)
5.58	31.4 ± 2.7	L-Tyr	>1,000
Dopamine	50.4 ± 27.2	m-L-Tyr	>1,000
5.59	29.5 ± 6.1	L-homo-Phe	>1,000
5.60	52.8 ± 18.7	L-homo-Tyr	>1,000
5.61	53.0 ± 32.8	levodopa	27.8 ± 10.3
5.62	39.5 ± 17.3	DL-dopa	~50
Caffeic acid	16.8 ± 3.1	5.64f	>200
5.63	40.4 ± 18.8	5.65b	>1,000
-	-	5.66g	>200

Beyond levodopa, the only other catechol based amino acid MBP that displayed good activity was caffeic acid with an IC₅₀ of 16.8±3.1 μM. While this was a seemingly good starting point, this scaffold was not further pursued, as caffeic acid is known to act through non-specific binding mechanisms, and has been identified as a potential Pan Assay Interference (PAIN) compound.³³ The phenolic amino acids L-Tyr, *m*-L-Tyr, and homo-L-Tyr were tested for activity, as these amino acid scaffolds contained the phenol moiety that was conserved in the original hit MBPs **5.4** – **5.6**, but none of these displayed any Arg1 inhibition at concentrations as high as 1,000 μM. This would seem to indicate that that the entirety of the MBP is needed for inhibition; and as for L-Tyr, this negative result was expected, as L-Tyr has not been reported as an inhibitor of Arg1.² Finally, neither of the hydroxamic acid amino acid compounds, **5.64f** and **5.66g**, had IC₅₀ values better than 200 μM. The most likely explanation for the lack of activity is

that the linker position between MBP and amino acid was at the wrong site, as variation of linker length had already been explored between these two compounds. Certainly, previous studies have established that in developing Arg1 inhibitors, precision in the linker, in terms of both length and position, are absolutely critical for good inhibition activity.^{8, 27, 34-35} As such, it is likely that positioning the linker at an alternate site on the MBP should result in much more potent Arg1 inhibitors, and represents work to be undertaken in future studies.

5.4 Conclusions

Human Arg1 functions to cleave L-arginine into L-ornithine and urea, and the over expression of this dinuclear Mn^{2+} metalloenzyme has been implicated in multiple disease states, including cancer and neurodegeneration. As such, Arg1 has become an exciting target for the development of small molecule inhibitors, with boronic acid based compounds featuring heavily in reported drug discovery efforts. To broaden the scope of potential Arg1 inhibitors, a library of MBP compounds was screened against Arg1, as metal-binding inhibitors have yet to be explored against Arg1. From this screen, the catechol, oxazoline, and hydroxamic acid MBP scaffolds were all identified as new leads against Arg1. Further derivatization on each of these scaffolds was used to identify sites for optimal elaboration. Finally, merging the catechol warhead with an amino acid lead to the identification of levodopa, which is both FDA approved and naturally occurring within the human body, as an inhibitor of Arg1, making levodopa of interest towards future studies of Arg1 inhibition. While hydroxamic acid based amino acid MBPs failed to yield potent inhibitors in this study, it is likely that altering the position of the amino acid linker will grant more active compounds. Furthermore, only amino acid derivatives of these lead MBPs were examined in this study, it is possible that pursuing other means of elaborating these

identified MBP scaffolds will lead to more potent Arg1 inhibitors. Overall, this work demonstrated the use of a multi-pronged inhibitor strategy against Arg1, and should help to lay the groundwork for future studies of MBP inhibitors against this metalloenzyme.

5.5 Experimental

Synthesis

Unless otherwise noted, all reagents and solvents were purchased from commercial suppliers and used with no additional purification. Silica gel column chromatography was performed using a CombiFlash Rf⁺ Teledyne ISCO system, using hexane, ethyl acetate, CH₂Cl₂ or MeOH as eluents. Reverse phase separations utilized a C18-column on the same instrument with a 0.1% formic acid in water and MeOH as eluents. Separations were monitored via a Teledyne ISCO RF⁺ PurIon ESI-MS detector with 1 Da resolution. ¹H NMR spectra were obtained using either Varian 400 or 500 MHz spectrometers at the Department of Chemistry and Biochemistry at UC San Diego. ¹H NMR data is reported in parts per million relative to the residual non-deuterated solvent signals, and spin multiplicities are given as s (singlet), *br* s (broad singlet), d (doublet), dd (doublet of doublets), t (triplet), dt (doublet of triplets), q (quartet), and m (multiplet). When available, coupling constants (J) are reported in hertz (Hz). The purity of compounds was determined to be at least 95% by analytical HPLC analysis. Standard resolution and high resolution mass spectrometry, as well as analytical HPLC, were performed at either the UC San Diego Molecular Mass Spectrometry Facility or on the previously described Teledyne ISCO RF⁺ PurIon ESI-MS detector. Compounds **5.4–5.8**, **5.11**, **5.15**, **5.18–5.21**, **5.58**, and **5.61–5.63**, as well as dopamine, caffeic acid, L-Tyr, *m*-L-Tyr, L-homo-Phe, L-homo-Tyr, levodopa, and DL-

dopa were purchased from commercial suppliers. Compounds **5.6**, **5.22–5.25**, **5.54**, and **5.55** were prepared as previously reported.³⁶

Synthesis for Catechol Derivatives

General Method for Methyl Ether Deprotection: In a flame-dried round bottom flask, the starting methyl ether compound (1 eq.) was dissolved in 10 mL CH₂Cl₂, and the reaction was placed under a nitrogen atmosphere and cooled to 0 °C. Then BBr₃ in heptanes (3 eq.) was added dropwise, and the reaction was allowed to slowly warm to 25 °C for 16 h. Then the reaction was cooled to 0 °C, and slowly quenched via the addition of ~7 mL MeOH. The quenched reaction was concentrated under reduced pressure, and the resulting crude was purified via column chromatography. Like fractions containing the desired product were combined and concentrated under reduced pressure to obtain final products.

4-Methoxy-[1,1'-biphenyl]-3-ol (5.9a): To a solution of 5-bromo-2-methoxyphenol (0.500 g, 2.46 mmol), phenylboronic acid (330 mg, 2.71 mmol), and S-Phos (101 mg, 246 μmol) in 15 mL 1,4-dioxane, a solution of potassium phosphate (1.57 g, 7.39 mmol) in a minimal amount of water was added. Then PdCl₂(dppf)-CH₂Cl₂ adduct (101 mg, 123 μmol) was added to the solution in one portion, and the reaction mixture was heated to reflux at 85 °C for 1 h. Upon completion, the reaction was hot filtered through a thin pad of celite, and the filtrate was concentrated under reduced pressure. The resulting crude was purified via column chromatography, running gradient from 100% hexanes to 100% ethyl acetate. The product eluted in 40% ethyl acetate in hexanes. Like fractions were combined and concentrated under reduced pressure to obtain **5.9a** (0.448 g, 2.24 mmol, 91%) as a light yellow solid. ¹H NMR

(400 MHz, DMSO- d_6): δ 9.09 (*br s*, 1H), 7.53 (dd, $J_1 = 8.4$, $J_2 = 1.2$, 2H), 7.40 (t, $J = 8.0$, 2H), 7.27 (dt, $J_1 = 7.6$, $J_2 = 1.2$, 1H), 7.06 – 7.02 (m, 2H), 6.97 (d, $J = 8.0$, 1H), 3.79 (s, 3H); ESI-MS(-): m/z 199 [M - H]⁻.

[1,1'-Biphenyl]-3,4-diol (5.9b): Following the general methyl ether deprotection protocol, from **5.9a** (0.350 g, 1.75 mmol) and BBr₃ in heptanes (5.0 mL, 5.0 mmol) **5.9b** (0.314 g, 1.68 mmol, 96%) was obtained as a light yellow solid. ¹H NMR (400 MHz, DMSO- d_6): δ 9.05 (*br s*, 1H), 9.01 (*br s*, 1H), 7.50 (d, $J = 8.0$, 2H), 7.37 (t, $J = 7.6$, 2H), 7.24 (t, $J = 7.6$, 1H), 7.03 (s, 1H), 6.92 (d, $J = 8.0$, 1H), 6.80 (d, $J = 8.0$, 1H); ESI-MS(-): m/z 185 [M - H]⁻.

3-Methoxy-[1,1'-biphenyl]-2-ol (5.10a): Following the same protocol used in **5.9a**, from 2-bromo-6-methoxyphenol (0.500 g, 2.46 mmol), **5.10a** (0.418 g, 2.09 mmol, 85%) was obtained as a light yellow solid. ¹H NMR (400 MHz, DMSO- d_6): δ 8.59 (*br s*, 1H), 7.53 – 7.50 (m, 2H), 7.38 (dt, $J_1 = 7.2$, $J_2 = 1.6$, 2H), 7.28 (dt, $J_1 = 7.2$, $J_2 = 1.6$, 1H), 6.96 – 6.93 (m, 1H), 6.88 – 6.81 (m, 2H), 3.83 (s, 3H); ESI-MS(-): m/z 199 [M - H]⁻.

[1,1'-Biphenyl]-2,3-diol (5.10b): Following the general methyl ether deprotection protocol, from **5.10a** (0.410 g, 2.05 mmol) and BBr₃ in heptanes (6.14 mL, 6.14 mmol), **5.10b** (0.207 g, 1.11 mmol, 54%) was obtained as a tan, crystalline solid. ¹H NMR (400 MHz, DMSO- d_6): δ 9.50 (*br s*, 1H), 8.27 (*br s*, 1H), 7.52 – 7.50 (m, 2H), 7.37 (dt, $J_1 = 7.2$, $J_2 = 0.8$, 2H), 7.26 (dt, $J_1 = 7.6$, $J_2 = 1.2$, 1H), 6.92 (dd, $J_1 = 6.8$, $J_2 = 0.8$, 1H), 6.72 – 6.66 (m, 2H); ESI-MS(-): m/z 185 [M - H]⁻.

Benzo[d]isoxazole-6,7-diol (12): A suspension of 2,3,4-trihydroxybenzaldehyde (0.500 g, 3.24 mmol), hydroxylamine hydrochloride (0.225 g, 3.24 mmol), and potassium carbonate (0.448 g, 3.24 mmol) in 2 mL of ethanol was stirred at 25 °C for 3 days and then heated to reflux at 100 °C for 2 h. Then the reaction contents were concentrated under reduced pressure and the crude was purified by column chromatography, running gradient from 100% CH₂Cl₂ to 15% MeOH in CH₂Cl₂. Like fractions were combined and concentrate under reduced pressure to obtain the impure product. The resulting solid was recrystallized from IPA with minimal CH₂Cl₂ to obtain **12** (0.193 g, 1.27 mmol, 39%) as a white solid. ¹H NMR (400 MHz, DMSO-*d*₆): δ 8.17 (s, 1H), 6.71 (d, *J* = 8.4, 1H), 6.33 (d, *J* = 8.4, 1H); ESI-MS(-): *m/z* 150.27 [M - H]⁻.

2-Bromo-1-(2,3,4-trihydroxyphenyl)ethan-1-one (13a): A solution of CuBr₂ (1.33 g, 5.95 mmol) in 20 mL ethyl acetate and a solution of 1-(2,3,4-trihydroxyphenyl)ethan-1-one (0.500 g, 2.97 mmol) in 20 mL chloroform were both pre-heated to 70 °C. After 5 min at 70 °C, the acetophenone solution was added to the flask containing CuBr₂, and the reaction continued to heat at 70 °C under nitrogen atmosphere for 16 h. Then the solids were hot filtered off and discarded. The filtrate was concentrated under reduced pressure, and the resulting crude was purified by column chromatography, running gradient from 100% CH₂Cl₂ to 15% MeOH in CH₂Cl₂. The product eluted slowly across 2-10% MeOH in CH₂Cl₂. Like fractions were combined and concentrated under reduced pressure to obtain **13a** (0.528 g, 1.10 mmol, 36%) as an impure deep yellow oil that was used directly in the next step without any additional purification. ¹H NMR (400 MHz, DMSO-*d*₆): δ 7.44 (d, *J* = 9.2, 1H), 6.53 (d, *J* = 8.8, 1H), 4.65 (s, 2H); ESI-MS(-): *m/z* 245 [M - H]⁻.

6,7-Dihydroxybenzofuran-3(2H)-one (13b): To a solution of **13a** (0.510 g, 1.00 mmol) in 20 mL IPA, potassium carbonate (0.855 g, 6.19 mmol) was added. The reaction was heated to reflux at 100 °C for 20 h. Then the reaction was allowed to cool to 25 °C, was concentrated under reduced pressure and purify the crude by reverse phase column chromatography, running gradient from 100% water to 100% MeOH. The product eluted impure in 100% water. Like fractions were combined, acidified with a small amount of HCl, and extracted into organic using 3×20 mL ethyl acetate. The combined organic was washed with brine, dried over magnesium sulfate, the solids were filtered off and discarded. The filtrate was concentrate under reduced pressure and re-purified by normal phase column chromatography, running gradient from 100% CH₂Cl₂ to 15% MeOH in CH₂Cl₂. The desired product eluted in 6% MeOH in CH₂Cl₂. Like fractions were combined and concentrated under reduced pressure to obtain **13b** (0.041 g, 0.25 mmol, 24%) as a very pale yellow solid. ¹H NMR (400 MHz, Acetone-*d*₆): δ 8.70 (*br s*, 2H), 7.04 (d, *J* = 8.4, 1H), 6.67 (d, *J* = 8.4, 1H), 4.64 (s, 2H); ESI-MS(-): *m/z* 165 [M - H]⁻.

7,8-Dihydroxy-4H-chromen-4-one (14): To a solution of 1-(2,3,4-trihydroxyphenyl)ethan-1-one (0.500 g, 2.97 mmol) in 10 mL toluene, N,N-dimethylformamide dimethyl acetal (1.2 mL, 8.9 mmol) was added. The reaction was heated at 100 °C for 2 h, until the starting material was consumed by TLC. Then the reaction was concentrated under reduced pressure, and the crude solid was taken up in 10 chloroform with 1 mL of 12 M HCl, and heated to reflux at 100 °C for 2 h, after which the reaction was cooled to 25 °C, diluted with water, and extracted into organic using 20×3 mL ethyl acetate. The combined organic was washed with brine, dried over magnesium sulfate, and the solids were filtered off and discarded. The filtrate was concentrated under reduced pressure, and the resulting crude was purified by column chromatography,

running gradient from 100% CH₂Cl₂ to 15% MeOH in CH₂Cl₂. The desired product eluted in 10% MeOH in CH₂Cl₂. Like fractions were combined and concentrated under reduced pressure to obtain **15** (0.055 g, 0.33 mmol, 10%) as a yellow solid. ¹H NMR (400 MHz, DMSO-*d*₆): δ 10.30 (*br s*, 1H), 9.40 (*br s*, 1H), 8.18 (dd, *J*₁ = 5.6, *J*₂ = 1.2, 1H), 7.36 (dd, *J*₁ = 8.4, *J*₂ = 1.2, 1H), 6.91 (dd, *J*₁ = 8.8, *J*₂ = 2.4, 1H), 6.17 (dd, *J*₁ = 6.0, *J*₂ = 2.0, 1H); ESI-MS(-): *m/z* 177.28 [M - H]⁻.

3-Aminobenzene-1,2-diol hydrobromide (16): Following the general methyl ether deprotection protocol, from 2,3-dimethoxyaniline (0.500 g, 3.26 mmol) and 1 M BBr₃ in heptanes (16.3 mL, 16.3 mmol) **16** (0.670 g, 3.25 mmol, 99%) was obtained as a tan solid. ¹H NMR (400 MHz, DMSO-*d*₆): δ 9.96 (*br s*, 1H), 9.73 (*br s*, 2H), 9.63 (*br s*, 1H), 6.85 (dd, *J*₁ = 7.6, *J*₂ = 1.6, 1H), 6.76 (dd, *J*₁ = 8.0, *J*₂ = 1.6, 1H), 6.69 (t, *J* = 8.0, 1H); ESI-MS(+): *m/z* 126 [M + H]⁺.

4-Aminobenzene-1,2-diol hydrobromide (17): Following the general methyl ether deprotection protocol, from 3,4-dimethoxyaniline (0.500 g, 3.26 mmol) and 1 M BBr₃ in heptanes (16.3 mL, 16.3 mmol), **17** (0.600 g, 2.90 mmol, 89%) was obtained as a tan solid. ¹H NMR (400 MHz, DMSO-*d*₆): δ 9.76 (*br s*, 2H), 9.52 (*br s*, 1H), 9.25 (*br s*, 1H), 6.80 – 6.78 (m, 2H), 6.62 (dd, *J*₁ = 8.4, *J*₂ = 2.4, 1H); ESI-MS(+): *m/z* 126 [M + H]⁺.

Synthesis for Oxazoline Derivatives

General Method for Oxazoline Cyclization A: To a solution of 2-nitrilephenol (1 eq.) in toluene (5 mL), ZnCl₂ (0.02 eq.) and aminoethanol (1.5 eq.) were sequentially added. The

mixture was purged with nitrogen and heated to reflux at 130 °C for 20 h. After cooling to 25 °C, the reaction was concentrated under reduced pressure and the residue was taken up in water and ethyl acetate. The aqueous phase was extracted with ethyl acetate (5×5 mL), and the combined organic phase was dried over magnesium sulfate, and the filtrate was concentrated under reduced pressure. The resulting pink-brown residue was purified by column chromatography with a gradient of 0% to 20% ethyl acetate in hexanes, unless otherwise noted. Desired fractions were combined and concentrated under reduced pressure to obtain the desired oxazoline derivative. Compounds that were isolated as oils were cooled to -20 °C for 1 h to solidify, and remained solid thereafter.

General Method for Oxazoline Cyclization B: To a solution of starting amino-acid derivative (1 eq.) in dry CH₂Cl₂ (10 mL) at 0 °C, was added thionyl chloride (1.5 eq.). The reaction was allowed to warm to 25 °C and stirred for 16 h. The reaction was washed with sat. sodium bicarbonate solution (20 mL), and the aqueous phase extracted with 3:1 CH₂Cl₂ to isopropanol (3×15 mL). The organic phase was dried over magnesium sulfate, and the filtrate was concentrated under reduced pressure. The resulting pink-brown residue was purified by column chromatography with a gradient of 0% to 20% ethyl acetate in hexanes, unless otherwise noted. Desired fractions were combined and concentrated under reduced pressure to obtain the desired oxazoline derivative. Compounds that were isolated as oils were cooled to -20 °C for 1 h to solidify and remained solid thereafter.

General Amide Coupling Protocol: To a solution of starting carboxylic acid (1.0 eq.) in DMF (20 mL), was sequentially added EDC (3.0 eq.) and HOBt (2.0 eq.) and the reaction stirred at 60

°C for 1 h. Then triethylamine (3.0 eq.) and ethanolamine (1.0 eq.) were sequentially added and the reaction continued to stir at 60 °C overnight. Upon cooling to 25 °C, the reaction was diluted with brine (50 mL) and ethyl acetate (30 mL). The organic and aqueous phases were separated, and the organic phase was washed with additional brine (20 mL). The combined aqueous phase was extracted with ethyl acetate (20 mL) and the combined organic phase was dried over magnesium sulfate. The solids were filtered off and discarded, and the filtrate was concentrated under reduced pressure. The resulting crude was purified by column chromatography with a gradient of 0% to 100% ethyl acetate in hexanes, unless otherwise noted. Like fractions were combined and concentrated under reduced pressure to obtain the desired amide product

2-(4,5-Dihydrooxazol-2-yl)phenol (5.5): From the general method for oxazoline cyclization A, from 2-hydroxybenzotrile (0.300 g, 2.52 mmol), ZnCl₂ (6.86 mg, 50.4 μmol), and ethanolamine (167 μL, 2.77 mmol) in toluene (5 mL) at 120 °C for 24 h, the desired product **5.5** (0.083 g, 0.51 mmol, 20%) was obtained as a clear oil that solidified upon cooling to -20 °C to a pale tan solid. ¹H NMR (400 MHz, DMSO-*d*₆): δ 12.23 (*br s*, 1H), 7.61 (d, *J* = 8.0, 1H), 7.42 (t, *J* = 8.8, 1H), 6.97 (d, *J* = 8.4, 1H), 6.92 (t, *J* = 7.6, 1H), 4.46 (t, *J* = 9.2, 2H), 4.05 (t, *J* = 9.6, 2H); ¹³C NMR (500 MHz, DMSO-*d*₆): δ 165.8, 159.5, 134.1, 128.2, 119.4, 116.9, 110.6, 67.5, 53.4; HRMS (ESI-TOF): *m/z* calcd for C₉H₉NO₂+H⁺: 164.0706 [M+H]⁺; found: 164.0706.

2-(4,5-Dihydro-1H-imidazol-2-yl)phenol (5.26): From the general method for oxazoline cyclization A, from 2-hydroxybenzotrile (0.500 g, 4.20 mmol), ZnCl₂ (11.4 mg, 83.9 μmol), and ethane-1,2-diamine (308 μL, 4.62 mmol) in toluene (5 mL) at 130 °C for 22 h, the desired product **5.26** (0.270 g, 1.67 mmol, 40%) as a clear yellow oil that solidified upon standing to a

crystalline, pale yellow solid. ^1H NMR (400 MHz, DMSO- d_6): δ 7.54 (d, $J = 8.0$, 1H), 7.25 (t, $J = 7.2$, 1H), 6.76 (d, $J = 8.4$, 1H), 6.68 (t, $J = 7.6$, 1H), 3.69 (s, 4H); ^{13}C NMR (500 MHz, DMSO- d_6): δ 166.6, 163.7, 133.0, 127.9, 118.5, 116.3, 110.9, 47.1; HRMS (ESI-TOF): m/z calcd for $\text{C}_9\text{H}_{10}\text{N}_2\text{O}+\text{H}^+$: 163.0866 $[\text{M}+\text{H}]^+$; found: 163.0867.

2-(4,5-Dihydrothiazol-2-yl)phenol (5.27): From the general method for oxazoline cyclization A, from 2-hydroxybenzotrile (0.500 g, 4.20 mmol), ZnCl_2 (11.4 mg, 83.9 μmol), and 2-aminoethane-1-thiol hydrochloride (525 mg, 4.62 mmol), in toluene (5 mL) at 130 $^\circ\text{C}$ for 20 h, the desired product **5.27** (0.340 g, 1.90 mmol, 45%) was obtained as a yellow oil that upon cooling to -20 $^\circ\text{C}$, solidified to a pale yellow solid. ^1H NMR (400 MHz, DMSO- d_6): δ 7.43 – 7.37 (m, 2H), 6.97 – 6.91 (m, 2H), 4.46 (t, $J = 8.4$, 2H), 3.44 (t, $J = 7.2$, 2H); ^{13}C NMR (500 MHz, DMSO- d_6): δ 172.0, 158.8, 133.7, 131.0, 119.7, 116.9, 117.2, 116.3, 63.6, 31.9; HRMS (ESI-TOF): m/z calcd for $\text{C}_9\text{H}_9\text{NOS}+\text{H}^+$: 180.0478 $[\text{M}+\text{H}]^+$; found: 180.0479.

2-(5,6-Dihydro-4H-1,3-oxazin-2-yl)phenol (5.28): From the general method for oxazoline cyclization A, from 2-hydroxybenzotrile (0.500 g, 4.20 mmol), ZnCl_2 (11.4 mg, 83.9 μmol), and 3-aminopropan-1-ol (353 μL , 4.62 mmol), in toluene (5 mL) at 130 $^\circ\text{C}$ for 21 h, the desired product **5.28** (0.400 g, 2.25 mmol, 54%) was obtained as a clear oil that upon cooling to -20 $^\circ\text{C}$, solidified to a white crystalline solid. ^1H NMR (400 MHz, DMSO- d_6): δ 7.59 (dd, $J_1 = 7.6$, $J_2 = 2.0$, 1H), 7.30 (dt, $J_1 = 8.4$, $J_2 = 1.6$, 1H), 6.83 (dd, $J_1 = 8.0$, $J_2 = 0.4$, 1H), 7.87 (dt, $J_1 = 7.6$, $J_2 = 0.4$, 1H), 4.40 (t, $J = 5.2$, 2H), 3.53 (t, $J = 6.0$, 2H), 1.98 – 1.93 (m, 2H); ^{13}C NMR (500 MHz, DMSO- d_6): δ 160.9, 159.3, 133.0, 126.9, 118.1, 117.3, 114.5, 65.9, 40.8, 21.4; HRMS (ESI-TOF): m/z calcd for $\text{C}_{10}\text{H}_{12}\text{NO}_2+\text{H}^+$: 178.0865 $[\text{M}+\text{H}]^+$; found: 178.0864.

Hydroxy-N-(2-hydroxyethyl)-2-naphthamide (5.29a): To a solution of 1-hydroxy-2-naphthoic acid (1.00 g, 5.31 mmol) in THF (25 mL), was added ethanolamine (893 μ L, 15.9 mmol), and triethylamine (2.22 mL, 15.9 mmol). Then 50% T3P in ethyl acetate (4.7 mL, 7.97 mmol) was added in one portion to initiate the reaction. The reaction was purged with nitrogen and heated to reflux at 70 °C for 16 h. Upon cooling to 25 °C, the reaction was diluted with ethyl acetate (20 mL) and washed with water (3 \times 20 mL). The combined aqueous phase was acidified with a small amount of 1 M HCl and then back-extracted with ethyl acetate (10 mL). The combined organic phase was dried over magnesium sulfate and the solids were filtered off and discarded. The filtrate was concentrated under reduced pressure and the resulting residue was purified by column chromatography with a gradient of 0% to 100% ethyl acetate in hexanes. The product eluted in 70% ethyl acetate in hexanes. Desired fractions were combined and concentrated under reduced pressure to obtain the product, **5.29a** (0.300 g, 1.30 mmol, 24%), as a white solid. $^1\text{H NMR}$ (400 MHz, DMSO- d_6): δ 8.95 (*br t*, $J = 4.8$, 1H), 8.25 (*d*, $J = 8.0$, 1H), 7.90 – 7.85 (*m*, 2H), 7.62 (*dt*, $J_1 = 6.8$, $J_2 = 0.8$, 1H), 7.54 (*dt*, $J_1 = 6.8$, $J_2 = 0.8$, 1H), 7.36 (*dd*, $J_1 = 9.2$, $J_2 = 1.6$, 1H), 4.83 (*br s*, 1H), 3.57 (*br s*, 2H), 3.42 (*br t*, $J = 6.0$, 2H); ESI-MS(+): m/z 232 $[\text{M} + \text{H}]^+$.

2-(4,5-Dihydrooxazol-2-yl)naphthalen-1-ol (5.29b): From the general method for oxazoline cyclization B, from **5.29a** (0.180 g, 0.778 mmol) and thionyl chloride (0.085 mL, 1.17 mmol) in CH_2Cl_2 (10 mL), the desired product **5.29b** (0.053 g, 0.25 mmol, 32%) was obtained as a pale yellow solid. $^1\text{H NMR}$ (400 MHz, DMSO- d_6): δ 8.27 (*d*, $J = 8.4$, 1H), 7.86 (*d*, $J = 8.4$, 1H), 7.66 – 7.52 (*m*, 3H), 7.34 (*d*, $J = 8.8$, 1H), 4.54 (*t*, $J = 9.6$, 2H), 4.10 (*t*, $J = 9.6$, 2H); $^{13}\text{C NMR}$

(500 MHz, DMSO- d_6): δ 166.9, 159.3, 136.2, 129.2, 128.1, 126.2, 124.8, 123.6, 123.6, 118.1, 103.1, 67.9, 52.4; HRMS (ESI-TOF): m/z calcd for $C_{13}H_{11}NO_2+H^+$: 214.0863 $[M+H]^+$; found: 214.0865.

1-2-Hydroxy-N-(2-hydroxyethyl)-5-methylbenzamide (5.30a): Following the above general amide coupling protocol, from 3-hydroxy-2-naphthoic acid (1.00 g, 6.57 mmol), EDC (3.78 g, 19.7 mmol), HOBt (2.01 g, 13.1 mmol), triethylamine (2.7 mL, 19.7 mmol), and ethanolamine (397 μ L, 6.57 mmol) in 20 mL DMF at 60 °C for 40 h, the desired product **5.30a** (0.356 g, 1.53 mmol, 29%) was obtained as a yellow solid. 1H NMR (400 MHz, DMSO- d_6): δ 12.06 (*br s*, 1H), 9.06 (*br t*, $J = 5.2$, 1H), 8.55 (s, 1H), 7.84 (d, $J = 8.4$, 1H), 7.72 (d, $J = 8.0$, 1H), 7.48 (t, $J = 6.8$, 1H), 7.37 (t, $J = 6.8$, 1H), 7.27 (s, 1H), 4.87 (*br t*, $J = 5.2$, 1H), 3.59 (q, $J = 5.6$, 1H), 3.44 (q, $J = 5.6$, 1H); ESI-MS(+): m/z 232 $[M + H]^+$.

3-(4,5-Dihydrooxazol-2-yl)naphthalen-2-ol (5.30b): From the general method for oxazoline cyclization B, from **5.30a** (0.350 g, 1.51 mmol) and thionyl chloride (0.166 mL, 2.27 mmol) in CH_2Cl_2 (10 mL), the desired product **5.30b** (0.190 g, 0.891 mmol, 59%) was obtained as a fluffy white solid. 1H NMR (400 MHz, DMSO- d_6): δ 11.99 (*br s*, 1H), 8.33 (s, 1H), 7.95 (d, $J = 8.4$, 1H), 7.75 (d, $J = 8.0$, 1H), 7.51 (t, $J = 7.2$, 1H), 7.35 – 7.34 (m, 2H), 4.53 (t, $J = 9.6$, 2H), 4.13 (t, $J = 9.6$, 2H); ^{13}C NMR (500 MHz, DMSO- d_6): δ 165.5, 155.1, 136.6, 129.8, 129.3, 128.9, 127.0, 126.5, 124.2, 112.9, 110.7, 67.5, 53.8; HRMS (ESI-TOF): m/z calcd for $C_{13}H_{11}NO_2+H^+$: 214.0863 $[M+H]^+$; found: 214.0866.

2-Hydroxy-N-(2-hydroxyethyl)-1-naphthamide (5.31a): Following the above general amide coupling protocol, from 2-hydroxy-1-naphthoic acid (1.00 g, 6.57 mmol), EDC (3.78 g, 19.7 mmol), HOBt (2.01 g, 13.1 mmol), triethylamine (2.7 mL, 19.7 mmol), and ethanolamine (397 μ L, 6.57 mmol) in 20 mL DMF at 60 °C for 30 h, the desired product **5.31a** (0.155 g, 0.671 mmol, 13%) was obtained as a yellow solid. $^1\text{H NMR}$ (400 MHz, DMSO- d_6): δ 9.97 (*br s*, 1H), 8.19 (*br t*, $J = 5.6$, 1H), 7.94 (*br s*, 1H), 7.80 – 7.77 (m, 2H), 7.71 (d, $J = 8.4$, 1H), 7.42 (t, $J = 8.0$, 1H), 7.28 (t, $J = 8.0$, 1H), 7.16 (d, $J = 8.8$, 1H), 3.34 (s, 4H); ESI-MS(+): m/z 232 [$\text{M} + \text{H}$] $^+$.

1-(4,5-Dihydrooxazol-2-yl)naphthalen-2-ol (5.31b): From the general method for oxazoline cyclization B, from **5.31a** (0.150 g, 0.649 mmol) and thionyl chloride (0.071 mL, 0.973 mmol) in CH_2Cl_2 (10 mL), the desired product **5.31b** (0.050 g, 0.234 mmol, 36%) was obtained as a white solid. $^1\text{H NMR}$ (400 MHz, DMSO- d_6): δ 8.67 (d, $J = 8.8$, 1H), 7.96 (d, $J = 9.2$, 1H), 7.84 (d, $J = 8.0$, 1H), 7.53 (t, $J = 6.8$, 1H), 7.35 (t, $J = 8.0$, 1H), 7.19 (d, $J = 8.8$, 1H), 4.63 (t, $J = 9.6$, 2H), 4.07 (t, $J = 9.6$, 2H); $^{13}\text{C NMR}$ (500 MHz, DMSO- d_6): δ 168.4, 162.5, 135.0, 131.7, 129.4, 128.3, 128.0, 124.8, 123.6, 119.8, 102.0, 68.1, 51.1; HRMS (ESI-TOF): m/z calcd for $\text{C}_{13}\text{H}_{11}\text{NO}_2 + \text{H}^+$: 214.0863 [$\text{M} + \text{H}$] $^+$; found: 214.0865.

2-Hydroxy-3-methylbenzotrile (5.32a): To 98% formic acid (20 mL), was added 2-hydroxy-3-methylbenzaldehyde (1.00 g, 7.34 mmol), potassium acetate (0.865 g, 8.81 mmol), and hydroxylamine hydrochloride (0.612 g, 8.81 mmol). The reaction was placed under nitrogen, and heated to reflux at 100 °C for 24 h. Upon cooling to 25 °C, the reaction was concentrated under reduced pressure, and the residue was taken up in 1:1 ethyl acetate to water (40 mL). The aqueous phase was separated from the organic phase, and the organic phase was washed with

additional water (2×20 mL). The combined aqueous phase was back extracted with ethyl acetate (15 mL) and the combined organic was dried over magnesium sulfate. The solids were filtered off and discarded, and the filtrate was concentrated under reduced pressure. The resulting crude was purified by column chromatography with a gradient of 0% to 20% ethyl acetate in hexanes. The product eluted in 11 % ethyl acetate in hexanes. Desired fractions were combined and concentrated under reduced pressure to obtain intermediate **5.32a** (0.559 g, 4.20 mmol, 57%) as a white solid. ¹H NMR (400 MHz, DMSO-*d*₆): δ 10.07 (*br s*, 1H), 7.42 (d, *J* = 7.6, 1H), 7.38 (d, *J* = 7.6, 1H), 6.87 (t, *J* = 7.6, 1H), 2.20 (s, 3H); ESI-MS(-): *m/z* 132 [M - H]⁻.

2-(4,5-Dihydrooxazol-2-yl)-6-methylphenol (5.32b): From the general method for oxazoline cyclization A, from **5.32a** (0.559 g, 4.20 mmol), ZnCl₂ (11.4 mg, 83.9 μmol), and ethanolamine (381 μL, 6.30 mmol) in toluene (5 mL) at 130 °C for 24 h, the desired product **5.32b** (0.554 g, 3.13 mmol, 75%) was obtained as a clear oil that solidifies upon standing to a white solid. ¹H NMR (400 MHz, DMSO-*d*₆): δ 12.44 (*br s*, 1H), 7.44 (dd, *J*₁ = 8.0, *J*₂ = 2.0, 1H), 7.28 (dd, *J*₁ = 7.2, *J*₂ = 0.8, 1H), 6.80 (t, *J* = 7.6, 1H), 4.43 (t, *J* = 9.6, 2H), 4.04 (t, *J* = 9.6, 2H), 2.18 (s, 3H); ¹³C NMR (500 MHz, DMSO-*d*₆): δ 166.1, 157.8, 134.7, 125.7, 125.4, 118.8, 109.9, 67.4, 53.4, 16.1; HRMS (ESI-TOF): *m/z* calcd for C₁₀H₁₂NO₂+H⁺: 178.0863 [M+H]⁺; found: 178.0866.

2-(4,5-Dihydrooxazol-2-yl)-5-methylphenol (5.33): From the general method for oxazoline cyclization A, from 2-hydroxy-4-methylbenzotrile (0.559 g, 4.20 mmol), ZnCl₂ (11.4 mg, 83.9 μmol), and ethanolamine (381 μL, 6.30 mmol) in toluene (5 mL) at 130 °C for 20 h, the desired product **5.33** (0.296 g, 1.67 mmol, 40%) was obtained as a clear oil that solidifies upon standing to a white solid. ¹H NMR (400 MHz, DMSO-*d*₆): δ 12.14 (*br s*, 1H), 7.48 (dd, *J*₁ = 8.0, *J*₂ = 1.2,

1H), 6.79 (s, 1H), 6.73 (dd, $J_1 = 7.2$, $J_2 = 0.8$, 1H), 4.43 (t, $J = 9.6$, 2H), 4.03 (t, $J = 9.2$, 2H), 2.28 (s, 3H); ^{13}C NMR (500 MHz, DMSO- d_6): δ 165.8, 159.5, 144.5, 128.0, 120.4, 117.1, 108.1, 67.3, 53.3, 21.8; HRMS (ESI-TOF): m/z calcd for $\text{C}_{10}\text{H}_{12}\text{NO}_2 + \text{H}^+$: 178.0863 $[\text{M} + \text{H}]^+$; found: 178.0865.

3-Hydroxy-N-(2-hydroxyethyl)-2-naphthamide (5.34a): Following the above general amide coupling protocol, from 2-hydroxy-5-methylbenzoic acid (1.00 g, 6.57 mmol), EDC (3.78 g, 19.7 mmol), HOBT (2.01 g, 13.1 mmol), triethylamine (2.7 mL, 19.7 mmol), and ethanolamine (397 μL , 6.57 mmol) in 20 mL DMF at 60 °C for 16 h, the desired product **5.34a** (0.260 g, 1.33 mmol, 20%) was obtained as a clear, pale pink oil that solidified upon standing to a white, crystalline solid. ^1H NMR (400 MHz, DMSO- d_6): δ 12.29 (*br s*, 1H), 8.74 (*br t*, $J = 5.2$, 1H), 7.67 (d, $J = 1.6$, 1H), 7.18 (dd, $J_1 = 8.4$, $J_2 = 2.4$, 1H), 6.77 (d, $J = 8.4$, 1H), 4.78 (*br t*, $J = 5.2$, 1H), 3.54 – 3.50 (m, 2H), 3.32 (s, 2H), 2.23 (s, 3H); ESI-MS(-): m/z 194 $[\text{M} - \text{H}]^-$.

2-(4,5-Dihydrooxazol-2-yl)-4-methylphenol (5.34b): From the general method for oxazoline cyclization B, from **5.34a** (0.260 g, 1.33 mmol) and thionyl chloride (0.146 mL, 1.17 mmol) in CH_2Cl_2 (10 mL), the desired product **5.34b** (0.189 g, 1.07 mmol, 80%) was obtained as clear oil that solidified upon standing to a white solid. ^1H NMR (400 MHz, DMSO- d_6): δ 11.97 (*br s*, 1H), 7.40 (s, 1H), 7.22 (d, $J = 8.4$, 1H), 6.86 (dd, $J_1 = 8.4$, $J_2 = 1.6$, 1H), 4.43 (t, $J = 9.6$, 2H), 4.03 (t, $J = 9.6$, 2H), 2.22 (s, 3H); ^{13}C NMR (500 MHz, DMSO- d_6): δ 165.8, 157.4, 134.7, 128.0, 128.00, 116.7, 110.2, 67.4, 53.4, 20.4; HRMS (ESI-TOF): m/z calcd for $\text{C}_{10}\text{H}_{12}\text{NO}_2 + \text{H}^+$: 178.0865 $[\text{M} + \text{H}]^+$; found: 178.0864.

(R)-2-(5-Methyl-4,5-dihydrooxazol-2-yl)phenol (5.35): From the general method for oxazoline cyclization A, from 2-hydroxybenzotrile (0.500 g, 4.20 mmol), ZnCl₂ (11.4 mg, 83.9 μmol), and (R)-1-aminopropan-2-ol (473 mg, 6.30 mmol) in toluene (5 mL) at 130 °C for 20 h, the desired product **5.35** (0.440 g, 2.48 mmol, 59%) was obtained as a clear oil that solidified upon cooling to -20 °C to a white crystalline solid. ¹H NMR (400 MHz, DMSO-*d*₆): δ 12.28 (*br s*, 1H), 7.59 (d, *J* = 8.0, 1H), 7.41 (t, *J* = 7.6, 1H), 6.96 (d, *J* = 8.0, 1H), 6.90 (t, *J* = 8.0, 1H), 4.97 – 4.88 (m, 1H), 4.16 (dd, *J*₁ = 14.0, *J*₂ = 9.6, 1H), 3.61 (dd, *J*₁ = 14.4, *J*₂ = 7.6, 1H), 1.37 (d, *J* = 6.4, 3H); ¹³C NMR (500 MHz, DMSO-*d*₆): δ 165.2, 159.6, 134.0, 128.2, 119.3, 116.9, 110.7, 76.4, 59.6, 21.0; HRMS (ESI-TOF): *m/z* calcd for C₁₀H₁₂NO₂+H⁺: 178.0863 [M+H]⁺; found: 178.0864.

(S)-2-(5-Methyl-4,5-dihydrooxazol-2-yl)phenol (5.36): From the general method for oxazoline cyclization A, from 2-hydroxybenzotrile (0.500 g, 4.20 mmol), ZnCl₂ (11.4 mg, 83.9 μmol), and (S)-1-aminopropan-2-ol (473 mg, 6.30 mmol) in toluene (5 mL) at 130 °C for 20 h, the desired product **5.36** (0.270 g, 1.52 mmol, 36%) was obtained as a clear oil that solidified upon cooling to -20 °C to a white crystalline solid. ¹H NMR (400 MHz, DMSO-*d*₆): δ 12.28 (*br s*, 1H), 7.60 (d, *J* = 8.0, 1H), 7.41 (t, *J* = 7.2, 1H), 6.96 (d, *J* = 8.4, 1H), 6.90 (t, *J* = 7.6, 1H), 4.97 – 4.87 (m, 1H), 4.17 (ddd, *J*₁ = 14.4, *J*₂ = 9.6, *J*₃ = 2.8, 1H), 3.61 (ddd, *J*₁ = 14.4, *J*₂ = 7.6, *J*₃ = 2.8, 1H), 2.49 (d, *J* = 1.6, 3H); ¹³C NMR (500 MHz, DMSO-*d*₆): δ 165.2, 159.6, 134.0, 128.2, 119.3, 116.9, 110.7, 76.4, 59.6, 21.0; HRMS (ESI-TOF): *m/z* calcd for C₁₀H₁₂NO₂+H⁺: 178.0863 [M+H]⁺; found: 178.0864.

(R)-2-(5-Methyl-4,5-dihydrooxazol-2-yl)phenol (5.37): From the general method for oxazoline cyclization A, from 2-hydroxybenzotrile (0.500 g, 4.20 mmol), ZnCl₂ (11.4 mg, 83.9 μmol), and D-alaninol (491 μL, 6.30 mmol) in toluene (5 mL) at 130 °C for 20 h, the desired product **5.37** (0.400 g, 2.26 mmol, 54%) was obtained as a clear oil. ¹H NMR (400 MHz, DMSO-*d*₆): δ 12.24 (*br s*, 1H), 7.60 (d, *J* = 8.0, 1H), 7.42 (t, *J* = 7.6, 1H), 6.97 (d, *J* = 8.4, 1H), 6.91 (t, *J* = 8.0, 1H), 4.57 (dt, *J*₁ = 8.4, *J*₂ = 0.8, 1H), 4.47 – 4.38 (m, 1H), 4.00 (dt, *J*₁ = 7.2, *J*₂ = 0.8, 1H), 1.27 (d, *J* = 6.4, 3H); ¹³C NMR (500 MHz, DMSO-*d*₆): δ 164.7, 159.6, 134.0, 128.2, 119.3, 116.83, 110.6, 73.5, 60.7, 21.6; HRMS (ESI-TOF): *m/z* calcd for C₁₀H₁₂NO₂+H⁺: 178.0863 [M+H]⁺; found: 178.0864.

(S)-2-(5-Methyl-4,5-dihydrooxazol-2-yl)phenol (5.38): From the general method for oxazoline cyclization A, from 2-hydroxybenzotrile (0.500 g, 4.20 mmol), ZnCl₂ (11.4 mg, 83.9 μmol), and L-alaninol (491 μL, 6.30 mmol) in toluene (5 mL) at 130 °C for 20 h, the desired product **5.38** (0.320 g, 1.81 mmol, 43%) was obtained as a clear oil. ¹H NMR (400 MHz, DMSO-*d*₆): δ 12.24 (*br s*, 1H), 7.60 (d, *J* = 8.0, 1H), 7.42 (t, *J* = 8.4, 1H), 6.96 (d, *J* = 8.8, 1H), 6.91 (t, *J* = 7.6, 1H), 4.567 (dt, *J*₁ = 9.2, *J*₂ = 2.4, 1H), 4.47 – 4.38 (m, 1H), 4.00 (dt, *J*₁ = 7.6, *J*₂ = 2.0, 1H), 1.28 (dd, *J*₁ = 6.4, *J*₂ = 2.0, 3H); ¹³C NMR (500 MHz, DMSO-*d*₆): δ 164.7, 159.6, 134.1, 128.2, 119.4, 116.9, 110.6, 73.5, 60.7, 21.6; HRMS (ESI-TOF): *m/z* calcd for C₁₀H₁₂NO₂+H⁺: 178.0863 [M+H]⁺; found: 178.0864.

5-Bromo-2-(4,5-dihydrooxazol-2-yl)phenol (5.39): From the general method for oxazoline cyclization A, from 4-bromo-2-hydroxybenzotrile (1.00 g, 5.05 mmol), ZnCl₂ (13.8mg, 101 μmol), and ethanolamine (0.458 mL, 7.57 mmol) in toluene (5 mL) at 130 °C for 20 h, the

desired product **5.39** (0.030 g, 0.12 mmol, 3%) was obtained as a white solid. $^1\text{H NMR}$ (400 MHz, $\text{DMSO-}d_6$): δ 12.55 (*br s*, 1H), 7.53 (dd, $J_1 = 8.4$, $J_2 = 1.6$, 1H), 7.23 (d, $J = 2.8$, 1H), 7.13 – 7.10 (m, 1H), 4.47 (dt, $J_1 = 9.2$, $J_2 = 1.6$, 2H), 4.05 (dt, $J_1 = 9.6$, $J_2 = 1.6$, 2H); ESI-MS(+): m/z 242.22 $[\text{M} + \text{H}]^+$.

4-Bromo-2-(4,5-dihydrooxazol-2-yl)phenol (5.40): From the general method for oxazoline cyclization A, from 5-bromo-2-hydroxybenzotrile (1.00 g, 5.05 mmol), ZnCl_2 (13.8mg, 101 μmol), and ethanolamine (0.458 mL, 7.57 mmol) in toluene (5 mL) at 130 $^\circ\text{C}$ for 20 h, the desired product **5.40** (0.128 g, 0.529 mmol, 10%) was obtained as a white solid. $^1\text{H NMR}$ (400 MHz, $\text{DMSO-}d_6$): δ 12.31 (*br s*, 1H), 7.66 (dd, $J_1 = 2.4$, $J_2 = 0.8$, 1H), 7.59 – 7.56 (m, 1H), 6.96 (dd, $J_1 = 8.8$, $J_2 = 0.8$, 1H), 4.47 (t, $J = 9.6$, 2H), 4.07 (t, $J = 9.6$, 2H); ESI-MS(+): m/z 242.23 $[\text{M} + \text{H}]^+$.

2-(4,5-Dihydrooxazol-2-yl)-5-methoxyphenol (5.41): To a solution of 2-hydroxy-4-methoxybenzoic acid (1.00 g, 5.95 mmol) in 30 mL DMF, EDC (2.28 g, 11.9 mmol) and HOBt (1.82 g, 11.9 mmol) were sequentially added. The reaction was heated at 70 $^\circ\text{C}$ for 1 h, then ethanolamine (1.08 mL, 17.8 mmol) and TEA (2.5 mL, 17.8 mmol) were added at to the reaction mixture, and the reaction continued to heat at 70 $^\circ\text{C}$ overnight. Upon cooling to 25 $^\circ\text{C}$, the reaction solution diluted with 30 mL, brine and extracted into organic with 3 \times 20 mL ethyl acetate. The combined organic was dried over magnesium sulfate, and the solids were filtered off and discarded. The filtrate was concentrated under reduced pressure, and the resulting residue was purified by column chromatography, running gradient from 100% hexanes to 100% ethyl acetate. The desired product eluted in 35% ethyl acetate in hexanes. Like fractions were

combined and concentrated under reduced pressure to obtain the desired product as an impure off-white solid. This solid was further purified by RP chromatography, running gradient from 100% water to 100% MeOH; the desired product eluted in 10% MeOH in water. Like fractions were combined and concentrated under reduced pressure to obtain **5.41** (0.0259 g, 134 μ mol, 2%) was obtained as an off-white solid. $^1\text{H NMR}$ (400 MHz, Acetone- d_6): δ 12.29 (*br s*, 1H), 7.55 (d, $J = 9.6$, 1H), 6.50 – 6.47 (m, 2H), 4.46 (t, $J = 9.2$, 2H), 4.07 (t, $J = 9.2$, 2H), 3.83 (s, 3H); ESI-MS(+): m/z 194.20 $[\text{M} + \text{H}]^+$.

2-(4,5-Dihydrooxazol-2-yl)-4-methoxyphenol (5.42): Following the same protocol used in **5.41**, from 2-hydroxy-5-methoxybenzoic acid (1.00 g, 5.95 mmol), **5.42** (0.043 g, 0.22 mmol, 4%) was obtained as an off-white solid. $^1\text{H NMR}$ (400 MHz, Acetone- d_6): δ 7.14 (d, $J = 3.2$, 1H), 7.03 (dd, $J_1 = 9.2$, $J_2 = 3.2$, 1H), 6.89 (d, $J = 9.2$, 1H), 4.50 (t, $J = 9.2$, 1H), 4.12 (d, $J = 9.2$, 1H), 3.77 (s, 3H); ESI-MS(+): m/z 194.24 $[\text{M} + \text{H}]^+$.

2-Hydroxy-N-(2-hydroxyethyl)-4-(trifluoromethyl)benzamide (5.43a): Following the above general amide coupling protocol, from 2-hydroxy-4-(trifluoromethyl)benzoic acid (1.00 g, 4.85 mmol), EDC (2.79 g, 14.6 mmol), HOBt (1.49 g, 9.70 mmol), triethylamine (2.0 mL, 15 mmol), and ethanolamine (880 μ L, 14.6 mmol) in 20 mL DMF at 45 $^\circ\text{C}$ for 72 h, the desired product **5.43a** (0.250 g, 1.00 mmol, 21%) was obtained as a clear, pale pink oil that solidified upon standing to a white, crystalline solid. $^1\text{H NMR}$ (400 MHz, DMSO- d_6): δ 8.95 (*br t*, $J = 5.6$, 1H), 8.06 (d, $J = 8.0$, 1H), 7.23 (d, $J = 8.8$, 1H), 7.21 (s, 1H), 4.82 (*br t*, $J = 5.2$, 1H), 3.54 (q, $J = 5.6$, 2H), 3.38 (q, $J = 5.6$, 2H); ESI-MS(+): m/z 248.24 $[\text{M} + \text{H}]^+$.

2-(4,5-Dihydrooxazol-2-yl)-5-(trifluoromethyl)phenol (5.43b): From the general method for oxazoline cyclization B, from **5.43a** (0.220 g, 0.883 mmol) and thionyl chloride (0.100 mL, 1.37 mmol) in CH₂Cl₂ (10 mL), the desired product **5.43b** (0.161 g, 0.696 mmol, 79%) was obtained as a white solid. ¹H NMR (400 MHz, DMSO-*d*₆): δ 12.57 (*br s*, 1H), 7.81 (d, *J* = 8.0, 1H), 7.30 (*s*, 1H), 7.24 (d, *J* = 8.0, 1H), 4.51 (t, *J* = 9.6, 2H), 4.10 (t, *J* = 9.6, 2H); ESI-MS(+): *m/z* 232.23 [M + H]⁺.

(R)-2-(5-Phenyl-4,5-dihydrooxazol-2-yl)phenol (5.44): From the general method for oxazoline cyclization A, from 2-hydroxybenzotrile (500 mg, 4.20 mmol), ZnCl₂ (11.4 mg, 0.839 μmol), and (*R*)-2-amino-1-phenylethan-1-ol (864 mg, 6.30 mmol) in toluene (5 mL) at 130 °C for 20 h, the desired product **5.44** (0.308 g, 0.129 mmol, 30%) was obtained as a white solid. ¹H NMR (400 MHz, DMSO-*d*₆): δ 12.13 (*br s*, 1H), 7.67 (d, *J* = 8.0, 1H), 7.47 – 7.36 (m, 5H), 7.01 (d, *J* = 8.4, 1H), 6.93 (dt, *J*₁ = 7.6, *J*₂ = 0.4, 1H), 5.84 (t, *J* = 8.0, 1H), 4.52 (dd, *J*₁ = 14.4, *J*₂ = 10.0, 1H), 3.95 (dd, *J*₁ = 14.8, *J*₂ = 7.6, 1H); ESI-MS(+): *m/z* 240.15 [M + H]⁺.

(S)-2-(5-Phenyl-4,5-dihydrooxazol-2-yl)phenol (5.45): From the general method for oxazoline cyclization A, from 2-hydroxybenzotrile (500 mg, 4.20 mmol), ZnCl₂ (11.4 mg, 0.839 μmol), and (*S*)-2-amino-1-phenylethan-1-ol (864 mg, 6.30 mmol) in toluene (5 mL) at 130 °C for 20 h, the desired product **5.45** (0.310 g, 0.130 mmol, 31%) was obtained a clear yellow oil that solidified upon standing. ¹H NMR (400 MHz, DMSO-*d*₆): δ 12.12 (*br s*, 1H), 7.67 (d, *J* = 7.6, 1H), 7.47 – 7.36 (m, 5H), 7.01 (d, *J* = 8.4, 1H), 6.93 (dt, *J*₁ = 7.2, *J*₂ = 1.2, 1H), 5.84 (dd, *J*₁ = 10.0, *J*₂ = 7.6, 1H), 4.53 (dd, *J*₁ = 14.4, *J*₂ = 10.0, 1H), 3.95 (dd, *J*₁ = 14.8, *J*₂ = 7.6, 1H); ESI-MS(+): *m/z* 240.15 [M + H]⁺.

Synthesis for Hydroxamic Acid Derivatives

General Method for Hydroxamic Acid Formation A: To solution of starting 2-hydroxybenzoate (1 eq.) in 20 mL MeOH, KOH (4.5 eq.) and hydroxylamine hydrochloride (2.0 eq.) were sequentially added. Then the reaction mixture was heated to reflux at 75 °C for 5 h, during which the solution changed from clear to deep, bright yellow. Upon cooling to 25 °C, the reaction mixture was cooled to 25 °C, acidified to ~ pH 6 with acetic acid, and concentrated under reduced pressure. The resulting residue was taken up in 60 mL of 1:1 water and ethyl acetate, and the organic was separated from the aqueous. The aqueous was washed with an additional 2×15 mL ethyl acetate, then the combined organic was dried over magnesium sulfate, and the solids were filtered off and discarded. The filtrate was concentrated under reduced pressure, and the resulting crude was purified by column chromatography running gradient from 100% hexanes to 100% ethyl acetate in hexanes. The desired product typically eluted in 40% ethyl acetate in hexanes. Like fractions were combined and concentrated under reduced pressure to obtain the product as a slightly impure yellow solid. The solid was then recrystallized from 3:1 ethyl acetate to hexanes, and the resulting solid was collected via vacuum filtration and washed with a small amount of cold 3:1 ethyl acetate to hexanes to obtain the desired final products.

General Method for Hydroxamic Acid Formation B: To solution of picolinic acid (1 eq.) in 10 mL of 1:1 CH₂Cl₂ to THF was added 5 drops cat. DMF followed by thionyl chloride (1.2 eq.). The reaction was allowed to stir at 25 °C for 30 min to form the in situ acid chloride, noting that a white precipitate immediately formed upon thionyl chloride addition. Then the reaction

contents were concentrated under reduced pressure, and the resulting in situ acid chloride was taken up in an additional 10 mL CH₂Cl₂. TEA (2.0 eq.) and hydroxylamine hydrochloride (2.0 eq.) were sequentially added to the solution, and the reaction was allowed to stir at 25 °C for 1.5 h. Upon reaction completion, the solution was quenched via the addition of DI water, and the organic and aqueous layers were separated. The aqueous was washed with an additional 3×10 mL CH₂Cl₂, and the combined organic was washed with brine. The organic was dried over magnesium sulfate, and the filtrate was concentrated under reduced pressure. The resulting crude was purified by column chromatography, running gradient from 100% hexanes to 100% ethyl acetate. The product typically eluted in 50% ethyl acetate in hexanes. Like fractions were combined and concentrated under reduced pressure to obtain the desired final products.

N,2-Dihydroxy-3-methylbenzamide (5.46): From the general method for hydroxamic acid formation A, from methyl 2-hydroxy-3-methylbenzoate (0.500 g, 3.01 mmol), KOH (0.760 g, 13.5 mmol), and hydroxylamine hydrochloride (0.418 g, 6.02 mmol) in MeOH (20 mL) at 75 °C for 5 h, **5.46** (0.152 g, 0.909 mmol, 30%) was obtained as a white, spindle crystalline product. ¹H NMR (400 MHz, DMSO-*d*₆): δ 11.63 (*br s*, 1H), 9.37 (*br s*, 1H), 7.49 (d, *J* = 7.2, 1H), 7.27 (d, *J* = 6.4, 1H), 6.73 (t, *J* = 7.6, 1H), 2.14 (s, 3H); ESI-MS(+): *m/z* 168.16 [M + H]⁺.

N,2-Dihydroxy-4-methylbenzamide (5.47): From the general method for hydroxamic acid formation A, from methyl 2-hydroxy-4-methylbenzoate (0.500 g, 3.01 mmol), KOH (0.760 g, 13.5 mmol), and hydroxylamine hydrochloride (0.418 g, 6.02 mmol) in MeOH (20 mL) at 75 °C for 5 h, **5.47** (0.151 g, 0.903 mmol, 30%) was obtained as a light tan powdery solid. ¹H NMR

(400 MHz, DMSO- d_6): δ 12.29 (*br s*, 1H), 11.37 (*br s*, 1H), 9.26 (*s*, 1H), 7.55 (*d*, $J = 8.0$, 1H), 6.70 (*s*, 1H), 6.66 (*dd*, $J_1 = 8.4$, $J_2 = 0.8$, 1H), 2.24 (*s*, 3H); ESI-MS(+): m/z 168.16 [M + H]⁺.

N,2-Dihydroxy-5-methylbenzamide (5.48): From the general method for hydroxamic acid formation A, from methyl 2-hydroxy-5-methylbenzoate (0.500 g, 3.01 mmol), KOH (0.760 g, 13.5 mmol), and hydroxylamine hydrochloride (0.418 g, 6.02 mmol) in MeOH (20 mL) at 75 °C for 5 h, **5.48** (0.250 g, 1.50 mmol, 50%) was obtained as a light tan crystalline solid. ¹H NMR (400 MHz, DMSO- d_6): δ 11.90 (*br s*, 1H), 11.37 (*br s*, 1H), 9.29 (*s*, 1H), 7.49 (*s*, 1H), 7.18 (*d*, $J = 8.4$, 1H), 6.78 (*d*, $J = 8.4$, 1H), 2.20 (*s*, 3H); ESI-MS(+): m/z 168.14 [M + H]⁺.

N,2-Dihydroxy-3-methoxybenzamide (5.49): From the general method for hydroxamic acid formation A, from methyl 2-hydroxy-3-methoxybenzoate (0.548 g, 3.01 mmol), KOH (0.760 g, 13.5 mmol), and hydroxylamine hydrochloride (0.418 g, 6.02 mmol) in MeOH (20 mL) at 75 °C for 7 h, **5.49** (0.225 g, 1.23 mmol, 41%) was obtained as a tan crystalline solid. ¹H NMR (400 MHz, DMSO- d_6): δ 12.37 (*br s*, 1H), 11.47 (*br s*, 1H), 9.35 (*s*, 1H), 7.23 (*d*, $J = 8.0$, 1H), 7.06 (*d*, $J = 8.0$, 1H), 6.76 (*t*, $J = 8.0$, 1H), 3.76 (*s*, 3H); ESI-MS(+): m/z 184.12 [M + H]⁺.

N,2-Dihydroxy-4-methoxybenzamide (5.50): From the general method for hydroxamic acid formation A, from methyl 2-hydroxy-4-methoxybenzoate (0.548 g, 3.01 mmol), KOH (0.760 g, 13.5 mmol), and hydroxylamine hydrochloride (0.418 g, 6.02 mmol) in MeOH (20 mL) at 75 °C for 7 h, **5.50** (0.089 g, 0.47 mmol, 16%) was obtained as a tan crystalline solid. ¹H NMR (400 MHz, DMSO- d_6): δ 11.31 (*br s*, 1H), 9.21 (*s*, 1H), 7.60 (*d*, $J = 8.4$, 1H), 6.44 – 6.41 (*m*, 2H), 3.74 (*s*, 3H); ESI-MS(+): m/z 184.16 [M + H]⁺.

N,2-Dihydroxy-5-methoxybenzamide (5.51): From the general method for hydroxamic acid formation A, from methyl 2-hydroxy-5-methoxybenzoate (0.548 g, 3.01 mmol), KOH (0.760 g, 13.5 mmol), and hydroxylamine hydrochloride (0.418 g, 6.02 mmol) in MeOH (20 mL) at 75 °C for 7 h, **5.51** (0.318 g, 1.74 mmol, 58%) was obtained as a tan crystalline solid. ¹H NMR (400 MHz, DMSO-*d*₆): δ 11.75 (*br s*, 1H), 11.42 (*br s*, 1H), 9.34 (*s*, 1H), 7.23 (*d*, *J* = 3.2, 1H), 6.99 (*dd*, *J*₁ = 8.8, *J*₂ = 2.8, 1H), 6.82 (*d*, *J* = 8.8, 1H), 3.70 (*s*, 3H); ESI-MS(+): *m/z* 184.13 [M + H]⁺.

3-Amino-N,2-dihydroxybenzamide (5.52): From the general method for hydroxamic acid formation A, from methyl 3-amino-2-hydroxybenzoate (0.750 g, 4.49 mmol), KOH (1.13 g, 20.2 mmol), and hydroxylamine hydrochloride (0.624 g, 8.97 mmol) in MeOH (20 mL) at 45 °C for 16 h, **5.52** (0.054 g, 0.32 mmol, 7%) was obtained as a tan crystalline solid. ¹H NMR (400 MHz, DMSO-*d*₆): δ 11.50 (*br s*, 1H), 9.29 (*br s*, 1H), 6.89 – 6.86 (*m*, 1H), 6.75 – 6.71 (*m*, 1H), 6.60 – 6.54 (*m*, 1H); ESI-MS(+): *m/z* 169.01 [M + H]⁺.

N,2-Dihydroxy-N-methylbenzamide (5.53): From the general method for hydroxamic acid formation A, from methyl 2-hydroxybenzoate (0.500 g, 3.29 mmol), KOH (0.830 g, 14.8 mmol), and N-methylhydroxylamine hydrochloride (0.549 g, 6.57 mmol) in MeOH (20 mL) at 75 °C for 5 h, **5.53** (0.094 g, 0.56 mmol, 17%) was obtained as a light tan crystalline solid. ¹H NMR (400 MHz, DMSO-*d*₆): δ 7.90 (*d*, *J* = 8.0, 1H), 7.35 (*dt*, *J*₁ = 8.4, *J*₂ = 1.2, 1H), 6.91 (*d*, *J* = 8.0, 1H), 6.85 (*dt*, *J*₁ = 8.0, *J*₂ = 1.2, 1H), 3.39 (*s*, 3H); ESI-MS(+): *m/z* 167.06 [M + H]⁺.

N-Hydroxy-6-methylpicolinamide (5.56): From the general method for hydroxamic acid formation B, from 6-methylpicolinic acid (0.350 g, 2.55 mmol), thionyl chloride (224 μ L, 3.06 mmol), 5 drops cat. DMF, TEA (0.71 mL, 5.1 mmol), and hydroxylamine hydrochloride (0.355 g, 5.10 mmol) in CH_2Cl_2 (15 mL) at 25 $^\circ\text{C}$ for 1.5 h, **5.56** (0.063 g, 0.41 mmol, 16 %) was obtained as an off white solid. ^1H NMR (400 MHz, $\text{DMSO-}d_6$): δ 11.19 (s, 1H), 9.06 (s, 1H), 7.82 (t, $J = 7.6$, 1H), 7.73 (d, $J = 7.6$, 1H), 7.40 (d, $J = 7.6$, 1H), 2.50 (s, 3H); ESI-MS(+): m/z 153.10 $[\text{M} + \text{H}]^+$.

N-Hydroxy-5-methylpicolinamide (5.57): From the general method for hydroxamic acid formation B, from 5-methylpicolinic acid (0.500 g, 3.65 mmol), thionyl chloride (319 μ L, 4.38 mmol), 5 drops cat. DMF, TEA (1.00 mL, 7.29 mmol), and hydroxylamine hydrochloride (0.507 g, 7.29 mmol) in CH_2Cl_2 (15 mL) at 25 $^\circ\text{C}$ for 1.5 h, **5.57** (0.043 g, 0.28 mmol, 8%) was obtained as an off white solid. ^1H NMR (400 MHz, $\text{DMSO-}d_6$): δ 11.33 (s, 1H), 9.00 (s, 1H), 8.42 (s, 1H), 7.85 (d, $J = 8.0$, 1H), 7.76 (dd, $J_1 = 8.0$, $J_2 = 0.4$, 1H), 3.33 (s, 3H); ESI-MS(+): m/z 153.10 $[\text{M} + \text{H}]^+$.

Synthesis for Unnatural Amino Acid MPB Derivatives

3-(Aminomethyl)benzene-1,2-diol (59): Following the previous methyl ether deprotection protocol, from (2,3-dimethoxyphenyl)methanamine (0.25 g, 1.5 mmol) and neat BBr_3 (4.5 mL, 4.5 mmol) in 10 mL CH_2Cl_2 at 0 – 25 $^\circ\text{C}$ for 16 h, **59** (0.17 g, 1.2 mmol, 81%) was obtained as a yellow solid. ^1H NMR (400 MHz, $\text{DMSO-}d_6$): δ 8.47 (*br s*, 4H), 6.82 (d, $J = 7.6$, 1H), 6.75 (d, $J = 7.6$, 1H), 6.76 (dt, $J_1 = 8.0$, $J_2 = 1.2$, 1H), 3.91 (s, 2H); ESI-MS(+): m/z 140 $[\text{M} + \text{H}]^+$.

3-(2-Aminoethyl)benzene-1,2-diol (60): Following the previous methyl ether deprotection protocol, from 2-(2,3-dimethoxyphenyl)ethan-1-amine (0.250 g, 1.38 mmol) and neat BBr_3 (4.1

mL, 4.1 mmol) in 10 mL CH₂Cl₂ at 0 – 25 °C for 16 h, **60** (0.050 g, 0.33 mmol, 24%) was obtained as an off-white crystalline solid. ¹H NMR (400 MHz, DMSO-*d*₆): δ 9.34 (*br s*, 1H), 7.93 (*br s*, 3H), 6.70 (dd, *J*₁ = 7.2, *J*₂ = 2.0, 1H), 6.58 – 6.53 (m, 2H), 2.94 (t, *J* = 6.8, 2H), 2.79 (t, *J* = 8.8, 2H); ESI-MS(+): *m/z* 154 [M + H]⁺.

(S)-2-((Tert-butoxycarbonyl)amino)-3-(3-formyl-4-hydroxyphenyl)propanoic acid (5.64a):

A solution of (tert-butoxycarbonyl)-L-tyrosine (6.0 g, 1 eq., 21 mmol) in freshly prepared 108 mL of 10 % aqueous NaOH was pre-heated to 80 °C and placed under a nitrogen atmosphere. Then chloroform (6.0 mL, 75 mmol) was slowly added dropwise via addition funnel over the course of 20 min to the pre-heated reaction, at a rate of ~1 drop per 5 s. The reaction was then heated for an additional 4 hrs at 80 °C, and was then cooled to 25 °C. It was observed that upon reaction completion, the reaction solution had changed from clear dark yellow/brown. Once cool, the reaction mixture was gently acidified with 4 M HCl, and the product was extracted into organic using 3×20 mL ethyl acetate. The combined organic was washed with brine, dried over magnesium sulfate, and the solids were filtered off and discarded. The filtrate was concentrated under reduced pressure, and the resulting crude was purified by column chromatography, running gradient from 100% CH₂Cl₂ to 10% MeOH. The desired product eluted in 5% MeOH in CH₂Cl₂, co-eluting with a small amount of unreacted starting material, as had been previously described in the literature reference.³⁷ Like fractions containing the desired product were combined and concentrated under reduced pressure to obtain **5.64a** (1.79 g, 5.80 mmol, 27 %) as a light yellow oil that solidified upon standing. ¹H NMR (400 MHz, DMSO-*d*₆): δ 10.56 (*br s*, 1H), 10.22 (s, 1H), 7.51 (s, 3H), 7.39 (d, *J* = 8.0, 1H), 7.10 (d, *J* = 8.4, 1H), 6.90 (d, *J* = 8.4, 1H), 4.06 – 4.01 (m, 1H), 2.94 (dd, *J*₁ = 13.6, *J*₂ = 4.4, 1H), 2.75 (dd, *J*₁ = 13.2, *J*₂ = 10.4, 1H), 1.29 (s, 9H); ESI-MS(-): *m/z* 308.03 [M - H]⁻.

Benzyl (S)-3-(4-(benzyloxy)-3-formylphenyl)-2-((tert-butyl

butoxycarbonyl)amino)propanoate (5.64b): To a solution of **5.64a** (1.79 g, 5.79 mmol) dissolved in 50 mL DMF, potassium carbonate (1.68 g, 12.2 mmol) and (bromomethyl)benzene (1.44 mL, 12.2 mmol) were sequentially added. The reaction mixture was placed under a nitrogen atmosphere and allowed to stir at 25 °C for 16 h. Upon reaction completion, the reaction mixture was diluted with 50 mL ethyl acetate, and washed with 50 mL brine. The aqueous was back-extracted with 10 mL ethyl acetate, and the combined organic was dried over magnesium sulfate, and the solids were filtered off and discarded. The filtrate was concentrated under reduced pressure, and the resulting crude was purified by column chromatography, running gradient from 100% hexanes to 50% ethyl acetate in hexanes. The desired product eluted in 25% ethyl acetate in hexanes. Like fractions were combined and concentrated under reduced pressure to obtain **5.64b** (2.04 g, 4.17 mmol, 72%) as a clear, pale yellow, viscous oil. ¹H NMR (400 MHz, DMSO-*d*₆): δ 10.38 (s, 1H), 7.58 – 7.21 (m, 12H), 5.24 (s, 2H), 5.08 (s, 2H), 4.22 – 4.16 (m, 1H), 3.02 – 2.97 (m, 1H), 2.90 – 2.84 (m, 1H), 1.29 (s, 9H); ESI-MS(+): *m/z* 512.18 [M + Na]⁺.

(S)-2-(Benzyloxy)-5-(3-(benzyloxy)-2-((tert-butoxycarbonyl)amino)-3-oxopropyl)benzoic acid (5.64c): To a solution of **5.64b** (2.00 g, 4.09 mmol) in 27 mL *t*-butanol, 16.3 mL of a 1.25 M NaHPO₄ buffer at pH 8 was added, and the reaction was placed under a nitrogen atmosphere. Then, with vigorous stirring, a suspension of KMnO₄ (3.87 g 24.5 mmol) in 25 mL DI water was added over the course of ~2 min, and the reaction mixture was allowed to stir at 25 °C for 3 h. Upon completion, the reaction mixture was quenched via the addition of sat. Na₂SO₄ solution,

and the reaction was acidified with 6 M HCl, until the solution turned completely clear. The product was extracted into organic using 3×20 mL ethyl acetate, and the combined organic was washed with brine, dried over magnesium sulfate, and the solids were filtered off and discarded. The filtrate was concentrated under reduced pressure, and the resulting residue was purified by column chromatography, running gradient from 100% hexanes to 100% ethyl acetate. The desired product eluted in 50% ethyl acetate in hexanes. Like fractions were combined and concentrated under reduced pressure to obtain **5.64c** (1.03 g, 2.05 mmol, 50%) as a clear, slightly fragrant oil. ¹H NMR (400 MHz, Acetone-*d*₆): δ 7.82 (s, 1H), 7.58 (d, *J* = 8.0, 2H), 7.44 – 7.33 (m, 9H), 7.20 (d, *J* = 8.4, 1H), 6.32 (*br* d, *J* = 8.0, 1H), 5.32 (s, 2H), 5.16 (s, 2H), 4.49 – 4.23 (m, 1H), 3.17 (dd, *J*₁ = 14.0, *J*₂ = 5.2, 1H), 3.03 (dd, *J*₁ = 13.6, *J*₂ = 8.8, 1H), 1.35 (s, 9H); ESI-MS(-): *m/z* 504.17 [M - H]⁻.

Benzyl (S)-3-(4-(benzyloxy)-3-(hydroxycarbamoyl)phenyl)-2-((tert-butoxycarbonyl)amino)propanoate (5.64d): A solution of **5.64c** (0.400 g, 0.791 mmol) in 10 mL CH₂Cl₂ was cooled to 0 °C. Then thionyl chloride (69.3 mL, 0.949 mmol) was added to the solution, followed by the addition of ~2 drops cat. DMF. The reaction was stirred at 25 °C for 1 h to generate the in situ acid chloride. Then the solution containing the in situ acid chloride was slowly added dropwise to a solution of hydroxylamine hydrochloride (0.275 g, 3.96 mmol) and triethylamine (0.55 mL, 4.0 mmol) in 33 mL of a 10:1 THF to water. Upon addition of the acid chloride solution, a large amount of HCl gas evolved, and the reaction mixture turned light orange-brown. The reaction mixture was allowed to stir at 25 °C for 2 h, until reaction was complete by TLC. The reaction mixture was quenched with 1 M HCl, and extracted into organic using 3×15 mL ethyl acetate. The combined organic was washed with brine, dried over

magnesium sulfate, and the solids were filtered off and discarded. The resulting residue was purified by column chromatography, running gradient from 100% hexanes to 100% ethyl acetate. The desired product eluted in 50% ethyl acetate in hexanes. Like fractions were combined and concentrated under reduced pressure to obtain benzyl **5.64d** (0.225 g, 0.432 mmol, 55%) as a white solid. $^1\text{H NMR}$ (400 MHz, Acetone- d_6): δ 10.49 (*br s*, 1H), 8.57 (*br s*, 1H), 7.92 (s, 1H), 7.55 (d, $J = 7.2$, 1H), 7.45 – 7.32 (m, 9H), 7.11 (d, $J = 8.8$, 1H), 6.29 (*br d*, $J = 8.0$, 1H), 5.35 (s, 2H), 5.14 (s, 2H), 4.46 – 4.41 (m, 1H), 3.14 (dd, $J_1 = 13.6$, $J_2 = 5.2$, 1H), 3.02 (dd, $J_1 = 14.0$, $J_2 = 8.8$, 1H), 1.34 (s, 9H); ESI-MS(+): m/z 543.22 $[\text{M} + \text{Na}]^+$.

(S)-2-((Tert-butoxycarbonyl)amino)-3-(4-hydroxy-3-(hydroxycarbamoyl)phenyl)propanoic acid (5.64e): To a solution of **5.64d** (0.175 g, 0.336 mmol) in 15 mL MeOH, and under a nitrogen atmosphere, palladium on carbon (36 mg, 10% Wt, 33.6 μmol) was added in one portion. Then the reaction was placed under a hydrogen atmosphere at 1 atm, and the reaction mixture was allowed to stir at 25 °C under 1 atm of hydrogen for 4 h. Upon reaction completion, the reaction mixture was filtered through a pad of celite and the yellowish filtrate was concentrated under reduced pressure. The crude was taken up in water, made basic with NaOH, and the aqueous was washed with 2 \times 10 mL ether. Upon back extraction of the organic, the aqueous layer was acidified using HCl, and the product was extracted into organic using 3 \times 15 mL ethyl acetate. The combined organic was washed with brine, dried over magnesium sulfate, and the solids were filtered off and discarded. The filtrate was concentrated under reduced pressure to obtain **5.64e** (0.107 g, 0.313 mmol, 93%), as a light, purple/brown oil that was used directly in the next step without any additional purification. $^1\text{H NMR}$ (400 MHz, DMSO- d_6): δ 12.02 (*br s*, 2H), 11.34 (*br s*, 1H), 9.29 (*br s*, 1H), 7.57 (s, 1H), 7.23 (d, $J = 8.0$, 1H), 7.06 (d, $J =$

8.0, 1H), 6.79 (d, $J = 8.4$, 1H), 4.08 – 4.02 (m, 1H), 2.90 (dd, $J_1 = 13.6$, $J_2 = 4.4$, 1H), 2.71 (dd, $J_1 = 13.2$, $J_2 = 10.0$, 1H), 1.90 (s, 9H).

(S)-2-Amino-3-(4-hydroxy-3-(hydroxycarbamoyl)phenyl)propanoic acid (5.64f): To a suspension of **5.64e** (0.106 g, 0.311 mmol) in 1 mL CH₂Cl₂, TFA (1.00 mL, 13.0 mmol) was added dropwise. The reaction mixture was allowed to stir at 25 °C for 1.5 h, until the reaction appeared complete by TLC. Then the reaction contents were concentrated under reduced pressure to obtain a purplish brown residue, which was then purified by RP chromatography, running gradient from 5% MeOH in water to 100% MeOH. The desired product eluted rapidly in 5% MeOH in water. Like fractions containing the desired product were combined and concentrated under reduced pressure to obtain **5.64f** (0.0474 g, 0.313 mmol, 63%) as an off white solid. ¹H NMR (400 MHz, DMSO-*d*₆): δ 7.60 (s, 1H), 7.24 (d, $J = 7.2$, 1H), 6.84 (d, $J = 8.4$, 1H), 3.85 (s, 1H), 3.06 (d, $J = 10.8$, 1H), 2.92 – 2.87 (m, 1H); HRMS (ESI-TOF): m/z calcd for C₁₀H₁₂N₂O₅-H⁻: 239.0673 [M-H]⁻; found: 239.0674.

(S)-5-(2-((Tert-butoxycarbonyl)amino)-2-carboxyethyl)-2-hydroxybenzoic acid (5.65a): Following the same protocol used in **5.64e**, from **5.64d** (0.085 g, 0.17 mmol) and palladium on carbon (8.9 mg, 10% Wt, 8.4 μ mol) in 15 mL MeOH under 1 atm hydrogen at 25 °C for 16 h, **5.65a** (0.044 g, 14 mmol, 81%) was obtained as a white solid. ¹H NMR (400 MHz, Acetone-*d*₆): δ 7.81 (s, 1H), 7.47 (d, $J = 8.4$, 1H), 6.90 (d, $J = 8.4$, 1H), 6.10 (*br* d, $J = 7.6$, 1H), 4.42 – 4.37 (m, 1H), 3.18 (dd, $J_1 = 14.0$, $J_2 = 4.8$, 1H), 2.99 (dd, $J_1 = 14.0$, $J_2 = 8.4$, 1H), 1.36 (s, 9H); ESI-MS(-): m/z 324.09 [M - H]⁻.

(S)-5-(2-Amino-2-carboxyethyl)-2-hydroxybenzoic acid-TFA (5.65b): To a solution of **5.65a** in 1 mL CH₂Cl₂, TFA (1.00 mL, 13.0 mmol) was added dropwise. The reaction mixture was allowed to stir at 25 °C for 3 h. Upon completion, the reaction contents were concentrated under reduced pressure to obtain the desired product, **5.65b** (0.046 g, 0.14 mmol, 100%) as a TFA salt that was off-white in color. ¹H NMR (400 MHz, DMSO-*d*₆): δ 8.23 (*br s*, 3H), 7.69 (*s*, 1H), 7.37 (*d*, *J* = 8.4, 1H), 6.92 (*d*, *J* = 8.4, 1H), 4.16 (*s*, 1H), 3.05 – 3.03 (*m*, 2H); ESI-MS(-): *m/z* 224.21 [M - H]⁻.

(S)-2-((Tert-butoxycarbonyl)amino)-4-(4-hydroxyphenyl)butanoic acid (5.66a): To a solution of (S)-2-amino-4-(4-hydroxyphenyl)butanoic acid hydrobromide (1.00 g, 3.62 mmol) in 25 mL dioxane and 10 mL DI water, 9.0 mL 1 M NaOH was added, and the reaction was cooled to 0 °C. After cooling, di-tert-butyl dicarbonate (0.901 g, 4.13 mmol) was added in one portion, and the reaction was stirred at 0 °C for 10 min, then at 25 °C for 2 h. Upon completion, the reaction mixture was basified to ~pH 11 with 6 M NaOH, and washed with 2×10 mL ether, discarding the organic. The aqueous was acidified with HCl, and the product was extracted into organic using 3×10 mL ethyl acetate. The combined organic was washed with brine, dried over magnesium sulfate, and the solids were filtered off and discarded. The filtrate was concentrated under reduced pressure to obtain **5.66a** (1.22 g, 4.13 mmol, theoretical yield). The product was obtained with excess dioxanes present, despite excessive time under vacuum, and was used directly in the next step with no additional purification. ¹H NMR (400 MHz, DMSO-*d*₆): δ 12.39 (*br s*, 1H), 9.14 (*br s*, 1H), 7.16 (*d*, *J* = 8.0, 1H), 6.95 (*d*, *J* = 8.0, 2H), 6.64 (*d*, *J* = 8.0, 2H), 3.81 – 3.76 (*m*, 1H), 2.52 – 2.46 (*m*, 2H), 1.83 – 1.77 (*m*, 2H), 1.38 (*s*, 9H); ESI-MS(+): *m/z* 318.10 [M + Na]⁺.

(S)-2-((Tert-butoxycarbonyl)amino)-4-(3-formyl-4-hydroxyphenyl)butanoic acid (5.66b):

Following the same protocol used in **5.64a**, from **5.66a** (1.20 g, 4.06 mmol) and chloroform (1.44 mL, 17.9 mmol) in 43 mL of freshly prepared 10% NaOH at 80 °C for 3 h, **5.66b** (0.376 g, 1.16 mmol, 29%) was obtained as a yellow oil. ¹H NMR (400 MHz, DMSO-*d*₆): δ 12.45 (*br s*, 1H), 10.52 (*br s*, 1H), 10.21 (*s*, 1H), 7.47 (*s*, 1H), 7.34 (*d*, *J* = 8.4, 1H), 7.21 (*d*, *J* = 8.4, 1H), 6.91 (*d*, *J* = 8.4, 1H), 3.79 (*s*, 1H), 2.59 – 2.40 (*m*, 2H), 1.87 – 1.71 (*m*, 2H), 1.38 (*s*, 9H); ESI-MS(-): *m/z* 322.10 [M - H]⁻.

Benzyl (S)-4-(4-(benzyloxy)-3-formylphenyl)-2-((tert-butoxycarbonyl)amino)butanoate (5.66c):

Following the same protocol used in **5.64b**, from **5.66b** (0.375 g, 1.16 mmol), potassium carbonate (337 mg, 2.44 mmol), and (bromomethyl)benzene (0.289 mL, 2.44 mmol) in 25 mL DMF at 25 °C for 16 h, **5.66c** (0.338 g, 0.671 mmol, 58%) was obtained as a clear oil. ¹H NMR (400 MHz, DMSO-*d*₆): δ 10.38 (*s*, 1H), 7.53 – 7.23 (*m*, 13H), 5.25 (*s*, 2H), 5.15 – 5.04 (*m*, 2H), 3.93 (*s*, 1H), 2.60 (*m*, 2H), 1.91 – 1.80 (*m*, 2H), 1.38 (*s*, 9H); ESI-MS(+): *m/z* 526.16 [M + Na]⁺.

(S)-2-(Benzyloxy)-5-(4-(benzyloxy)-3-((tert-butoxycarbonyl)amino)-4-oxobutyl)benzoic acid (5.66d):

Following the same protocol used in **5.64c**, from **5.66c** (0.320 g, 0.635 mmol), a suspension of KMnO₄ (0.602 g, 3.81 mmol) in 3.8 mL water, all in 10 mL *t*-butanol and 7.9 mL NaHPO₄ buffer at pH 8, at 25 °C for 1h, **5.66d** (0.117 g, 0.225 mmol, 35%) was obtained as a white, oily solid. ¹H NMR (400 MHz, DMSO-*d*₆): δ 7.48 – 7.10 (*m*, 12H), 7.08 (*d*, *J* = 8.8, 1H),

5.15 – 5.04 (m, 4H), 3.94 (dd, $J_1 = 12.8$, $J_2 = 7.2$, 1H), 2.58 – 2.53 (m, 2H), 1.90 – 1.81 (m, 2H), 1.38 (s, 9H); ESI-MS(-): m/z 518.17 [M - H]⁻.

Benzyl (S)-4-(4-(benzyloxy)-3-(hydroxycarbamoyl)phenyl)-2-((tert-butoxycarbonyl)amino)butanoate (5.66e): Following the same protocol used in **5.64d**, from **5.66d** (0.110 g, 212 μ mol), thionyl chloride (19 μ L, 0.254 mmol), ~2 drops cat DMF in 2.5 mL CH₂Cl₂ at 0 °C for 1 h, and then with TEA (0.15 mL, 1.1 mmol) and hydroxylamine hydrochloride (0.074 mg, 1.1 mmol) in 11 mL of 10:1 THF to water at 25 °C for 2h, **5.66e** (0.074 g, 0.14 mmol, 65%) was obtained as a clear oil that solidified upon standing to a white solid. ¹H NMR (400 MHz, Acetone-*d*₆): δ 10.49 (*br s*, 1H), 8.54 (*br s*, 1H), 7.88 (s, 1H), 7.54 (d, $J = 7.6$, 2H), 7.44 – 7.29 (m, 9H), 7.12 (d, $J = 8.4$, 1H), 6.50 (d, $J = 8.0$, 1H), 5.34 (s, 2H), 5.21 – 5.11 (m, 2H), 4.24 – 4.19 (m, 1H), 2.76 – 2.65 (m, 2H), 2.10 – 2.00 (m, 2H), 1.42 (s, 9H); ESI-MS(+): m/z 535.00 [M + H]⁺, 557.22 [M + Na]⁺.

(S)-2-((Tert-butoxycarbonyl)amino)-4-(4-hydroxy-3-(hydroxycarbamoyl)phenyl)butanoic acid (5.66f): Following the same protocol used in **5.64e**, from **5.66e** (0.074 g, 0.14 mmol) and palladium on carbon (15 mg, 10% Wt, 14 μ mol) in 15 mL MeOH under 1 atm hydrogen at 25 °C for 4 h, **5.66f** (0.025 g, 71 μ mol, 51%) was obtained as a clear oil that was used directly in the next step without any additional purification. ¹H NMR (400 MHz, Acetone-*d*₆): δ 11.84 (*br s*, 1H), 11.01 (*br s*, 1H), 7.53 (s, 1H), 7.31 (d, $J = 8.4$, 1H), 6.86 (d, $J = 8.4$, 1H), 6.34 (d, $J = 8.0$, 1H), 2.76 – 2.62 (m, 2H), 2.13 – 2.00 (m, 2H), 1.44 (s, 9H); ESI-MS(+): m/z 377.13 [M + Na]⁺.

(S)-2-Amino-4-(4-hydroxy-3-(hydroxycarbamoyl)phenyl)butanoic acid (5.66g): Following the same protocol used in **5.64f**, from **5.66f** (0.025 g, 71 μ mol) and TFA (0.50 mL, 6.5 mmol) in 1 mL CH₂Cl₂ at 25 °C for 1 h, **5.66g** (0.0066 g, 26 μ mol, 37%) was obtained as a pale blush colored solid. ¹H NMR (400 MHz, CD₃OD): δ 7.60 (s, 1H), 7.27 (d, *J* = 8.4, 1H), 6.88 (d, *J* = 7.2, 1H), 3.98 – 3.95 (s, 1H), 2.80 – 2.69 (m, 2H), 2.23 – 2.11 (m, 2H); HRMS (ESI-TOF): *m/z* calcd for C₁₁H₁₄N₂O₅-H⁻: 253.0830 [M-H]⁻; found: 253.0831.

Assay Protocol:

Arg1 Assay Protocol: Human Arg1 was purchased from Abcam, and the substrate was prepared as previously reported,²⁹ and the assay was performed in a clear 96-well plate. Each well contained a total volume of 100 μ L, including buffer (50 mM HEPES, 50 mM NaCl, 2 mM MnCl₂, pH 8.5), inhibitor (varying concentration), thio-arginine substrate (0.5 mM), and Elman's reagent as a developer (0.5 mM). The enzyme and inhibitor were incubated together at 37 °C for 30 min, after which the reaction was initiated by the addition of a 1:1 solution of substrate and developer. The change in absorbance was monitored for 30 min at 420 nm at 37 °C. The negative control wells contained no inhibitor and were arbitrarily set as 100% enzyme activity. IC₅₀ values were determined by incubating various concentrations of inhibitor with the enzyme using the aforementioned conditions, and dose response curves were generated, fitted, and analyzed using GraphPad Prism graphing software using four-variable response parameters.

5.6 Acknowledgements

Chapters 5 is, in part, a reprint of materials published in the following paper: Targeting Metalloenzymes for Therapeutic Intervention, Chen, Y.A.;* Adamek, R.N.;;* Dick, B.L.;

Credille, C.V.; Morrison, C.N.; Cohen, S.M.; *Chem. Rev.* **2018**, *118*, ASAP article. DOI: 10.1021/ACS.CHEMREV.8B00201. The dissertation author was the primary researcher and the primary author for the reprinted data presented herein. Reprinted with permission from Chemical Reviews. Copyright 2018 American Chemical Society.

*These authors contributed equally to this work.

Chapter 5 is, in part, submitted for publication as the following manuscript: Identification of Adenosine Deaminase Inhibitors by Metal-binding Pharmacophore Screening, Adamek, R.N.; Ludford, P.; Duggan, S.M.; Tor, Y.; Cohen, S.M.; *ChemMedChem* **2020** (*in submission*). The dissertation author was the primary researcher and the primary author for the reprinted data presented herein.

5.7 References

1. Kossel, A.; Dakin, H., Über die Arginase. *Hoppe-Seyler's Zeitschrift für Physiologische Chemie* **1904**, *41*, 321-331
2. Pudlo, M.; Demougeot, C.; Girard-Thernier, C., Arginase Inhibitors: A Rational Approach Over One Century. *Med. Res. Rev.* **2017**, *37*, 475-513.
3. Morris, S. M., Jr.; Bhamidipati, D.; Kepka-Lenhart, D., Human Type II Arginase: Sequence Analysis and Tissue-Specific Expression. *Gene* **1997**, *193*, 157-61.
4. Vockley, J. G.; Jenkinson, C. P.; Shukla, H.; Kern, R. M.; Grody, W. W.; Cederbaum, S. D., Cloning and Characterization of the Human Type II Arginase Gene. *Genomics* **1996**, *38*, 118-23.
5. Di Costanzo, L.; Sabio, G.; Mora, A.; Rodriguez, P. C.; Ochoa, A. C.; Centeno, F.; Christianson, D. W., Crystal Structure of Human Arginase I at 1.29-Å Resolution and Exploration of Inhibition in the Immune Response. *Proc. Natl. Acad. Sci. U. S. A.* **2005**, *102*, 13058-63.
6. Christianson, D. W., Arginase: Structure, Mechanism, and Physiological Role in Male and Female Sexual Arousal. *Acc. Chem. Res.* **2005**, *38*, 191-201.
7. Christianson, D. W.; Cox, J. D., Catalysis by Metal-Activated Hydroxide in Zinc and Manganese Metalloenzymes. *Annu. Rev. Biochem.* **1999**, *68*, 33-57.

8. Cox, J. D.; Cama, E.; Colleluori, D. M.; Pethe, S.; Boucher, J. L.; Mansuy, D.; Ash, D. E.; Christianson, D. W., Mechanistic and Metabolic Inferences from the Binding of Substrate Analogues and Products to Arginase. *Biochemistry-Us* **2001**, *40*, 2689-2701.
9. Caldwell, R. B.; Toque, H. A.; Narayanan, S. P.; Caldwell, R. W., Arginase: An Old Enzyme with New Tricks. *Trends Pharmacol. Sci.* **2015**, *36*, 395-405.
10. Rodriguez, P. C.; Ochoa, A. C., Arginine Regulation by Myeloid Derived Suppressor Cells and Tolerance in Cancer: Mechanisms and Therapeutic Perspectives. *Immunol. Rev.* **2008**, *222*, 180-91.
11. Bronte, V.; Serafini, P.; Mazzoni, A.; Segal, D. M.; Zanovello, P., L-Arginine Metabolism in Myeloid Cells Controls T-Lymphocyte Functions. *Trends Immunol.* **2003**, *24*, 302-6.
12. Serafini, P.; De Santo, C.; Marigo, I.; Cingarlini, S.; Dolcetti, L.; Gallina, G.; Zanovello, P.; Bronte, V., Derangement of Immune Responses by Myeloid Suppressor Cells. *Cancer Immunol. Immunother.* **2004**, *53*, 64-72.
13. Gabrilovich, D. I.; Nagaraj, S., Myeloid-Derived Suppressor Cells as Regulators of the Immune System. *Nat. Rev. Immunol.* **2009**, *9*, 162-74.
14. De Santo, C.; Serafini, P.; Marigo, I.; Dolcetti, L.; Bolla, M.; Del Soldato, P.; Melani, C.; Guiducci, C.; Colombo, M. P.; Iezzi, M.; Musiani, P.; Zanovello, P.; Bronte, V., Nitroaspirin Corrects Immune Dysfunction in Tumor-Bearing Hosts and Promotes Tumor Eradication by Cancer Vaccination. *Proc. Natl. Acad. Sci. U. S. A.* **2005**, *102*, 4185-90.
15. Farkona, S.; Diamandis, E. P.; Blasutig, I. M., Cancer Immunotherapy: The Beginning of the End of Cancer? *BMC Med.* **2016**, *14*, 73.
16. Ribas, A.; Wolchok, J. D., Cancer Immunotherapy Using Checkpoint Blockade. *Science* **2018**, *359*, 1350-1355.
17. Pardoll, D. M., The Blockade of Immune Checkpoints in Cancer Immunotherapy. *Nat. Rev. Cancer.* **2012**, *12*, 252-64.
18. De Strooper, B., Lessons from a Failed Gamma-Secretase Alzheimer Trial. *Cell* **2014**, *159*, 721-6.
19. Mullard, A., BACE Failures Lower AD Expectations, Again. *Nat. Rev. Drug Discov.* **2018**, *17*, 385.
20. Mullard, A., BACE Inhibitor Bust in Alzheimer Trial. *Nat. Rev. Drug Discov.* **2017**, *16*, 155.
21. Liu, P.; Fleete, M. S.; Jing, Y.; Collie, N. D.; Curtis, M. A.; Waldvogel, H. J.; Faull, R. L.; Abraham, W. C.; Zhang, H., Altered Arginine Metabolism in Alzheimer's Disease Brains. *Neurobiol. Aging* **2014**, *35*, 1992-2003.

22. Kan, M. J.; Lee, J. E.; Wilson, J. G.; Everhart, A. L.; Brown, C. M.; Hoofnagle, A. N.; Jansen, M.; Vitek, M. P.; Gunn, M. D.; Colton, C. A., Arginine Deprivation and Immune Suppression in a Mouse Model of Alzheimer's Disease. *J. Neurosci.* **2015**, *35*, 5969-82.
23. Hansmannel, F.; Sillaire, A.; Kamboh, M. I.; Lendon, C.; Pasquier, F.; Hannequin, D.; Laumet, G.; Mounier, A.; Ayrat, A. M.; DeKosky, S. T.; Hauw, J. J.; Berr, C.; Mann, D.; Amouyel, P.; Campion, D.; Lambert, J. C., Is the Urea Cycle Involved in Alzheimer's Disease? *J. Alzheimers Dis.* **2010**, *21*, 1013-21.
24. Yi, J.; Horvay, L. L.; Friedlich, A. L.; Shi, Y.; Rogers, J. T.; Huang, X., L-Arginine and Alzheimer's Disease. *Int. J. Clin. Exp. Pathol.* **2009**, *2*, 211-38.
25. Polis, B.; Samson, A. O., Arginase as a Potential Target in the Treatment of Alzheimer's Disease. *Advances in Alzheimer's Disease* **2018**, *7*, 199-140.
26. Ovsepian, S. V.; O'Leary, V. B., Can Arginase Inhibitors Be the Answer to Therapeutic Challenges in Alzheimer's Disease? *Neurotherapeutics* **2018**, *15*, 1032-1035.
27. Baggio, R.; Elbaum, D.; Kanyo, Z. F.; Carroll, P. J.; Cavalli, R. C.; Ash, D. E.; Christianson, D. W., Inhibition of Mn-2(2+)-Arginase by Borate Leads to the Design of a Transition State Analogue Inhibitor, 2(S)-Amino-6-Borohexanoic Acid. *J Am Chem Soc* **1997**, *119* (34), 8107-8108.
28. Golebiowski, A.; Paul Beckett, R.; Van Zandt, M.; Ji, M. K.; Whitehouse, D.; Ryder, T. R.; Jagdmann, E.; Andreoli, M.; Mazur, A.; Padmanilayam, M.; Cousido-Siah, A.; Mitschler, A.; Ruiz, F. X.; Podjarny, A.; Schroeter, H., 2-Substituted-2-Amino-6-Borohexanoic Acids as Arginase Inhibitors. *Bioorg. Med. Chem. Lett.* **2013**, *23*, 2027-30.
29. Han, S.; Viola, R. E., A Spectrophotometric Assay of Arginase. *Anal. Biochem.* **2001**, *295*, 117-9.
30. Kuhn, N. J.; Ward, S.; Piponski, M.; Young, T. W., Purification of Human Hepatic Arginase and its Manganese (II)-Dependent and pH-Dependent Interconversion Between Active and Inactive Forms: A Possible pH-Sensing Function of the Enzyme on the Ornithine Cycle. *Arch. Biochem. Biophys.* **1995**, *320*, 24-34.
31. Di Costanzo, L.; Ilies, M.; Thorn, K. J.; Christianson, D. W., Inhibition of Human Arginase I by Substrate and Product Analogues. *Arch. Biochem. Biophys.* **2010**, *496*, 101-8.
32. Hoveyda, H. R.; Karunaratne, V.; Rettig, S. J.; Orvig, C., Coordination Chemistry of 2-(2'-Hydroxyphenyl)-2-Oxazolines with Aluminum, Gallium, and Indium: First Tris(ligand)Metal(III) Complexes of this Naturally Occurring Binding Group. *Inorg. Chem.* **1992**, *31*, 5408-5416.
33. Bisson, J.; McAlpine, J. B.; Friesen, J. B.; Chen, S. N.; Graham, J.; Pauli, G. F., Can Invalid Bioactives Undermine Natural Product-Based Drug Discovery? *J. Med. Chem.* **2016**, *59*, 1671-90.

34. Golebiowski, A.; Paul Beckett, R.; Van Zandt, M.; Ji, M. K.; Whitehouse, D.; Ryder, T. R.; Jagdmann, E.; Andreoli, M.; Mazur, A.; Padmanilayam, M.; Cousido-Siah, A.; Mitschler, A.; Ruiz, F. X.; Podjarny, A.; Schroeter, H., 2-Substituted-2-amino-6-borono-hexanoic acids as arginase inhibitors. *Bioorg Med Chem Lett* **2013**, *23* (7), 2027-30.
35. Ilies, M.; Di Costanzo, L.; North, M. L.; Scott, J. A.; Christianson, D. W., 2-Aminoimidazole Amino Acids as Inhibitors of the Binuclear Manganese Metalloenzyme Human Arginase I. *J. Med. Chem.* **2010**, *53*, 4266-76.
36. Agrawal, A.; Johnson, S. L.; Jacobsen, J. A.; Miller, M. T.; Chen, L. H.; Pellecchia, M.; Cohen, S. M., Chelator Fragment Libraries for Targeting Metalloproteinases. *Chemmedchem* **2010**, *5*, 195-199.
37. Preparation of Amino Acid-Related Imidazopyridine Benzamide Derivatives as Anticancer Agents. US7618981, 2009.